2019

Lithic industries and chronology of Middle Paleolithic sites in Southwest China

Yue Hu
University of Wollongong

UNIVERSITY
OF WOLLONGONG
AUSTRALIA

Lithic industries and chronology of Middle Paleolithic sites in Southwest China

Yue Hu

Supervisors:
Bo Li
Ben Marwick
Sam Lin
Richard G. Roberts
Richard Fullagar

This thesis is presented as part of the requirement for the conferral of the degree:
Doctor of Philosophy

University of Wollongong
School of Earth, Atmospheric and Life Sciences

July 2019

Abstract

The characteristics and development of Palaeolithic in China and more broadly in East Asia have been hotly debated. At the centre of the debate is whether there were lithic technological changes in East Asia during the Middle and Late Pleistocene. It has been argued that the lithic industries in this region were dominated by simple core-flake production system until the Late Pleistocene when Upper Palaeothic forms appeared. The lack of advanced stone tool technology in East Asia would imply that hominin populations in this region were possibly culturally and genetically isolated during the early and middle Pleistocene. One of the main reasons that caused such a debate is the scarce of well-defined 'Middle Paleolithic' sites in East Asia, because many of these sites were excavated decades ago and, hence, lacked reliable chronology and detailed and systematic lithic study. To contribute to our understanding of Paleolithic culture in East Asia during the late Middle Pleistocene period, this study presents detailed lithic analysis and chronological study on two Paleolithic sites in Southwest China, Guanyindong and Tianhuadong caves.

In order to establish reliable chronological frameworks for the sites, the recently developed single-grain optically stimulated luminescence (OSL) techniques were applied to date quartz grains extracted from the artefact-bearing sediments from the sites. Since a part proportion of the quartz grains have saturated OSL signal, the standardised growth curve (SGC) method was applied to avoid underestimation in age due to truncated equivalent dose distribution. It shows that the SGC method can be successfully applied to date sediments from this region. OSL ages of 170–80 and 90–50 thousands years ago were obtained for the Guanyindong and Tianhuadong sites, respectively, which suggests that both sites should be assigned to Middle Palaeolithic period.

Evidence of complex systems of lithic production from the two studied sites are reported. Based on detailed analysis of over 2000 stone artefacts from the Guanyindong assemblage, a total of 45 stone artefacts were identified to be made with Levallois concept, including 11 cores, 31 flakes and 4 tools. Apart from Levallois, the lithic assemblages from the sites provide evidence of diverse lithic production systems, including Quina, Kombewa, and discoid systems, which show that the late Middle Pleistocene inhabitants in this region had used a variety of tool-making strategies to adapt to climatic and ecological conditions, raw material availability and demographic contexts. These new findings are similar and contemporary to those typically found in west Eurasia, suggesting that during late Middle Pleistocene hominins in this area had the comparable abilities as those in Europe and Africa, and, thus, challenge the longstanding view that there is a lack of distinct progress in lithic technology during the Early and Middle Palaeolithic period in East Asia.

Acknowledgments

I would like to extend my sincere gratitude to people who have had provided their kindest help. The thesis could not have been accomplished without their support.

Firstly, I would like to specially thank my supervisors Dr. Bo Li and Dr. Ben Marwick for their constructive guidance and patient assistance since the beginning of my PhD project. Dr. Bo Li not only gave me the opportunity and helped coordinating the project but also provided me countless guidance on OSL dating and valuable discussion on Palaeolithic archaeology, letting alone all the assistance on field investigations and sampling, laboratory measurements. Since worked with Dr. Ben Marwick in his archaeological site in Myanmar, he has always been a patient, kind, supportive person to me throughout of my study period. He gave me numerous valuable guidances on R programming, stone artifacts analysis, fieldwork and writing skills. I truly appreciate the helps and supports from both of them. What I learnt from them can always benefit my academic career. I also feel grateful to Dr. Sam Lin, who spent a lot of time with me in analysing stone artifacts in Beijing. He also patiently illustrated and explained lithic technologies to me. I really want to thank him for his generosity.

Secondly, I also would like to thank Prof. Richard Roberts who supported my first field excavation and gave generous suggestions for my publication as well as lots of guidance on my study. Richard Fullgar, one of my co-supervisors, also gave me a lot of instruction at the beginning of my PhD project. I also wanted to thank Prof. Zenobia Jacobs for her valuable advice on my study, such like publication, presentation, and her supports to my laboratory work. Speaking of laboratory work, I really wanted to thank our OSL dating team, especially Dr Terry Lachlan and Yasaman Jafari, who have given me lots of help in the laboratory work. Besides, during my PhD project in UOW, I received a lot of help from other staff members School of Earth, Atmospheric and Life Sciences (SEALS). Their assistances are always in time, effective and substantial. I also wanted to thank my nice colleagues in UOW. It's really a joyful time to get to know each one of them and spend four years together.

Besides, I am truly gratful to the colleagues from China. A special mention of those who contributed most directly, they include Prof. Weiwen Huang, Prof. Yamei Hou, Prof Jiafu Zhang, Prof. Youping Wang, Ning Ma, Yushan Lou, Yemao Hou, Jianping Yue, Yujie Guo, Lei Lei, Xingwen Li. And also many thanks to C. Tryon, J. Feathers and any other anonymous reviwers who have given me valuable comments and suggestions of the context. Last and surly not least gratitude goes to my family who have always been there supporting me. And, finally I apologize to all other unnamed people who helped me in numerous ways to make the thesis possible. Thank you all.

Certification

I, Yue Hu, declare that this thesis submitted in fulfilment of the requirements for the conferral of the degree Doctor of Philosophy, from the University of Wollongong, is wholly my own work unless otherwise referenced or acknowledged. This document has not been submitted for qualifications at any other academic institution.

Yue Hu

9th July 2019

List of Names or Abbreviations

TL	Thermoluminescence
OSL	Optically stimulated luminescence
IR	Infrared
IRSL	Infrared stimulated luminescence
SAR	Single-aliquot regenerative-dose
SGC	Standardised growth curve
nm	Nanometer (unit of the wavelength of light)
cm	Centimeter (unit of the measure of stone artefacts)
μm	microns (unit of grain size)
mW	Milli-Watt (unit of stimulation power of light)
L_x	The OSL intensity of regenerative-dose signal
L_n	The OSL intensity of natural signal
T_x	The OSL intensity of test-dose signal for regenerative doses
T_n	The OSL intensity of test-dose signal for natural doses
D_e	Equivalent dose
BIC	Bayes Information Criterion
ka	Thousand years (1 ka = 1,000 years)
Ma	Million years (1 Ma = 1,000,000 years)
MIS	Marine isotopic stage
UP	Upper Palaeolithic
MP	Middle Palaeolithic
LP	Lower Palaeolithic
ESA	Early Stone Age
MSA	Middle Stone Age
LSA	Late Stone Age
GIUR	Geometric Index of Unifacial Reduction
CV	Coefficient of variations

Table of Content

List of Figures

List of Tables

Chapter 1: Introduction

1.1 The evolution of stone techonology

Although human fossils are most important evidence in studying human dispersals and migrations, they are extremely rare and are absent or poorly preserved in most archaeological sites. In contrast, stone tools made by past humans are widespread and present in many archaeological sites. Compared to human fossils, stone artefacts are much better preserved and are continuously identified through most of the Palaeolithic site. As 'road signs' of human activities (Bar-Yosef and Belfer-Cohen, 2013), stone tools reflects the recognition, tradition, teaching and learning systems of prehistoric human, and, hence, may provide important evidence on distinguishing specific social groups that developed various technologies for making tools.

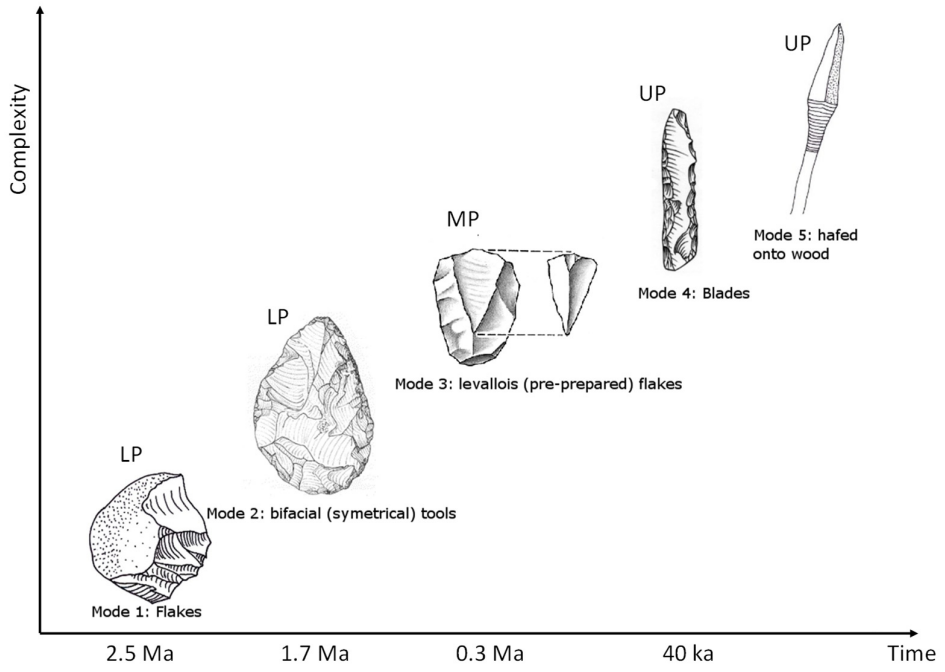

Figure 1-1: Schematic model of the evolution of stone tool technology (modified from Adam Benton, 2012. 'Human ancestors used tools earlier than previously thought?', Evoanth. Weblink: https://evoanth.wordpress.com/2012/04/17/human-ancestors-used-tools-earlier-than-previously-thought/).

Stone tools were made by at least ~3.3 million years ago (Ma) in Africa (Harmand et al., 2015). Since their first appearance, stone technology exibited multiple stages of evolution, from simple core-flake chopping tools to prepared-core techniques and then to complex microlithic component tools (Figure 1-1). The Palaeolithic period was divided into three sub-periods according to the appearance of new stone technologies. In Eurasia, these periods are the Lower Palaeolithic (LP), Middle Palaeolithic (MP) and Upper Palaeolithic (UP). In Africa, the term Stone Age is used as a synonym for the Paleolithic, i.e., Early Stone Age (ESA), Middle Stone Age (MSA) and Late Stone Age (LSA). Considering technological features in detail, the stone techniques were classified into five groups (Mode 1 to Mode 5) (Clark, 1969). Mode 1 was widely distributed in Africa and Eurasia during LP at ~2.5 Ma (Delagnes and Roche, 2005; Kimbel et al., 1996; Semaw et al., 1997; Zhu et al., 2018). It is characterized by pebble cores and flake tools. The representative industries of Mode 1 include Oldowan (e.g. Harmand et al., 2015; Leakey, 1971; Semaw et al., 1997). Mode 2, which also belongs to LP, was developed in Africa since ~1.75 Ma ago and was spread into Eurasia along with the dispersal of *Homo erectus* and derived species such as *Homo heidelbergensis* (Diez-Martín et al., 2015; Roberts et al., 1994). It is characterized by large bifacial cutting tools made from flakes and cores, such as Acheulean handaxes, cleavers, and picks (e.g. Asfaw et al., 1992; Hou et al., 2000; Kuman and Clarke, 2000). Mode 3, corresponding to MP and MSA, arouse about 300–400 thousand years ago (ka), is characterized by flake tools struck from prepared cores (Tryon, 2006; Tryon et al., 2005). In Europe and west Asia, a representative Mode 3 industry is the Mousterian culture affinitive to Neanderthal (e.g. Krause et al., 2007; Langley et al., 2008; Mellars, 1995; Moncel et al., 2011; Patrick et al., 1998; Richter et al., 2017; Shea, 2003). Mode 4 (UP and LSA, ~40 ka) are diagnosed by prismatic blade cores and blades, retouched into various specialized forms such as end-scrapers, burins, backed blades and points (Shea, 2011) as well as composite tools. In some places, Mode 4 is considered to have been made and spread by modern humans before 40 ka (e.g. Foley and Lahr, 1997; Gemble, 1986; Higham et al., 2011; Schick and Toth, 1993). Typical industries of Mode 4 include Aurignacian, Gravettian, Solutrean. Mode 5 (Later UP, Mesolithic, Epipaleolithic) is distinguished by retouched microliths and other retouched components of composite tools.

Although stone tools were found worldwide through the entire Palaeolithic, the temporal and spatial distribution is uneven. In most regions of Africa and western Eurasia, stone technology appeared to have developed continuously and abundantly from Mode 1 to Mode 5. Nevertheless, in East Asia, the evolution of stone technology is relatively ambiguous. In the 1940s, Movius (1944, 1948) suggested a geographic line (Figure 1-3), so-called ‘Movius Line’, that separated the Old World into two regions according to the ‘presence’ and ‘absence’ of Acheulean bifaces (Dennell, 2016). In particular, it was argued that east of the Movius Line (mostly in reference to East and Southeast Asia) lacks Mode 2 Acheulean bifaces and was characterized by unstandardized cores and flakes throughout the LP and MP (Movius, 1969; Movius, 1948). Such a strong technological division was subsequently abandoned since the discoveries of bifacial handaxes in East Asia (Gamble, 2001; Kei, 2012; Hou et al., 2000; Huang, 1989; Norton et al., 2006; Pei, 1958; Petraglia and Shipton, 2008; Wang, 2007; Xie, 2007; Yang et al., 2014; Yi and Clark, 1983; Zhang et al., 2010). However, the lack of archaeological evidence for prepared-core technologies (Mode 3), in particular the Levallois concept, in East Asia during the Middle

Pleistocene has led to the suggestion of a standstill technological trajectory in East Asia during this period (Gao and Norton, 2002).

1.2 Levallois concept

The Levallois concept, also known as one of prepared-core technologies, is a specific hierarchical core reduction strategy, involving multiple stages of shaping a mass of stone core in a predetermined way so that a flake of predetermined size and shape can be detached from a single preferred surface (débitage) (Figure 1-2) (Boëda, 1995). This technique is distinctive from the earlier methods of lithic reduction (e.g., Acheulean biface), and is considered as more complex than earlier methods of lithic reduction. One of the main advantages of the Levallois technique, compared to the preceding techniques, is that it provides a greater control over the size and shape of the flake products (Eren and Lycett, 2012a). It was named after the type site in the Levallois-Perret suburb of Paris, France.

The Levallois concept gradually appeared since 400–300 ka ago in Africa and Eurasia (Adler et al., 2014; Akhilesh et al., 2018; Rolland, 1995; Shimelmitz et al., 2016; Tryon et al., 2005; White and Ashton, 2003). Debates surrounding the appearance and interpretation of the Levallois concept include topics relating to hominin behavioral evolution (e.g. Kuhn and Hovers, 2013; Moncel et al., 2011; Tryon and Tyler, 2013; Wurz, 2013), human species (Hublin, 2009), social and cognition development and economics (Eren and Lycett, 2012a; Wynn and Coolidge, 2004). The graduate disappearance of Mode 2 large bifacial cutting tools and the appearance of the more complex Levallois tools, at ~300–200 ka ago (Adler et al., 2014; Fontana et al., 2013; Picin et al., 2013; Tryon and McBrearty, 2002; White and Ashton, 2003) marks the transition from the ESA (and LP) to MSA (and MP). Since this period is broadly contemporary with the appearance and spread of *Homo sapiens* in Africa, this technology has been considered to be closely associated with the evolution and spread of Neanderthals and modern humans (Foley and Lahr, 1997).

The products and the procedure of Levallois have been regarded as structured and planned by the prehistoric flintknappers. Hence this technique has been considered to reflect an important stage in hominin cognitive evolution and linguistic capacities (e.g. Eren and Lycett, 2012; Hayden, 1993; Schlanger, 2008; Wynn and Coolidge, 2004). Some scholars believe that early Levallois knappers possessed a long-term working memory that allows them to demonstrate what we recognize as ‘expert’ levels of performance (Wynn and Coolidge, 2004). Similarly, linguistic capacities are believed to be involved to maintain connections with peers or generations and to link the processes of Levallois reduction to social complexity (see Holloway, 1992; Lieberman, 1975). Furthermore, the utilization of the prepared core technique also suggests a demographic change and increased connectivity of social networks (Eren and Lycett, 2012a; Powell et al., 2009), since the productivity of predetermined procedure requires more time and energy. Consequently, this division largely depended on the development of language and social structure. This assumption emphasize on the necessity of making Levallois products.

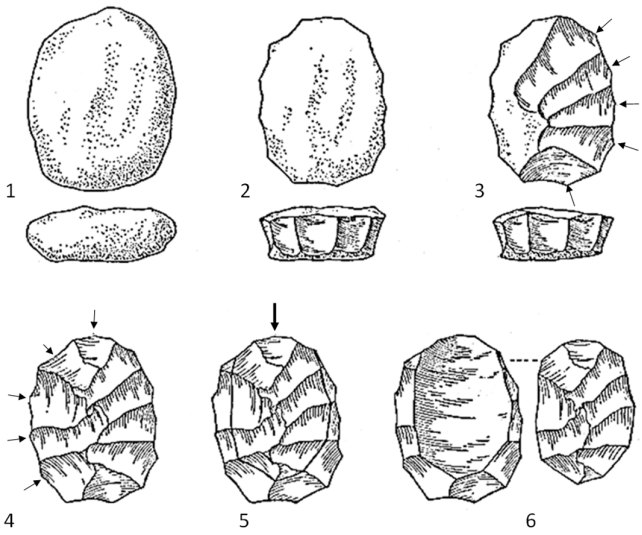

Figure 1-2: Schematic illustration of six stages (1–6) of Levallois reduction process (from Bordes, 1961a). 1, an unretouched blank; 2, removals around the periphery of the core; 3, using the previous removals as platforms to remove flakes; 4, create a convex surface; 5, removal of the central flake; 6, the predetermined products.

The advantage of Levallois concept has been discussed for decades. While some believed that 'Levallois' flake production is a wastefulness of knapping effort (Noble, 1996) and the advantage of Levallois flakes are not obvious in sharp usable edges and standardization compared with regular flakes (Sandgathe, 2004), others maintain the possibility of an 'ability to draw on a cognitive capacity of long-term working memory' (Wynn and Coolidge, 2004) and the efficiency of Levallois products can be demonstrated by using experimental methods (Brantingham and Kuhn, 2001; Lycett and Eren, 2013).

After first appearing in Africa (Tryon and McBrearty, 2002, 2006), the Levallois technique have been found in the Near East, the Indian subcontinent and Europe (e.g., Lycett, 2007a; Misra, 2001; Rolland, 1995; Shea, 2003; Tryon, 2006; Tryon and McBrearty, 2006; White et al., 2006). The Levalloiso-Mousterian "culture" is conservatively believed to have been produced by at least three hominin species: *Homo sapiens*, *Homo neanderthalensis* and late *Homo heidelbergensis* (Archaic *Homo sapiens* sensu lato) (Eren and Lycett, 2012a; Grun and Stringer, 2000; Grun et al., 2005; Hublin, 2009; Mercier et al., 1993; Schwarcz et al., 1988; Stringer, 2002; Stringer et al., 1989; Valladas et al., 1988; Vandermeersch, 1982). In contrast, Levallois technologies are scarce in eastern Asia (Gao and Norton, 2002; Schick, 1994; Schick, 1998; Schick and Zhuan, 1993).

Figure 1-3 summarises the distribution of sites in Africa and Eurasia dated to Late Middle Pleistocene period (from MIS 9 to 3) where Levallois technology was discovered. It can be seen that, while Levallois sites have become ubiquitous in west Eurasia and Africa prior to MIS 7 (~200 ka), evidence of this technology in East Asia remains scarce. The absence of Levallois technology in East Asia also reinforces the division between East and West. Until recently, the earliest known evidence was from a few sites

dated back to ~30–40 ka ago. One of these is the Shuidonggou site, a Late Upper Pleistocene site in north China, which preliminarily yielded Initial Upper Palaeolithic blade-rich assemblages and was reported as containing Levallois complex (Boëda et al., 2013). In addition to Shuidonggou, Jinsitai also provides evidence of Levallois reduction in northern China (Wang, 2010), suggesting a geographic extension between Western and Eastern Asia via the Altai and Mongolia (Boëda et al., 2013).

Given this uneven distribution of the Levallois sites, it has been believed that this technology is largely absent in East Asia during most of the Late Middle Pleistocene period, so a 'Movius Line sensu lato' (Norton and Bae, 2008; Norton et al., 2006) appears to have remained supported (Lycett, 2007b; Schick, 1994; Schick and Zhuan, 1993). The uneven global distribution has also made it difficult to determine how the Levallois technology originated, and its relationship to later technologies and human evolution. Although it is becoming a consensus that the Levallois have much deeper chronological roots in Acheulean or Mode 2 assemblages across the Old World from the Early Pleistocene onwards, the Levallois concept is probably originated in multiple regional (Adler et al., 2014; Debono and Goren-Inbar, 2001; White and Ashton, 2003). For instance, early Levallois technology found with bifaces in the Southern Caucasus suggests Levallois technology evolved out of the existing local Acheulian (or Mode II) technological systems (Adler et al., 2014). This supports a hypothesis of isolated technological convergence (Tryon et al., 2005), rather than a single-origin and dispersal model. The recent discovery of Levallois technology in India around 385–172 ka ago (Akhilesh et al., 2018) also raised the need to re-evaluate the relationship between the origins of Middle Palaeolithic culture in South Asia and the dispersal of modern humans.

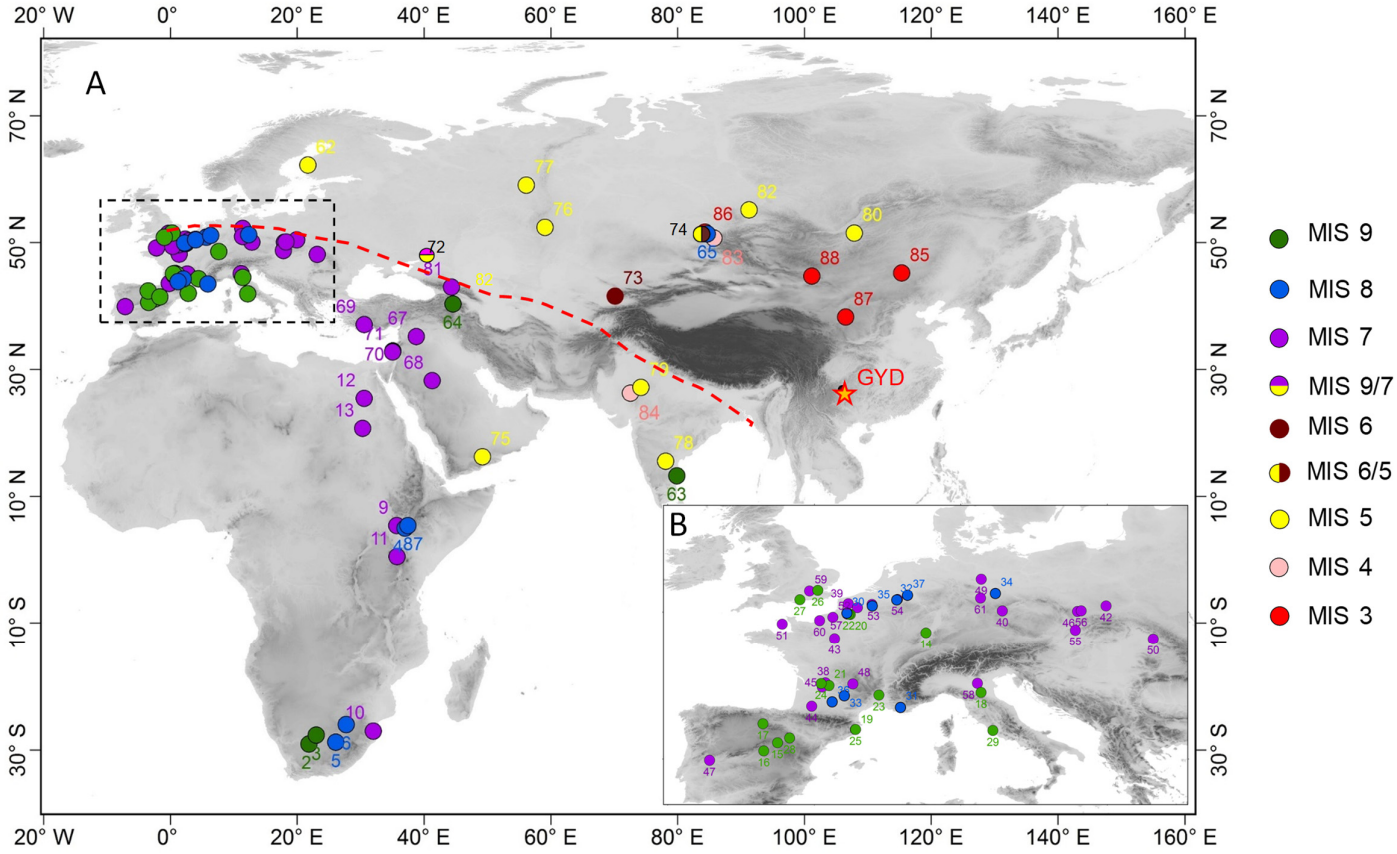

Figure 1-3: Distribution of Levallois technology during Late Middle Pleistocene (from MIS 9 to 3) in Africa and Eurasia. The dashed red line shows the 'Movius Line'. The rectangular in A is shown in an enlarged scale in B. Detailed information on the sites are provided in Table 1-1. The Marine Isotope Stage (MIS) corresponding to the chronology of individual sites are indicated by different colours of the symbols. Note that there are a large number of sites younger than MIS 7 in Europe and Africa, but they are not shown here.

Table 1-1. Summary of the sites shown in Figure 1-3, together with their corresponding ages and dating methods used. For some sites, precise numerical ages are not available because absolute dating methods were not applied and their ages were roughly estimated by stratigraphic correlation only, so only MIS stages were provided for these sites.

ID	Site	Country	Age (ka)	MIS stage	Dating method	Reference
1	Guanyindong	China		6–4	OSL/U-series	This study
	AFRICA					
2	Bundu farm	South Africa	190–340	9	ESR	(Herries, 2011)
3	Kathu Pan	South Africa	291 ± 45	9	OSL/ESR/U-seires	(Porat et al., 2010)
4	Kibish formation	Ethiopia	~195	7	Ar/Ar	(Brown and Fuller, 2008; Tryon and Faith, 2013)
5	ETH72-8B & Kulkuletti (Gademotta formation)	Ethiopia	~280	8	Ar/Ar	(Tryon and Faith, 2013)
6	Florisbed	South Africa	268 ± 26	8	ESR, OSL	(Grün et al., 1996)
7	Sterkfontein cave	South Africa	252 ± 42	8	ESR/stratigraphy	(Herries, 2011)
8	Gademotta	Ethiopia	180–280	8	Ar/Ar	(Douze and Delagnes, 2016; Herries, 2011)
9	Kulkuletti	Ethiopia	~280 ± 8	8	Ar/Ar	(Douze and Delagnes, 2016; Herries, 2011)
10	Border cave	South Africa	217–238	7	ESR	(Herries, 2011)
11	Kapthurin formation	Kenya	200–250	7	Tephra	(Tryon, 2006; Tryon and Faith, 2013)
12	Kharga oasis & site REF-4	Egypt	220 ± 20	7	U-series	(Hawkins et al., 2001)
13	Sai island	Sudan	152–223	7	OSL	(Van Peer et al., 2003)
	EUROPE					
14	Achenheim	France	258 ± 23	9	stratigraphy	(Buraczynski and Butrym, 1987)
15	Ambrona	Spain	336 ± 36	9	ESR / U-series	(Falguères et al., 2006)
16	Aridos 1	Spain		9	stratigraphy	(Santonja and Villa, 1990)
17	Atapuerca	Spain	345 ± 26	9	ESR / U-series	(Falguères et al., 1999)
18	Dall'Olio Cave	Italy		9	stratigraphy	(Fontana et al., 2013)
19	Domeny	Spain	> 317 ± 49	9	Ar/Ar, stratigraphy	(Carbonell and Rodríguez, 2008)
20	Gentelles base	France		9	stratigraphy	(Fontana et al., 2013)
21	La Micoque	France	288–350	9	ESR/U-series	(Falguères et al., 1997)
22	Cagny Lépinette	France		9	stratigraphy	(Tuffreau, 2001)
23	Orgnac 3	France	> 303	9	Ar/Ar, U-Th	(Michel et al., 2013)
24	Petit bost	France	325 ± 30	9	TL	(Jaubert and Bordes, 2008)
25	Puig den Roca	Spain	< 317 ± 49	9	Ar/Ar, stratigraphy	(Carbonell and Rodríguez, 2008)
26	Purfleet	UK	~ 324	9	TL, stratigraphy	(White and Ashton, 2003)
27	Solent River	UK		9	stratigraphy	(Westaway et al., 2006)
28	Torralba	Spain	> 243 ± 18	9	U-series, stratigraphy	(Santonja and Villa, 2006)
29	Torre in Pietra	Italy		9	stratigraphy	(Grimaldi, 1998)
30	Argoeuves	France		8	stratigraphy	(Tuffreau, 1982)
31	Baume Bonne	France		8	stratigraphy	(Gagnepain and Gaillard, 2003)
32	Kesselt -Op de Schanz	Belgium		8	stratigraphy	(Michel et al., 2013)
33	Les Bossés	France	274 ± 12	8	TL	(Jarry et al., 2007)
34	Markkleeberg	Germany		8	stratigraphy	(Van Baelen et al., 2007)
35	Mesvin	Belgium	283 ± 30	8	U-Th	(Ryssaert, 2006a)

36	Raspide 2	France		8	stratigraphy	(Colonge et al., 2010)
37	Rheindahlen	Germany		8	stratigraphy	(Thissen, 2006)
38	Abri Vaufrey	France	208 ± 8	7	U-series	(Blackwell and Schwarcz, 1988)
39	Bapaume les (Pas-De-Calais)	France	~195	7	IRSL	(Balescu and Tuffreau, 2004)
40	Bečov I	Czech Republic		7	stratigraphy	(Wisniewski and Fridrich, 2010)
41	Biache-Saint-Vaast	France	230 ± 18	7	ESR/U-series/TL	(Bahain, 2007)
42	Biśnik Cave	Poland	230 ± 51	7	TL	(Cyrek et al., 2014)
43	Bonneval	France	240	7	TT-OSL	(Sun et al., 2010)
44	Campsas	France		7	stratigraphy	(Jaubert and Servelle, 1996)
45	Cantalouette	Ukraine	223 ± 20	7	TL/stratigraphy	(Brenet et al., 2008)
46	Dzierżysław	Poland		7	stratigraphy	(Wiśniewski, 2014)
47	Galeria Pesada	Portugal	241 ± 22	7	ESR/U-series	(Marks et al., 2002)
48	Gran Rois	France		7	stratigraphy	(Balescu and Tuffreau, 2004)
49	Hundisburg	Germany		7	stratigraphy	(Adler et al., 2014)
50	Korolevo	Ukraine	220 ± 35	7	OSL	(Haesaerts and Koulakovskaya, 2006)
51	La Cotte de St.Brelade	UK	238 ± 35	7	TL	(Callow and Cornford, 1986)
52	Le Pucheuil	France		7	stratigraphy	(Delagnes and Ropars, 1996)
53	Le Rissori(MSJ)	Belgium		7	stratigraphy	(Adam, 2002)
54	Maastricht Belvédère	Netherlands	258 ± 19	7	TL/ESR	(Vandenberghe et al., 1993)
55	Nové Mesto nad Váhom	Slovakia		7	stratigraphy	(Wiśniewski, 2014)
56	Raciborz Studienna 2	Poland		7	stratigraphy	(Wiśniewski, 2014)
57	Salouël	France	> 200 ± 57	7	ESR/U-series	(Ameloot-van der Heijden et al., 1996)
58	San Bernardino	Italy	184 ± 6	7	ESR	(Picin et al., 2013)
59	Thames valley	UK		7	stratigraphy	(Scott et al., 2011)
60	Therdonne	France	178 ± 11	7	TL/stratigraphy	(Locht et al., 2010)
61	Weimar-Ehringsdorf	Germany	230	7	U-Th	(Mallick and Frank, 2002)
62	Susiluola Cave	Finland	> 100	5	OSL, TL, stratigraphy	(Rolland, 2010)
	ASIA					
63	Attirampakkam	India	385 ± 64	9	OSL	(Akhilesh et al., 2018)
64	Nor Geghi	Armenia	335–325	9	Ar/Ar, stratigraphy	(Adler et al., 2014)
65	Denisova Cave	Russia	220–280	8	TL	(Derevianko et al., 2003)
66	Hayonim	Israel	~ 220	7	TL/ESR	(Mercier et al., 2007)
67	Hummal	Syria	150–220	7	TL	(Tensorer et al., 2007)
68	Jebel Qattar JQ-1	Saudi Arabia	211 ± 16	7	OSL	(Petraglia et al., 2012)
69	Karain cave	Turkey	250–200	7	TL/ESR	(Otte et al., 1998)
70	Misliya cave	Israel	166–212	7	TL	(Valladas et al., 2013)
71	Tabun(Mount Carmel)	Israel	256 ± 26	7	TL/ESR	(Mercier and Valladas, 2003)
72	Mikhailovskoe	Russia		9–7	stratigraphy	(Hoffecker, 2003)
73	Obi-Rakhmat Grotto	Uzbekistan	55–73	6	ESR, OSL	(Krivoshapkin et al., 2010)
74	Ust-Karakol 1	Russia	133 ± 33	6–5	TL	(Derevianko et al., 2005; Slavinskiy and Rybin, 2015)
75	Aybut al Auwal	Oman	106	5	OSL	(Rose et al., 2011)
76	Bogdanovka	Russia		5	stratigraphy	(Shirokov et al., 2011)
77	Garchi I	Russia	~115	5	OSL	(Pavlov et al., 2004; Svendsen et al., 2010)
78	Jwalapuram (JPW 3a)	India	74–77	5	OSL	(Petraglia et al., 2007)

79	Katoati	India	50–100 or older	5	OSL	(Blinkhorn et al., 2013)
80	Khotyk	Russia		5	TL	(Rolland, 2010)
81	Myshtulagty Lagat	Russia	70–250	5–7	Ar/Ar, stratigraphy	(Hidjrati et al., 2003)
82	Ust'-Izhul	Russia	~125	5	IRSL	(Chlachula et al., 2003)
83	Kara-Bom	Russia	~62	4	ESR	(Derevianko et al., 2005; Vasil'ev et al., 2002)
84	Shergarh Tri-Junction	India	60–43	4	OSL	(Andrews et al., 1998; Blinkhorn, 2014)
85	Jinsitai	China	50–40	3	C-14	(Wang et al., 2010; Li et al., 2018)
86	Okladnikov Cave	Russia	45–33	3	U-series, C-14	(Krause et al., 2007; Vasil'ev et al., 2002)
87	Shuidonggou Locality I	China	38–34	3	C-14	(Boëda et al., 2013; Li et al., 2013a; Liu et al., 2009)
88	Tsagaan Agui	Mongolia	52–23	3	TL	(Derevianko et al., 2000)

1.3 Characterisitics of Middle Paleolithic assemblages

Generally, the MP in west Eurasia and Africa began at ~300 ka (Delagnes et al., 2007; Richter, 2010) during which small flake tools started overwhelming the large core tools (Dibble et al., 2006; Kuhn, 2013). The small flake tools, resulted from a more diverse flake-production system, include multiple variants of Levallois concept (Boëda, 1994; Boëda, 1995), discoid production, blade production, the "Quina" method (Bar-Yosef and Kuhn, 1999; Boëda, 1991; Bourguignon, 1996; Boëda, 1990; Hiscock et al., 2009; Peresani, 2003), and a range of less commonly documented techniques (Faivre, 2012; Geneste Jean-Michel, 1996; Slimak, 1999). Corresponding to the varieties of technological system, were changes in mobility strategies, cognitive, social and adaptive changes (Gamble, 1999), such as the use of fire (Berna and Goldberg, 2007; Goldberg et al., 2012), hafting (Boëda et al., 1996; Cârciumaru et al., 2012; Rots, 2009), use of pigment (D'Errico, 2008; Soressi and D'Errico, 2007) and demographic growth, were developed in the expanded hunting territories (Kuhn, 2013; Shennan, 2001).

Form an anthropological perspective, early modern humans evolved in Africa (Hublin et al., 2017; McDougall et al., 2005; Richter et al., 2017; White et al., 2003) and Neanderthal replaced (or probably evolved from) *Homo heidelbergensis* in West Eurasia (Arsuaga et al., 2014; Hublin, 2009). Around 120 ka, when the 'classic' MP techno-complexes rise, both Neanderthal in Europe and western Asian and early modern humans in Africa created a large range of variable forms in core reduction and tool manufacture. One of the key features of lithic production shared by the MP assemblage in West is the diversity of flake production (Delagnes and Meignen, 2006; Kuhn, 2013). These regional developments in lithic technologies can be observed over the Old World. Therefore, from the human evolution and migration perspective, the MP was a key period in understanding the timing and nature of the dispersal of archaic and modern humans out of Africa and into Asia, and their interactions with local hominin populations (Bae et al., 2017). The eastern hemisphere is especially important for answering these questions because of a long Pleistocene record of multiple hominin species, including *Homo erectus*, Denisovans, *Homo floresiensis* and *Homo sapiens*, with *Homo sapiens* potentially deriving from several dispersal events (Martinón-Torres et al., 2017).

1.3.1 MP in western Eurasia

This area covers a large landscape including most part of Europe, the Levant and western Asia. During MP, standardized flake productions were largely based on débitage, generally but not always, involving the Levallois technique (Wil Roebroeks, 1999). However, the Levallois concept is the most abundant and widespread production system except regions with low quality raw materials (Delagnes and Meignen, 2006). Considerable variability of technologies can be found in Europe, such as four types of Mousterian with different traditions in the later part of MP (Bordes, 1961a), namely, Typical, Quina, Denticulates and Mousterian of Acheulean tradition. Moreover, blade forms are present at a small number of sites (e.g. Conard, 1990; Révillion, 1995; Révillion and Tuffreau, 1994). Even within the Levallois technique, the sequence of preferential and recurrent methods can be found. These all indicate a more regional and significant variability during MP than the period preceeding or afterward.

Many well-dated MP sites in Europe are known to date to marine isotopic stage (MIS) 7 (~200 ka), such as Ehringsdorf in Germany, Maastricht-Belvédère in the Netherlands and Biache-Samt-Vaast in northern France (Roebroeks, 1999). This pattern continues through MIS 6 and 5, after which Mousterian sites appear in abundance, especially in France, such as Grotte Vaufrey (MIS 6; typical Mousterian sites; Geneste, 1988a), Combe-Grenal (MIS3; Quina Mousterian; Turq, 2000); La Borde (Denticular Mousterian; >MIS 5b; Jaubert et al., 1990); Coursac (MTA; MIS 5, Geneste, 1985) and rest of Europe such as Lynford Quarry (Boismier et al., 2003), Vindija Cave (Devièse et al., 2017), Zafarraya (Hublin et al., 1995), Pech de l'Aze I (Dibble et al., 2018). This emergence of Mousterian assemblages like these may represent the gradual replacement of Neanderthals over earlier *Homo* species.

Generally, the MP industries of Eastern Europe, Levantine, Central Asia and North African MP share similar tool types and techniques (Shea, 2003). Also, compared with East Eurasia, west Asia, such as Levant and central Asia, have similar trajectories of stone technology as in Europe. The early modern human and Neanderthal both occupied this area and are responsible for Mousterian stone tools during the timespan of the MP. However, whether it is a gradual or sudden replacement, or short or long co-existence of early modern humans and Neanderthals remains a complicated issue (Fu et al., 2015; Klein, 1999; Shea, 2003). There are hundreds of MP sites that were discovered in this area such as Tabun (Jelinek, 1982; Shimelmitz et al., 2016), Qesem (Barkai et al., 2003; Shimelmitz et al., 2011), Hayonim (Meignen, 2002; Mercier et al., 2007), Kebara (Bar-Yosef et al., 1992), Qafzeh Cave (Hovers, 2009; Schwarcz et al., 1988) and Umm el Tlel (Syria) (Boëda et al., 1996; Shea, 2003), etc. The principle MP industry in Levant is called 'Levantine -Mousterian' which is after the 'Acheulo-Yabrudian" of Lower Palaeolithic, and then transited into "Ahmarian" industry after ~ 40 ka (Gilead, 1991; Kadowaki et al., 2015). One of the most distinguished attributes of Levantine-Mousterian is the production of triangular and sub-triangular flakes that are obtained by recurrent Levallois method and various standardized Levallois points. Unlike Europe and East Asia, the Levant provided a relative stable climate and food resources that enabled the sustained development of lithic industries (Enzel and Bar-Yosef, 2017; Farrand, 1979).

Overall, the MP of Europe and the east of Mediterranean are dominated by Mousterian cultural where the Levallois technique and other standardized flake production systems were widely distributed. The tool

makers are mainly early modern humans and Neanderthals. These attributes differ from East Asia where the existing evidence shows the overwhelming lithic industries are flake-based tools and flakes that achieved by non-prepared core technologies.

1.3.2 MSA in Africa

Africa is a continent that human species, lithic technologies, and other social behaviors have been continuously and constantly evolved (Wood and Richmond, 2000). The earliest appearance of Mode 1 technologies (Harmand et al., 2015; Semaw et al., 1997; Semaw S, 2003), Acheulean handaxe (Mode 2) production (Asfaw et al., 1992), and the earliest evidence of the Levallois (Mode 3) technique (Tryon, 2006; Tryon and McBrearty, 2002; Tryon et al., 2005) were all found in Africa. The MSA in Africa (McBrearty and Brooks, 2000) is associated with both anatomically modern humans (*Homo sapiens*) and archaic *Homo sapiens* (Clark et al., 2003; Schlebusch et al., 2017).

Numerous sites associated with MSA complexes have been found in Africa. In northern Africa, especially the area close to Mediterranean, Levallois tools were found in some industries such like, Jebel Irhoud , El-Azrag (Pasty, 1997) and Haua Fteah (Douka et al., 2014). The pattern of technological behaviors and *Homo* species from this region are analogous to those found in Europe and Levant. In eastern Africa, abundant sites associated with fossils of *Homo sapiens* were found. The method and predetermined productions of Levallois concept are highly variable (Tryon and Tyler, 2013), ranging from the earlier larger preferential blanks to later smaller Levallois blanks. One of the earliest Levallois concept products are found in Kapthurin formation, which also provides the best stratigraphic sequence of MSA assemblages (Tryon, 2006; Tryon et al., 2005). Early (around MIS 7) Levallois stone tools are also found in sites such like Sai Island 8-B-11 (Van Peer et al., 2003), Omo-Kibish, KHS of Kibish Formation (Tryon and Tyler, 2013), ETH72-7B, ETH72-1 of Gademotta Formation (Tryon and Tyler, 2013). Most sites here are well-dated, yielding most reliable chronology, for example, the oldest (>276 ka) MSA site was discovered at Gademotta, in Ethiopia (Morgan and Renne, 2008; Tryon and Tyler, 2013). Compared with other regions in Africa, MSA sites found in Central Africa are less recorded, however, they reflects similar technological behaviors to eastern Africa. Most of MSA sites in the southern Africa are cave sites, such like Blombos Cave (Jacobs et al., 2006b), Sibudu Cave (Wadley and Jacobs, 2004), Howieson's Poort (Jacobs et al., 2008). Some of those sites are characterized by finely shaped flake tools with bifacial points, hafting weapons and blade products and various modern human behaviors, including early evidence for symbols and personal ornaments (Mellars, 2006b). However, these markers are discontinuous and vanished between ~75 and 60 ka till the LSA at ~40 ka when they reappeared and became more common (Ambrose, 1998; Henshilwood et al., 2002; Powell et al., 2009; Zilhão, 2007).

In summary, Africa provides the most complete and almost the oldest MP traits as well as a lengthy and complex evolution trajectory of human species. Like in Eurasia, the lithic industries demonstrated high variation. Geographically, the north parts of continent, where a different climate exists (Castañeda et al., 2009; deMenocal, 2004; Ziegler et al., 2013), had Mousterian culture features in MSA. The east parts yielded the richest and oldest sites that contain MSA patterns such as Levallois, blades, and discoid

pieces. These technologies were considered to have evolved from pre-existing Acheulean industries in ESA. Early blade techniques, for example, appeared in Acheulean sites in East Africa (Johnson and McBrearty, 2010). For the Levallois technique, it was believed to be developed from multiple independent pathways (Tryon et al., 2005; Tryon and Tyler, 2013; White et al., 2011) in Acheulian sites from both Africa and Eurasia. In the later part of MSA, this region displayed a more complex pattern with the emergence of modern human behaviors, similar to other places of the Old World.

1.3.3 North Asia and South Asia

In north Asia, many sites have been found with MP and UP complexes. In the Altai region, most sites can be designed to MP period. Well-known sites from this region include cave sites, such as Ust Kanskaya, Denisova, Strashnaya, Okladnikov, and open-air sites, such as Kara-Bom, Ust-Karakol 1 and 2, and Tumechin 1 and 2 (Derevianko et al., 2005; Jacobs et al., 2019). Three MP traditions were observed, which are Denisovan, Kara-Bom and Sibiryachikha (Krivoshapkin et al., 2018). Levallois industries were well demonstrated in Denisova cave at 300–69 ka (Derevianko, 2014; Krivoshapkin et al., 2018) and Kara-Bom at 60–40 ka (Derevianko et al., 2005; Krivoshapkin et al., 2018). The stone tool makers of these industries are likely to be either Denisovan or Neanderthal or both, which were living in this area with genetic flow between these two groups (Slon et al., 2017; Slon et al., 2018).

During the Lower Palaeolithic period, the industries of the Indian subcontinent were generally divided into either the Acheulian (biface) or the Soanian (non-biface) traditions (Lycett, 2007a; Pappu et al., 2011). Acheulean assemblages were abundantly found in various palaeoenvironmental and climatic contexts (Mishra et al., 1995; Misra, 2001) and then followed by the earliest emergence of Levallois concept in Attirampakkam site dated to 385–172 ka (Akhilesh et al., 2018). The rise of the MP throughout the Indian subcontinent was indicated by the gradual disuse of bifaces, the predominance of small tools, the appearance of distinctive and diverse Levallois flake and point strategies, and a blade component (Akhilesh et al., 2018). Also in Pakistan, the Levallois concept is found at Rohri Hills, Ongar and Karachi Gulf (Biagi, 2006).

1.4 Middle Paleolithic in East Asia

The characteristics and development of Palaeolithic in China (and more broadly in East Asia) has been hotly debated (e.g. Boriskovsky, 1978; Gao, 1999; Gao and Norton, 2002; Huang et al., 2009; Kei, 2012; Movius, 1948; Norton and Bae, 2008; Wang, 2017). Conventionally, the Chinese Palaeolithic followed a similar approach used in western Eurasia, namely by dividing the Palaeolithic period into three stages: Lower, Middle and Upper Palaeolithic (see reviews in Gao, 1999; Huang, 2000). A key issue in debates in East Asian Palaeolithic archaeology is the existence of the MP in this region. As mentioned above, while distinctive lithic technologies (e.g., Levallois prepared cores) can be found in many MP sites in western Eurasia, sites in East Asia of the same period generally lack distinctive Mode 3 technologies. As a consequence, the MP in China has often been defined on the basis of chronology and by association with the remains of archaic *Homo sapiens* (Lin, 1996), rather than on the characteristics of stone

technology. In particular, sites dated to the late Middle Pleistocene to early Upper Pleistocene (140−30 ka) and those associated with archaic *Homo sapiens* remains have been designated as MP (Gao and Norton, 2002). Most sites described as MP were found in North China and most parts of South China. Some especially representative sites in China include Zhoukoudian localities 15 and 4, Xujiayao, Dingcun, Dali and Linjing (Athreya and Wu, 2017; Gao and Norton, 2002; Jia et al., 1979; Li et al., 2017c, 2019; Li and Lotter, 2019; Pei, 1939, 1958; Wang, 2000).

Technological evolution in East Asia prior to the appearance of blade and microblade technologies at ~40 ka has been regarded as slow and conservative (Bar-Yosef and Wang, 2012; J. Norton et al., 2009; Lin, 1996; Schick, 1994; Schick and Zhuan, 1993; Zhang, 1985, 1990). Based on the analysis of four criteria—raw material procurement, core reduction, retouch and technology—from Late Middle Pleistocene archaeological sites of China, Gao and colleagues (Gao, 1999; Gao and Norton, 2002; Li, 2014) observed that the raw materials of most of their studied sites are poor-quality local sources, the tools were either made on pebbles or directly-used flakes without any retouch, flaking is opportunistic and simple, and modification is casual with the absence of clear temporal trends (Gao, 2013). Based on these, they suggested that the European-inspired 3-stages division should be abandoned in China. Instead, they suggest a two-stage model (Early and Late Palaeolithic) with the early-to-late transition defined by the emergence of blade and microblade technologies at ~40 ka (Gao and Norton, 2002). However, this two-stage model has been challenged by some other studies (e.g. Huang, 2000; Huang et al., 2009; Kei, 2012). It is suggested that some technologies once viewed as 'simple' had changed gradually, and some of the technologies from upper Palaeolithic industries have deep roots from Lower and Middle Palaeolithic (Du, 2006; Li et al., 2019; Li and Lotter, 2019; Li, 1993; Wang, 2005).

Another problem with the 'Middle Paleolithic' in East Asia is that most of these sites described as MP were excavated decades ago and, hence, lack reliable chronologies from absolute dating methods, and lack detailed and systematic studies of the lithic assemblages. For example, Guo et al. (2016) applied newly developed luminescence dating technique to three MP sites from the Nihewan Basin. Similar to many other MP sites in China, these sites were previously assigned to MP (> 140 ka) based on stratigraphic correlation. However, Guo et al. (2016) found that two of the sites were actually older than 250 ka, and only one of them (~86 ka) is correctly assigned. Their study highlights the need to reassess the putative MP sites in East Asia.

Apart from this chronological issue, recent studies re-analysing stone artefacts from several sites in China have provided new insights in to the MP lithic characteristics in this region. After reexamination on the stone artefacts from Dali (dated to 300-247 ka), Li and Lotter (2019) found that core reduction strategies are mostly expedient, dominated by simple unifacial unidirectional flaking. However, some formal tools at Dali demonstrated comparatively complex technologies, which are diverse in type and reflect a relatively standardized production strategy. Furthermore, several 'atypical' Levallois cores associated with varied types and standard tools are identified in Linjing (~125–90 ka), a site from where two archaic human crania that show a mosaic of features of archaic East Asian humans, Neanderthals and early modern humans were found (Li et al., 2019; Li et al., 2017c). Furthermore, elements of predetermined technologies such like predetermined core shapes and proto-laminar cores, were reported

in some Early Pleistocene sites such like Donggutuo (~1.1 Ma) (Wang et al., 2005) from Nihewan basin (Hou, 2003, 2004), although this is still controversial (Keates, 2010). In southwest China, Levallois products in the Panxian Dadong cave were also reported (Huang et al., 1997; Otte, 2017; Zhang et al., 2015).

1.5 Research questions and study sites

1.5.1 Research questions

As mentioned above, compared to west Eurasia and Africa, the development and characteristics of the East Asia Palaeolithic remains ambiguous and have been hotly disputed for decades (An, 1965; Guo et al., 2017; Li et al., 2013a; Madsen et al., 2001; Pei et al., 2012; Teihard de Chardin TD, 1924). If the claimed absence of complex MP stone tool technology in East Asia is true, then one may argue that hominin populations in this region were probably culturally and genetically isolated during the Early and Middle Pleistocene. However, recent studies have suggested a continuous genetic flow in East Asia during Late Middle Pleistocene. For example, the ~100 kyr Xuchang crania with its mosaic of Eurasian and Neanderthal features indicate population interactions across Eurasia (Li et al., 2017b). A Middle Pleistocene demographic event is also indicated by DNA from the Late Pleistocene Tianyuan individual that indicates a divergence of Asians from Europeans that had occurred prior to 40 kyr (Fu et al., 2013). The recent discovery of a ~170 ka Denisovan Mandible from the northeastern Tibet Plateau (Chen et al., 2019) suggested that the Denisovans might have been widely distributed in East Asia. The study of the Denisova Cave in Siberia indicates that Denisovans might have started making MP Mode 3 assemblages as early as ~300 ka ago (Jacobs et al., 2019). This raises the question of why the Denisovans abandoned this complex technology when they moved southward to East Asia.

Secondly, the lack of Mode 3 technology in East Asia has been explained as a result of the lack of a strong ancestral Acheulean (Mode 2) tradition in this region (Lycett, 2007b). This is based on the assumption that Acheulian bifacial technologies and Levallois technologies are homologous, sharing a common technological ancestry. However, the emerging evidence of Mode II bifacial tools from archaeological sites in East and Southeast Asia (Brumm and Moore, 2012; Hou et al., 2000; Li et al., 2016b; Norton et al., 2006; Yang et al., 2017) raised questions about why the East Asian Acheulean technology did not result in the development of prepared-core Mode 3 technology.

Thirdly, as mentioned above, most of the assigned MP sites in East Asia have been poorly dated. This is mainly because that most of the sites are open-air sites and were excavated decades ago. The chronology of these sites has been deduced from stratigraphic correlations between sites, which is unreliable and has a large uncertainty. As a result, many of these assemblages may likely to have been incorrectly assigned to Palaeolithic stages. Absolute dating of these sites has been challenging because of a lack of reliable dating techniques, e.g., their ages are beyond the datable range of radiocarbon (< 50 ka). It is not until recently that the development of new generation luminescence dating techniques that allows dating of

these Middle to Late Middle Pleistocene sites possible (Roberts et al., 2015; Wintle, 2008). The question is: what ages do new luminescence methods indicate for putative MP sites in China?

Furthermore, many of the assemblages claimed as MP in East Asia have been studied decades ago, when a systematic and detailed lithic analysis methodology was not available. In the last decade, the spatial and temporal diversities of MP in Eurasian Mousterian complexes have been studied in great detail (Delagnes and Meignen, 2006; Guibert et al., 2008; Monnier and Missal, 2014; Morin et al., 2014; Shea, 2014; Thiébaut et al., 2014). Many interpretative models and methodologies have been introduced to measure and explain variation (Boëda et al., 1990; Geneste, 1985; Pigeot, 1991; Schlanger, 1996; Tixier et al., 1980), economic contexts of land use, subsistence, and raw material management, environmental factors and mobility (Bamforth, 1991; Dibble, 1987; Kuhn, 1995; Nelson, 1991). It is necessary to improve our understanding of technological behaviours of the MP in East Asia through the application of these new approaches to East Asian assemblages.

Finally, although firm evidence of Levallois technology by 30–40 ka has been found in North China, the presence of Levallois complex in south China is ambiguous. So far the only proposed evidence has been found at the Panxiandadong, a Middle Pleistocene site, which is claimed to have yielded Levallois-like products (Huang et al., 1997, 2009; but see Gao, 2013 for a different view), and needs further verification. For this reason, more studies on the lithic assemblages from the other sites from this region are needed to answer the question whether Levallois technique is present in South China or not. If yes, what is the difference between this technique with those found in Africa and Europe and what is their relationship? Were they developed independently or transmitted from the other regions? In order to answer these questions, we need to first investigate the characteristics of the lithic technology in South China and its relationship to the other regions (including north China, south Asia and west Asia).

1.5.2 Study region and sites

To address the above research questions, in this thesis I focus on two cave sites from Southwest China, one is the Guanyindong Cave in the Guizhou Province and the other is the Tianhuadong Cave in the Yunnan Province (Figure 1-4).

A number of sites containing human fossils have been discovered in Southeast Asia (SEA), suggesting a diversity of hominin taxa in this region. Recent studies corroborated this diversity and its potential for discovering new hominin taxa in southern China and Southeast Asia. For example, the presence of *Homo floresiensis* skeletal remains at Liang Bua, Flores, Indonesia (e.g., Morwood et al., 2004) and the more recently discovered *Homo luzonensis* from Callao Cave, Luzon, Philippines (Détroit et al., 2019) suggests the possibility of additional *Homo* species in SEA, probably concurrent with *Homo sapiens* (Sutikna et al., 2016), which reflects the importance role that Southeast Asia play in the evolution of the genus Homoas well. The distribution of Denisovan DNA also adds to the possibility of novel hominin species in SEA (e.g., Krause et al., 2010; Reich et al., 2010). More recently, an important find at Fuyan Cave in Daoxian, southern China is the *Homo sapiens* teeth dated to 80–120 ka years ago (Liu et al., 2015). This compelling evidence suggests a successful migration of *Homo sapiens* out of Africa well before the conventionally accepted time of 50–60 ka years ago (Mellars, 2006a). Further evidence are

presented from the ~65 ka Palaeolithic site of Madjedbebe in north Australia (Clarkson et al., 2017) and the 73–63 ka modern human fossils site of Lida Ayer in Sumatra (Westaway et al., 2017). Lying on the southern migrating route of modern human (Abdulla et al., 2009), southwest China is a critical area in studying dispersal of hominin and modern human from west to east (and probably from north to the south as well). It may provide key evidence in the expansion and interaction of hominin or modern human in northeast of Movius line (Movius, 1948) from the Middle Pleistocene through to the Late Pleistocene.

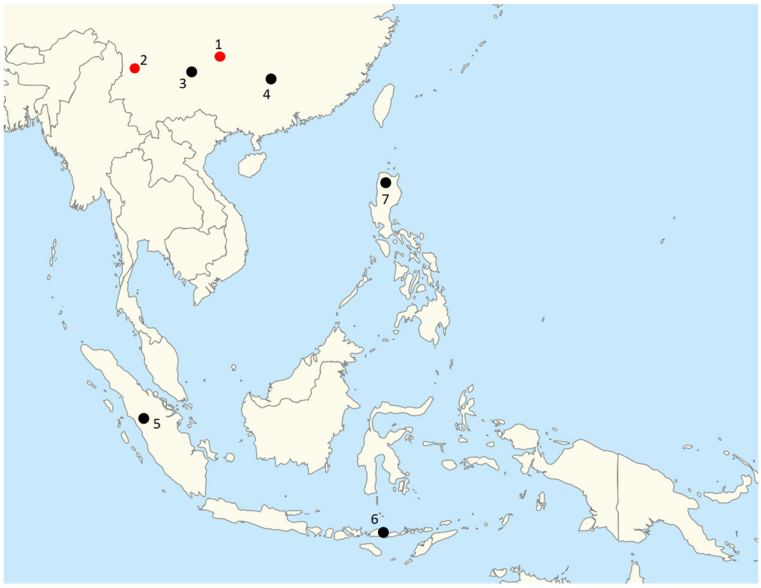

Figure 1-4: Map of Southeast Asia showing my study sites (Guanyindong and Tianhuadong) and other key sites mentioned in this section. 1, Guanyindong Cave; 2, Tianhuadong Cave; 3, Panxiandadong Cave; 4, Fuyan Cave; 5, Lida Ayer; 6, Liang Bua; 7, Callao Cave.

Unfortunately, with respect to lithic assemblages, Palaeolithic sites with abundant stone artefacts in South China are scarce compared to Europe and Africa, and even north China. Furthermore, most of these South China sites have been poorly dated or even not dated with radiometric methods at all (Dennell, 2009; Guo et al., 2016). Guanyindong site is one of the few sites in this region that have abundant stone artefacts (over 3000 artefacts were excavated). It is important in terms of lithic assemblages which shares the features with Eurasia and also bears distinctive local characters since its location lies in southwest China. Previous work at Guanyindong suggests that its lithic assemblage represents a different character from those found in north China (Li and Wen, 1986) and Europe (Li et al., 2009b; Pei, 1965). However, my initial exploration of the lithic assemblage in Guanyindong suggests that the Levallois technique may be present in this site. Therefore, a detailed lithic analysis of the assemblage from Guanyindong forms one of the core components of this thesis. In order to further contribute to our understanding of the long-term development of lithic technologies in southwest China, I have also selected studied an additional site in this region, Tianhuadong Cave. Tianhuadong site is a newly discovered site, located in the west of Yunnan province. Dating work has not been previously

conducted, but radiocarbon dating of the site has failed (Ruan et al., 2017), suggesting that this site is older than 50 ka. The two selected sites cover a distant area of southwest China (the distance between Guanyindong and Tianhuadong is about ~ 700 km). These two sites were included in this PhD project to study the spatial and temporal evolution of the lithic technology in this region during the Middle and Late Pleistocene.

1.5.3 Aims of this study

This thesis focusses on chronological and lithic analysis on the two selected Palaeolithic sites in Southwest China. My specific aims are to:

1) Provide a reliable chronology for two key Palaeolithic sites (Guanyindong cave and Tianhuadong cave) in southwest China, based on novel optically stimulated luminescence (OSL) dating techniques. I will test and apply advanced luminescence techniques to date the sediments and thus infer ages of the associated archaeological materials from these sites;

2) Describe the characteristics of lithic assemblages from these sites. This aim can be divided into several specific aims:

a) Identify the characteristics, origins and development of lithic technology in Southwest China.

b) Investigate the relationships between lithic technologies and human dispersal in this region.

c) Investigate the possible reasons for the temporal and spatial differences in lithic technology between the Guanyindong and Tianhuadon, and between these two sites and elsewhere, by considering climatic and environmental changes, mobility, economic concerns, and demography, etc.

d) Compare the Guanyindong and Tianhuadon assembalges with lithic technologies from other regions, including Africa, Europe, North China and South Asia.

1.6 Organisation of this thesis

The following chapters of this thesis are organised as follows:

Chapter 2 provides a detailed background to the two studied sites, including geological and archaeological settings, stratigraphy and previous chronology.

Chapter 3 presents the materials and methods used for lithic and chronological studies.

Chapter 4 presents the detailed OSL dating results for the Guanyindong Cave site.

Chapter 5 focusses on the identification of Levallois technology in Guanyindong Cave.

Chapter 6 presents lithic analysis results on the Guanyindong assemblage.

Chapter 7 presents detailed OSL dating results for the Tianhuadong Cave and briefly describes the lithic assemblage of the site.

Chapter 8 provides a synthetic discussion and summary of the results of the proceeding chapters.

Chapter 2: Study sites

Two Paleolithic sites, Guanyindong and Tianhuadong caves from southwest China, were investigated in this study. Their importance has been introduced in Chapter 1. This chapter presents detailed background for the two sites, including geological, archaeological, stratigraphic and sampling information.

2.1 Guanyindong Cave

2.1.1 Geological and archaeological background

Guanyindong Cave (26°51′26″N, 105°58′7″E, 1464 m a.s.l.) is located in the Qianxi county of Guizhou province (Figure 2-1A), the eastern end of the Yunnan-Guizhou Plateau, Southwest China. This region has a typical karst landscape (Figure 2-1B) with a general elevation of 1400–2000 m, and is composed of carboniferous and Permian limestones, cataclastic rocks, basalt, and coal deposits. The main ecosystem types include evergreen broad-leaved forest, coniferous and broad-leaved mixed forest, and montane elfin forest. With a subtropical humid climate (humid in summer and dry in spring), this region is controlled by the East Asian summer monsoon and the cold fronts of the winter monsoon and the southwest warm-wet air masses (Zhang et al., 2004). The mean annual temperature is about 14 °C, with the highest monthly mean temperature (20–21 °C) in summer and the lowest (4–5 °C) in winter. Mean annual precipitation in this region is ~1400 mm.

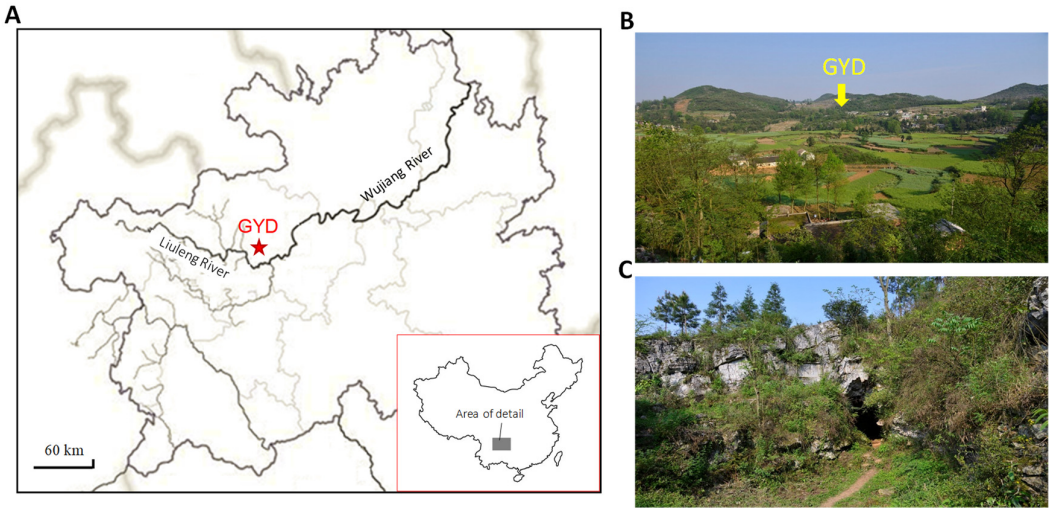

Figure 2-1: (A) Map showing the Guizhou province of China and the location of the Guanyindong Cave. (B) Southward view of the Guanyindong Cave. (C) The main entrance of the cave.

Guanyindong Cave is a limestone cave (Figure 2-1B and C) developed during the Late Tertiary or beginning of the Quaternary (Li and Wen, 1986), and is one of the highest and most developed karst caves in this region. The cave, extending from east to west, was developed from a fracture that was mainly formed by an east-west strike, joint with several south-north branches (Figure 2-2A). The main

entrance, which is also the main excavation area, is located at the west end of the cave. The cave, about 90 m long and 2–4 m wide, has a narrow roof that gradually broadens down to the floor. The distance from floor to roof is about 2–8 m high. The cave floor is about 15 m above the bottom of the karstic depression.

The sedimentary deposits slope down from the entrance to the inside of the cave (Figure 2-2B), and there is a general trend of decreasing grain size of sediments from outside to inside, indicating that the source of the deposit came mainly from the outside. Stalactites and stalagmites are well developed inside the cave, and some of them are connected, forming stalagnates. Thick flowstone plates were developed surrounding the stalagnates at various areas in the cave, these plates cover the majority of sediment in the cave, but the thickness of the plates varies.

The Guanyindong Cave site was first discovered in 1964 by a field team organized by the Institute of Vertebrate Paleontology and Paleoanthropology and the Provincial Museum of Guizhou. Four excavation seasons were conducted in 1964, 1965, 1972 and 1973, respectively. Several trenches (Profiles 1, 2a, 2b and 3) were opened within the cave (Figure 2-2A) in 1960s, which yielded about a hundred stone artefacts. The main excavation was conducted in 1970s at the west cave entrance (Figure 2-2B), where most of fauna fossils and stone artefacts were found (Li and Wen, 1986). The stone artefacts, more than 2000 in total, found in the first 4 excavations were stored in the Institute of Vertebrate Paleontology and Paleoanthropology. The materials analysed in this study (Chapters 5 and 6) are all from this batch. The last excavation season was conducted in the north entrance of the cave in 1980s by the Provincial Museum of Guizhou, which yielded about 800 stone artefacts; these are stored in Guizhou Province and are not included in this study.

2.1.2 Stratigraphy

According to the excavation report by the original excavators (Li and Wen, 1986; Pei et al., 1965), the stratigraphy of the sediments at the main entrance was divided into 9 layers (Layers 1–9) (Figure 2-2B) and 3 groups (Layer 1 does not belong to any of those groups. It is a surface layer): Group A (Layer 2), Group B (including Layers 3–8) and Group C (Layer 9). While Layer 1 and Group B extend from the outside to the inside of the cave, Layer 2 (Group A) was found in front of the cave entrance only (Figure 2-2B). Most sediments from Layer 1, Groups A and B in the main excavation area had been removed during the previous excavations. In 2015, we visited the cave and found a residual profile, named S1, which is a ~3 m residual profile at the south-wall at the cave entrance (Figure 2-2 and Figure 2-3). The Layer 1, Groups B and C were still visible at S1 (Figure 2-3). In 2018, we re-visited the site and found another residual profile, S2, at the south-wall outside the cave and is about 14 m away from the cave entrance (Figure 2-2B and Figure 2-4, where the Layer 1 and Layer 2 are exposed. The stratigraphic features of the two profiles are consistent with those described by the excavators (Pei et al., 1965). The features of each layer are described in Table 2-1.

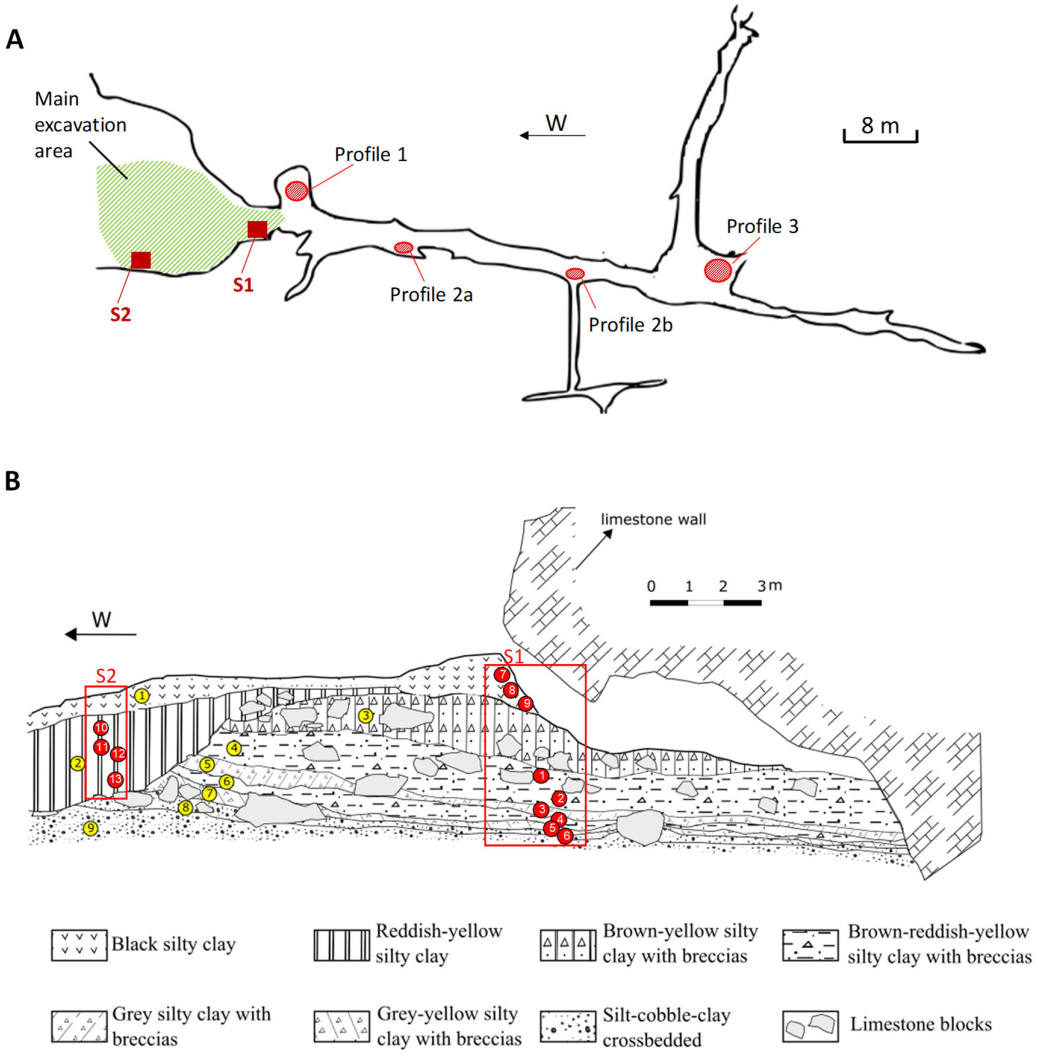

Figure 2-2: Plan view and stratigraphy of the Guanyindong Cave. (A) Plan view of the cave, main excavation area and the residual profiles from south wall. The red circles are the location of Profile 1, 2a, 2b and 3. The red squares shows the locations of the residual profiles S1 and S2 studied in this thesis. (B) Detail of the numbered stratigraphic layers at the main entrance of the cave. The stratigraphic layer numbers are shown in yellow circles. The red rectangles show the locations of the residual profiles S1 and S2. The red rectangles show the locations of the two south-wall sections (S1 and S2) where OSL samples were taken. The locations of OSL samples are shown in red circles, with the number of sample code shown inside (e.g., number 1 represents GYD-OSL1). OSL dating results are presented in Chapter 4. Both panels were modified from Li and Wen (1986).

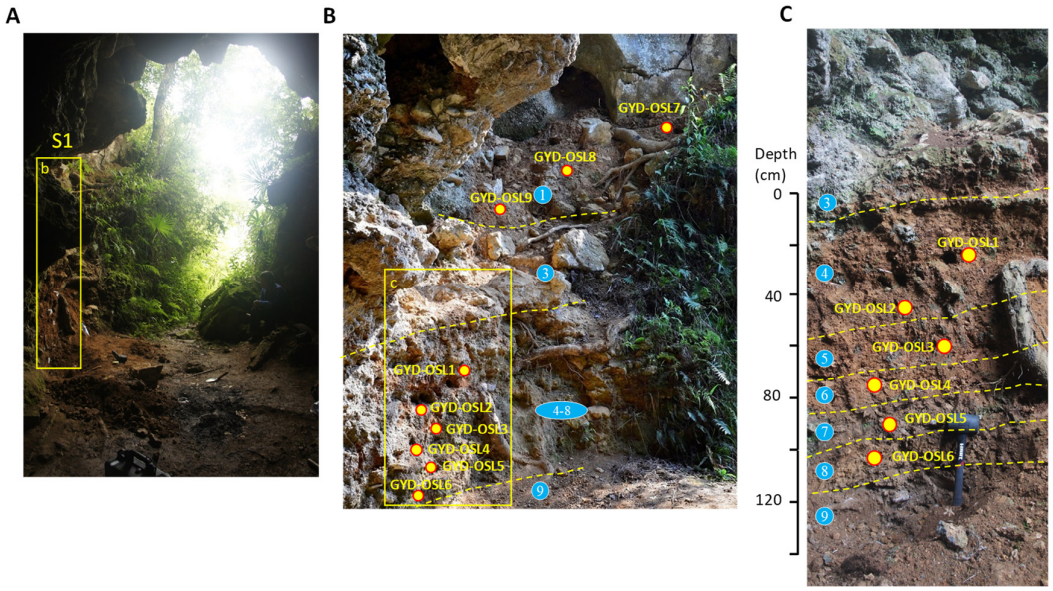

Figure 2-3: General view of the residual profile S1 from the cave entrance. (A) Photo taken from the interior of the cave, showing the location of the residual profile S1 at the south wall (marked by rectangle with details shown in B and C). (B) Photo showing details of the residual profile S1 at the south wall and the location of all OSL samples from Layer 1 and Layers 4–8. The details of Layers 4–9 inside the yellow rectangle are shown in C. (C) Photo showing the details of sedimentary layers 3–9 of Group B, and the location of OSL samples. The stratigraphic layer numbers are shown in blue circles and the location of OSL samples are marked by yellow circles with sample names shown next to each of them. The dashed yellow lines in b and c show the boundaries between the layers.

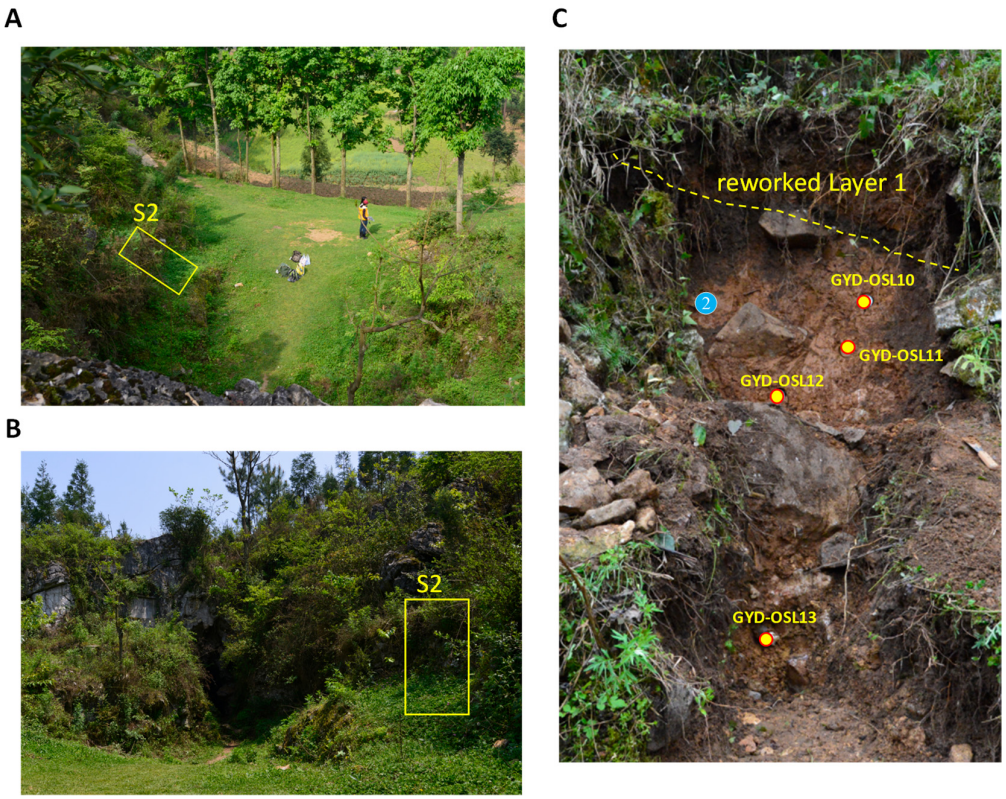

Figure 2-4: General view of the residual profile S2 outside the cave entrance. (A) Photo taken from top of the cave, showing the location of the residual profile S2 (marked by rectangle). (B), Photo taken from outside the cave, showing the location of the residual profile S2 (yellow rectangle). (C) Photo showing the details of sedimentary layers (Layer 2 and reworked Layer 1) of residual profile S2, and the location of OSL samples. The dashed yellow line shows the boundary between Layers 1 and 2. The stratigraphic layer numbers are shown in blue circles and the location of OSL samples are marked by yellow circles with sample names shown next to each of them.

Table 2-1. Description of stratigraphic layers and number of stone artefacts extracted from each layer.

Layer	Thickness (cm)	Sedimentary features	Number of stone artefacts
1	~15–70	Archaeologically sterile and consists of black silty clay	0
Group A			
2	~40–240	Reddish-yellow silty clay, containing abundant rock debris and plenty of stone artefacts and fragments of mammal fossils. This layer sits unconformably on top of Group B.	879
Group B			
3	~50–100	A loose layer with brown-yellow and grey-yellow silty clay, containing fragments of limestone and breccias. According to the excavation report, this layer yielded only a small number of stone artefacts and fossils.	20
4	~40–50	Brown-yellow and red-yellow silty clay with some fragments of limestone breccias. The top of this layer is capped by a flowstone layer (3–5 cm in thickness). Many stone artefacts and fossils were found from this layer.	68
5	~20	Grey silty clay with abundant limestone fragments, which yielded plenty of stone artefacts and fossils.	801
6	~10	Similar to Layer 4 but with the absence of large limestone fragments. This layer yielded more stone artefacts and fossils than Layer 4.	236
7	~15	A grey-yellow silty clay layer containing stone artefacts and fossils with abundant small limestone fragments.	139
8	~10	Yellow silty clay, containing limestone and breccias fragments. Stone artefacts and fossils were found from this layer too.	20
Group C			
9	> 10 cm	Archaeologically sterile and consists of layers of sand, gravels and breccias.	0

2.1.3 Fossil assemblage

The fossils from Group A are mostly fragments (Li and Wen, 1986), indicating that the material of Group A was probably reworked before deposition. Only a few species were identified, including *Rhinoceros sinensis Owen*, *Stegodon sp.*, *Hystrix sp.* and *Bovinae*. In contrast to Group A, the fossils from Group B were much better preserved, and abundant species can be identified, including 23 families [*Eulota (Cathaica) sp.*, Testudinidae indet., *Macaca sp.*, *Hystrix cf. subcristata Swinhoe*, *Rhizomys cf. sinensis Gray*, *Vulpes cf. vulgaris* L., *Ursus thibetanus kokeni* M. et G., *Ailuropoda melanoleuca fovealis* M. et G., *Mustelidae indet.*, *Crocuta ultima Matsumoto*, *Panthera cf. tigris* L., *Gomphotheriidae indet.*, *Stegodon cf. orientalis* Owen, *Stegodon guizhouensis* Li et Wen sp. nov., *Equus sp., Megatapirus augustus* M. et *G.*, *Rhinoceros sinensis* Owen, *Sus cf. scrofa L.*, *Muntiacus sp.*, *Cervus (cf. Pseudaxis) sp.*, *Rusa sp.,* Bovinae, and *Capricornis sumatraensis* Bechstein] and 13 species (*Gastropoda*, *Chelonia*, *Primates*, *Rodentia*, *Carnivora*, *Proboscidea*, *Perissodactyla* and *Artiodactyla*). Most of these species belong to the Middle Pleistocene *Ailuropoda-Stegodon* fauna group, which is commonly found at cave sites in south China.

2.2 Tianhuadong site

2.2.1 Geological and archaeological background

Tianhuadong (N26°02.211', E100°27.648', 1805 m a.s.l.) is a cave site located on the east side of limestone valley, Heqing country, Yunnan Province, southwest China (Figure 2-5A). The cave, ~200 m long, has a 13 m wide entrance. It covers an area of ~2400 m^2. Sixteen kilometres to the north of the cave is the Jinsha River, and ~100 m to the west is a branch of Caifeng River. This cave has been used as a temple for many years, so it is difficult to investigate and excavate inside the cave. For this reason, investigations were carried out in 2010, 2013 and 2016 on a gentle slope in front of the cave (Figure *2-5*B) by the Institute of Cultural Relics and Archaeology of Yunnan province. A 1x2 m trench (T1), extending from west to east, was opened (Figure 2-5). A total of 1,121 stone artefacts were excavated. They include 289 from within the stratigraphic layers that recovered from the test trench excavated in 2013 and 832 collected from the surface in 2010, 2013, and 2016. These stone artefacts are stored in the Institute of Cultural Relics and Archaeology of Yunnan province.

2.2.2 Stratigraphy

The deposits cavated are mainly red mild clay with a stable and homogeneous sedimentary structure. The sedimentary profile of the trench was divided into five layers (Figure 2-6) and is described as follows:

1) Layer 1 (0–25 cm thick) is a disturbed top soil layer. It consists of brown-yellow mild clay. A total of 81 stone artefacts and a small number of animal fossils were recovered from this layer.

2) Layer 2 was divided into two sub-layers, Layer 2a (15–40 cm thick) and 2b (35–70 cm thick). Layer 2a is a light brown red mild clay layer with dense structure and solid texture. Weak carbonate cementation was developed. A total of 100 stone artefacts were recovered from this layer. Layer 2b is a brown red mild clay layer, with similar structure and texture as Layer 2a. Only a few (n=14) stone artefacts and animal fossil fragments were found from Layer 2b.

3) Layer 3 (10–45 cm thick) consists of brown mild clay with carbonate cementation. It bears numerous (n = 56) of stone artefacts, animal fossil fragments and some charcoal fragments.

4) Layer 4 (15–70 cm thick) is red brown mild clay with carbonate cementation. Numerous animal fossil fragments and a small number (n = 32) of stone artefacts were recovered.

5) Layer 5 (15–30 cm thick) is a brown red mild clay layer with carbonate cementation. Only a small amount of animal fossil fragments and charcoal fragments were recovered.

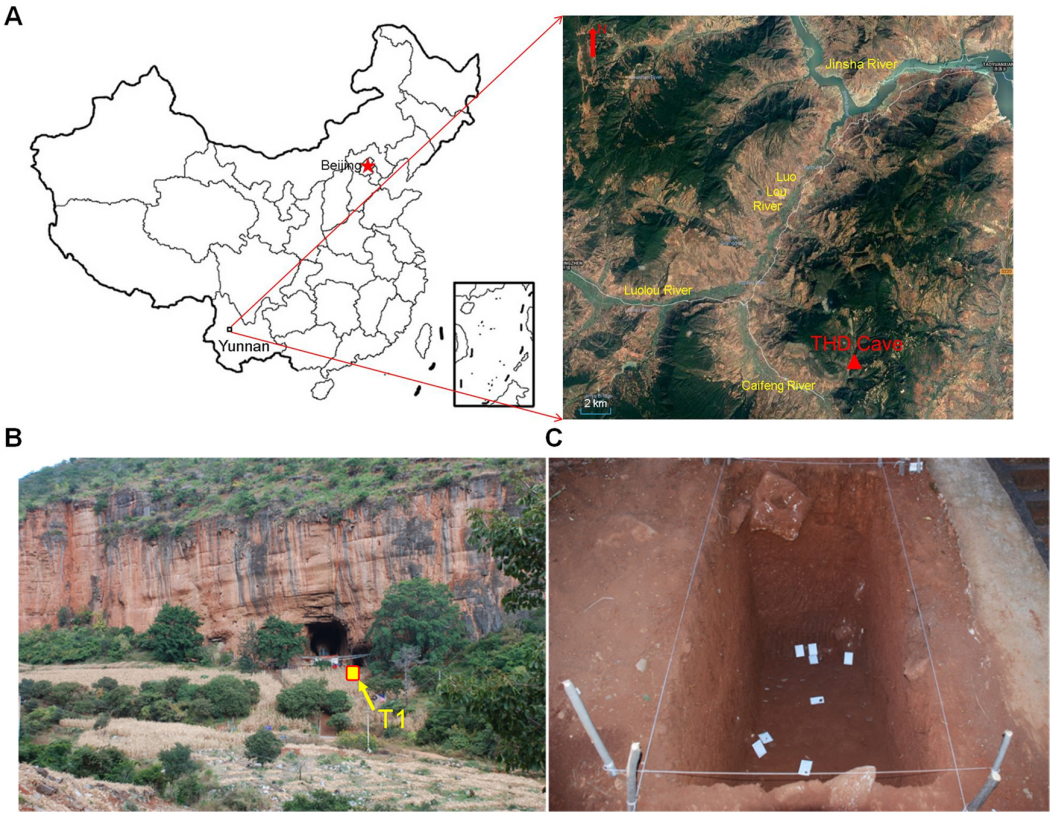

Figure 2-5: (A) Geographic locations of the Tianhuadong site. (B) Photo showing the cave entrance and the excavation area (T1) in front of the cave. (C) Photo showing the excavated trench.

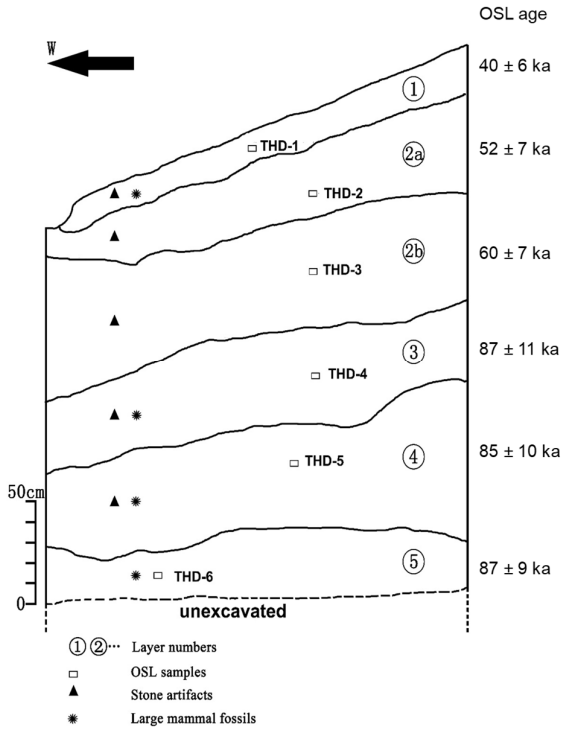

Figure 2-6: Schematic diagram of the stratigraphy, cultural relics and localities of OSL samples of the north wall of T1. Figure modified from Ruan et al. (2018). See Chapter 7 for details about OSL ages.

Apart from the top layers (1 and 2a), there is no obvious evidence of reworking induced by water flows. According to observations by local farmers, the deposits from the near surface (~ 0.5 m) were removed during previous engineering activities. Therefore, the stone artefacts collected from the surface are expected to originate from the overlaying deposits that have been removed and the underlying deposits (mainly Layer 1) been reworked during the engineering activities. More than half of the stone artefacts and fossils recovered from both the surface and lower deposits show signs of weathering on their surface. This is probably due to the acid depositional environment associated with red clay, a typical depositional environment in south China. Most of the stone artefacts recovered from the deposits and collected from the surface show no little traces of abrasion on their edges, indicating that they were neither exposed for a long period nor transported for a long distance. This suggests that the artefacts were recovered in-situ, although more detailed taphonomic work is needed to fully understand the site formation process.

Chapter 3: Materials and Methods

The materials and methods from this study fall into two categories. One category is the stone artefacts from the Guanyindong and Tianhuadong sites, and the other is the sediments collected for dating from the excavated profiles at the study sites. This chapter presents detailed information about the materials and the methodologies used to study them.

3.1 Lithic analysis

To reconstruct the reduction sequence from raw material procurement to tool manufacture, a technological approach (Boëda et al., 1990; Inizan, 1999) was used to study the entire assemblage. I consider raw material procurement and exploittation and tool manufacturing, core reduction and flake debitage. Sub-divisions for each sequence were categorized with reference to the Western European MP. Both qualitative, including technological, typological and metrical attributes, and quantitative methods, including the amount and patterns, were utilized to demonstrate and analyse attributes of the assemblage at various aspects.

3.1.1 Typological and technological approach

The sorting procedures for stone artefacts are according to the typology developed and summarized by Bordes (Bordes, 1961b; Bordes, 1969; Dibble, 1994) and Inizan et al. (1999). The four main categories consist of cores, flakes, tools, chunks and debris. The main categories are defined in Table 3-1. For cores, we divided them in Levallois cores, discoid cores, truncated faceting, elongated cores, and ordinary cores, which are further divided as single-platform, double-platform and multiply-platform cores, based on the quantity of platforms they have. Complete flakes were classified into ordinary flakes, Levallois flakes, débordant flakes, elongated flakes, kombewa flakes, tablets, natural backed knife, and crests. Other flakes include flake fragments, retouched flakes and retouched flake fragments. Because retouched pieces account for a large component in the assemblage, we further classified them into side-scrapers, denticulates, notches, points, borers, burins, backed knives, end-scrapers, choppers and cleavers based on their technological and morphological characters according to Borders (Dibble, 1994). The chunks and debris are those artefacts that present artificial marks but without any retouch or served as cores or flakes.

3.1.2 Metrical and morphometric data

Metrical and morphometric data were collected using a digital calliper and an electronic scale. Except basic raw materials and metrical data (mainly including length, width and thickness, and mass)were measured for each artefacts and different attributes for different categories were differentiated. For the chunks and debris, only mass were measured.

Table 3-1. The definitions of some key categories mentioned in the chapter

Category	Definition
Discoid cores	Cores with circular outline and an asymmetrical biconvex section. They are formed by removing flakes using centripetally directed percussions (Inizan, 1999). The less convex of the two faces is formed by the removal negatives of the flakes. The other faces are often cortical in the middle, with a margin formed by the preparation negatives of the striking platforms or by an area of cortex.
Truncated faceting	Cores started from a flake and then knapped along the periphery of the flake and take its ventral side as working surface, ending up as cores with the flake scars on ventral side (Dibble et al., 2006).
Elongated cores	Cores from which elongated flakes are detached.
Kombewa cores	The convexity of a lower surface of a flake is used for detaching a second flake, and thus the second flake has two bulbs (see the definition of kombewa flake below).
Ordinary cores	Simple flaking cores which different quantity of platforms.
Complete flakes	Flakes with platform, percussion point, bulb, completed proximal, mesial and distal part.
Flake Fragments	Pieces lack any part of a complete flake.
Retouched flake (or flake fragments)	Complete flakes or flake fragments that are retouched.
Débordant flakes	Levallois core edge flake. The aim of removal of this flake is to maintain the lateral convexity of the Levallois core (Boëda et al., 1990).
Elongated flakes	Flakes are relatively long (length ≥ 2×width).
Kombewa flakes	Flakes with two bulbs left on both upper and lower surface (Dauvois, 1981; Owen, 1938; Tixier et al., 1980).
Tablets	A flake with its exterior surface as its core's entire original platform surface, and facets on its margins that are portions of previous flake scars of the core' (Dibble, 1994).
Natural backed knife	A flake with a cortex abrupt edge opposite a natural sharp cutting edge.
Crests	A flake to initialize a production of blades through bifacial flaking along one edge of a nodule (Dibble, 1994).
Chunks and debris	Artefacts that present artificial marks but without any retouch or served as cores or flakes.

3.1.2.1 Raw materials

The classification of raw materials is based on their physical properties, including homogeneity, crystal structure, grain size, etc. Sub-division was not conducted because their fracture properties are similar within a category (e.g., chert and limestone).

3.1.2.2 Cores

For cores, the following information was collected: type, geometry (column, conic, cubic, irregular, cicular and wedged), maximum dimension, medial width, distal width, distal thickness, platform types, platform width, platform thickness, scar number, scar length, cortex percentage, cortex texture, cortex location, heat damage, platform preparation, and rotations (see Figure 3-1 for examples of the variables). Types comprise Levallois, discoid, blade, truncated faceting, single, double, and multiply platform cores. The Levallois cores were identified based on Boëda's six criteria (Boëda, 1995). The other types were

identified in accordance to their definitions. Only large and main scars (> 2 cm) were counted. Cortex percentage is estimated with ~10% uncertainty and cortex textures are mainly rough, smooth and tabular. Platform preparation chiefly consists of plain, faceted, cortex. The rotation number indicates possible platform transform times during the reduction of a core.

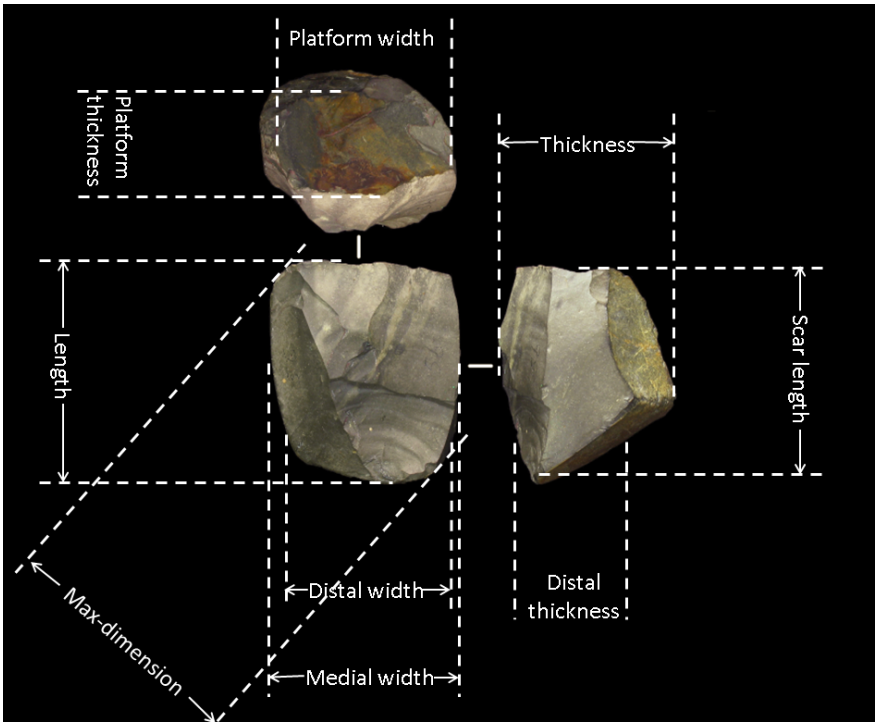

Figure 3-1: Key morphometric variables of cores.

3.1.2.3 Flakes

For flakes, we collected their types (including complete, fragment, retouched or sub-types such like Levallois and débordant), maximum dimension, length, oriented width, width at 25%, 50% and 75% max dimension, oriented thickness, thickness at 25%, 50% and 75% max dimension, platform width, platform thickness, platform shape (triangle, rectangle, quadrangle, gull-wing, fusiform, trapezoid and irregular), dorsal scar number (i.e., the completed flake scars left on the dorsal surface), dorsal scar directions, cortex percentage, cortex texture (rough, smooth, angular), cortex location (platform, proximal, medial and distal), heat and damage, termination , and platform preparation (plain, faceted, cortex, dihederal, focus and missing). Key morphometric terms are demonstrated in Figure 3-2 and Figure 3-3.

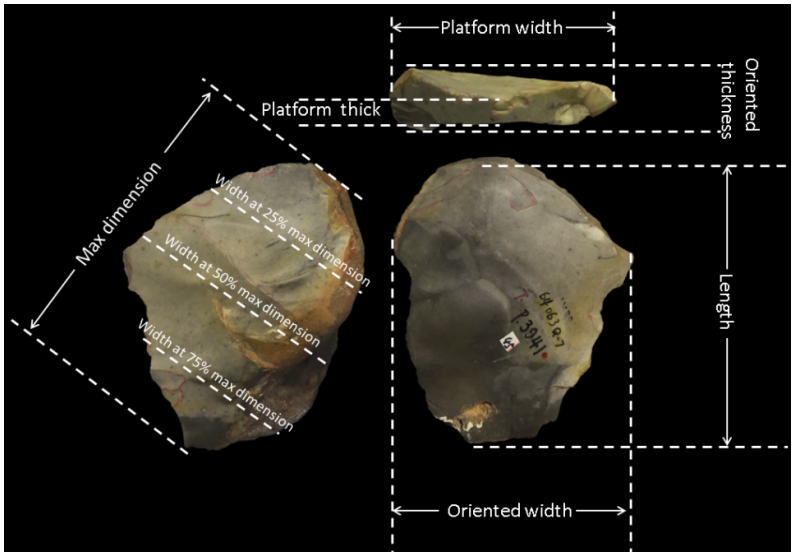

Figure 3-2: Skematic model showing key morphometric variables of flakes.

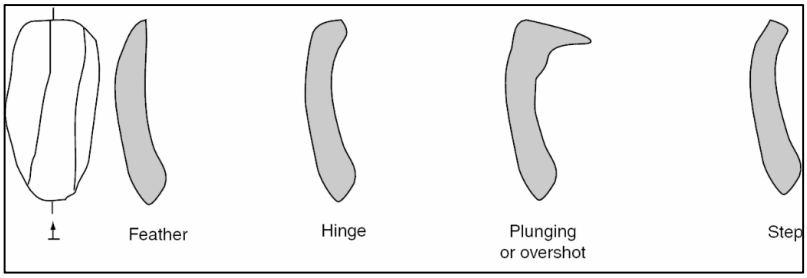

Figure 3-3: Flake termination types (from Shea, 2013)

3.1.2.4 Retouched pieces

For retouched pieces, attributes including number of layers, number of edges, edge types, number of burins, retouch diameter (for curvature), retouch depth (for curvature), notch number, notch location, notch length and depth, edge angle, GUIR and index of invasiveness were recorded. The number of layers was estimated by the overlaps of retouching phases. Edge types include straight (i.e., the edge shape is straight), convex (i.e., the edge shape is convex), concave (i.e., the edge shape is concave), denticulate (i.e., the edge shape is denticulate), end (end-scraper), beak, pointed (borer), and notch. The edge angle was calculated by measuring the width at the 3 mm depth of the edge and then transfer the value into angle degree (*Figure 3-4*) (Eren and Lycett, 2016). To estimate the invasion and intensity of retouching, two concepts "Index of Invasiveness" (Clarkson, 2002) and "Geometric Index of Unifacial Reduction (GIUR)" were applied (Figure 3-5 and Figure 3-6) (Hiscock and Clarkson, 2005; Hiscock and Tabrett, 2010; Kuhn, 1990).

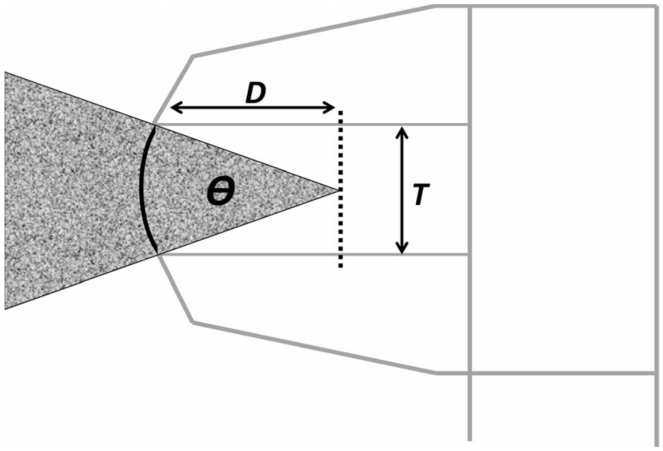

Figure 3-4. The measurement of edge angle (from Eren and Lycett, 2016)

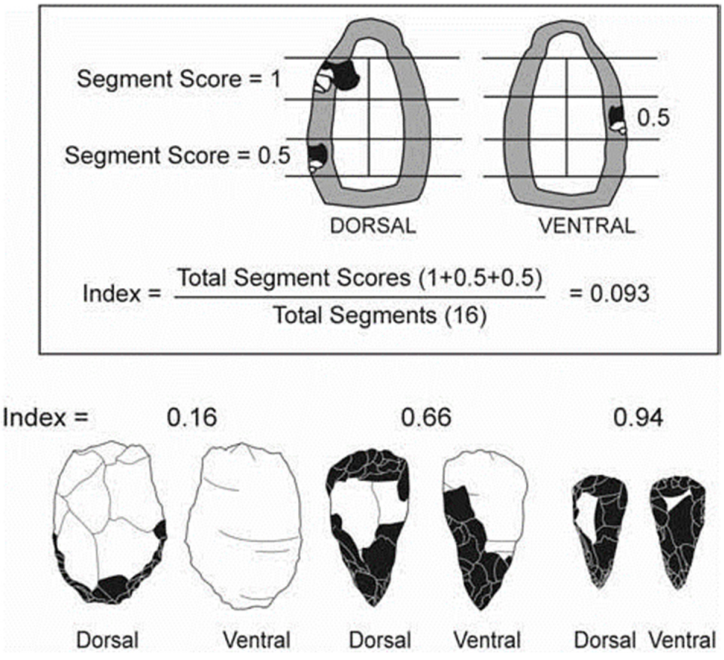

Figure 3-5: Index of invasiveness (from Clarkson, 2002).

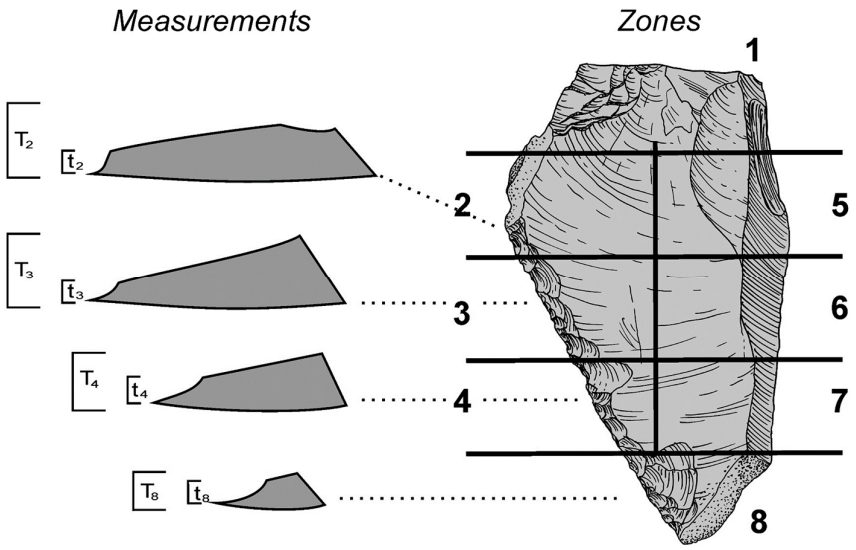

Figure 3-6: GIUR measurement (from Hiscock and Clarkson, 2009).

3.1.3 Data collection method

Data were recorded in Excel spreadsheets. Statistical analysis, interaction patterns among categories and attributes, tables and charts were compited using R and RStudio. To best illustrate the artefacts, we also used CT scanner housed in the IVPP to produce 3D animations of several typical Levallois cores. The raw data and R code used to produce the statistics and graphs presented in this thesis are openly available online at ttps://doi.org/10.1038/s41586-018-0710-1.

3.2 Optical dating

3.2.1 Basic principle of luminescence dating

Defects in crystals, such as quartz and feldspar, may result in charge imbalances across a mineral. When crystals are subjected to ionising radiation, e.g., alpha, beta and gamma radiation, the defects may capture free charges generated by the ionising radiation. These defect 'traps' can hold the trapped charges for a period of time that depends on the energy barrier of the traps, i.e., the energy that a trapped charge requires to escape from the traps. Once the crystals are heated or exposed to light, the trapped charges may obtain sufficient energy to escape, after which they may be captured by another trap or recombined with a hole centre. Such a recombination process of de-trapped charges releases the energy stored in the traps. And result in emission of light, and the emitted light is called luminescence. The

emission stimulated by heating is called thermoluminescence (TL) and, similarly, that resulted from exposure to light is called optically stimulated luminescence (OSL).

The application of luminescence in dosimetry can be traced back to 1950s. TL was firstly applied in in archaeological dating in 1960s (Aitken, 1985; Ichikawa, 1965). The basic concept is that luminescence signal intensity is proportional to the number of trapped charges, and, hence, proportional to the radiation dosage received by the mineral. When minerals from archaeological samples, such as pottery, tile and brick, were heated during production, the trapped charges were ejected and recombined with holes, which would reset the luminescence 'clock' of the heated material. After these archaeological samples were buried, they were exposed to ionising radiation emitted from naturally occurring radioactive elements, such as U, Th and K, within and surround the samples. Such an environmental radiation resulted in a time-dependent accumulation of trapped charges in the mineral lattice. As a result, the age can be estimated by dividing the equivalent dose (D_e, a measure of the radiation energy in unit Gy absorbed by grains during their period of burial) by the environmental dose rate or annual dose (the rate of supply of ionizing radiation to the grains over the burial period, in unit Gy per thousand year (ka)) (Aitken, 1985):

$$Age(ka) = \frac{Paleodose\ or\ Equivalent\ Dose\ (Gy)}{Annual\ Dose\ (Gy/ka)}$$

The D_e can be estimated by measuring the amount of luminescence accumulated in minerals, and the dose rate can be estimated by measuring the concentrations of the radioactive elements within the sample and surrounding materials, i.e., U, Th and K and the cosmic ray flux.

The use of OSL for dating sediment (also termed 'optical dating') was first introduced in 1980s (Huntley et al., 1985). While TL dating has the luminescence clock reset by heating, OSL dating relies on optically resetting the luminescence signals. For example, the luminescence of sedimentary minerals would be reset by exposure to sunlight during their transportation. Their OSL signals would accumulate again after burial. Hence, OSL dating provides an estimate of the time since mineral grains such as quartz or feldspars were last exposed to sunlight (Aitken, 1998; Huntley et al., 1985; Roberts et al., 2015).

3.2.1.1 The numerator - equivalent dose

The equivalent dose is estimated by comparing the natural OSL signals in the sample with those generated by laboratory irradiation. The D_e is equal to the laboratory radiation dose that can produce the same OSL signal intensity as the natural signal. Two groups of procedures or protocols have been developed for determining D_e, additive-dose and regenerative-dose methods (Figure 3-7). All these procedures involves preheating the sample to an elevated temperature for a given period to get rid of any thermally unstable signals (e.g. Li, 1991; Wintle and Murray, 2006) and to transfer charges from shallow traps into the deep traps (Wintle and Murray, 1999).

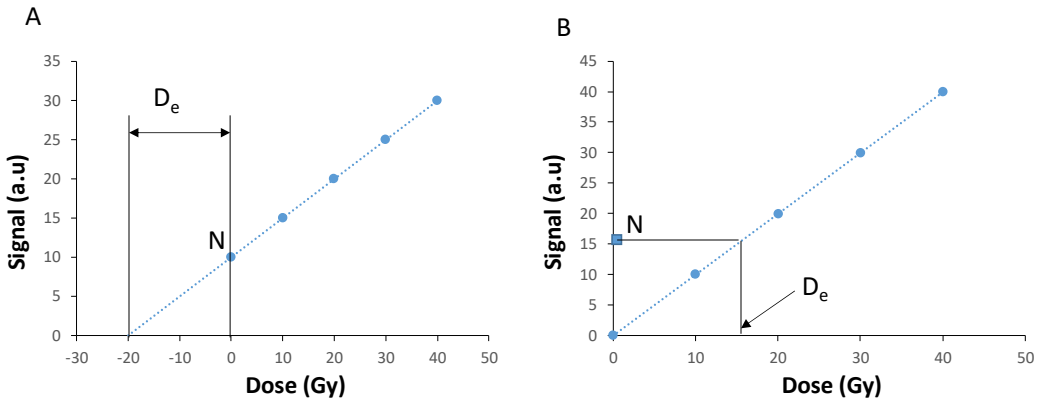

Figure 3-7: Illustrations of the two methods used in luminescence dating. (A) Additive-dose method; (B) Regenerative-dose method.

The additive-dose method (Tite, 1966) involves dividing the natural samples into several groups (Figure 3-7A). One of the groups is used for measuring natural signal. The other groups are given different laboratory doses. The measured signals from natural and laboratory-irradiated samples are plotted against laboratory doses given to each group to establish an additive-dose growth curve. The D_e value can be estimated by extrapolating the curve to a background or residual level. The additive-dose method works best when the TL or OSL signal lies on the linear part of the dose response curve (DRC). It may, however, introduce a significant error because of an inappropriate use of fitting function if the samples have D_e in the non-linear range of DRC or when there is supralinearity in the extrapolated portion in DRC.

To overcome the problem of additive-dose method for dealing non-linear DRC, the regenerative-dose method was proposed (1980). In this method, the aliquots of natural samples are first measured to observe the natural signals. After that, they are given different laboratory doses to regenerate luminescence signals. A DRC is then obtained by plotting the regenerated signals against the corresponding regenerative doses. The D_e can be calculated from the horizontal intersection of the natural signal level and the DRC (Figure 3-7B). The advantage of this method is that it avoids the problem of extrapolation. Hence, it can be applied to samples whose D_e are in the non-linear response region. The drawback of this method, however, is that it becomes inaccurate if there is a significant sensitivity change between the measurement of the natural signal and the regeneration signals, which has been commonly observed as a result of bleaching, preheating or laboratory irradiation (e.g. Wintle and Murray, 1999). In order to deal with the sensitivity change problem, a 'single-aliquot regenerative-dose' (SAR) procedure was developed (Galbraith et al., 1999; Murray and Roberts, 1998; Murray and Wintle, 2000). The SAR protocol involves monitoring and correcting for sensitivity changes using a test-dose signal (T_x), which is kept the same throughout the procedure, after the measurements of each natural or

regenerative-dose signals (L_n or L_x). A step-by-step procedure is provided in Table 3-2. The sensitivity-corrected OSL signal (L_x/T_x) are used to establish a DRC, and the sensitivity-corrected natural signal (L_n/T_n) is projected onto this curve to estimate D_e.

Table 3-2. The single-aliquot regenerative-dose (SAR) protocol.

Step	Treatment	Observed
1	Regenerative dose, D_i [a]	
2	Preheat	
3	OSL measurement	L_n or L_x
4	Test dose, D_t	
5	Preheat or cut-heat	
6	OSL measurement	T_n or T_x
7	Return to step1	

[a] For the 'natural' sample, i = 0 and $D_0 = 0$. The whole sequence is repeated for several regenerative doses including a zero dose and a repeat dose.

The reliability of sensitivity corrections in the SAR procedure is routinely checked by measuring two identical regenerative doses and calculating their ratios (so-called 'recycling ratio'). If the sensitivity correction is successful, the recycling ratio should be statistically indistinguishable. It is suggested that a recycling ratio within the range of 1.0 ± 0.1 should be acceptable (Murray and Wintle, 2000). Apart from the recycling ratio test, in order to monitor recuperation or thermal transfer of charges from thermally unstable traps into optically sensitive traps (Aitken, 1998; Aitken and Smith, 1988), a zero dose is usually incorporated into the SAR cycle. The ratio between the sensitivity-corrected signal for the zero dose and that for the natural dose is then calculated to assess the extent of thermal transfer or recuperation. A recuperation ratio less than 5% is considered as acceptable (Murray and Wintle, 2000).

Several other tests have been proposed to test the suitability of the SAR protocol. One is to check if the D_e depends on preheat temperatures or not, which is called a preheat plateau test (Murray and Roberts, 1998; Murray and Wintle, 2000). This is achieved by measuring D_e values using different preheat temperatures. Results obtained from within the 'plateau' temperature region are considered as most reliable. Apart from the preheat plateau test, the SAR protocol is also usually tested using a dose recovery test (Galbraith et al., 1999; Murray and Roberts, 1998). In this test, the natural grains from the sample are bleached using sunlight or laboratory light sources. After that, a known laboratory dose is given as an 'unknown' surrogate dose to be measured. A success in a dose recovery test provides a minimum check of the reliability of the SAR procedure. Given the multiple self-diagnostic features of the SAR protocol mentioned above, it has been successfully and widely adopted in geological and archaeological dating of sediments (Lian and Roberts, 2006; Murray and Olley, 2002; Preusser et al., 2009; Roberts et al., 2015; Stokes et al., 2003; Wintle, 2008).

3.2.1.2 The denominator – dose rate

The natural radiation dose comes mainly from the alpha, beta and gamma radiation emitted from radioactive elements (e.g. ^{40}K, ^{235}U, ^{238}U, ^{87}Rb and ^{232}Th) in the sediments (Aitken, 1985) plus a small contribution from cosmic rays (Prescott and Hutton, 1988, 1994). These radiation sources have different

effective ranges in sediments. The cosmic ray has the longest penetrating distance, ranging from several to tens of meters. The gamma ray has a penetration distance of ~30 cm, so it is important to make in-situ measurement of the gamma dose rate for samples from a heterogeneous deposit setting. The β particles have much shorter penetration distance (a few millimeters), which means that there is a considerable loss of energy for the β particles when they penetrate the sandy-size grains (63–2000 μm in diameter). For this reason, attenuation factors are needed to estimate effective beta dose rate, which have been calculated and provided by several studies (e.g. Brennan, 2003; Fain et al., 1999; Mejdahl, 1979). For the α particles, however, all their energies are deposited within ~20–30 microns in a mineral grain due to their heavy mass and high ionization capacity. In practice, the sandy grains used for dating are etched with HF acid to remove the outer rims of the grains to get rid of the alpha-irradiated layers, so that calculation of alpha dose rate is avoided.

Table 3-3. Dose rate conversion factors for U, Th and K. Data from Guérin et al. (Guérin et al., 2011)

Concentration	Dose rate conversion factor (Gy/ka)		
	alpha	beta	gamma
1 ppm, Uranium	2.795	0.1457	0.1116
1 ppm, Thorium	0.738	0.0227	0.0479
1%, Potassium		0.798	0.249

Because these radioactive elements (mainly U, Th and K) contributing to the environmental dose have very long half-lives (in the order of billion years), their radioactivity can be assumed to be constant over the applicable time range of luminescence dating (usually younger than a million years). As a result, the environmental dose rates measured based on the present-day radioactivity can be assumed to represent the effective dose rate for the samples during their burial period. It must be noted, however, that this assumption is only valid when the decay chains (such as U and Th) remains equilibrium over time and there is no leaching or enrichment of K, which is not always met for geochemically active deposits (Olley et al., 1996).

In practice, the environmental dose rate is estimated based on measuring the concentrations of radioactive elements (mainly U, Th and K) in the sample itself and its surroundings. The concentrations are then converted into dose rates according to published converting factors (Table 3-3). The cosmic ray contribution can be estimated based on the elevation, latitude, longitude and burial depth of the sample (Prescott and Hutton, 1994). Apart from the above considerations, the attenuation of radiation energy by moisture in the sediments also needs to be taken into account (Aitken, 1985), which can be calculated using the water content given as the ratio of the weight of water to that of dry sample (Aitken, 1985; Zimmerman, 1971).

In summary, the environmental dose rate of quartz grains of diameter s can be calculated as

$$D_{ex}(s) = \frac{D_{U\beta}[1-\Phi_U(s)] + D_{Th\beta}[1-\Phi_{Th}(s)] + D_{K\beta}[1-\Phi_K(s)]}{1+1.25W} + \frac{D_\gamma}{1+1.14W} + D_{\cos}$$

Where $D_{U\beta}$, $D_{Th\beta}$ and $D_{K\beta}$ are the external beta dose rates from U, Th and K, respectively, and D_{γ} is the gamma dose rate from U and Th, and D_{cos} is the dose rate from cosmic ray, and Φ_K, Φ_U and Φ_{Th} are the effective absorption factors of the beta dose rates for K, U and Th, respectively, and W is water content.

3.2.2 Sample collection and preparation procedure

In this study, sediments samples of interest are collected from the stratigraphic profiles using stainless steel tubes (25 cm long and 5 cm diameter). The tubes were pushed or hammered into a freshly cleaned vertical section of the sediment profile. The two tube ends were immediately covered with lids and sealed with opaque duct tapes to ensure a safe transportation and prevent exposure to light. For all the samples, an additional bag of materials were collected for each sample for dosimetry measurement.

All samples are prepared under a subdued red to orange light condition (>590 nm) in the dark rooms at the University of Wollongong. Firstly, both ends of OSL sample tubes are removed to get rid of materials that may be exposed to sunlight during the sampling processes. The materials from the centre of the tubes were then put into a large beaker with water. They were then wet sieved to obtain sandy fractions (> 60 μm diameter). The sandy fraction were then stirred and washed in an ultrasonic bath (Branson, type 5250) several times to remove clay minerals. After that, they were treated with 10% HCl to remove any carbonates, followed with several washes in the ultrasonic bath to remove the remaining acid and reaction solution. The samples were then treated with H_2O_2 for over 24 hours to remove any organic matters followed with several washes in the same way. The samples were then dried in an oven at a temperature of 50 ºC. The dried sediments were then sieved to retrieve different grain sizes using sieves of sizes 90 μm, 125 μm, 150 μm, 180 μm, 212 μm, and 250 μm, respectively.

To extract quartz from the sediments, we first used heavy liquids made from the solution of sodium polytungstate to separate feldspar, quartz and other heavy minerals (Mejdahl, 1985). This is based on the fact that different minerals have different densities. The feldspars usually have density less than 2.62 g/cm^3, while quartz usually falls within the range of 2.75 g/cm^3 and 2.62 g/cm^3. Heavy liquid separate, however, is not perfect and the quartz fractions separated by them always contain other minerals (especially feldspars). In order further purify the quartz fraction, 40% hydrofluoric acid (HF) is applied for 40 minutes to get rid of the contaminated feldspar grains, based on the fact that feldspar are much easier and quicker to react with HF than quartz. Another benefit of using HF etching is that it can remove the outer layer (10–20 μm) of the quartz grains that were irradiated by α particles, so that estimation of alpha dose contribution is avoided. After HF etching, the samples were treated with 10% HCl for several minutes to remove any fluorides formed during HF etching. The purity of quartz fractions was then checked by applying infrared stimulation, based on the fact that feldspars are IR sensitive but quartz is not. (e.g. Hütt et al., 1988; Smith et al., 1990). If a strong IRSL signal is detected, the HF etching procedure was repeated until pure quartz was obtained.

3.2.3 Measurement facilities

As mentioned above, luminescence dating involves measurement of two quantities, D_e and dose rate. In this study, the measurement of D_e was achieved in a luminescence detection system and the dose rates were measured using several techniques, which are outlined below.

3.2.3.1 Luminescence detection system

In the luminescence dating laboratory at UOW, a total of 7 Risø automated TL/OSL readers, including one OSL/TL-DA-12, four OSL/TL-DA-15 and two OSL/TL-DA-20, are available for luminescence measurements. A photo and the schematic structure of the Risø system are shown in Figure 3-9. This system allows automated irradiation, preheating and TL/OSL measurements, all can be flexibly programmed in a controlling software 'SEQUENCE" running on the computer connected to the system. The system can load up to a total of 48 aliquots or discs in one sequence. There are several key components in the system, including a radiation source, a heater, stimulation light sources, a luminescence detector and optical filters.

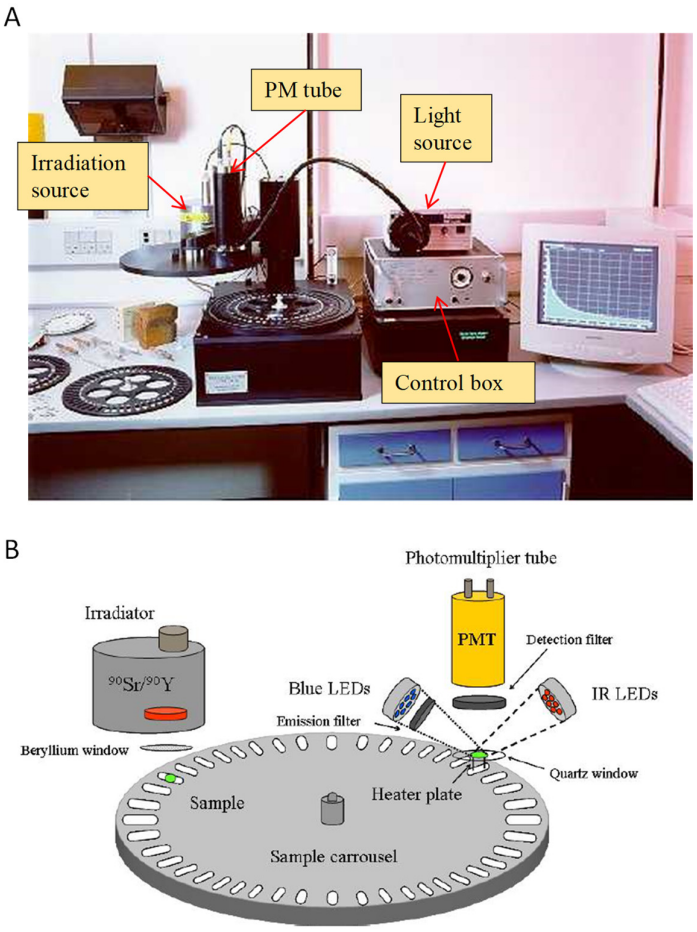

Figure 3-8: (A) Photo showing a Risø automated TL/OSL system. (B) The structure of the Risø automated TL/OSL reader (from user's manual).

3.2.3.1.1 Irradiation source

The system uses a $^{90}Sr/^{90}Y$ beta irradiation source sealed in a lead cylinder to achieve laboratory irradiation, which enables an irradiation time as short as 1 second to as long as 31 years. The dose rates of each irradiation sources were calibrated using a gamma-irradiated calibration quartz supplied by the Risø National Laboratory, Denmark. The quartz was irradiated with a known gamma dose of ~4.7 Gy. Calibration was conducted for both single aliquot and single grain discs. Since the ^{90}Sr has a half-life of ~28.79 years, the dose rate is expected to decrease over time. The real-time dose rate is estimated using the following equation:

$$D(t) = D_0 e^{-\lambda t}$$

where D_0 is the dose rate obtained on the calibration date, and λ is the decay constant ($\lambda = 0.024071$ per year) (Aitken, 1985).

3.2.3.1.2 Heater

Heating plays an important role in luminescence dating. For OSL dating, a preheat is usually applied after irradiation to remove unstable signals. The linear heating system in the Risø readers allows a heating rate from 1 to 20 °C/s and can heat the samples up to 700 °C.

3.2.3.1.3 Stimulation light sources

Several light sources, IR diodes, blue LEDs, green laser and IR laser, are equipped with the Risø readers at UOW. Both the IR diodes and laser are used for feldspar stimulation (e.g. Bøtter-Jensen et al., 1991; Spooner et al., 1990), and the blue LEDs and green laser are used for both quartz and feldspar stimulation (Huntley et al., 1985). The IR laser diodes (830±10 nm) are running at 400 mW/cm^2 at the sample. The blue LED units consists of six clusters of LEDs (470±20 nm) running at ~30 mW/cm^2 at the sample (Botter-Jensen et al., 2000).

3.2.3.1.4 Luminescence detection

The luminescence signal emitted from the sample is detected through a Bi-alkali photomultiplier tube (PMT) (EMI9235QA). Optical filters are attached in front of the PMT tube to block scattered stimulation light. The wavelength of the filters are carefully selected to allow only the selected emission band of can reach the PMT, which is based on previous studies on the emission spectrums of various minerals. For quartz OSL, Hoya U-340 filters with peak transmission around 340 nm are commonly used (e.g. Bøtter-Jensen et al., 1994; Huntley et al., 1991). For K-feldspars, a Schott BG-39 filter combined with a Corning 7-59 filter with transmission from 320 to 480 nm are usually used to allow for detecting a violet/blue emission (390-440 nm) (e.g. Huntley et al., 1991; Jungner and Huntley, 1991).

3.2.3.1.5 Single grain system

Conventionally, tens to thousand grains are mounted on a disc and measured simultaneously in a single aliquot method. In this case, the observed results represent an average of all the grains been measured. This may causes problem if the samples contains grains that are contaminated or insufficiently bleached. To avoid this problem, a single-grain technique has been developed (Galbraith et al., 1999; Roberts et al.,

1998; Roberts et al., 1999), in which grains are measured one by one and D_e results are obtained for individual grains. By investigating the variability and distribution of D_e values of individual grains, the single-grain technique can provide information on 1) the extent to which the grains were sufficiently bleached prior to deposition, 2) stratigraphic integrity of deposit that may be affected by post-depositional mixture or bioturbation, and 3) variability in luminescence behaviors among individual grains (Jacobs and Roberts, 2007), which may help to identify and reject poorly behaved grains that may result in erroneous D_e values. Given its advantages for dealing with complex depositional environments, it has been extensively applied to date archaeological sites (Roberts et al., 1998; Roberts et al., 1999; Henshilwood et al., 2002; Feathers, 2003; Jacobs et al., 2003; Duller, 2006; Jacobs et al., 2008; Arnold et al., 2014;).

The Risø single-grain measurement system (Figure 3-9A) is equipped with a green laser (532 nm) and/or an IR laser (Bøtter-Jensen et al., 2003) with a focussed spot of ~20 µm diameter, which is able to precisely locate and stimulate individual grains (Bøtter-Jensen et al., 2000; Duller et al., 1999a; Duller et al., 1999b). Sand-sized mineral grains are mounted onto specially-made aluminium discs (Figure 3-9B), which are drilled with 100 holes on each disc and each hole is 300 µm in diameter and 300 µm deep (Bøtter-Jensen et al., 2000). This allows each hole to hold one single grain of 180–212 µm in diameter or several grains of smaller sizes (e.g., up to 8 grains of 90–125 µm in diameter). In addition to the 100 holes for holding sample grains, three larger holes (500 µm diameter) are drilled in the margin of the disc (Figure 3-9B) as anchor points. To precisely locate and stimulate individual holes, the laser beam at low power (~1-2% of the maximum power) is used to scan the periphery of the disc to find the positions of the three anchor points. The 100 grain holes' coordinates are then precisely determined. The laser beam can then stimulate individual grains one by one with a very negligible cross-talk effect (Duller, 2012a).

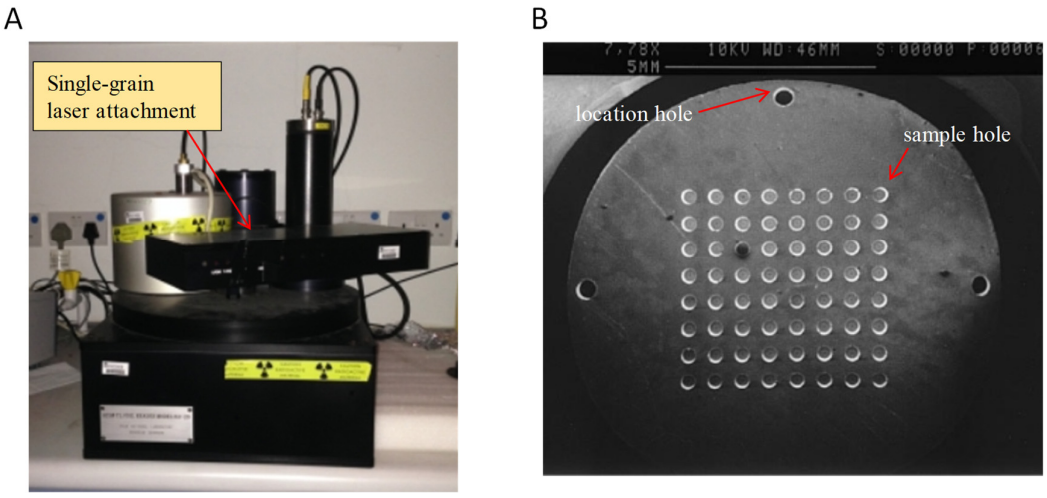

Figure 3-9: (A) Photo showing the single-grain laser sources attached to a Risø reader. (B) A scanning electron microscope image of a sample disc showing the eight by eight grid of 300 µm diameter holes used to hold the grains, and the two 500 µm holes on the periphery, drilled completely through the disc, which are used to locate the disc (Picture from Duller et al. (1999b).

3.2.3.2 Dosimetry measurement facilities

Several techniques and facilities for dosimetry determination have been facilitated at the luminescence dating laboratory of UOW. These include thick-source alpha counting (TSAC) for uranium and thorium, beta-counting for beta dose rate and a portable gamma spectrometer for in-situ gamma dose rate. Other chemical analysis techniques, such as X-ray fluorescence (XRF) and ICP-MS, are also available in the School of Earth and Environmental Sciences of UOW. In this study, both TSAC, beta counting and gamma spectrometer were used and they were introduced below.

3.2.3.2.1 Thick source alpha counting

The TSAC technique is able to detect the alpha particles emitted from the U and Th decay chains (Aitken, 1985; Turner et al., 1958). To determine beta and gamma dose rates from alpha counting requires an assumption of radioactive equilibrium. Alpha counting has the advantage of directly measuring alpha activity, unlike other chemical techniques, such as ICP-MS, which only measures parent concentrations. Three Daybreak 583 Alpha Counters are facilitated and used in this study. Each of the counters is composed of one photomultiplier tube (PMT) (EMI type 6097). About several grams of crushed sample powder is placed on top of a 42mm diameter sprinkling zinc sulphide (ZnS) screen in a plastic holder. The sample holder is placed directly on top of a photomultiplier tube (PMT) (EMI type 6097). The emitted alpha particles bombard the ZnS screen, which can generate scintillations of light that can be recorded and counted by the PMT. To obtain a precise result and reduce errors from counting statistics, at least 2000 counts are needed for each measurement. The counts rate α (counts per 1000 second) can then be converted into dose-rates according to the following conversion factors provided in previous studies (Aitken, 1985):

Alpha dose rate $D_a = 1.285\ \alpha$,

Beta dose rate $D_\beta = 0.072\ \alpha$

Gamma dose rate $D\gamma = 0.083\ \alpha$

3.2.3.2.2 Risø GM-25-5 beta counter

This instrument is designed to measure beta dose rate of a sample. The beta particles emitted from sediment are mainly from U, Th and K. Each beta counter is composed of five Geiger-Mueller (GM) cylindrical detectors (Figure 3-10A). The whole instrument is protected by a 10 cm thick lead shield to reduce the background radioactivity. A guard detector is also designed to detect and reject coincidence counts resulted cosmic ray (Figure 3-10B) (Bøtterjensen and Mejdahl, 1988). For each measurement, three sub-samples of crushed sample powders, one standard sample (Nussi) whose radioactivity (i.e., beta dose rate) is known, and one MgO powder (used as blank) are loaded into plastic sample holders (Figure 3-10C) and counted in the five GM counters simultaneously for at least 24 hours. The beta dose rate from the three sub-samples can be obtained by comparing the raw counts of the standard.

3.2.3.2.3 Portable gamma spectrometer

As mentioned in the last section, gamma rays have a penetration distance of ~30 cm in sediment. It is, therefore, important to make in-situ gamma dose rate measurement for any samples taken from non-uniform stratigraphic layers. One of my study sites, Guanyindong Cave, is such a site that contains complicated sedimentary features (see Chapter 4). We have used an ORTEC digiDART spectrometer to measure the in-situ gamma dose rates for our samples from the site (Figure 3-11A).

This instrument consists of multi-channel analyser consoles, including a 2-inch NaI (TI) detector and a controller. Each detector consists of a NaI (TI) crystal attached to a photomultiplier and sealed inside a stainless-steel cylinder for protection. The cylinder is 57 mm in diameter and 250 mm in length, which is roughly the same size as the OSL tubes used for taking samples. To measure the gamma rays, the detector is placed into the hole left after removing the OSL tubes from the profile. The detector is left in the hole for from 30 min to one hour to measure the energy spectrum of the gamma rays emitted by the sediments surrounding the detector (or the OSL sample). The spectrum is recorded by the controller and can be downloaded to a computer for conversion to an estimate of gamma dose rate (Figure 3-11B). Calibration of the detectors using standards of known radioactivity is performed using the doped concrete blocks at the Oxford University. The gamma dose rates were determined using the 'threshold' technique (Mercier and Falguères, 2007).

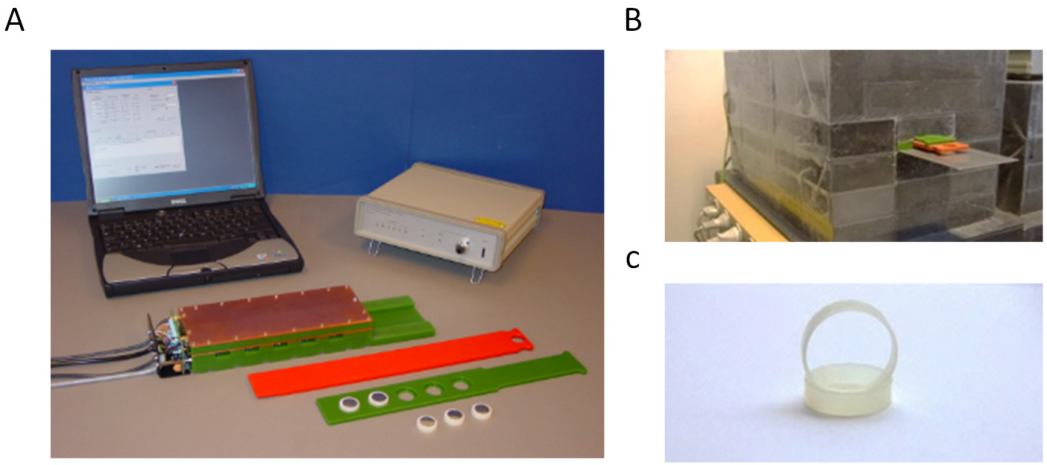

Figure 3-10: Photo showing the Risø GM-25-5 beta counter used in this study (photos from the Risø product website: https://www.nutech.dtu.dk/english/products-and-services/radiation-instruments/gm_multicounter*). (A) Photo showing the sample loading devices for five detectors. (B) Photo showing the lead shield of the beta counter. (C) Photo of the sample holder.*

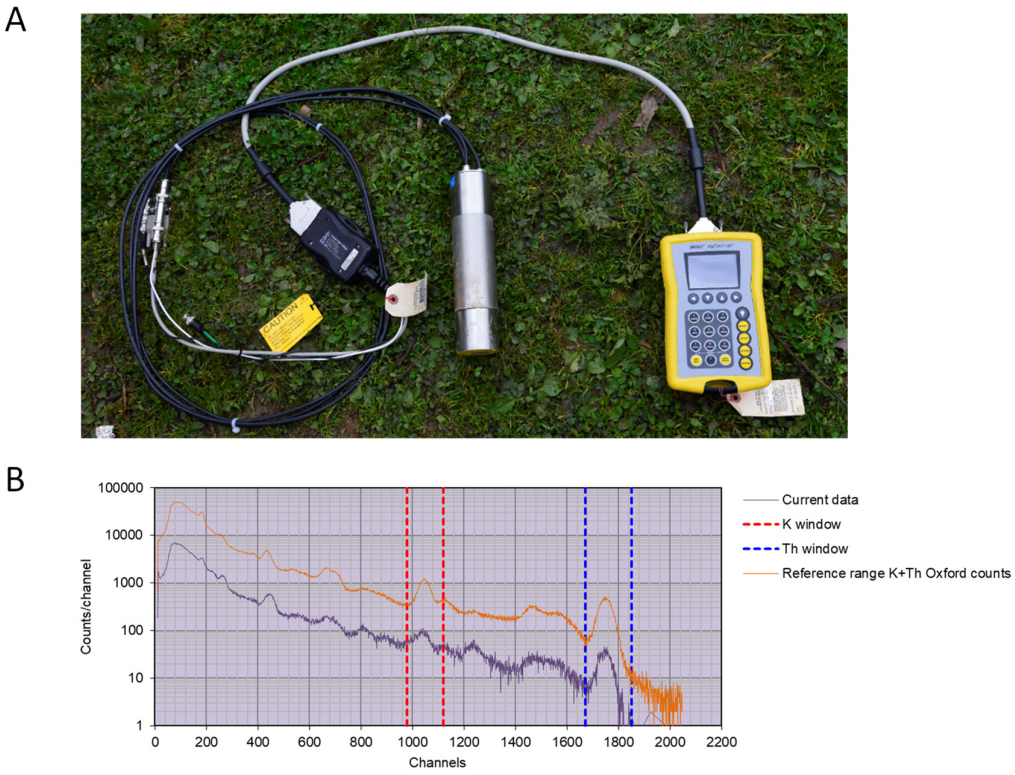

Figure 3-11: (A) Photo showing the ORTEC digiDART gamma spectrometer used in this study. (B) Energy spectrum for one of sample GYD-OSL1 from the Guanyindong site.

Chapter 4: Chronology of the Guanyindong site

The content of this chapter is based on the article published in *Nature* in 2019 (see Appendix B). Some changes have been made for purpose of including it in this thesis, such as excluding the descriptions of the background of the site, sample preparations, instrument description, etc., which have been presented in Chapters 1–3.

Hu, Y., Marwick, B., Zhang, J.-F., Rui, X., Hou, Y.-M., Yue, J.-P., Chen, W.-R., Huang, W.-W., Li, B., 2019. Late Middle Pleistocene Levallois stone-tool technology in southwest China. Nature 565, 82–85.

4.1 Previous chronological studies on Guanyindong site

There were a few attempts to date the Guanyindong site since 1980s. The first dating work was conducted by Yuan et al. (1986) using U-series dating on fossil teeth recovered directly from the stratigraphy units of site. In their study, a total of 6 fossil teeth were dated, including one from Layer 2 (Group A), one from Layer 4, three from Layer 5 and one from Layer 8 (). Given the complexity and difficulty of quantifying uranium migration into and out of skeletal tissues, the U-series results on bones and teeth should be regarded as minimum age estimates (Grün et al., 2014). The age of the fossil tooth from Layer 2 is 55 ± 3 ka, hence, providing a minimum estimate for the age of Group A. The other ages obtained for the fossil teeth from Group B range from ~75 to ~120 ka, placing a minimum age of ~120 ka for the Layer 4 and those below.

The second atempt was conducted by Shen and Jin (1992), based on U-series dating on carbonate and fossil teeth. In their study, samples were taken from three locations (named Profiles 1, 2a and 3 by Pei et al. (1965)) inside the cave (Figure 4-1). Profile 1 is located at the cave entrance, where the main excavation was conducted and most of the stone tools were discovered. Profiles 2a and 3 are two of the earliest test pits excavated by Pei et al. (1965) in 1960s located further inside the cave, where very few artefacts (~100 stone artefacts) were found and many of them were collected from the surface. Since the artefacts excavated inside the cave are not analysed in this study, only the results of the samples from the cave entrance reported in Shen and Jin's study is discussed.

A total of 8 samples were collected by Shen and Jin (1992) from the cave entrance (Figure 4-1). The first two samples (QGC-19-1 and QGC-19-2) were taken from the bottom tip of a hanging stalactite, yielding ages of 58 ± 3 and 42 ± 2 ka, respectively. The authors claimed that this stalactite "*has sign of residual red clay on the bottom surface*", indicating that this stalactite was in contact with the red-clay deposits from Layer 2 and, hence, should provide a maximum age estimate for Layer 2. However, this age is younger than the age ~55 ka of the fossil tooth extracted in-situ from Layer 2 reported by Yuan et al. (1986); the latter, however, should be viewed as a minimum age of Layer 2. Furthermore, according to the stratigraphic description by Li (1986) (see Figure 2-2B), the deposits of Layer 2 terminated outside the cave, so the 'red-clay attachement' on the stalactite should not be linked to the Layer 2, and, therefore, the its age should not be used to constrain the age of Layer 2. The OSL age of ~80 ka for the Layer 2 (see the next section) also confirm that their age estimates for Layer 2 are underestimated.

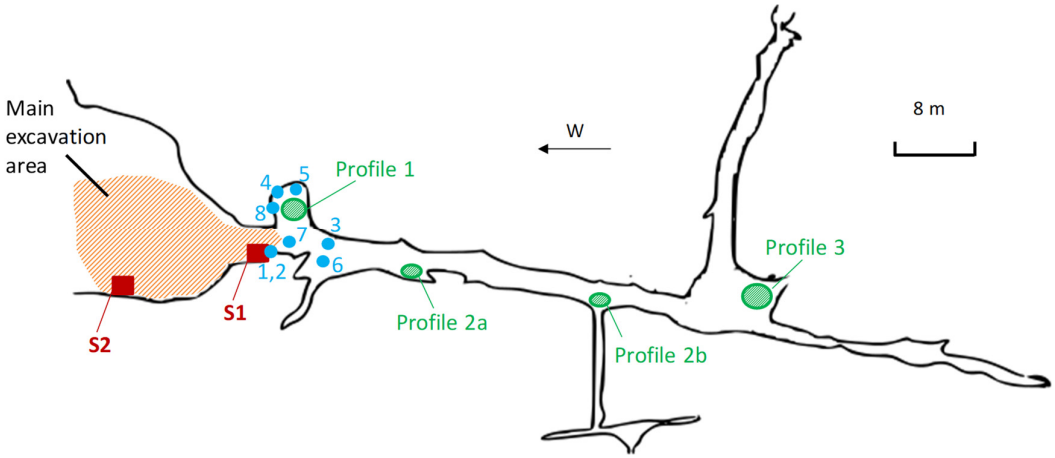

Figure 4-1: Plan view of the Guanyindong Cave, main excavation area and the residual profiles from the south wall. The blue dots and the numbers next to each of them represent the locations of U-series dating samples taken by Shen and Jin (see Chapter 4 for discussion of the U-series results); sample codes from 1 to 8 are QGC-19-1, QGC-19-2, QGC-4, QGC-21, QGB-4, QGC-7 and QGC-23, respectively. The green circles are the location of Profile 1, 2a, 2b and 3. The red squares show the locations of the residual profiles S1 and S2 where OSL samples were taken.

Table 4-1. Summary of dating results for different stratigraphic layers. The ages were obtained from samples that have reliable stratigraphic age control and associated dating methods. Note that the U-series ages of fossils should be regarded as minimum age estimates.

Layer	**Age (ka) / Method / Reference**
1	40–70 (OSL on 3 sediment samples) (this study)
Group A	
2	57 ± 3 (U-series on a rhinoceros tooth) (Yuan et al., 1986)
	87 ± 3 (weighted mean of 4 OSL samples) (this study)
Group B	
3	Not dated
4	119 ± 10 (U-series on a unknown fossil tooth) (Yuan et al., 1986)
	163 ± 12 (weighted mean of 2 OSL samples) (this study)
5	84 ± 5 (U-series on a *Bovinae* tooth) (Yuan et al., 1986)
	76 ± 4 (U-series on a unknown fossil tooth) (Yuan et al., 1986)
	104 ± 6 (U-series on a rhinoceros tooth) (Yuan et al., 1986)
	163 ± 12 (OSL on sediment) (this study)
6	73 ± 3 (U-series on a rhinoceros tooth) (Shen and Jin, 1992)
	181 ± 16 (U-series on stalagmite) (Shen and Jin, 1992)
	175 ± 32 (OSL on sediment) (this study)
7	167 ± 12 (OSL on sediment) (this study)
8	115 ± 7 (U-series on a *Cervidae* tooth) (Yuan et al., 1986)
	169 ± 14 (OSL on sediment) (this study)
Group C	
9	260 ± 30 (U-series on stalagmite) (Shen and Jin, 1992)

The third sample (QGC-4) is a piece of broken stalactite sitting on top of "*some residual deposits*" at the north wall, which yielded an age of >350 ka, so it should not be linked as any stratigraphic unit of the site. The fourth sample (QGC-12) is "*a piece of flowstone sitting on top of some residual deposits attached to the north wall of the cave*". This sample yielded an age of 52 ± 2 ka. According to Shen and

Jin, this sample has the same elevation as the Layer 4, so they regarded this age as an estimate of the age of Layer 4. However, this age is significant younger than the minimum age (~119 ka) obtained from the fossil teeth directly taken from Layer 4 reported by Yuan et al. (1986), suggesting that the correlation of the sample and Layer 4 simply based on their elevation is unreliable.

The fifth sample (QGC-21) is a piece of carbonate 'curtain' taken on the north wall but a few tens of centimeters below QGC-12. This sample yielded an age of 147 ± 14 ka. Given the failed correlation of the overlying sample QGC-12 as mentioned above, the stratigraphic location of QGC-12 remains unclear. The sixth sample (QGB-4) is a rhinoceros tooth recovered from the Layer 6 from the residual sediment profile at the south wall (where our OSL samples were taken). The age of this sample is 73 ± 3 ka, and should be viewed as a minimum age for this layer. The seventh sample (QGC-7) is "*a small piece of stalagmite sitting on top of the flowstone from Layer 6*" of the residual profile at the south wall. The age of this sample is 185 ± 15 ka, providing a reliable constraint of the age for this layer. The last sample (QGC-23) is an in-situ stalagmite from the bottom of the profile at the north wall, which yielded an age of 260 ± 30 ka. This age should provide a reliable constraint of the maximum age for Layer 8 or Group B.

In conclusion, previous U-series dating on fossil teeth and carbonate have provided controversial results, mainly because many of the carbonate samples analysed are lack of firm stratigraphic control. As a result, only those samples with a reliable stratigraphic control can provide useful constraints on the chronological framework of this site (Table 4-1). For this reason, all of the U-series ages of fossil teeth extracted directly from sediments should be viewed as minimum ages for the associated layers, and only one stalagmite sample (QGC-7) taken directly from Layer 6 from the residual profile at the south wall yielded reliable age estimate for this layer.

4.2 OSL dating

In order to confirm the age of the Guanyindong assemblage, OSL dating was applied to determine the ages of the deposits from Layer 1, Layer 2 (Groups A) and Layer 3-8 (Group B) (Figure 2-2B).

4.2.1 Sample description and preparation

A total of 13 sediment samples were collected for OSL dating from two residual profiles (S1 and S2) at the south-wall of the cave entrance (Figure 2-2), including 3 samples from Layer 1 at S1, 4 from Layer 2 at S2, 2 from Layer 4 at S1 and 1 from each of the layers 5–8 at S1 (Figure 2-3 and Figure 2-3). No sample was taken from Layer 3, because suitable materials could not be found for dating from S1 (Figure 2-3). The samples were collected by hammering opaque plastic tubes, each about 5 cm in diameter and ~25 cm long, into the cleaned section face. The tubes were sealed in black plastic bags for safe transport. Apart from the tubes, additional sediment at each sample location was collected and placed in plastic zip-lock bags for measuring their current moisture contents and radioactivity.

The samples were prepared using the procedure described in Chapter 3. All the samples were dominated by silt (<63 μm), and a limited amount of 180–212 μm quartz grains were extracted from our samples.

So apart from the limited number of 180–212 μm grains, the D_e using smaller grains (in the range of 90–180 μm) for each sample were also determined.

4.2.2 Dose rate and measurement facilities

The environmental dose rate for etched quartz is due mainly to beta and gamma radiation, from the decay of ^{238}U, ^{235}U, ^{232}Th (and their daughter products) and ^{40}K in the deposits surrounding the dated grains, and cosmic rays. Beta dose rates were measured directly by low-level beta counting (see Chapter 3 for details). Gamma dose rates were measured at each sample location by an *in situ* gamma spectrometer, to take account of any spatial heterogeneity in the gamma radiation field within 30 cm of each OSL sample. To accommodate the gamma detector, after removing the plastic sample tubes we further drilled the holes to a depth of 30 cm using a hand auger. A two-inch probe was inserted into the hole, and counts were collected for 30 min. The cosmic-ray dose rates were estimated following Prescott and Hutton (1994), based on the geomagnetic latitude and altitude of Guanyindong site, as well as the thickness of sediment above each sample. Since our samples were collected from the cave entrance, the overhead limestone shielding and the configuration of the cave were taken into account, by making a correction for the zenith angular distribution of cosmic rays (Smith et al., 1997). A relative uncertainty of 10% was assigned to account for the systematic uncertainty in the primary cosmic-ray intensity. Since the cosmic ray constitutes only 1–5% of the total dose rate for these samples (Table 4-2), the OSL ages are not highly sensitive to errors associated with the cosmic-ray dose rate.

Each of the measured beta and gamma dose rates and the calculated cosmic-ray dose rate were corrected for attenuation by water. For the samples from profile S1, the measured water contents of the 6 samples from Group B range from 20% to 24% (with a mean value of 22%) (Table 4-1), but lower values (11–17%) were obtained for the 3 samples from Layer 1. In contrast, higher values (28–32%) were found for all the samples taken from Group A at profile S2. The difference in the water contents between the two profiles is expected as S1 has been exposed for several decades after the last excavation in 1970s, so the measured present-day water contents should be underestimated. In contrast, S2 was protected by stones and covered by vegetation, which should retain water content better than S1. It is, therefore, expected that the water content obtained from S2 should be more representative to the long-term water content for S1. In order to assess the water content more reliably, additional sedimentary samples from two of the original trenches (Profile 2a and 3) inside the cave, where moisture contents are also better retained, were taken. For the 15 samples (with burial depth ranging from ~50 to ~300 cm) measured, their water contents range from 15 to 40%, and the mean and standard deviation are 30% and 8.5% respectively. So, instead of using the in-situ water content, a value of 30% was used as an estimate of the long-term water content for our OSL samples from Groups A and B and a value of 20% for those from Layer 1. A 25% relative standard error was assigned to these estimates, in order to accommodate any likely variations of water content over the burial period. It is noted that the measured in-situ water contents are within the 2 sigma range of the assumed values.

Table 4-2. Dose rate data, equivalent doses (D_e) and OSL ages for sediment samples from the Guanyindong site.

Sample	Layer / Group	Depth (cm)	Grain size (μm)	Water content (%) [a]	Gamma dose rate (Gy/ka)	Beta dose rate (Gy/ka)	Cosmic dose rate (Gy/ka) [b]	Total dose rate (Gy/a)	D_e (Gy) [c]	Age (ka) [c]	Final age (ka) [c,d,e]
S1											
GYD-OSL7	1	10	90–125	20 ± 5 (17)	0.97 ± 0.03	0.99 ± 0.05	0.031	2.00 ± 0.05	81 ± 4	41 ± 2	41 ± 2
GYD-OSL8	1	50	90–125	20 ± 5 (14)	0.89 ± 0.02	1.18 ± 0.09	0.030	2.10 ± 0.09	99 ± 4	47 ± 3	47 ± 3
GYD-OSL9	1	75	90–125	20 ± 5 (11)	0.60 ± 0.02	1.04 ± 0.08	0.027	1.66 ± 0.08	115 ± 5	69 ± 5	69 ± 5
GYD-OSL1	4/B	210	90–150	30 ± 8 (20)	0.59 ± 0.05	0.69 ± 0.04	0.024	1.30 ± 0.07	208 ± 14	160 ± 14	161 ± 12
			180–212		0.59 ± 0.05	0.66 ± 0.04	0.024	1.28 ± 0.07	211 ± 27	165 ± 23	
GYD-OSL2	4/B	235	90–125	30 ± 8 (21)	0.39 ± 0.04	0.89 ± 0.06	0.023	1.30 ± 0.07	224 ± 18	173 ± 17	165 ± 12
			180–212		0.39 ± 0.04	0.84 ± 0.06	0.023	1.25 ± 0.07	198 ± 16	158 ± 15	
GYD-OSL3	5/B	245	90–125	30 ± 8 (24)	0.44 ± 0.04	0.97 ± 0.06	0.023	1.43 ± 0.08	237 ± 13	165 ± 13	163 ± 12
			180–212		0.44 ± 0.04	0.92 ± 0.06	0.023	1.38 ± 0.08	206 ± 42	149 ± 32	
GYD-OSL4	6/B	260	90–180	30 ± 8 (23)	0.49 ± 0.04	1.16 ± 0.08	0.022	1.67 ± 0.09	292 ± 50	175 ± 31	175 ± 32
GYD-OSL5	7/B	270	90–180	30 ± 8 (20)	0.42 ± 0.04	0.89 ± 0.06	0.022	1.34 ± 0.07	224 ± 12	167 ± 12	167 ± 12
			180–212		0.42 ± 0.04	0.87 ± 0.06	0.022	1.31 ± 0.07	217 ± 36	166 ± 29	
GYD-OSL6	8/B	290	90–180	30 ± 8 (20)	0.42 ± 0.04	0.54 ± 0.03	0.022	0.99 ± 0.05	168 ± 12	170 ± 14	170 ± 14
S2											
GYD-OSL10	2/A	80	90–125	30 ± 8 (28)	1.25 ± 0.03	1.59 ± 0.10	0.132	2.96 ± 0.11	272 ± 11	92 ± 5	92 ± 5
GYD-OSL11	2/A	95	90–125	30 ± 8 (32)	1.04 ± 0.02	1.54 ± 0.11	0.126	2.70 ± 0.11	201 ± 24	75 ± 9	75 ± 9
GYD-OSL12	2/A	120	90–125	30 ± 8 (31)	0.87 ± 0.02	1.28 ± 0.09	0.120	2.28 ± 0.09	202 ± 17	89 ± 8	89 ± 8
GYD-OSL13	2/A	190	90–125	30 ± 8 (30)	1.11 ± 0.02	1.36 ± 0.10	0.108	2.57 ± 0.10	214 ± 16	83 ± 7	83 ± 7

[a] Values used for dose rate and age calculations, with measured (field) water contents shown in parentheses.
[b] Values after correction for the zenith angular distribution of cosmic rays.
[c] The uncertainties provided after the ± symbol represent the uncertainty at 1σ.
[d] A systematic error of 2% was added (in quadrature) to the propagated random errors in the final ages to allow for any bias associated with the calibration of the laboratory beta sources.
[e] For samples with two grain sizes measured, their final ages were obtained based on the weighted mean of the ages obtained from each of the two grain sizes.

OSL measurements were made on an automated Risø TL-DA-20 luminescence reader (see Chapter 3 for details). All the quartz OSL measurements were made by mounting the grains onto standard Risø single grain discs, where each grain hole contained 1 grain of 180–212 μm in diameter, or about 8 grains of 90–125 μm in diameter. Spatial variation in the dose rate for individual grain positions was calibrated using gamma-irradiated quartz standards from the instrument manufacturer Risø. The ultraviolet OSL emissions were detected by an Electron Tubes Ltd 9235QA photomultiplier tube fitted with Hoya U-340 filters.

4.2.3 SAR performance test

All OSL measurements were made using a single-aliquot regenerative-dose (SAR) procedure (Galbraith et al., 1999; Murray and Wintle, 2000). The SAR procedure involves measuring the OSL signals from the natural (burial) dose and from a series of regenerative doses, each of which was preheated at 240°C for 10 s prior to optical stimulation by the green laser beam for 2 s at 125°C. A fixed test dose (~16 Gy) was given after each natural and regenerative dose, with the induced test dose OSL signals used to correct for any sensitivity changes during the SAR sequence. A cut heat to 180°C was applied to the test dose. A duplicate regenerative dose was included in the procedure, to check on the validity of sensitivity correction, and a 'zero dose' measurement was made to monitor the extent of any 'recuperation' or 'thermal transfer' induced by the 240°C preheat. As a check on possible contamination from feldspars, the OSL IR depletion-ratio test (Duller, 2003) at the end of the SAR sequence, using an infrared bleach of 40 s at 50°C, was applied.

In order to test whether the SAR procedure is suitable for our samples, a dose recovery test was conducted on sample GYD-OSL2 using different combinations of preheat/cut heat (260/180, 240/180, 220/180, 200/160 and 180/160 °C) temperatures. Two single-grain discs were measured for each preheat temperature using the grains of 90–125 μm diameter. The grains were bleached for ~30 min using a Dr Hönle solar simulator (model: UVACUBE 400). The bleached grains were then given a dose of ~100 Gy, before being measured using the SAR procedure using different preheat and cut-heat temperatures. To select reliable single-grain D_e results, several rejection criteria similar to those proposed by Jacobs et al. (2006a) were applied. Grains were rejected if they exhibited one or more of the following properties: (1) Test-dose signal (T_n) too dim, i.e., the initial intensity is below the instrument detection limit (3σ below the background intensity) and/or the relative standard error (RSE) on the test dose measurement was more than 20%. (2) High levels of recuperation (i.e., the ratio between the sensitivity-corrected OSL signals for the zero dose and the largest regenerative dose is higher than 5%). (3) Poor dose response curve (DRC), i.e., the regenerative signals are too scattered to be well-fitted with suitable functions (e.g., a linear or saturating exponential function); note that poor recycling ratio falls into this category. To assess the goodness-of-fit of the DRCs, the figure-of-merit (FOM) and reduced-chi-square (RCS) values were applied (Peng and Li, 2017; Peng et al., 2016), which are defined as follows:

$$FOM\,(\%) = 100 \times \frac{\sum_{i=1}^{n} | y_i^o - y_i^f |}{\sum_{i=1}^{n} y_i^f} \quad (1)$$

and

$$RCS = \frac{1}{N-n} \times \sum_{i=1}^{n} \frac{(y_i^o - y_i^f)^2}{\sigma_i^2} \quad (2)$$

where y_i^o and y_i^f denote the i^{th} observed and fitted values, respectively, N and n denote the number of observations and fitted model parameters, respectively, and σ_i is the standard error for the i^{th} observation. Both FOM and RCS provide quantitative measures of the extents of scatter of data points from the best-fit curves. Upper limits of 10% for the FOM and 5 for the RCS criteria, as recommended by Peng and Li (2017), were used, which have been shown to be able to select grains with satisfactory DRCs; (4) Natural OSL signal statistically equal to or greater than the saturation level of the corresponding dose response curve.

From 39 to 64 grains were accepted for each of the preheat temperatures after applying the above rejection criteria. The measured to given dose ratios (or dose recovery ratios) are summarised as radial plots in Figure 4-2A–E for each of the preheat temperatures, respectively. The central age model (CAM) (Galbraith et al., 1999) was applied to calculate the weighted mean recovery ratios for each preheat temperature, and these were shown in each of the radial plots (Galbraith and Roberts, 2012; Galbraith et al., 1999). The dose recovery results were plotted against the preheat temperature in Figure 4-2F. It is shown that the mean ratios are statistically consistent with unity at 1σ for the preheat temperatures at 220, 240 and 260°C, which suggests that the chosen SAR procedures can accurately recover a known dose under these conditions.

4.2.4 D_e determination

Based on the dose recovery tests, the preheat/cutheat of 240/180°C was chosen for measuring D_e values for all the samples. Figure 4-2G and H show the natural OSL decay curves of 10 grains from each of the two samples GYD-OSL2 and GYD-OSL6. Based on the measurements from the 180–212 μm diameter grains, it was found that the OSL intensity varies significantly from grain to grain, and most (~90%) of the grains yielded no OSL signal at all (or their signal intensity is below the instrumental limit of detection); fewer than 5% of the measured single grains contributes >90% of the total OSL signal (Figure 4-2I). Apart from the OSL intensity, the dose response curves from different grains also display a wide range of shapes associated with different saturation doses (e.g., Figure 4-3A).

Depending on the availability of separated grains, from 800 to 4200 grains of 180–212 μm diameter were measured for GYD-OSL1, 2, 3, 5 and 6, respectively (Table 4-3). However, only about 2% of measured grains could pass the rejection criteria described above, and about 90% of the grains were rejected due to signals being too weak. For this reason, smaller grains in the range of 90–180 μm were measured for all the samples. For the measurement of small grain size (< 180 μm diameter) fractions, each grain-hole of the standard single-grain disc may contain several grains (e.g., up to 8 grains of 90–125 μm diameter), which makes our measurements equivalent to small aliquot that contains a few grains only. There are several advantages of measuring smaller grains. First, several grains were measured together in each of the holes, so there is a higher probability to find a bright grains in each hole, which can save the

instrumental time considerably. Second, because of the low percentage (< 5%) of bright grains in our samples, the measured OSL signal from each of the grain holes are expected to be dominant by those from only one or two grains, thereby effectively making these measurements equivalent to single-grain measurements. This is further confirmed by the similar results obtained from the 180–212 µm diameter grains and smaller grains (Table 4-2). Using this method, from 500 to 1400 'small-aliquots' were measured for each of the samples (Table 4-3). As expected, the percentage of aliquots that have detectable OSL signals was significantly increased, ranging from 18% to 55%. About 20% of the small aliquots produced more than 80% of the total OSL signal (Figure 4-2I). Correspondingly, the proportion of grains that pass the rejection criteria was considerably increased (Table 4-3).

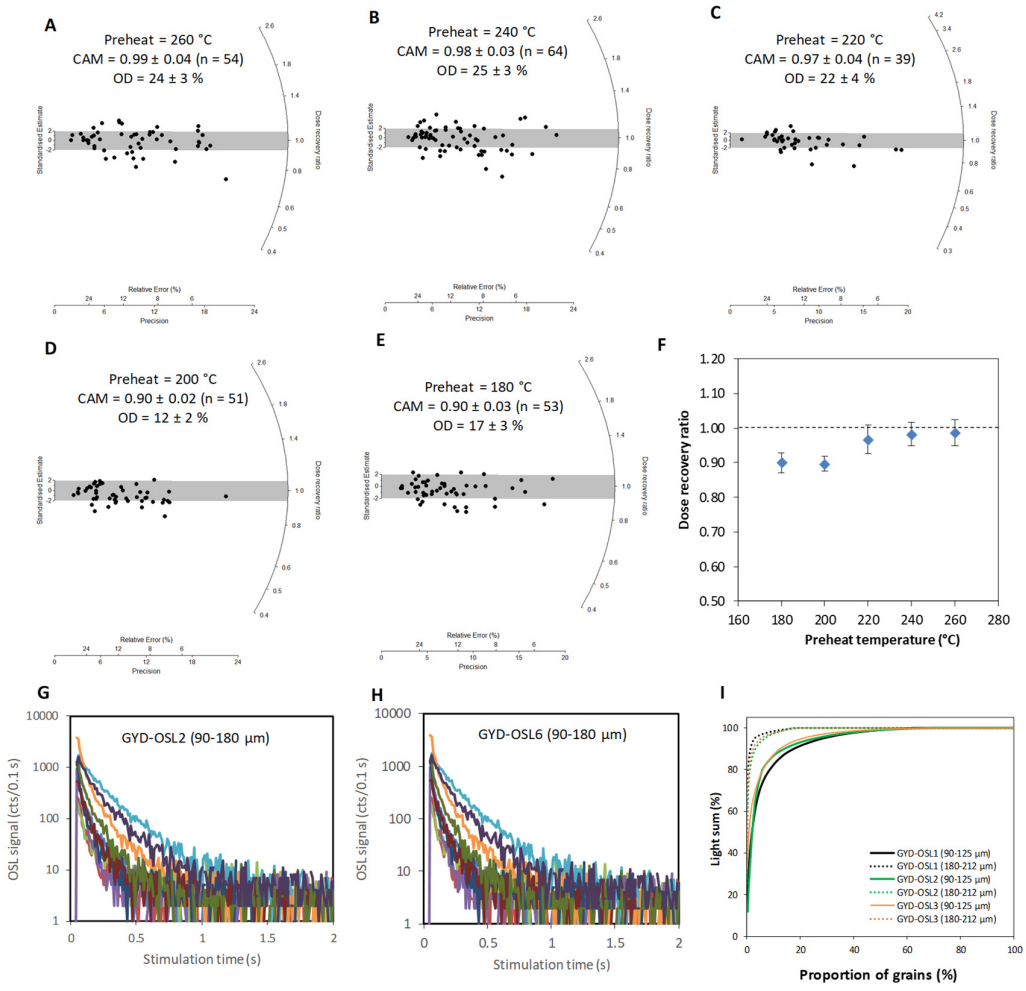

Figure 4-2: Dose recovery results and luminescence characteristics. (A–E) Radial plots showing the distributions of dose recovery ratios for individual grains from GYD-OSL2 for different preheat temperatures (from 260 to 180 °C, respectively) and the corresponding CAM and OD values. (F) The weighted mean dose recovery ratio plotted against preheat temperature. The vertical bars represent 1σ standard error. (G–H) Selected typical natural OSL decay curves of 10 grains from each of samples GYD-OSL2 and -OSL6, respectively. (I) Distribution of OSL signal intensities of individual quartz grains of different grain sizes from GYD-OSL1, -OSL2 and -OSL3. Data are plotted as the proportion of the total light sum that originates from the specified percentage of grains.

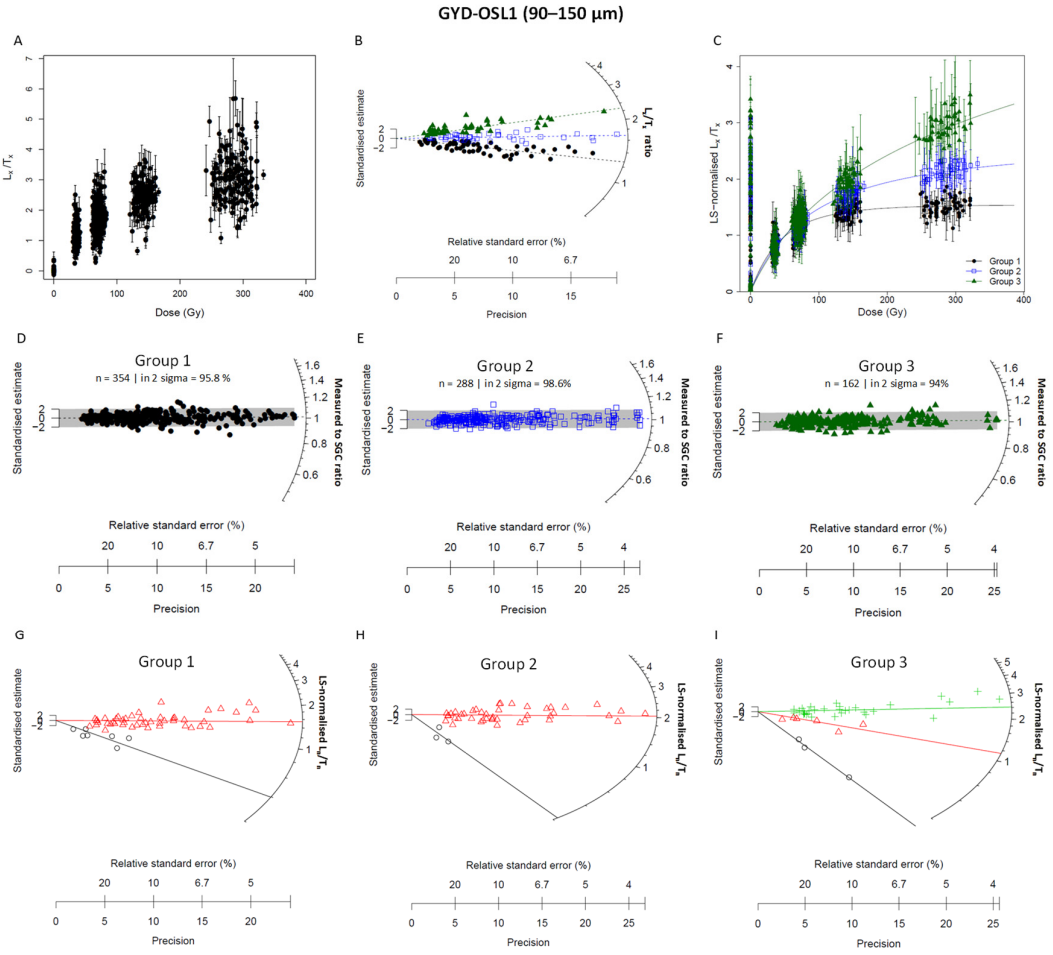

Figure 4-3: Single-grain DRCs and SGC results for the 90–150 µm grains of GYD-OSL1. (A) Comparisons of all the DRCs that pass the rejection criteria. (B) Radial plot showing the distribution of the ratios of L_x/T_x values between two regenerative doses of ~280 and ~70 Gy for all the accepted grains. Different symbols represent different groups of grains identified using FMM. (C) Comparison of the LS-normalised L_n/T_n and L_x/T_x for different groups. The data set for each group were fitted using a GOK function (full lines) and then normalised to unity at 50 Gy. (D–F) Radial plots showing the ratios between the LS-normalised L_x/T_x and the expected values from the best-fit SGC shown in (C); the shaded band captures 2σ range from unity. The total number of grains (n) and percentage falling inside the 2σ band are shown for each group. (G–I) Radial plots showing the LS-normalised natural signals (L_n/T_n); different age groups were identified using FMM and distinguished using different symbols. The full lines represent the central values of individual groups obtained using FMM. All the figures and data analysis were based on the building functions in R packages "Luminescence" (Kreutzer et al., 2012) and "numOSL" (Peng and Li, 2017).

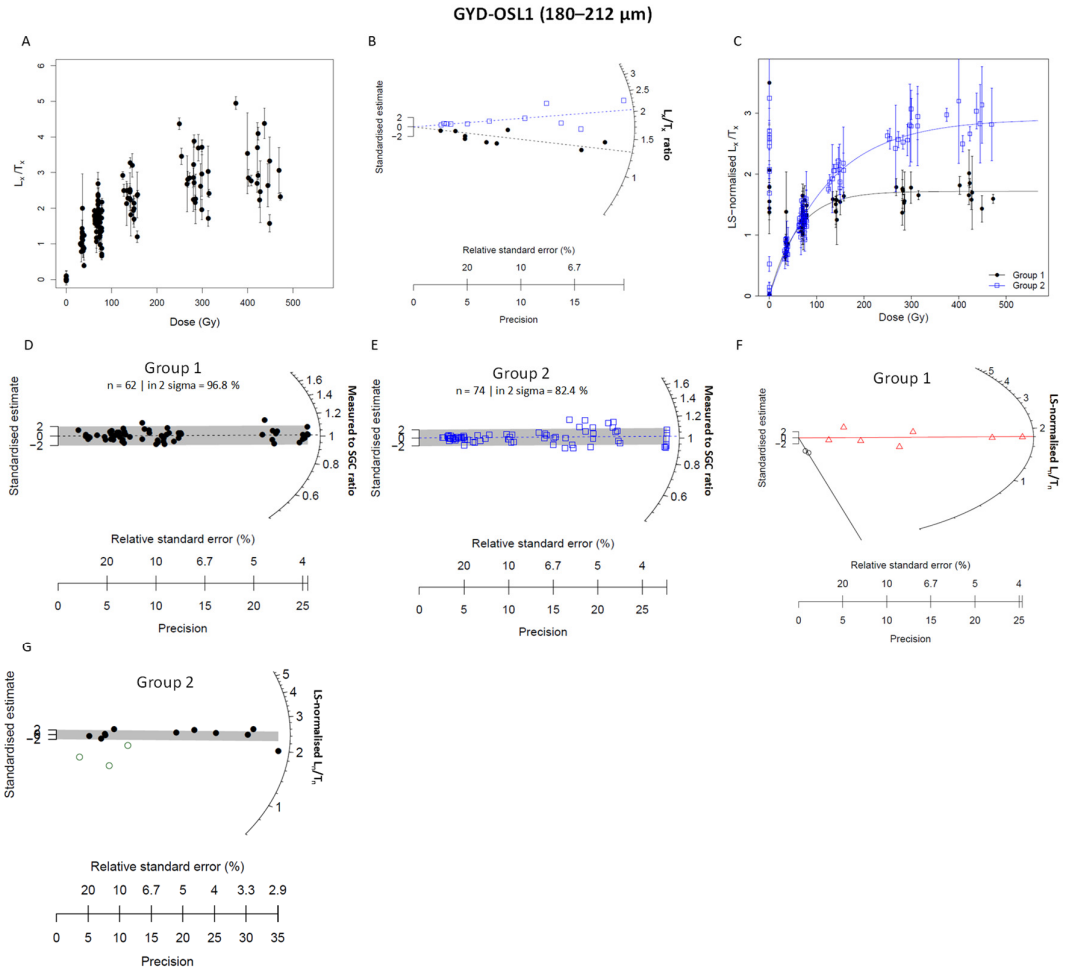

Figure 4-4: Single-grain measurement results for the 180–212 µm fraction of GYD-OSL1. (A–C) Results similar to those described in Figure 4-3A–C. (D–E) Results similar to those described in Figure 4-3D–F. (F) Results similar to those described in Figure 4-3G–I. (G) Radial plots showing the LS-normalised natural signals (L_n/T_n) for group 2; this distribution contains a small number of intrusive grains (open circles) identified as outliers using nMAD, so only the data points shown in filled circles were included in the final weighted mean L_n/T_n value calculated using the CAM.

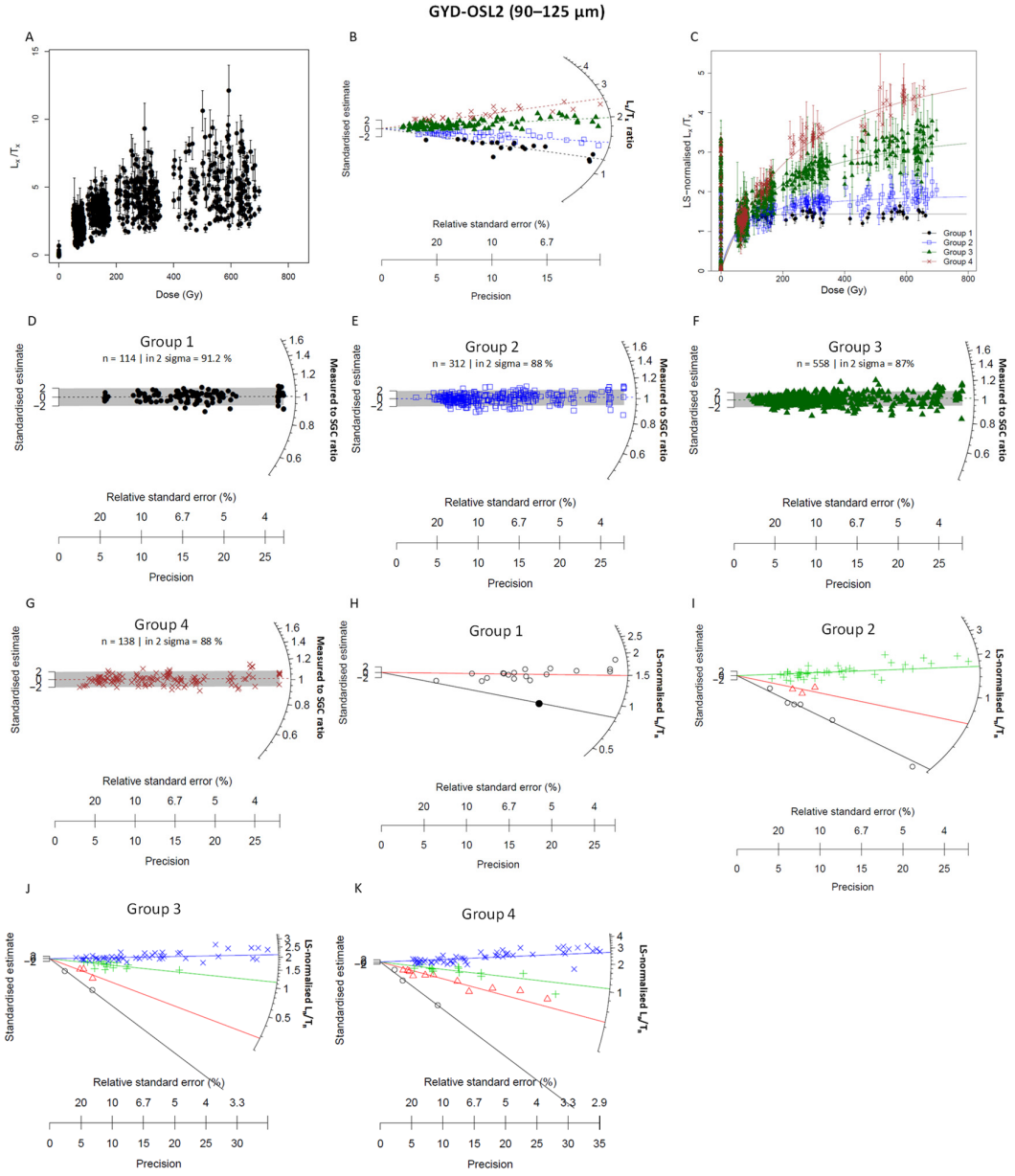

Figure 4-5: Single-grain measurement results for the 90–125 µm fraction of GYD-OSL2. (A–C) Results similar to those described in Figure 4-3A–C. (D–G) Results similar to those described in Figure 4-3D–F. (H–K) Results similar to those described in Figure 4-3G–I.

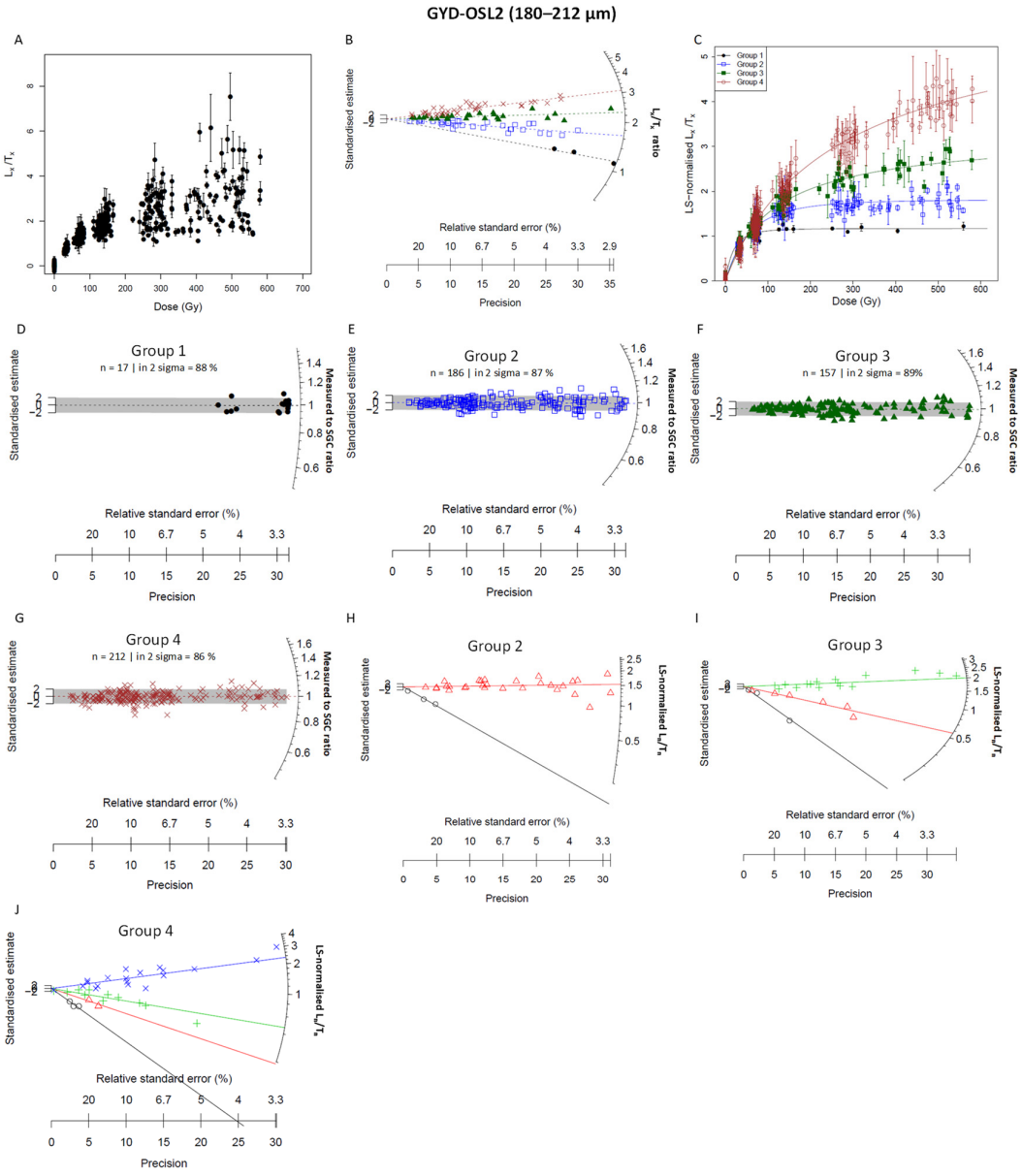

Figure 4-6: Single-grain measurement results for the 180–212 µm fraction of GYD-OSL2. (A–C) Results similar to those described in Figure 4-3A–C. (D–G) Results similar to those described in Figure 4-3D–F. (H–J) Results similar to those described in Figure 4-3G–I. Note that only 3 grains were identified as group 1 and all are 'modern' grains, so their natural signals are not plotted here.

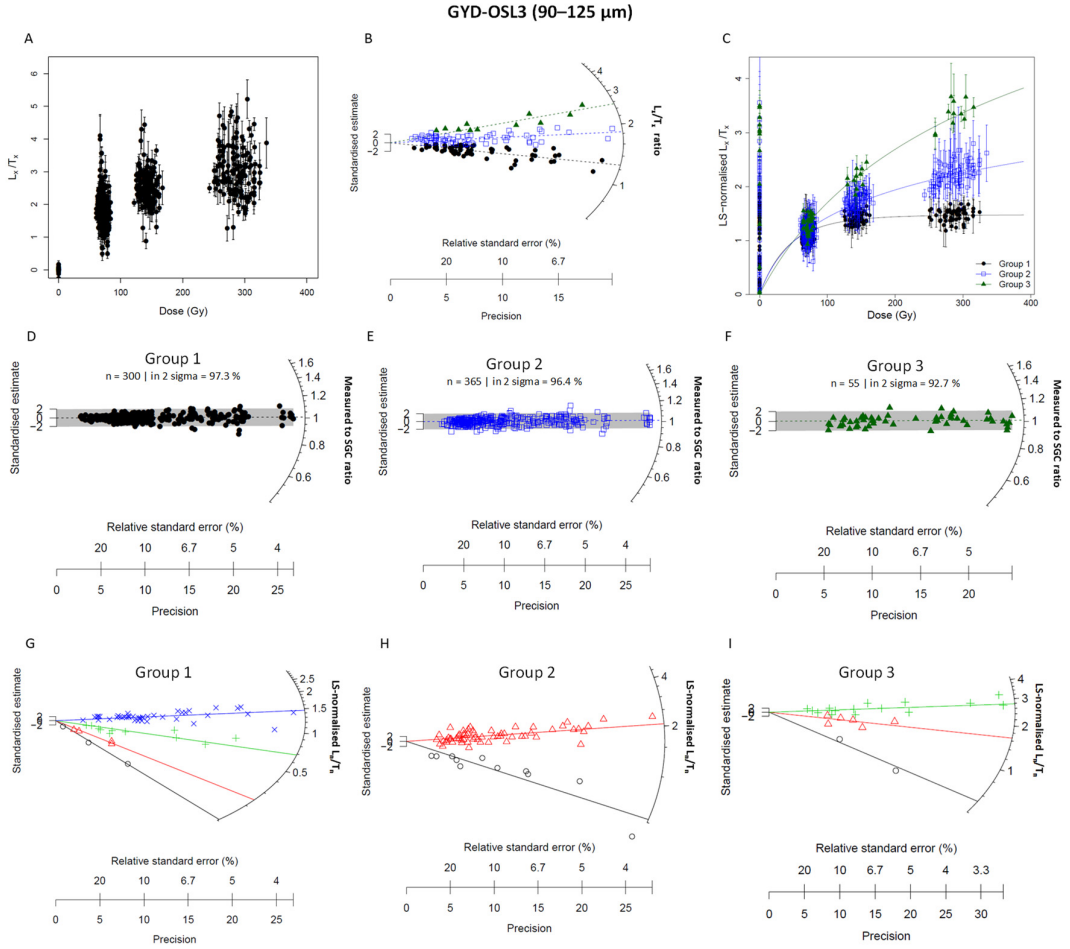

Figure 4-7: Single-grain measurement results for the 90–125 µm fraction of GYD-OSL3. (A–C) Results similar to those described in Figure 4-3A–C. (D–F) Results similar to those described in Figure 4-3D–F. (G–I) Results similar to those described in Figure 4-3G–I.

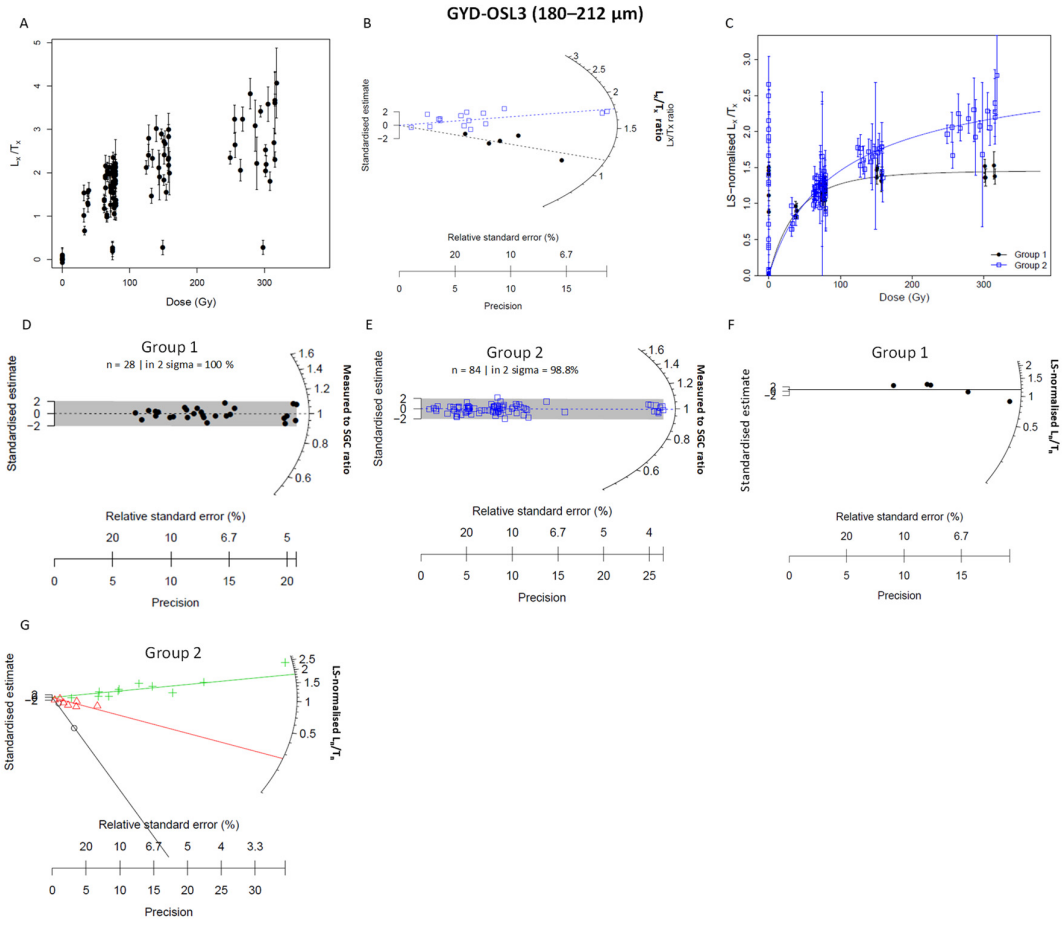

Figure 4-8: Single-grain measurement results for the 180–212 µm fraction of GYD-OSL3. (A–C) Results similar to those described in Figure 4-3A–C. (D–E) Results similar to those described in Figure 4-3D–F. (F–G) Results similar to those described in Figure 4-3G–I.

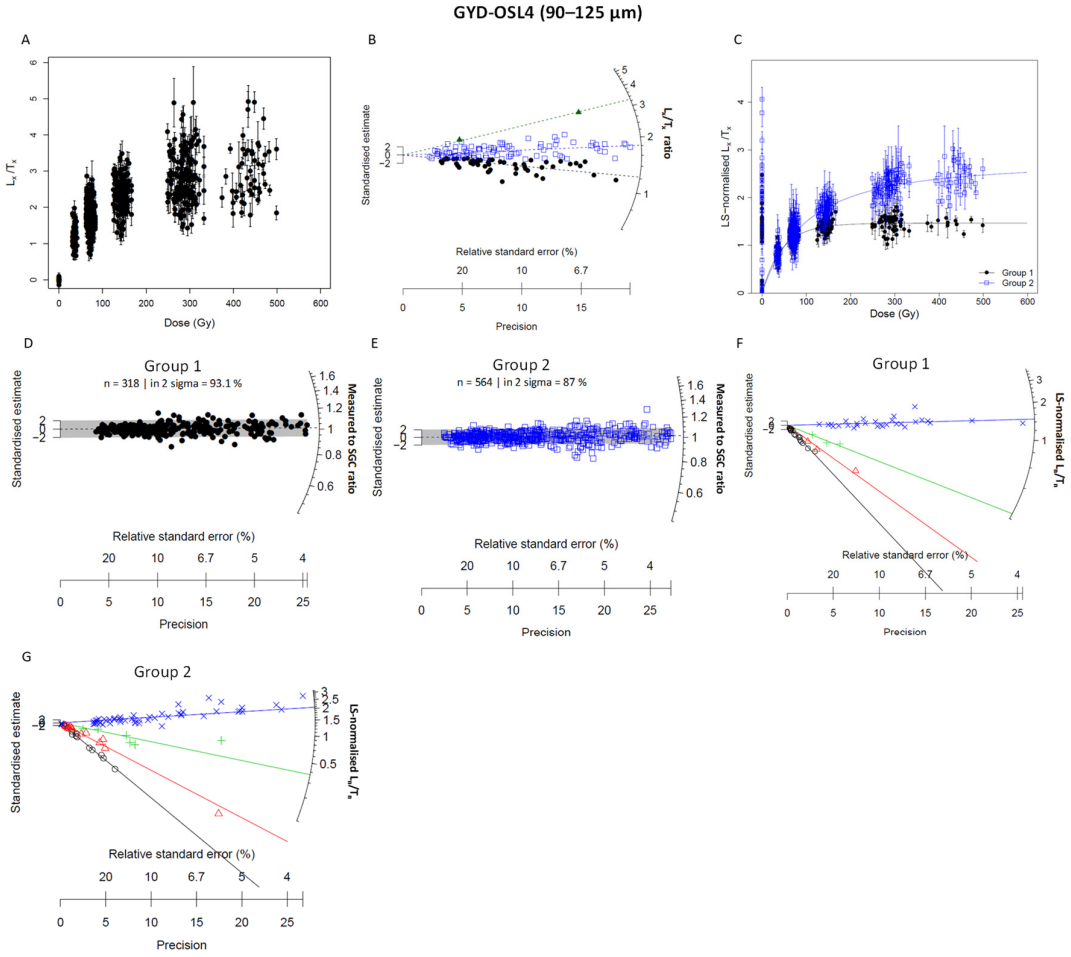

Figure 4-9: Single-grain measurement results for the 90–125 µm fraction of GYD-OSL4. (A–C) Results similar to those described in Figure 4-3A–C. (D–E) Results similar to those described in Figure 4-3D–F. (F–G) Results similar to those described in Figure 4-3G–I.

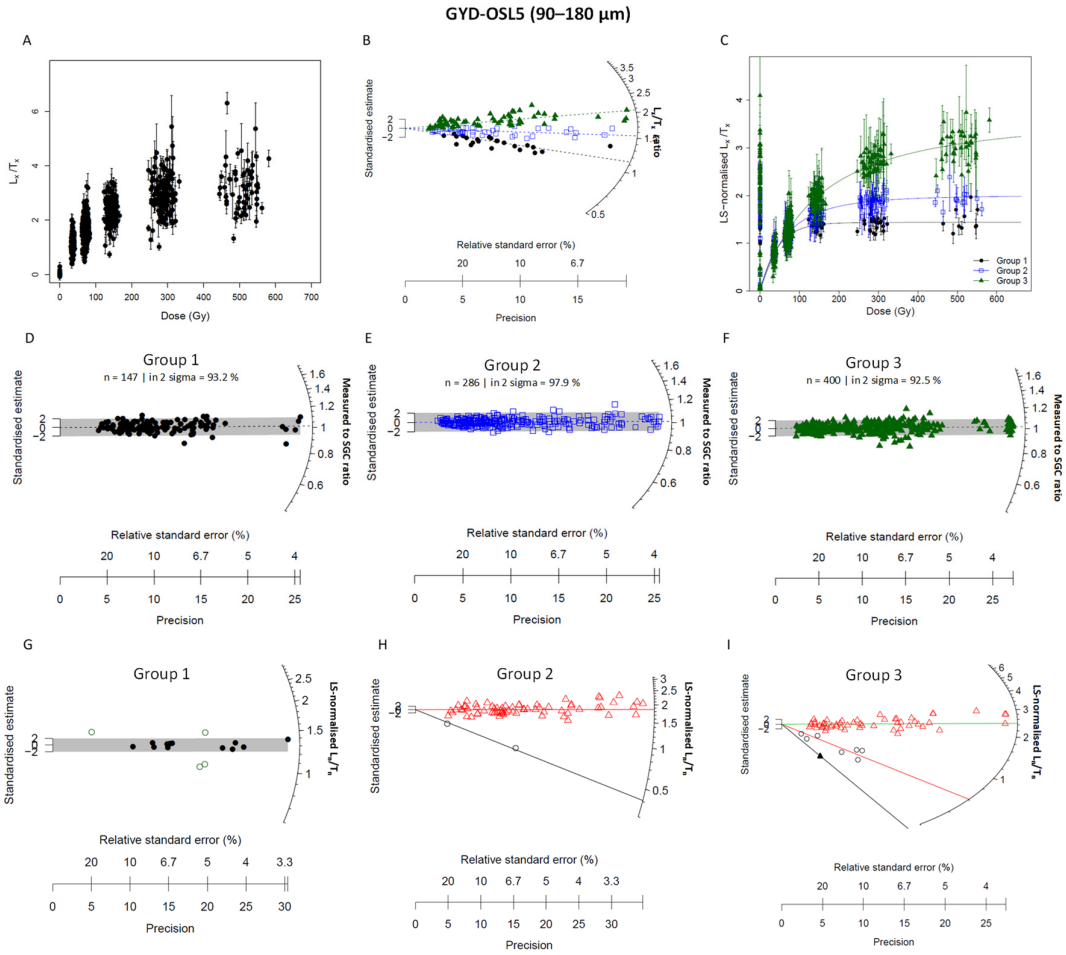

Figure 4-10: Single-grain measurement results for the 90–180 µm fraction of GYD-OSL5. (A–C) Results similar to those described in Figure 4-3A–C. (D–F) Results similar to those described in Figure 4-3D–F. (G–I) Results similar to those described in Figure 4-3G–I.

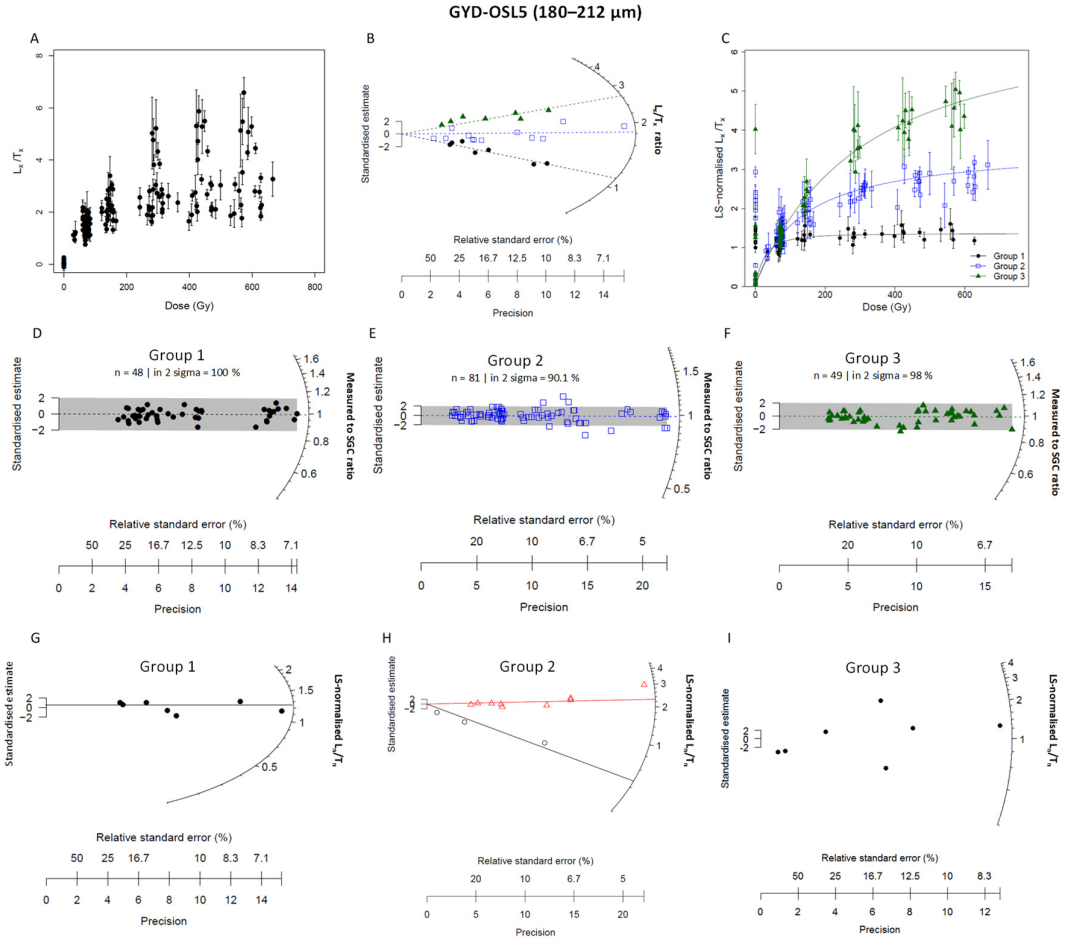

Figure 4-11: Single-grain measurement results for the 180–212 µm fraction of GYD-OSL5. (A–C) Results similar to those described in Figure 4-3A–C. (D–F) Results similar to those described in Figure 4-3D–F. (G–I) Results similar to those described in Figure 4-3G–I.

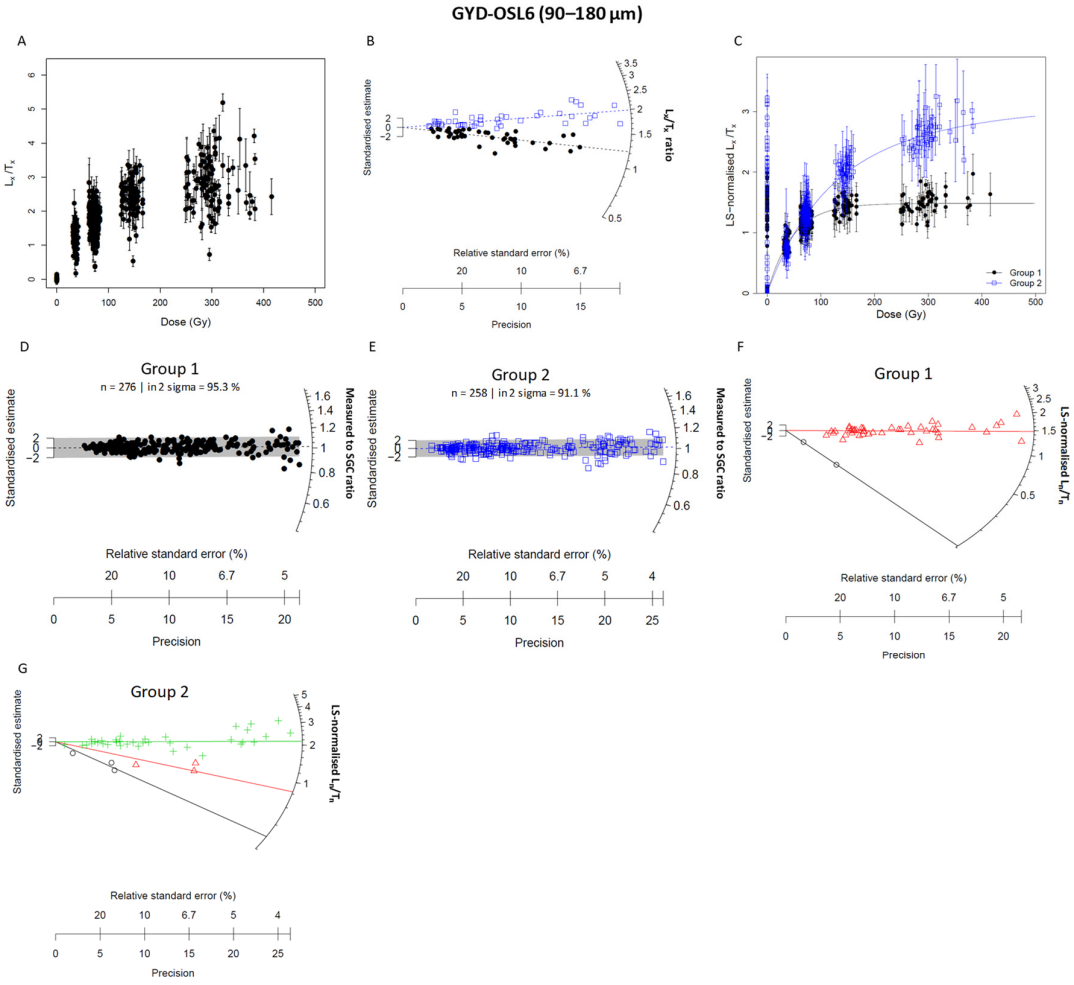

Figure 4-12: Single-grain measurement results for the 90–180 µm fraction of GYD-OSL6. (A–C) Results similar to those described in Figure 4-3A–C. (D–E) Results similar to those described in Figure 4-3D–F. (F–G) Results similar to those described in Figure 4-3G–I.

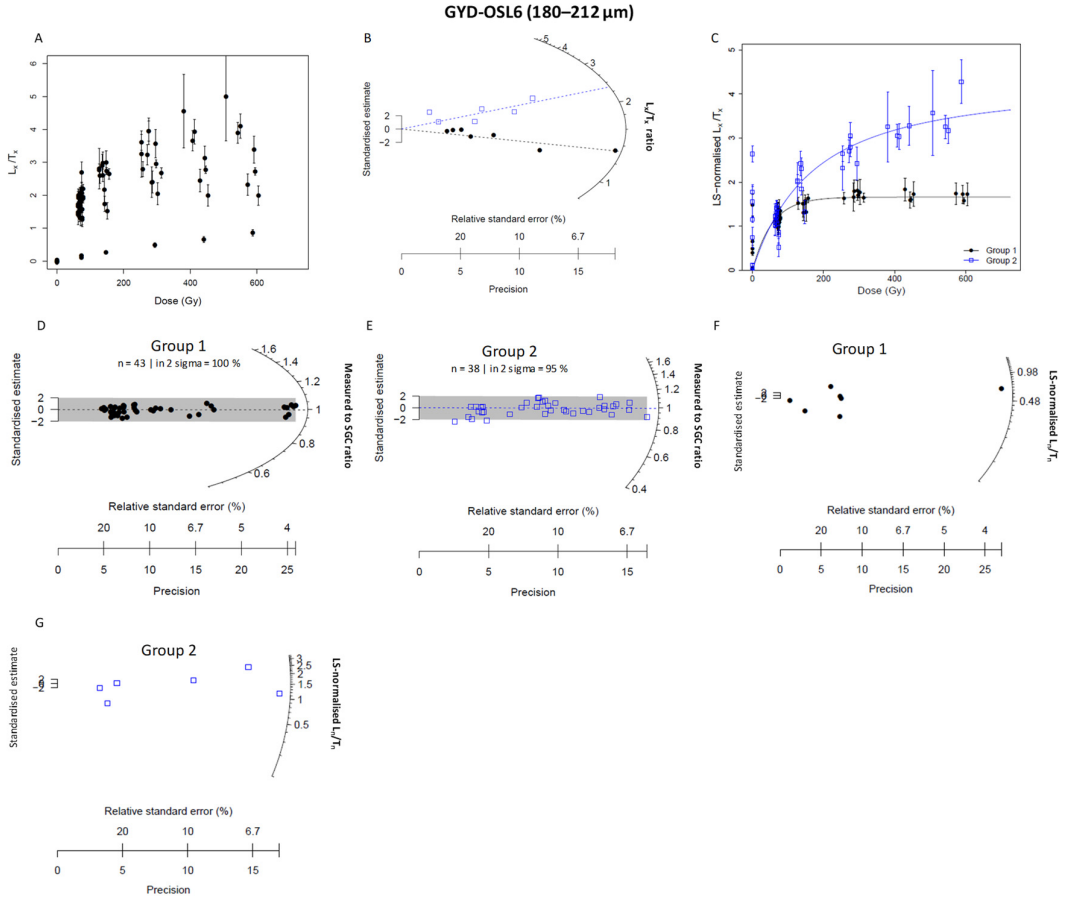

Figure 4-13: Single-grain measurement results for the 180–212 µm fraction of GYD-OSL6. (A–C) Results similar to those described in Figure 4-3A–C. (D–E) Results similar to those described in Figure 4-3D–F. (F–G) Results similar to those described in Figure 4-3G–I.

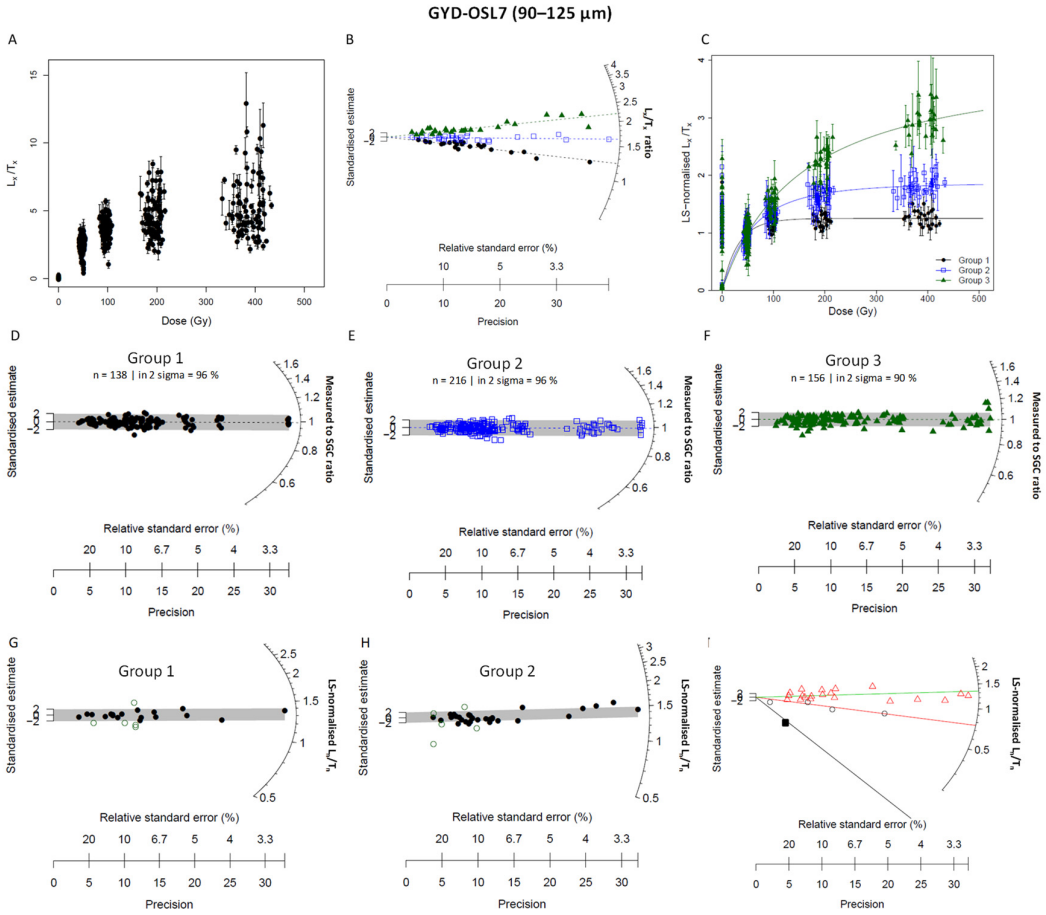

Figure 4-14: Single-grain measurement results for the 90–125 µm fraction of GYD-OSL7. (A–C) Results similar to those described in Figure 4-3A–C. (D–F) Results similar to those described in Figure 4-3D–F. (G–I) Results similar to those described in Figure 4-3G–I.

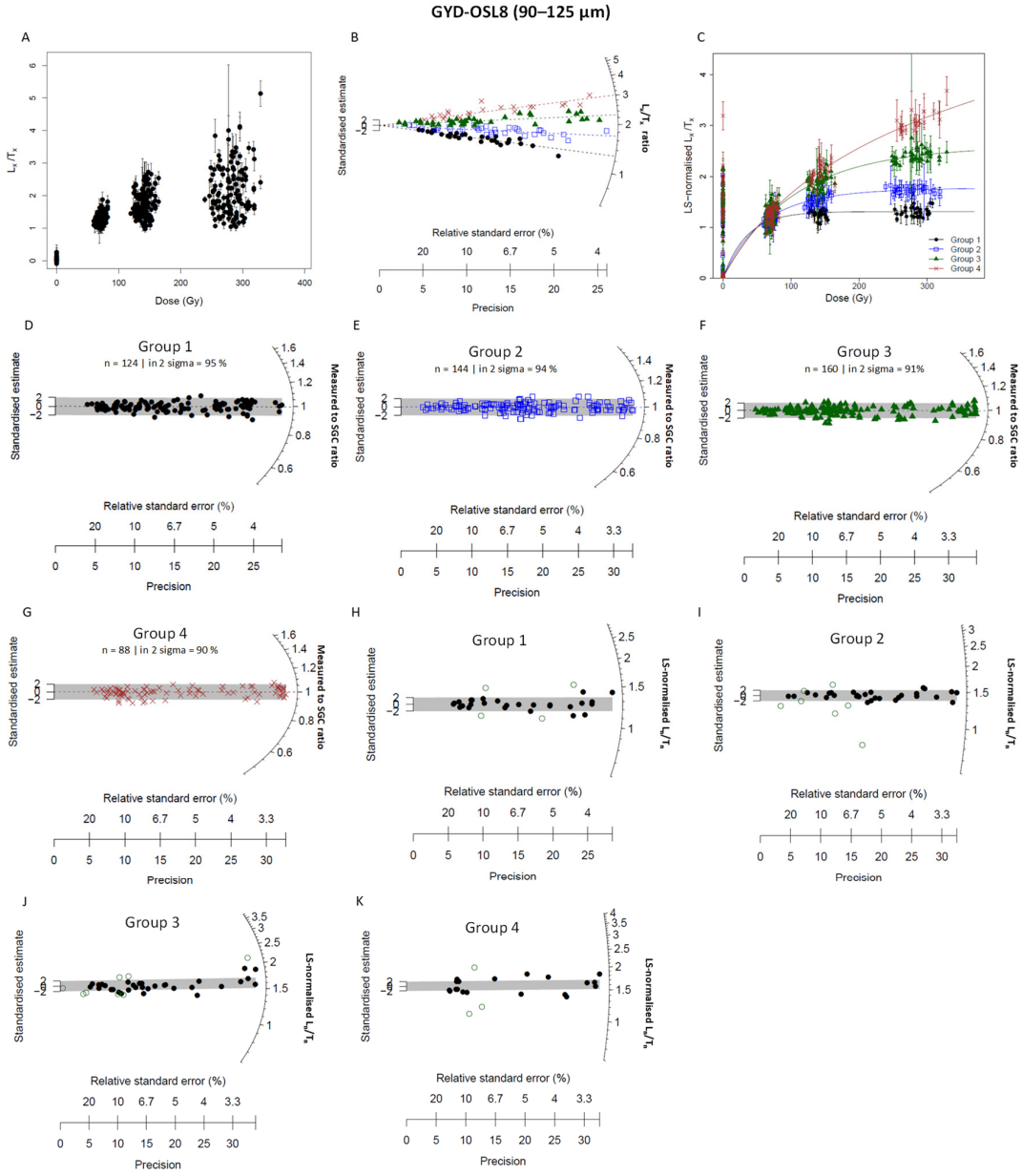

Figure 4-15: Single-grain measurement results for the 90–125 µm fraction of GYD-OSL8. (A–C) Results similar to those described in Figure 4-3A–C. (D–G) Results similar to those described in Figure 4-3D–F. (H–K) Results similar to those described in Figure 4-4G.

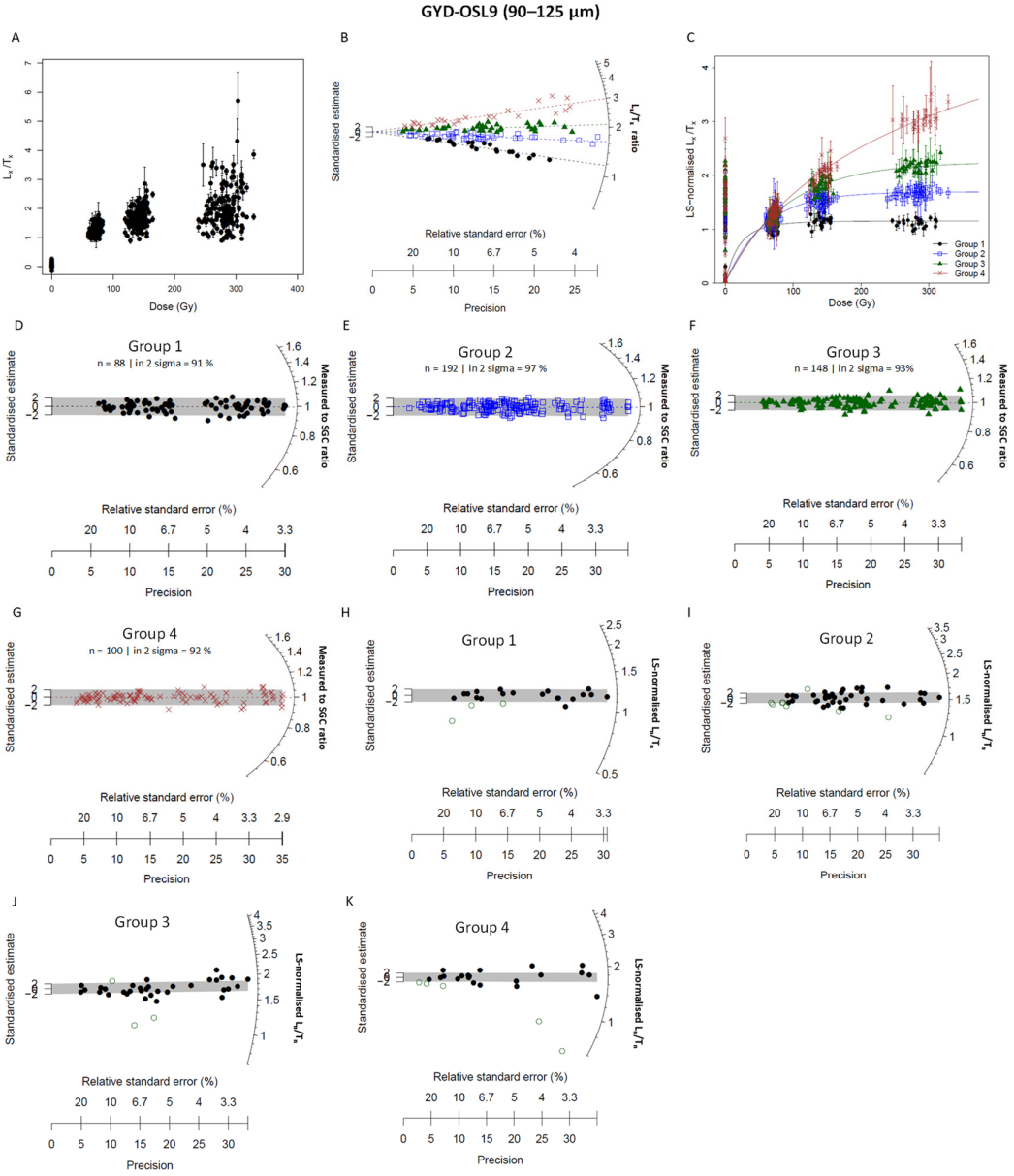

Figure 4-16: Single-grain measurement results for the 90–125 µm fraction of GYD-OSL9. (A–C) Results similar to those described in Figure 4-3A–C. (D–G) Results similar to those described in Figure 4-3D–F. (H–K) Results similar to those described in Figure 4-4G.

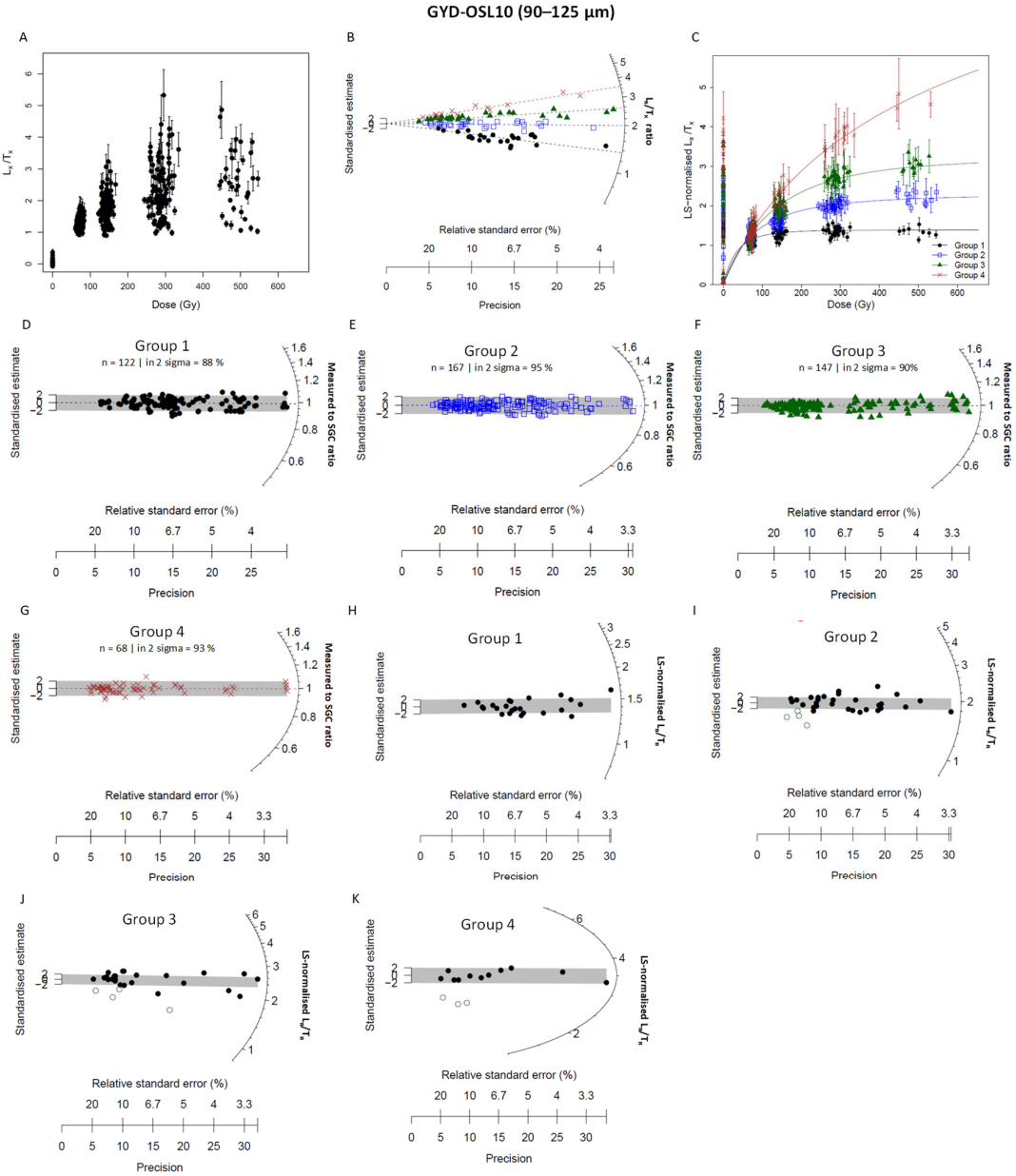

Figure 4-17: Single-grain measurement results for the 90–125 µm fraction of GYD-OSL10. (A–C) Results similar to those described in Figure 4-3A–C. (D–G) Results similar to those described in Figure 4-3D–F. (H–K) Results similar to those described in Figure 4-4G.

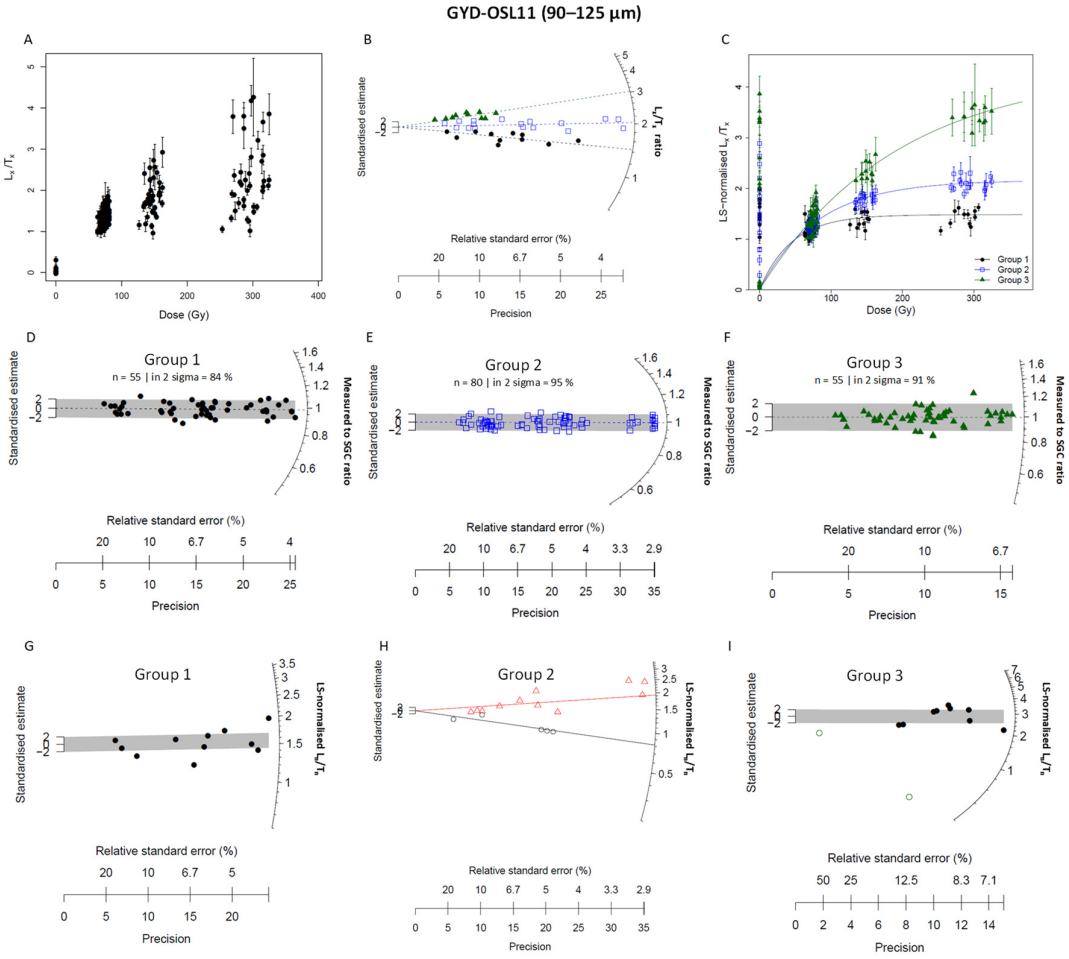

Figure 4-18: Single-grain measurement results for the 90–125 µm fraction of GYD-OSL11. (A–C) Results similar to those described in Figure 4-3A–C. (D–F) Results similar to those described in Figure 4-3D–F. (G) Results similar to those described in Figure 4-3G–I. (I) Results similar to those described in Figure 4-4G.

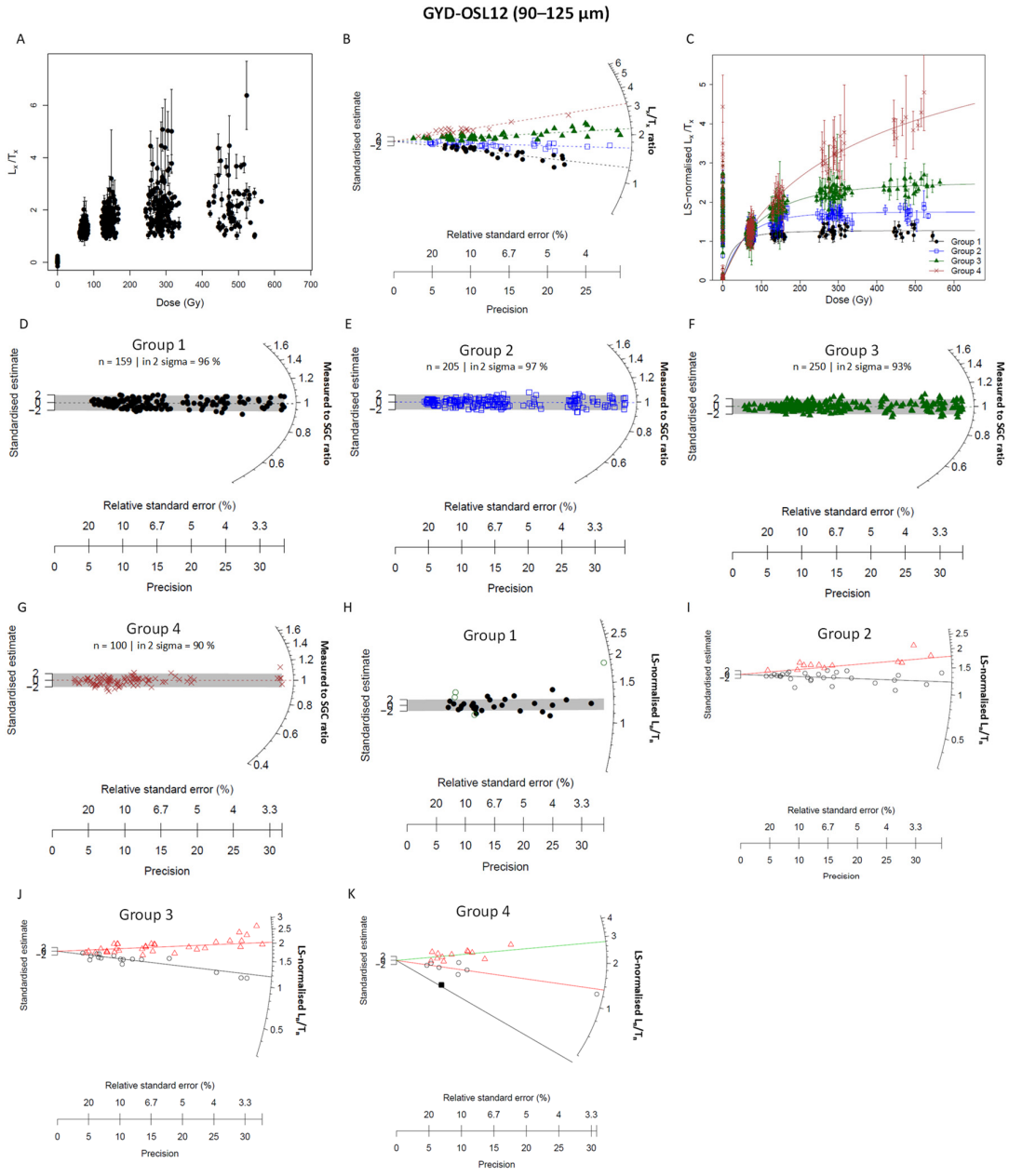

Figure 4-19: Single-grain measurement results for the 90–125 µm fraction of GYD-OSL12. (A–C) Results similar to those described in Figure 4-3A–C. (D–F) Results similar to those described in Figure 4-3D–F. (G–I) Results similar to those described in Figure 4-3G–I.

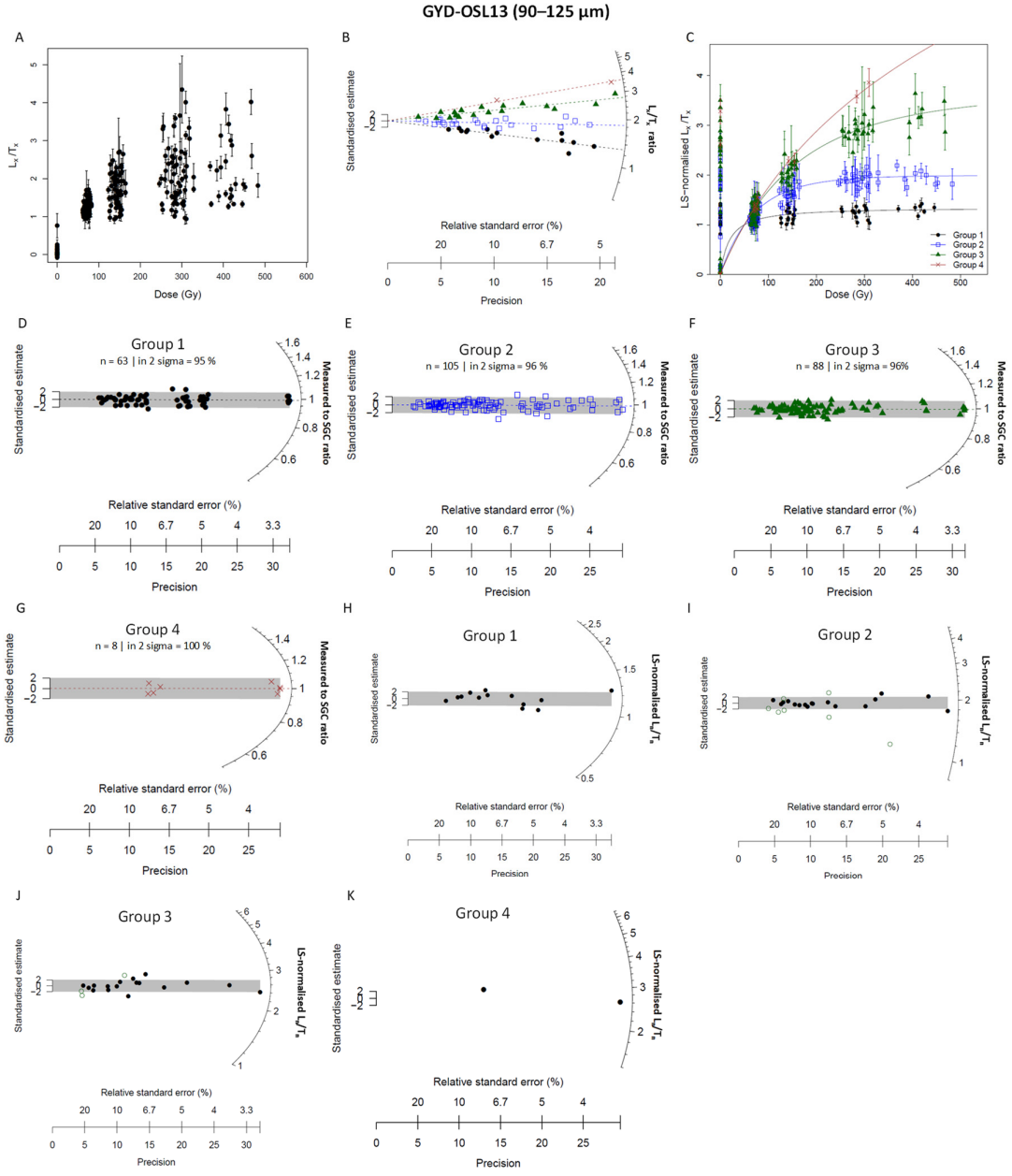

Figure 4-20: Single-grain measurement results for the 90–125 µm fraction of GYD-OSL13. (A–C) Results similar to those described in Figure 4-3A–C. (D–F) Results similar to those described in Figure 4-3D–F. (G–I) Results similar to those described in Figure 4-4G.

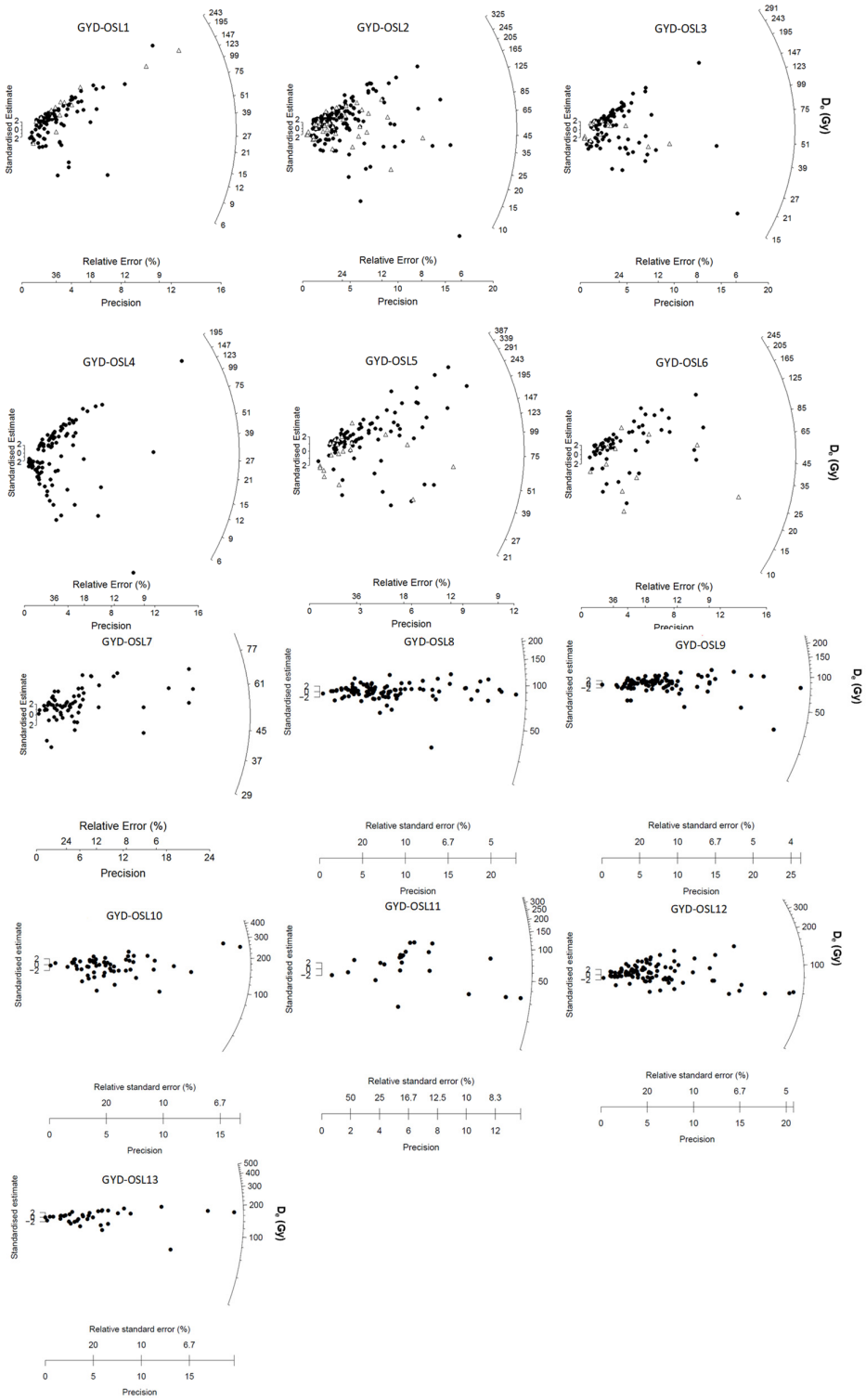

Figure 4-21: Single-grain SAR D_e results for all the samples. For the samples (GYD-OSL1, 2, 3, 5 and 6) with two grain sizes measured, the filled circles are the results from the fraction of 180–212 µm and the open triangles are those from the other fraction of smaller grain size (< 180 µm).

The distributions of individual D_e values passed through the rejection criteria are shown in radial plots in Figure 4-21 for all the samples. It can be seen that all the samples have shown a large range of D_e values, ranging from ~0 up to ~250 Gy. For those samples with two grain sizes measured, similar D_e distributions are observed between the two grain sizes from the same sample. These broad D_e distributions indicate that our samples were contaminated by 'younger' grains, especially for the samples taken from profile S1. This is not surprising because the residual profiles have been exposed for several decades since the last excavation in 1970s. As a result, one would expect some degree of bioturbation that might have intruded younger grains into the profiles. Evidence of such post-depositional mixture can be seen from the modern tree roots that penetrate deeply into the profile as shown in Figure 2-3. Fortunately, such recent bioactivity did not destroy the stratigraphic integrity of the residual profiles, because clear sedimentary beddings are still visible (Figure 2-3 and Figure 2-3) and consistent with the description in original excavation report.

4.2.5 Standardised growth curve analysis

The numbers of grains or aliquots that were rejected from each of the rejection criteria are summarised in Table 4-3. It is shown that there are considerable proportions of grains or aliquots (up to ~40%) that have natural signals saturated, e.g., the L_n/T_n value is statistically consistent or above the saturation level of the corresponding DRCs. As a result, finite D_e estimates cannot be obtained for these grains. Recent studies have suggested that rejecting a large number of 'saturated' grains may result in a significant underestimation in final D_e estimation due to the truncation of the full D_e distribution (Duller, 2012b; Gliganic et al., 2012; Guo et al., 2017; Li et al., 2016a; Thomsen et al., 2016). To avoid this problem, Li et al. (2017a) proposed a new method of analysing the L_n/T_n distribution and establishing standardised growth curves (SGCs) (Li et al., 2015; Roberts and Duller, 2004) for different grains or aliquots. In this new method, no grains are rejected because they are 'saturated', so a full and untruncated distribution of the L_n/T_n ratios is obtained, which allows reliable D_e estimation beyond the conventional limit of ~$2D_0$ using the standard SAR procedure. Given the large proportion of 'saturated' grains in our samples, the method of Li et al. (2017a) was, therefore, applied to estimate D_e for our samples.

The variability of the DRCs for our samples and the possibility of establishing SGCs was investigated, following the same method proposed by Li et al. (2016a). By analysing the L_x/T_x ratios between two regenerative doses, Li et al. (2016a) found that the single-grain and small-aliquot DRCs could be divided into three broad groups, termed 'early', 'medium' and 'later', which saturated at different dose levels. They also found that each group could be well-defined by a SGC. As suggested by Li et al. (2016a), SGC should be established using only those aliquots (grains) considered to be well-behaved so that reliable growth curves are produced. To do this, poorly-behaved grains or aliquots were identified and rejected using similar rejection criteria to those mentioned above but included all the 'saturated' ones. Figure 4-3A shows comparisons of all the DRCs that pass the rejection criteria for the 90–150 μm quartz grains from GYD-OSL1. It can be seen that the DRCs from the same samples are highly variable among different grains or aliquots, which prevents the establishment of a common SGC. To test whether the samples can be classified into several groups that share the same DRCs, the ratios between the L_x/T_x

values of two regenerative doses of ~280 and ~70 Gy were calculated, which reflects the saturation dose level of the corresponding DRC (Li et al., 2016a), e.g., higher ratios represent larger saturation doses or later saturation. The ratios were shown in the radial plots in Figure 4-3B.

To test whether there are several groups with each having similar saturation dose, the Finite Mixture Model (FMM) (Galbraith and Green, 1990; Galbraith and Roberts, 2012; Roberts et al., 2000) was used to identify the number of groups that have statistically indistinguishable L_x/T_x ratios and estimate the weighted mean ratios for each group and the probability of falling in each group for each grain or aliquot (Figure 4-3B). The DRCs from each group was analysed using a least-square normalisation (LS-normalisation) procedure (Li et al., 2016a) to establish corresponding SGCs for each of the groups (Figure 4-3C), which involves the following steps: (1) fit the L_x/T_x data from all grains from the same group using a best-fit model (e.g., single saturating exponential function); (2) re-scale the L_x/T_x data from each grain by multiplying a scaling factor so that the difference between re-scaled L_x/T_x values from that grain and the fitted common growth curve is minimised through an optimization procedure; each grain is treated individually so different scaling factors are determined for different grains; (3) repeat the steps 1 and 2 iteratively until there is negligible change in the re-scaled regenerative-dose signals and best-fit function. The scaling factors obtained for individual grains were then used to normalize their corresponding natural signals (L_n/T_n).

The dose-response data from the same groups were fitted using a general order kinetic function (Guralnik et al., 2015) of the form $f(x) = a[1-(1+bcx)^{(-1/c)}]+d$, where x is the dose and parameters *a, b, c* and *d* are constants. It can be seen that different groups have considerably different saturation dose levels, i.e., Group 1 saturated at ~100 Gy but Group 3 shows no sign of saturation up to 500 Gy. The ratio between the measured L_x/T_x and the expected values based on the SGC are statistically consistent with unity for all the groups; most of these ratios (~90% or more) are consistent with unity at 2σ (Figure 4-3D–F), confirming the validity of the grouping and SGC establishment. The same procedure was applied to all of our samples, and it was found that most of our samples can be fitted to 2–4 groups (Figure 4-3 to Figure 4-20) despite a large variation in their DRCs are observed.

Once the SGCs were established for individual groups, the natural signals (L_n/T_n) from each of the groups were re-normalised using the same scaling factors obtained during the LS-normalisation procedure. The distributions of the 'LS-normalised L_n/T_n values for each of the groups that were used to calculate final D_e values for each sample are shown in Figure 4-3 to 4-20 for all the samples. It can be seen that all the groups were dominated by a single population, although most of them contain a few grains that have significantly smaller L_n/T_n values. This is similar to the patterns observed from distribution of the SAR D_e values (Figure 4-21). However, since all of the grains that were rejected due to 'saturation' are included, it appears that all the samples have a dominant population and this population has the highest L_n/T_n (or D_e) values. Hence, the dominant population was considered to represent the true natural doses from the grains that remained intact since their burial.

Table 4-3. Number of single grains or aliquots measured, rejected and accepted for each sample, together with the reasons for their rejection.

Sample	Grain size (μm)	Number of measured grains/aliquots	Rejection criteria						Accepted D_e values [b]	Proportion of saturated [c]
			T_n below 3σ above BG [a]	RSE of T_n > 20% [a]	Recuperation > 5%	Poor DRC [a]	D_e by extrapolation	No L_n/T_n intersection		
GYD-OSL1	90–150	800	224	221	3	199	22	32	99 (12%)	35%
	180–212	1000	619	272	1	85	1	8	14 (1%)	39%
GYD-OSL2	90–125	800	148	210	2	203	42	15	180 (23%)	24%
	180–212	4200	2820	979	11	291	2	12	85 (2%)	14%
GYD-OSL3	90–125	600	138	134	0	187	19	24	98 (16%)	30%
	180–212	800	505	210	1	59	1	4	20 (3%)	20%
GYD-OSL4	90–180	1400	680	346	5	220	9	34	106 (8%)	29%
GYD-OSL5	90–180	1500	631	451	4	274	19	29	92 (6%)	34%
	180–212	1000	662	217	1	94	1	6	19 (2%)	27%
GYD-OSL6	90–180	1000	441	284	3	190	9	18	55 (6%)	33%
	180–212	800	558	170	1	56	0	0	15 (2%)	0%
GYD-OSL7	90–125	600	308	147	6	54	0	15	70 (12%)	18%
GYD-OSL8	90–125	500	147	116	16	92	0	25	104 (21%)	19%
GYD-OSL9	90–125	500	149	114	12	93	0	39	93 (19%)	30%
GYD-OSL10	90–125	1000	390	317	43	147	16	24	63 (6%)	39%
GYD-OSL11	90–125	600	248	222	15	77	6	9	23 (4%)	39%
GYD-OSL12	90–125	1000	412	269	28	148	14	24	105 (11%)	27%
GYD-OSL13	90–125	500	204	159	8	69	9	14	37 (7%)	38%

[a] BG, RSE and DRC represent background, relative standard error and dose response curve, respectively.

[b] The proportion of grains with acceptable D_e values is shown in the parentheses and was calculated as a ratio to the total number of measured grains.

[c] The proportion of saturated grains was calculated as the number of grains with D_e obtained by extrapolation and those without L_n/T_n intersection divided by the total number of grains that passed the first four criteria (columns 4–7).

The single-grain DRCs, SGCs and distribution of L_n/T_n values for individual groups of different samples are shown in figures from 4-3 to 4-20, respectively. For samples showing a single population of L_n/T_n values, CAM was applied to estimate the weighted mean L_n/T_n values. For those with only a few young grains intruded, these outliers were identified and removed based on the median absolute deviation as a means of screening data for outliers (Rousseeuw and Croux, 1993; Rousseeuw et al., 2006). For these cases, the normalised median absolute deviation (nMAD) was calculated using 1.4826 as the appropriate correction factor for a normal distribution, and rejected log L_n/T_n values with nMADs greater than 1.5. For the other samples where discrete D_e components could clearly be identified and are statistically supported, the FMM was applied to identify the number of populations for each distribution of LS-normalised L_n/T_n and to calculate the central value of each population. The FMM was fitted by varying the common overdispersion value (σ_b) between 0 and 0.5 to find the optimum fit when the lowest Bayes Information (BIC) score was reached (Arnold and Roberts, 2009; Galbraith and Roberts, 2012). The best-fit over-dispersion values (or σ_b) for FMM fall within 0.1–0.2 for all the samples. The best estimates of the LS-normalised L_n/T_n for each group were then projected onto the corresponding SGCs to estimate their D_e. The number of measured and accepted grains for each DRC group and their corresponding D_e results for all the samples are summarised in Table 4-4.

For some samples (e.g., the 180–212 μm grains of sample GYD-OSL5), insufficient number of grains were accepted so reliable results cannot be obtained. It can be seen that the Group 1 (i.e., the early saturated group) of most samples yielded infinite D_e value because the L_n/T_n statistically lies on the saturation level of the corresponding SGC. The number of 'saturated' grains decreases for other DRC groups with higher saturation dose levels, and finite results were obtained for the other groups that have higher saturation doses and their D_e values are statistically indistinguishable from each other for the same sample. For the samples with two different grain sizes measured, the D_e values from the two fractions are statistically consistent with each other. These results further confirm the validity of the grouping, SGC establishment and D_e estimates based on L_n/T_n and SGC.

4.2.6 Age estimates

The D_e values for each grain size fraction of the samples were estimated based on the weighted mean of the results for the non-saturated DRC groups that have produced finite D_e values. The final D_e and age estimates for the Guanyindong samples are listed in Table 4-4, together with the dose rate estimates. For the samples with two grain sizes measured, the ages obtained from both grain sizes are consistent with each other within one sigma, further supporting the argument that the small-aliquot measurements are analogue to single-grain measurements. For the samples with two different grain sizes measured, the age of each sample was, therefore, estiamted based on the weighted mean of the ages obtained from the two grain sizes.

Three samples from Layer 1 yielded age estimates of ~70–40 ka. Four samples from Group A yielded ages of ~90–80 ka, and six samples from Group B yielded ages of ~170–160 ka. The final age estimates for all the samples are shown together with the composite stratigraphy of the site in Figure 4-22. The OSL ages obtained for each of Groups A and B are statistically consistent with each other at two sigma. The dating results suggest that both Groups A and B were deposited in short periods, although there is a large gap in age (~90 ka) between Groups A and B, which is consistent with the observation of a sedimentary unconformity between the two groups (Figure 2-2B). The OSL chronology, hence, securely places the age of the Guanyindong archaeological deposits (Layers 2–8) between ~170 and ~80 ka.

The artefacts analysed in this study were collected during excavations in 1964–1973, when it was not typical to record artefact provenance at high spatial resolutions. Thus, only a small amount of the stone artefact assemblage contains provenance information that allows us to determine what period of time is represented. A total of 204 pieces of the studied stone artefacts have clear stratigraphic information, with 117 pieces from the lower layer (Group B, 170–160 ka) and 87 from the upper layer (Group A, ~90–80 ka). Only five Levallois pieces included information about which layer they were recovered from (3 from the upper layer, 2 from the lower layers). This small sample of artefacts with chronological context limits the robustness of any claims about change over time at Guanyindong Cave. Nevertheless, the patterns that are evident provide support to the main claim for Levallois technology appearing here at 170–80 ka.

Table 4-4. Summary of number of grains with saturated natural signal and D_e estimation results based on LS-normalised L_n/T_n for individual DRC groups and different grain sizes of each sample.

Sample	Grain size (μm)	DRC Group	Number of accepted DRCs	Number of saturated grains	Over-dispersion (%)	Age model [a]	D_e (Gy) [b]	Final D_e (Gy) [d]
S1								
GYD-OSL1	90–150	1	49	25	92 ± 9	FMM-2 (84%)	saturated	208 ± 14
		2	57	23	75 ± 7	FMM-2 (95%)	238 ± 31	
		3	47	7	114 ± 12	FMM-3 (72%)	199 ± 15	
	180–212	1	9	3	144 ± 36	nMAD (78%)	saturated	211 ± 27
		2	14	2	70 ± 14	nMAD (71%)	211 ± 27	
GYD-OSL2	90–125	1	21	11	40 ± 6	nMAD (90%)	saturated	224 ± 18
		2	66	26	69 ± 6	FMM-3 (89%)	204 ± 30	
		3	68	12	74 ± 7	FMM-4 (72%)	198 ± 20	
		4	82	9	99 ± 8	FMM-4 (67%)	260 ± 20	
	180–212	1	4	1	-	- [c]	-	198 ± 16
		2	32	10	59 ± 8	FMM-2 (91%)	157 ± 29	
		3	27	3	98 ± 14	FMM-3 (59%)	203 ± 33	
		4	36	2	139 ± 17	FMM-4 (53%)	211 ± 22	
GYD-OSL3	90–125	1	67	23	76 ± 7	FMM-4 (73%)	saturated	237 ± 13
		2	51	17	80 ± 8	FMM-2 (78%)	226 ± 15	
		3	23	4	50 ± 8	FMM-3 (65%)	258 ± 24	
	180–212	1	5	2	11 ± 5	CAM (100%)	saturated	206 ± 42
		2	20	3	207 ± 34	FMM-3 (55%)	206 ± 42	
GYD-OSL4	90–180	1	53	20	202 ± 22	FMM-4 (55%)	saturated	292 ± 50
		2	94	23	204 ± 16	FMM-4 (41%)	292 ± 50	
		3	2	0	135 ± 69	FMM-4 (0%)	- [c]	

GYD-OSL5	90–180	1	16	9	14 ± 3	nMAD (75%)	saturated	224 ± 12
		2	72	28	29 ± 3	nMAD (88%)	232 ± 30	
		3	52	12	67 ± 7	FMM-3 (79%)	222 ± 13	
	180–212	1	7	5	3 ± 9	CAM (100%)	saturated	217 ± 36
		2	12	3	71 ± 16	FMM-2 (75%)	217 ± 36	
		3	7	0	126 ± 37	- [c]	-	
GYD-OSL6	90–180	1	42	20	74 ± 8	FMM-2 (93%)	saturated	168 ± 12
		2	40	7	81 ± 9	FMM-3 (80%)	168 ± 12	
	180–212	1	7	1	125 ± 39	- [c]	-	
		2	8	0	98 ± 26	- [c]	-	
GYD-OSL7	90-125	1	22	14	12 ± 3	nMAD (82%)	saturated	81 ± 4
		2	34	2	37 ± 5	nMAD (91%)	85 ± 5	
		3	29	0	59 ± 8	FMM-3 (72%)	74 ± 6	
GYD-OSL8	90-125	1	31	22	12 ± 2	nMAD (87%)	saturated	99 ± 4
		2	36	3	24 ± 3	nMAD (78%)	109 ± 4	
		3	40	0	16 ± 2	nMAD (83%)	93 ± 3	
		4	22	0	36 ± 6	nMAD (82%)	93 ± 6	
GYD-OSL9	90-125	1	22	18	21 ± 4	nMAD (86%)	saturated	115 ± 5
		2	46	18	14 ± 2	nMAD (85%)	129 ± 39	
		3	39	4	23 ± 3	nMAD (87%)	122 ± 7	
		4	25	0	35 ± 5	nMAD (88%)	106 ± 7	
S2								
GYD-OSL10	90-125	1	25	18	9 ± 2	nMAD (96%)	saturated	272 ± 11
		2	34	13	27 ± 4	nMAD (88%)	248 ± 37	
		3	30	7	28 ± 4	nMAD (83%)	258 ± 29	
		4	14	2	36 ± 8	nMAD (79%)	276 ± 12	

GYD-OSL11	90-125	1	11	8	19 ± 5	CAM (100%)	saturated	201 ± 24
		2	16	3	45 ± 8	FMM-2 (75%)	181 ± 41	
		3	11	4	104 ± 23	nMAD (82%)	209 ± 29	
GYD-OSL12	90-125	1	32	16	16 ± 3	nMAD (88%)	saturated	202 ± 17
		2	41	12	27 ± 3	FMM-2 (37%)	saturated	
		3	50	8	29 ± 3	FMM-2 (66%)	192 ± 20	
		4	20	2	55 ± 9	FMM-3 (60%)	220 ± 30	
GYD-OSL13	90-125	1	14	7	11 ± 3	nMAD (93%)	saturated	214 ± 16
		2	24	14	20 ± 4	nMAD (71%)	290 ± 132	
		3	20	3	15 ± 3	nMAD (85%)	212 ± 16	
		4	2	0	9 ± 6	- [c]	-	

[a] The percentage of grains used for D_e estimation is shown in parentheses

[b] The D_e shown as 'saturated' means that the weighted mean of LS-normalised L_n/T_n is statistically consistent with the saturation level of the corresponding SGC.

[c] The number of accepted grains are insufficient for reliable statistical analysis, i.e., there is less than 5 grains that are statistically identified from the same age component.

[d] The final D_e were obtained based on the weighted mean of the finite D_e values obtained from each of the groups.

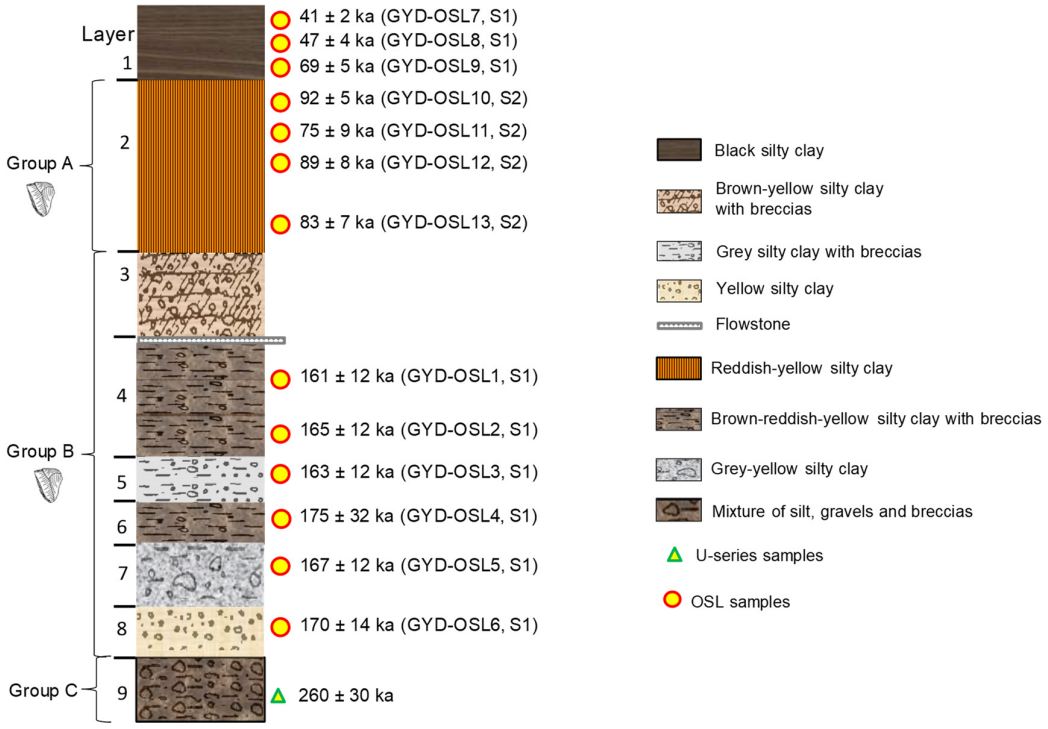

Figure 4-22: Schematic composite stratigraphy at the south wall of the cave entrance, with the depth, profile and ages of the OSL samples and U-series dating results (Shen and Jin, 1992) indicated. The sketches of stone tools indicate cultural layers. The errors of the OSL ages are expressed at 1σ.

4.3 Summary

Previous dating attempts have yielded controversial results, which prevents the establishment of essential chronological foundation to interpret human behavior and technological evolution in this region. The new OSL chronology provided a firm constraint on the sedimentary ages of the artefact-bearing deposits from Layer 1, Groups A and B (Figure 2-2 and Table 4-2). The OSL age for Layer 6 is consistent with the U-series age ~180 ka of the stalagmite sample (QGC-7) from the same layer, confirming the reliability of both dates. Based on the new OSL ages and previous U-series dating results, it is conclude that Layer 2 (Group A) was deposited at ~80–90 ka ago, corresponding to the last interglacial period or Marine Isotopic Stage 5a. The age estimate for Group A is further supported by its sedimentary feature. The deposits of Group A consist of reddish clay, indicating a strong paedogenesis process in a warm and humid interglacial condition. The poorly preserved fossils in Group A, as compared to those in Group B, further supports that the depositional environment of Group A is relatively warm and humid. The Layer 4–8 (Group B) were deposited between 160–170 ka ago. The age of the Guanyindong lithic assemblage can, therefore, safely placed between ~170 and ~80 ka.

The single-grain OSL dating results also demonstrated that single-grain OSL technique can be successfully applied to quartz extracted from the sediments of this region and it is a robust tool to date deposits that were affected by post-depositional disturbance.

Chapter 5: Levallois technology in Guanyindong

The content of this chapter is based on the article published in *Nature* in 2019 (see **Appendix B**). Some changes have been made for purpose of including it in this thesis, such as excluding the descriptions of the background of the site and chronology, etc., which have been presented in the preceeding chapters.

Hu, Y., Marwick, B., Zhang, J.-F., Rui, X., Hou, Y.-M., Yue, J.-P., Chen, W.-R., Huang, W.-W., Li, B., 2019. Late Middle Pleistocene Levallois stone-tool technology in southwest China. Nature 565, 82–85.

5.1 Definition and identification of Levallois concept

The concept of Levallois has a variety of definitions. At the center of most modern definitions of Levallois technology are the six technological criteria of Boëda (Boëda, 1995): 1) exploitation of the volume of raw material is organized in terms of two intersecting planes, or flaking surfaces; 2) the two surfaces are hierarchically related, one constituting the striking platform and the other the primary reduction surface; 3) the primary reduction surface is shaped such that the morphology of the product is pre-determined, which is fundamentally a function of the lateral and distal convexities of the surface; 4) the fracture plane for removing primary products is sub-parallel to the plane of intersection of the two surfaces; 5) the striking platform size and shape is adjusted to allow removal of flakes parallel to this plane, usually through retouch or faceting; and 6) Levallois flakes are removed via direct hard hammer percussion.

This reduction sequence concept is the prevailing definition of Levallois technology world-wide. As noted by Brantingham and Kuhn (Brantingham and Kuhn, 2001) and others (Eren and Lycett, 2012b; White et al., 2011) there are many possible core morphologies that are consistent with these six criteria. The specific actions required to achieve these criteria, such as cortex trimming, platform faceting and edge preparation, may be applied in different proportions and at different stages in the life of a core. Further variability is evident in patterns of surface preparation and the orientation of flake removals. Amidst this variability, three patterns of Levallois reduction have been documented, including flakes removed from along the circumference of the core (centripetal or radial), from two directions (orthogonal or opposed), or one from only direction (unidirectional, parallel, or convergent). Within these patterns there are two basic systems: preferential, in which only one large flake is produced per core preparation episode, and recurrent, where several large flakes are removed between each core preparation episode (Boëda, 1995).

These variations in technical attributes may result in a wide range of shapes, but this does not alter the fundamental model of Levallois reduction. This technical approach to defining and identifying Levallois technology differs from the older Bordesian typological concept of the Levallois. The Bordesian definition is based on the presence of specific, visually distinctive core and flake products, such as the classic turtle-shell core and large detached central flake (i.e. preferential Levallois flake) that are often

depicted in explanations of Levallois technology (Schlanger, 1996; Van Peer, 1992). A key point of contrast in the definitions of Boëda and Bordes is that for Boëda, the distinctive innovation in Levallois technology is the result of a process or sequence of actions that produces cores with a distinctive geometry, but for Bordes, the distinctive idea is the systematic production of artefacts with predetermined, visually distinctive shapes. Predetermination is important in Boëda's scheme also, but the visual distinctiveness and morphology of the product is less important. The broader implications are similar, that the artefact-maker used foresight and planning to create a stone artefact. But the implications for identifying a Levallois assemblage are substantially different. Boëda's concept permits many different flaking strategies within the Levallois, and wide latitude in the form and character of flake products (Mellars, 1995). On the other hand, if we use Bordes' Levallois definition we are constrained to forms that match his Mousterian typology, and similarly precise and delicate pieces.

One distinctive technological strategy that is common to both definitions of Levallois is the preparation of the core platform between each flake removal. This is a key point that separates Levallois from discoidal reduction, where there is no intervening phase of remodeling the core between flake removals, and an unhierarchical relation of the surfaces (but see Monnier et al. (2014) for some of the debates surrounding discoids and Levallois). Traces of core platform preparation are also important for identifying foresight and planning in stone artefact production, which is the key behavioural implication for early evidence of Levallois. Core preparation for removal of a target flake is also the main concept of Mode 3 technologies, of which the Levallois is the most intensively studied and best known subset. However, evidence of core preparation, although behaviorally significant, is not by itself sufficient to identify Levallois technology in an assemblage. Similarly, the hierarchical organization of the surfaces by itself, without signs of preparation, is not sufficient to identify Levallois. For example, Middle Pleistocene hierarchical cores that do not show maintenance of distal and lateral convexities, and only minimal treatment of the preparatory surface is conducted, mainly by large removals, are not identified as Levallois (Barzilai et al., 2006; Malinsky-Buller, 2016). Flakes resulting from these cores tend to be flat in terms of ventral curvature, with mostly plain striking platforms, showing no signs of platform preparation.

It appears in previous work that, when traces of core preparation are present and some of the Boëda criteria also, but the overall artefact morphology is not typical of Bordes' Mousterian typology that researchers hesitate to use the term 'Levallois'. Instead they use terms such as 'proto-Levallois', 'stripped-down Levallois' (White and Ashton, 2003), 'Levallois-like' (Brantingham et al., 2004; Brantingham et al., 2000; Niu et al., 2016; Shimelmitz et al., 2016), 'unsophisticated Levallois' (Cahen, 1981), 'para-Levallois' (Cahen et al., 1985; Watteyne, 1985), or 'reduced Levallois' (Roe, 2014). These terms are most common when discussing assemblages at the early chronological extreme of the European Middle Palaeolithic or African Middle Stone Age, or at geographic extremes of the classic Levallois area, such as China. In many cases this nomenclature reflects either transitional technologies from simple prepared cores to 'full' Levallois with core preparation and hierarchical surfaces (White and Ashton, 2003) or localized, independent convergences on Levallois technology that have no historical connection to the Bordesian core area of Levallois (Otte, 1995), or simply are pieces that are less

intensely modified, representing initial phases of knapping (Ryssaert, 2006b). This raises the question: where are the limits of the Levallois definition?

A particularly problematic detail in establishing the limits of the definition is means by which the hierarchical relationship between the two core surfaces was established and how the platform was prepared in order to orient it perpendicular to the axis of flaking. Brantingham and Kuhn (Brantingham and Kuhn, 2001) note that Boëda's definition gives little guidance on this. Several studies identify cores with a morphology of naturally asymmetric surfaces as Levallois, even though they lack the extensive flake removal to shape the core in preparation for the main flake removals (Brantingham and Kuhn, 2001; Chazan, 1997; Delagnes, 1995; Kuhn, 1995; Picin, 2017). Part of the problem here is the use of Boëda's criteria as a check-list rather than a guide. Boëda himself follows the check-list approach and defines cores as non-Levallois when one criterion is absent (Boëda, 1986: p104). In more recent research, there is a move away from this check list system and instead the adoption a more holistic approach, using the criteria as a guide (Bolton, 2015; Scott, 2006; White and Ashton, 2003).

5.2 Previous analyses of Guanyindong Cave lithics about Levallois concept

The classification of Levallois products remains a subjective matter, on which analysts often disagree (Boëda, 1991; Hovers, 2009; Perpère, 1986). As one of the most important Palaeolithic sites in Southern China, Guanyindong is no exception to this, with previous studies coming to differing conclusions about the presence of Levallois in the Guanyindong Cave assemblage.

One of the earliest English-language sources (Freeman, 1977) describes casts of five artefacts and identifies one as a transverse concave scraper made on a pseudo-Levallois point. Anticipating additional Levallois products, Freeman concludes that he 'would venture to guess that the collection will prove to have some proto-Levallois or true Levallois flakes when it is finally studied' (p. 101). Li et al. (Li et al., 2009a) came to a different conclusion after detailed examination of 1108 stone artefacts housed in the IVPP collections. They employ the *chaîne opératoire* concept to conduct a 'technological reading' of the assemblage. They identified three categories of cores representing three technological systems. Neither of these 'involve intentional preparation' (p. 3869) so they conclude the Guanyindong Cave artefacts are 'quite distinct from the concept Levallois' and reflect a 'different modes of cognition' (p. 3870). A third report mentioning Guanyindong stone artefacts summarizes the assemblage and notes that 'a few Levallois-like flakes were identified' (Gao, 2013).

Of the three previous English-language reports on the Guanyindong Cave stone artefacts, two claim to have observed traces of Levallois in the assemblage, and one argues that it is absent. In my view, the analysis of Li et al., which concluded that Levallois concepts are absent from GYD, is problematic because their use of *chaîne opératoire*-related methods that contribute to the irreproducibility of their results. The clarity and objectivity of *chaîne opératoire* methods have been widely questioned by stone artefact analysts. For example, Bar-Yosef and Van Peer argued that *chaîne opératoire* is '*overformalized and provides but an illusion of reading the minds of prehistoric knapper*' (Bar-Yosef and Van Peer,

2009). Similarly, Monnier and Missal (2014) have noted that use of *chaîne opératoire* concept is 'highly subjective; being based upon the analyst's experience and intuition" (p. 3). A well-known example of this problem can be found in the analysis of the assemblage from Biache Saint-Vaast level IIA. Boëda (1986) identified unidirectional and bidirectional recurrent Levallois core reduction, but Dibble (1995) found that the core reduction strategy changed from unidirectional to bidirectional as cores were more extensively reduced. This example highlights the difficulty of using the *chaîne opératoire* concept to obtain a result that can be reproduced by another analyst.

Therefore, the failure to identify Levallois in previous work may be attributed to the use of concepts of *chaîne opératoire* to interpret artefact attributes. This is prone to irreproducibility because of its subjectivity and arbitrary inference of prehistoric knappers' intentions and goals. Another important reason for the false-negative finding of previous work is the use of a check-list approach that rejects artefacts if just one criterion is absent.

5.3 Levallois technology in Guanyindong

The Guanyindong assemblage consists of flakes, retouched flakes, cores and broken nodules predominantly of chert (see Chapter 6 for more detailed information statistical analysis). Flakes are most abundant. While all stages of reduction and manufacture are represented, final stages are most abundant. Based on detailed analysis on 2217 stone artefacts, evidence of Levallois concepts was found on 45 specimens, including 11 cores, 30 flakes and 4 tools made on Levallois flakes (Figure 5-1 and Figure 5-2 Figure 5-3). Six of the cores, two of the flakes and one of the tools are described in details in Appendix A. Among the Levallois cores, eight of them exhibit patterns of recurrent Levallois concepts (see examples of line drawings from Figure 5-1.1, 4 and 6), each with two intersecting hierarchically-organised surfaces. The upper surfaces of these cores are covered with several scars removed to form convexities that influence the pattern of detachment of the final flake. The upper surface scars come from different directions forming a centripetal scar pattern. The scars of the predetermined flakes are parallel to the plane of the main flake release surface. The debitage surfaces of the cores have small flake scars along the edge, indicating preparation of their striking platforms. Three preferential Levallois cores are present (see line drawings from Figure 5-1.2, 3 and 5), and are identifiable by the prominent large final flake detachments that have truncated the distal regions of the previous preparatory flake scars. The scars of the main flake removal on these cores are parallel with the intersection of the upper and lower surfaces. The lower surfaces are extensively scarred and small platform preparation flake removals are present on the core circumference. The 3D morphology of three Levallois cores (shown in Figure 5-1.1, 2 and 3; Figure 5-2.1, 2 and 3) are also provided in the Appendix B (available at https://doi.org/10.1038/s41586-018-0710-1).

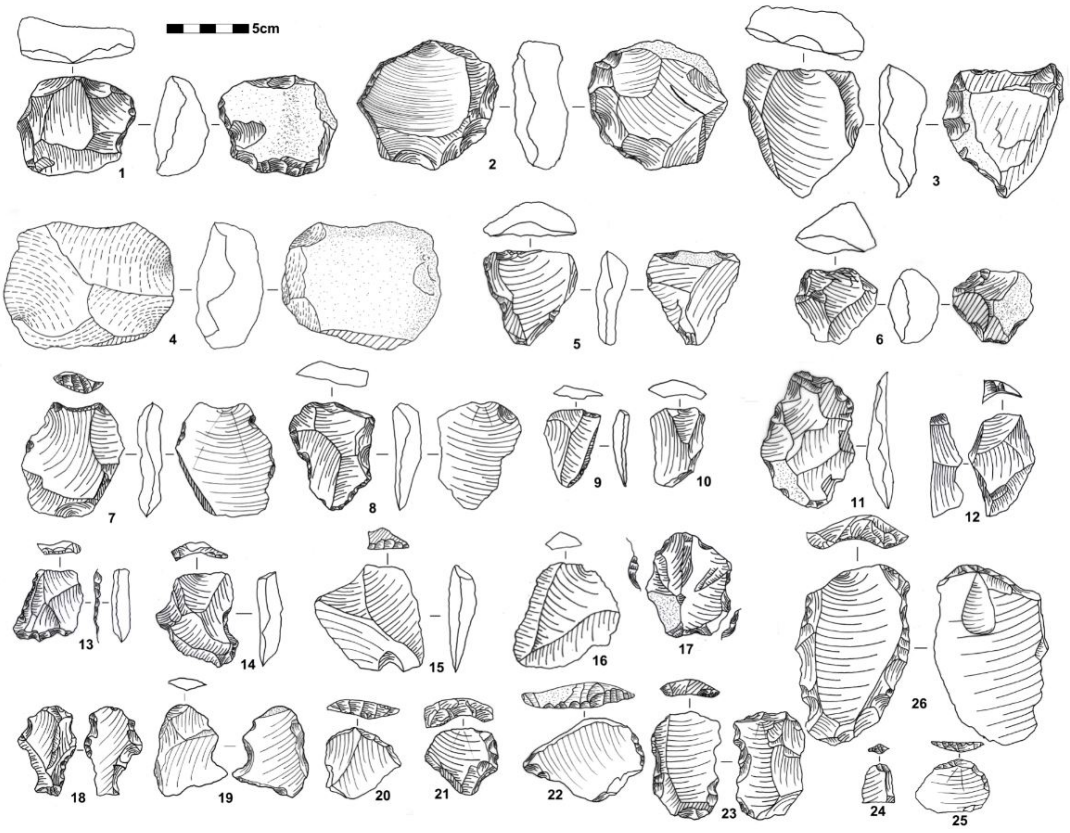

Figure 5-1: Line drawings of selected artefacts from Guanyindong Cave. 1, 4 and 6, Levallois recurrent cores; 2, 3 and 5, Levallois preferential cores; 7–11 and 14, Levallois flakes; 12, débordant; 15–16, pseudo-Levallois point; 13, 17–19, tools made on Levallois blanks; 20–26, flakes with prepared platforms. The photos of these artefacts are shown in the Figure 5-2 and Figure 5-3. The 3D structures of 2, 3 and 1 are shown in the Appendix B. The artefacts shown in 2, 3 and 17 were recovered from Group A, and those shown in 18 and 19 were from Group B.

Figure 5-2: Photos of selected Levallois cores. 1, 4 and 6, Levallois recurrent cores; 2, 3 and 5, Levallois preferential cores. The line draws of these artefacts are shown in Fig. 5-1(1–6). The artefacts shown in 2 and 3 were recovered from Group A.

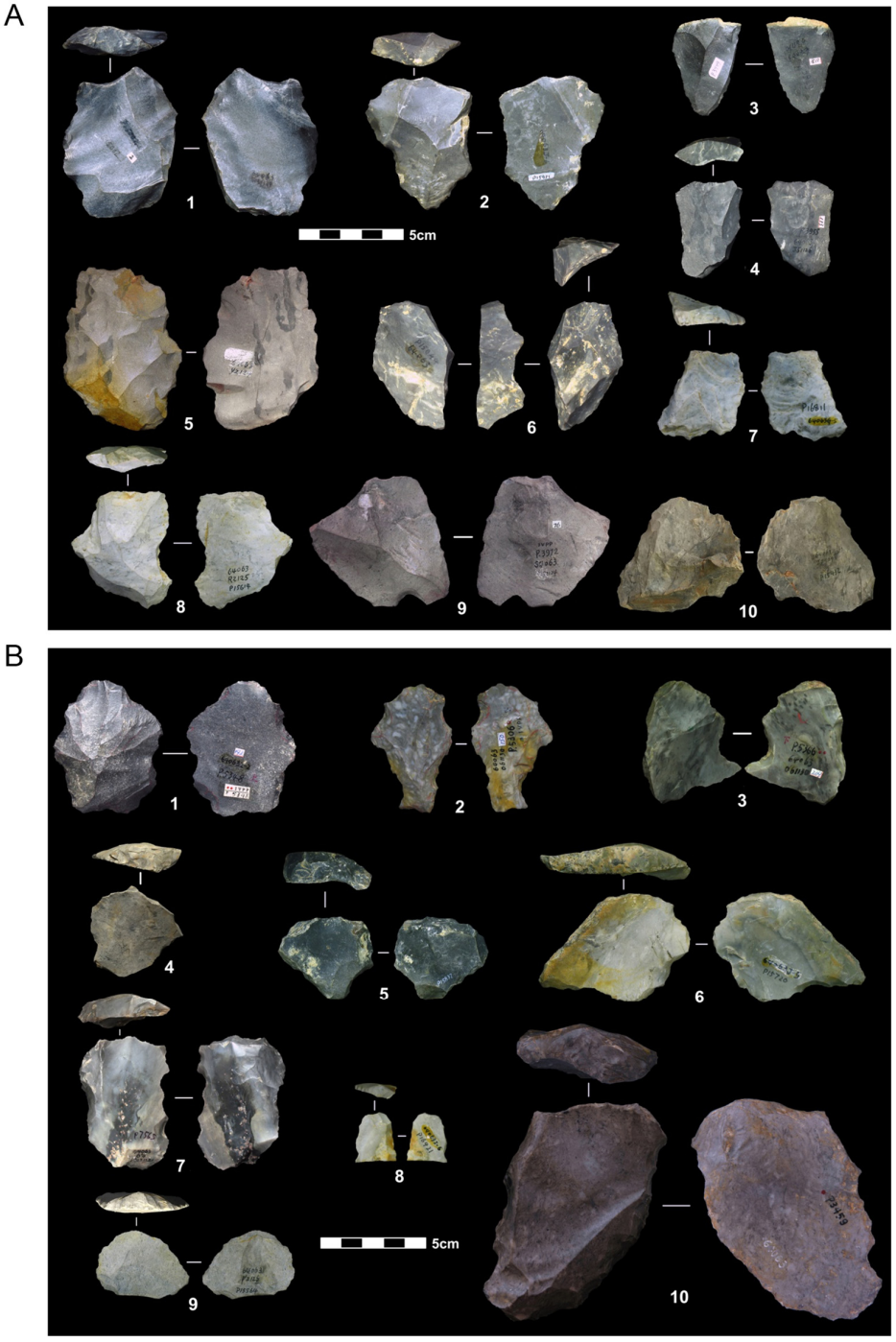

Figure 5-3: Photos of selected Levallois flakes, tool and flakes with prepared platform: (A) 1–5 and 8 Levallois flakes; 6, débordant; 7, tools made on Levallois blanks; 9-10, pseudo-Levallois point. The line draws of these artefacts are shown in Fig. 5-1(7–16). (B) 1–3, tools made on Levallois blanks; 4–10, flakes with prepared platforms. The line draws of these artefacts are shown in Fig. 5(17–26). The artefacts shown in 1 were recovered from Group A, and those shown in 2 and 3 were from Group B.

Many Levallois flakes at Guanyindong Cave exhibit distinctive Levallois characteristics. These include a facetted platform resulting from core preparation prior to flake detachment. Another characteristic is several smaller scars visible coming on to a flake's dorsal surface from several directions (Figure 5-1.7-11, and 14 and Figure 5-3A), often truncated at their distal ends by a larger central flake scar. These smaller scars may result from flaking to maintain the convexity of the core and prepare for the removal of the Levallois flake. Four Levallois flakes were retouched along the edges (Figure 5-1.13, 17-19 and Figure 5-3A7, B1-3). Besides these distinctive Levallois pieces, a number of non-Levallois flakes show signs of platform preparation (Figure 5-1.20-26 and Figure 5-3B), supporting the presence of more generalised strategies of prepared-core technology in Guanyindong Cave.

5.4 Standardization of Levallois products in Guanyindong

It has been suggested that Levallois debitage system is optimal in terms of raw material economy and flake utility since it increase the raw material's efficiency and the longest 'cutting edge' from a given blank can be created (Brantingham and Kuhn, 2001; Lycett and Eren, 2013). In other words, to meet specific requirements, Levallois flakes may exhibit a greater standardization in their attributes compared with the non 'preferred' flakes. In order to show the difference between Levallois flake and non-Levallois flakes, the coefficient of variations (CV) of Levallois and complete flakes (including retouched complete flakes) were compared on the base of several essential attributes (Table 5-1). The CV values of Levallois flakes are systematically smaller than those of complete flakes. The differences between the two groups were statistically significant (Mann-Whitney U = 13; exact p-value = 0.004), supporting the prediction that the Levallois flakes are more standardised than complete flakes (Lycett and Eren, 2013). Figure 5-4A–C shows the dimension comparison between Levallois and non-Levallois flakes. Mass and dimension are similar between Levallois and non-Levallois, but Levallois are thinner than non-Levallois flakes. Hence, it can be inferred that the use of Levallois concept was probably aiming to produce standard and thin flakes with proper size.

Table 5-1. Results of coefficient of variation (CV) analysis and descriptive statistics (revised from Eren, 2012). 'PLF': preferential Levallois flake; 'CF': complete flake.

Attribute	Mean (mm)		Standard deviation		CV (%)		Difference
	PLF	CF	PLF	CF	PLF	CF	
maximum dimension	54	57.2	17.5	23.9	32.5	41.7	9.2
oriented width	40.7	50.8	15.0	20.4	37.0	40.2	3.3
width at 25% of max dimension	32.7	32.4	11.4	14.79	34.9	45.3	10.4
width at 50% of max dimension	35.4	37.4	12.2	16.6	34.3	44.4	10.1
width at 75% of max dimension	28.4	32	10.6	15.3	37.2	47.9	10.7
length of flake (technological)	46.3	51.7	16.2	19.3	34.9	37.2	2.3
thickness at 25% of max dimension	11.1	15.6	4.6	8.11	41.5	52.0	10.5
thickness at 50% of max dimension	11.7	17.3	4.6	8.6	39.5	49.5	10.0
thickness at 75% of max dimension	9.3	15.7	3.7	7.6	39.5	48.2	8.7
Oriented thickness	11.7	18.8	4.0	8.8	34.2	46.9	12.7

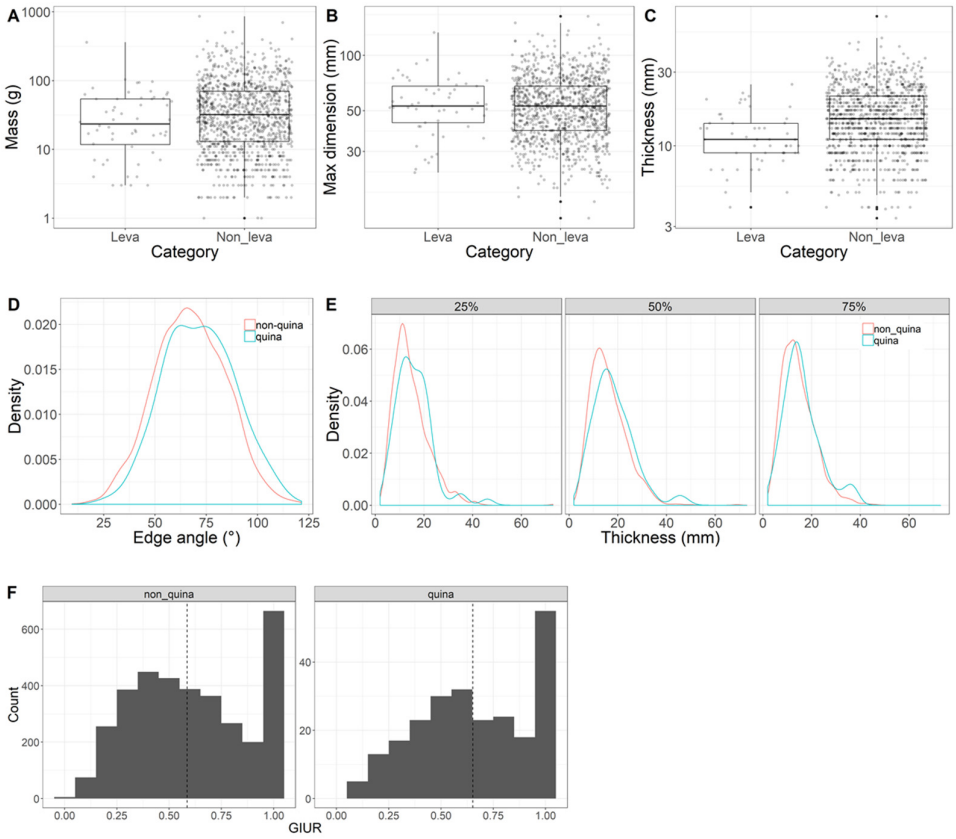

Figure 5-4: (A – C) Histograms showing comparison between levallois flakes and non-Levallois flakes on mass, maximum dimension and thickness at 50% of maximum dimension. (E) Density distribution of edge angle between Quina and non-Quina tools. (E) Density distribution of thickness at different locations (25%, 50% and 75% at maximum dimension) between Quina and non-Quina tools. (F) Histograms of GIUR of Quina and non-Quina tools.

5.5 Difference from previous lithic study on Levallois issue

Many previous studies had discussed the issue of Levallois (see 5.1). But only Li et al provided a detailed and systematic analysis on it. There are several differences between Li's results and outcomes of this study in many aspects. In their *chaîne opératoire* analysis, Li et al. describe three cores from Guanyindong Cave in detail (P4114, P4122, and P15948). This study concurs with their assessment of P4114 and P4122 that these cores are not Levallois. Contrary to Li et al, this study identifies P15948 as Levallois (see Figure 5-2.1, Figure 5-5 and the 3D structure in Appendix B), and here this piece is discussed in detail as an example of how the approach used in this study differs from Li et al.

Li et al. claimed that 1) each flaking sequence is unrelated; 2) there is only 1 flaking sequence; 3) all the flake scars come from the same direction, 4) convexity is obtained by flake ventral surface; and 5) the platform is not prepared. They, however, offer no explanation for one critical assumption which is why they found each flaking sequence to be unrelated. Based on the assumption they primarily disqualified this core from the Levallois concept. From my observation, the core was firstly prepared along most of

the edge left relative small flake scars (compared with the final flake they obtained) and tiny platform adjustment scars, and then knapper took the scars as platform for striking 6 flakes down from different directions, and all of their fracture planes are parallel to the plane of intersection of upper surface and lower surface. In my view, each flaking sequence is related because one sequence could not start before the other was complete. Moreover, there are three flaking sequences, not one as Li et al. claimed. In addition, rather than from the same direction, these scars are from multiple directions by using Levallois recurrent centripetal method. There are two flake scars they did not explain the sequence ascription.

Their fourth claim, that the blank of the core is a flake, is not convincing because this core is a slab or nodule with part of cortex left on the lower surface. The most distant ends of the piece have a similar thickness of about 20–30mm. It is not like typical Guanyindong flake which is thick at the proximal end and thin at the distal end. There are many cores that made from flakes in Guanyindong, they were described with the term “truncated faceting”. From these cores, we can see that the scars are either too small or too scarce to be classified as Levallois, and most of them are on the edge without extending across the whole ventral surface. Even if the ventral surface was flaked, we cannot say it was not prepared. For example, in Orgnac 3 in France, slabs are a common component of the Levallois assemblage, and half of Levallois cores take advantage of natural convexity of flake ventral surface to maintain the distal and literal convexities (Mathias, 2016; Moncel et al., 2011).

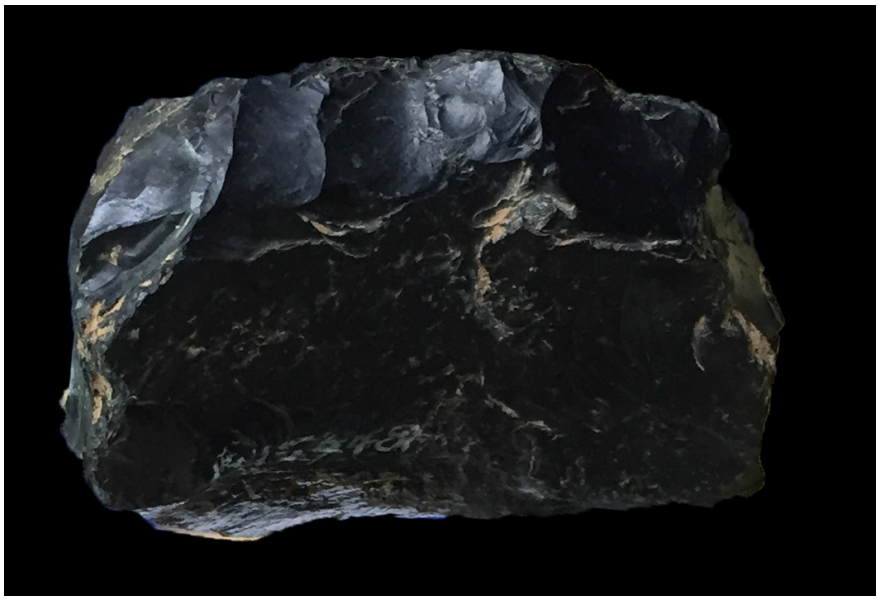

Figure 5-5: Detail of platform faceting on specimen 15948. This is the same specimen shown in Figure 5-2.1.

Finally, signs of preparation was observed on the platform of this piece (Figure 5-5), not a cortical surface as Li et al. report. Levallois attributes were found on P15948, which presents all stages of reduction and manufacture of Levallois core. The upper surface is covered with several scars come from different directions forming a centripetal scar pattern. Before flaking on the debitage surface, the core

had been knapped along the edge to prepare the striking platform. The fractures of the predetermined flakes are parallel to the plane of the flake release surface and striking platform surface.

In Li's Ph.D. thesis (Li, 2009) she describes 18 cores. Besides P15948, there are two more artefacts that were identified as Levallois cores (P5262 and P16311), but Li did not. For P5262 (see Appendix A for a detailed description), Li's conclusion is based on the assumption that the core was knapped from a naturally convex surface. But a natural convex surface was not found in this study, and instead observed preparation scars on its lateral and distal convexity, creating this geometry. Furthermore, a prepared platform was found, contrary to Li's observation of a cortical platform. For P16311, which has the least clear scar pattern of the three pieces noted here, Li identified a joint face, but there are scars resulting upper and lower surface structure typical of Levallois pieces. The key issue for each of their pieces remains the same: we did not make assumptions about the blank's geometry, but observed it directly.

5.6 Other prepared elements except Levallois

In addition to the Levallois assemblage, cores and flakes with prepared platforms and truncated-faceted pieces were also found in the assemblage. Eighteen cores are found with prepared platforms. This type of core features facetted scars on the striking platform in order to preparing a proper angle before knapping. Shapes of these cores are mainly irregular (67%) and conic (22%). Most of them (~56%) have only one platform. The average max dimension is 79.6 mm.

There are 43 flakes with faceted platforms, 72% of which were retouched to make tools. The majority of platform shapes are quadrangle (364%) and triangle (20.5%). The average platform width and thickness is 35.2 × 11.4 mm. The average max dimension of these flakes is 62.3 mm. Only a few flakes show traces of dorsal cortex (20%) and most of them have one or more previous flake scars remaining on the dorsal surface.

Core preparation is also present on 54 truncated-faceted pieces (Brantingham et al., 2000; Dibble, 1984; Dibble et al., 2006; Marwick et al., 2016) (also see chapter 6). These pieces usually started from a flake that was then knapped on the ventral side, ending up as cores with the flake scars on ventral side, indicating the production of invasive flakes from platforms along the dorsal edge. Other than on cores themselves, attributes indicating core preparation are also found on flakes (see examples from Figure 5-1.20-26 and Figure 5-3). Furthermore, evidence for maintaining core convexities is observed from 12 débordants (see examples from Figure 5-1.12 and Figure 5-3A), blanks that remove a large part of a core's lateral edge and are typically considered to be byproducts of core maintenance (Shimelmitz and Kuhn, 2017).

5.7 Timespan of Levallois and their environment context in Guanyindong

Since this site was excavated more than 40 years ago, information about the precise recovery locations of most of the stone artefacts is now lost and only 204 pieces of the studied stone artefacts have clear stratigraphic information (including 87 from Group A and 117 from Group B). Among these, 5 were identified as Levallois, and 3 of them (including 2 cores and 1 flake) are from Group A and 2 (all tools) are from Group B (Figure 5-1, Figure 5-2 and Figure 5-3). This suggests that Levallois concepts were present at this site throughout the whole occupation period.

So Levallois concepts at Guanyindong Cave first appeared in Group B, which was dated to Marine Isotope Stage (MIS) 6 (~180–130 ka) (see Chapter 4), a period contemporary to that when Levallois technology was widely adopted in Africa and Eurasia (Monnier et al., 2006). Syntheses of globally distributed benthic $\delta^{18}O$ records indicate that MIS 6 was a glacial period of cooler temperatures and lower sea levels than present (Lisiecki and Raymo, 2005). Microscopic freeze-thaw features in the MIS 6 sediments from the nearby site Panxian Dadong (Figure 1-4) suggest frequent freezing conditions during glacial periods, with temperatures of this region 5 °C or more cooler than present conditions during MIS 6 (Wang et al., 2005). This evidence, together with the composition of the Panxian Dadong faunal assemblage, indicate a mixed woodland environment including bamboo forests and open rocky areas with abundant grasses (Karkanas et al., 2008; Wang et al., 2004), suggesting that the landscape around Guanyindong Cave probably contained a reduced rainforest area compared to today, and a much-expanded open woodland environment.

5.8 Summary

Based on a more holistic approach, this study identified the Levallois in the Guanyindong Cave assemblage as large and flat preferential flakes, sometimes showing faceted platforms, and cores with hierarchical relationships and preferential removals. This study does not require traces of extensive shaping, instead following previous work that recognizes naturally asymmetric surfaces as compatible with an identification of Levallois technology. This study suggested that a full reduction sequence of Levallois concept presented in the assemblage, including Levallois cores, Levallois flakes, and tools made on flakes and convexity maintaining by-products. The evidence of prepared-core technique is also supported by the flakes and cores with faceted platforms and the fact that Levallois blanks do show more standardization than non-Levallois products.

Chapter 6: Analysis of lithic assemblage of Guanyindong

This chapter provides results of the Guanyindong assemblage other than Levallois pieces, including raw materials, core production, flake debitage and tool manufactory, and discusses the diversity of MP traits that present in the Guanyindong assemblage.

6.1 Introduction

The transition from Early Palaeolithic to Middle Palaeolithic in west Eurasia and Africa at ~300 thousand years ago (ka) includes significant milestones in human evolution such as the replacement of *Homo erectus* by *Homo sapiens* and other human species, and the numerical dominance of small flake tools over large cutting tools (Kuhn, 2013). During this period, a more diverse flake-production system appeared, including multiple variants of Levallois concept (Boëda, 1994; Boëda, 1995), discoid production, blade production, and the "Quina" method (Bar-Yosef and Kuhn, 1999; Boëda, 1991; Bourguignon, 1996; Boëda, 1990; Hiscock et al., 2009; Peresani, 2003), in addition to a range of less commonly documented techniques (Faivre, 2012; Geneste Jean-Michel, 1996; Slimak, 1999). Apart from novel technological system, this period also includes changes in mobility strategies, cognitive, social and adaptive behavious (Gamble, 1999), such as controlled use of fire (e.g. Berna and Goldberg, 2007; Goldberg et al., 2012), hafting (e.g. Boëda et al., 1996; Cârciumaru et al., 2012; Rots, 2009), use of pigment (D'Errico, 2008; Soressi and D'Errico, 2007), demographic growth, and expansion of hunting territories (Kuhn, 2013; Shennan, 2001).

The various changes and innovations happened in Middle Palaeolithic perplexed the technical behaviours in tool manufacture and management spatially and temporally. Within a given assemblage, although it is common that a system dominates, there is usually more than one system coexist (Beyries, 1993; Delagnes and Meignen, 2006; Jaubert and Farizy, 1995). These complicated diversities might be a result of changes in raw material availability, the intended function of tools, the range of technical knowledge (Delagnes and Meignen, 2006), population density and ecological environment, etc. The interaction of these factors may also have caused the discrepancy between East Asia and west Eurasia. For instance, the plausibility of the distinctive 'Middle Palaeolithic' in East Asia has been hotly debated since the mid-20th century (e.g. Boriskovsky, 1978; Gao, 1999; Gao and Norton, 2002; Kei, 2012; Movius, 1948; Norton Christopher and Jin Jennie, 2009). The lack of advanced stone tool technology in East Asia implies that hominin populations in this region were possibly culturally and genetically isolated during the early and middle Pleistocene (Wang, 2017). This theory, however, was challenged by the discovery of Levallois technology from the Guanyindong site dated to ~170 to 80 ka (Chapter 5). The findings from Guanyidnong suggest that the stone industry in East Asia during Middle and Late Pleistocene may have been more 'advanced' and 'distinctive' than what was thought. To contribute to this issue, this chapter presents further detailed study of the lithic assemblage from Guanyindong, which reveals a diverse lithic production that are comparable and contemporary to those found in west Eurasia and Africa during the same period.

6.2 Lithic assemblage of the Guanyindong site

To study the lithic characteristics of the Guanyindong assemblage, a total of 2,217 artefacts from the west entrance, including cores (n=249), flakes and flake fragments (n=1,199), retouched pieces (n=1,101), debris and chunks (n=769), were analysed in this study.

6.2.1 Raw materials

The raw materials of the assemblage is dominated by chert (77%) followed by limestone (21.7%) and basalt (0.9%). Other materials (such as sandstone and quartz) were only occasionally used (0.4%) (Table 6-1). The overwhelming exploitation of chert on core reduction and tool manufacture suggests that the Guanyindong hominins have deliberately selected chert as the raw material, being aware that chert is comparatively isotropic and fine-grained allowing them to have a closer control over the produce of 'pre-determined' objects. This procurement of homogenous raw material was achieved by strict selection on local materials or by importation through the effort in various environments. For Guanyindong, the majorities of raw material are accessible within 6 km (Leng, 2001; Li et al., 2009b). Specifically, chert is mainly available within the distance about 2–6 km, while limestone and volcanic rocks (such as basalt and quartz) are all available from local mountains, river bed and exposed sediments. Because the distance between sites and raw material source can be used to estimate the landscape that early hominin populations are physically and socially familiar with (Tryon and Tyler, 2013), so the raw material acquisition and artefacts transportation strategy can reflect the mobility strategies in hunting and foraging practices (Delagnes and Rendu, 2011).

Table 6-1. Stone artefact types and percentage of raw materials of Guanyindong site. The proportions are shown in the brackets following numbers.

	Chert	Limestone	Basalt	Other
cores	208 (83.9%)	38 (15.3%)	2 (0.8%)	0 (0%)
complete flake	141 (74.6%)	46 (24.3%)	0 (0%)	2 (1.1%)
flake breaks	6 (100%)	0 (0%)	0 (0%)	0 (0%)
debris	569 (74%)	190 (24.7%)	8 (1%)	2 (0.3%)
retouched chunks	43 (76.8%)	13 (23.2%)	0 (0%)	0 (0%)
retouched flakes and breaks	736 (78%)	192 (20.4%)	10 (1.1%)	5 (0.5%)
backed knife	5 (71.4%)	2 (28.6%)	0 (0%)	0 (0%)
bec	6 (85.7%)	1 (14.3%)	0 (0%)	0 (0%)
borer	47 (73.4%)	17 (26.6%)	0 (0%)	0 (0%)
bur	5 (83.3%)	1 (16.7%)	0 (0%)	0 (0%)
chopper	1 (50%)	0 (0%)	1 (50%)	0 (0%)
cleaver	1 (100%)	0 (0%)	0 (0%)	0 (0%)
denticulate	53 (69.7%)	21 (27.6%)	1 (1.3%)	1 (1.3%)
endscraper	30 (83.3%)	6 (16.7%)	0 (0%)	0 (0%)
natural backed	3 (60%)	2 (40%)	0 (0%)	0 (0%)
notch	68 (86.1%)	10 (12.7%)	1 (1.3%)	0 (0%)
point	23 (82.1%)	5 (17.9%)	0 (0%)	0 (0%)
scraper	464 (77.5%)	124 (20.7%)	7 (1.2%)	4 (0.7%)
tanged point	8 (88.9%)	1 (11.1%)	0 (0%)	0 (0%)
unidentifiable	22 (91.7%)	2 (8.3%)	0 (0%)	0 (0%)
overall	1703 (77%)	479 (21.7%)	20 (0.9%)	3 (0.4%)

Evidence showed that in Middle Pleistocene Europe most lithic materials were obtained from nearby sources (< 5 km) or relatively close localities (5–20 km), and stones collected between or beyond 20 km are rare (Fernandes et al., 2008). The distance between the site and main raw material source indicates that the Guanyindong tool-makers have been foraging and cruising a relative large landscape that require them to plan beyond the immediate needs, and be willing to spend more time and endeavour to obtain the raw materials they prefer (i.e., chert). This collecting distance in turn heavily affected the intensity of stone usage.

Table 6-2. Summary of mean, standard deviation (SD), variable coefficient (CV), quantile values at 25%, 50% and 75% for basic core attributes.

	Length (mm)	maximum dimension (mm)	medial width (mm)	distal width (mm)	thickness (mm)	distal thickness (mm)	mass (g)	platform	platform width (mm)	platform thickness (mm)	scar number	cortext percentage (%)
mean	47.2	75.1	58.0	49.2	51.8	38.7	198.9	1.5	50.9	43.7	2.9	14.5
SD	20.2	21.6	21.2	21.5	29.6	17.1	166.8	0.8	20.0	19.8	2.0	19.4
CV	0.4	0.3	0.4	0.4	0.6	0.4	0.8	0.5	0.4	0.5	0.7	1.3
25%	33.0	63.0	43.0	35.2	38.2	27.2	100.2	1.0	37.0	30.2	1.2	0.0
50%	43.5	72.0	55.0	45.0	47.0	37.0	149.5	1.0	50.0	40.0	2.0	7.5
75%	57.8	83.8	68.0	60.6	60.8	48.0	243.0	2.0	61.8	51.9	4.0	20.0

6.2.2 Core reduction

The primary attributes of 248 cores are summarised in Table 6-2. The median maximum dimension of them is 72 mm, which is larger than that of flakes (60 mm, Table 6-3). The median dimension is 43.5 x 55 x 47 mm. The median weight of the cores is 149.5 g. Chert dominates the raw material of cores (85%) (Table 6-1). Various geometries of cores were identified, including irregular (80.5%), conic (9.8%), column (6.7%) and small amounts of wedged and circular (~3%). Three types of cores can be identified according to the number of platforms (Figure 6-1A), single platform (60.5%), double platform (27.2%) and multiple platform (11.7%). According to technological reduction, most of them are ordinary cores, integrated with truncated faceting pieces (n=62; 24%), elongated core (n=15; 5%), discoid core (n=10; 4%), Levallois core (n=11; 4%), kombewa core (n=10; 4%), and small number of other types (i.e. bifacial core, hemispheric core). The majority (~80%) of cores have 1–4 flake scars, and some (16%) have 5–7 scars and only a small quantity (4%) have more than 7 scars (Figure 6-1B). The distribution of length of the scars on cores is shown in Figure 6-1C. The median length of scar is 26 mm.

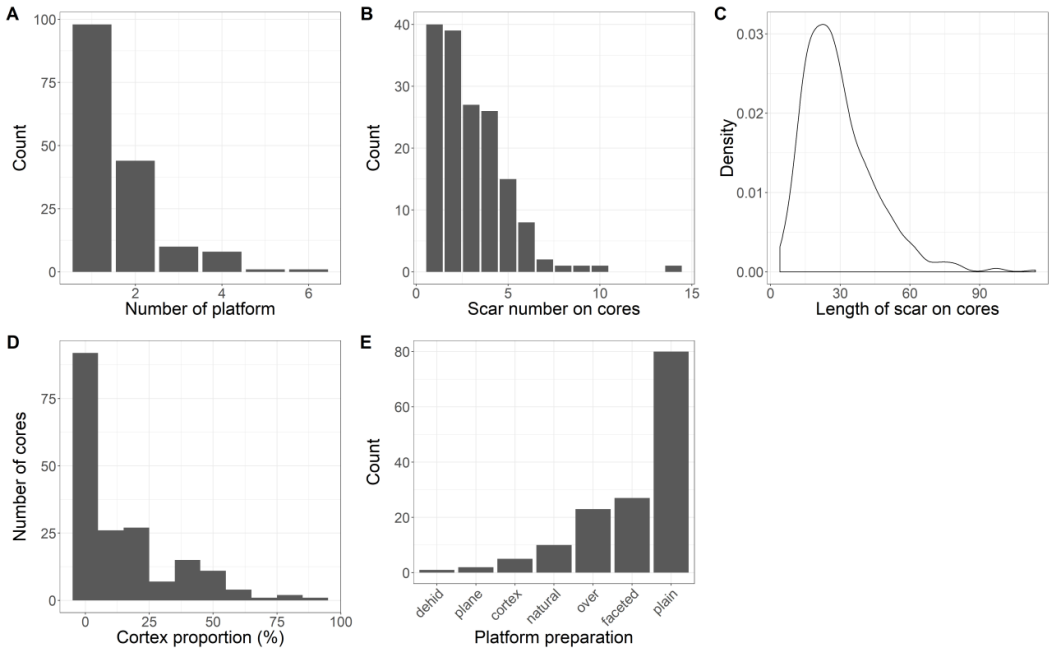

Figure 6-1: Statistical results of cores. (A, B, D, E) Histograms showing the number of cores with different number of platforms, scar number, cortex proportion and platform types. (C) Density distribution of the scar length on cores.

Most of cores (78%) are covered with zero or low percentage (< 25%) cortex (Figure 6-1D). The cortex locations are always on platforms and bottoms. The majority of platform type is plain (54%), followed by facetted platforms (18.2%) (Figure 6-1E). Most cores (83%) have 1 or 2 rotations, which means that they rotated the core 1 to 2 times to find a new platform to keep flaking when current platform and the original platform is no longer suitable for further striking. About 10% of the cores have 3 or more rotations.

Especially, there are plenty of cores been exploited from flakes, of which 4 patterns are observed based on the directions of knapping, unidirectional and bidirectional (Figure 6-2). Those cores are primarily exploited along the periphery of the flake, using the natural slab morphology of a flake as platform and volumetric consumption. There is another flake core type called truncated faceting that can be attributed as a preparation method.

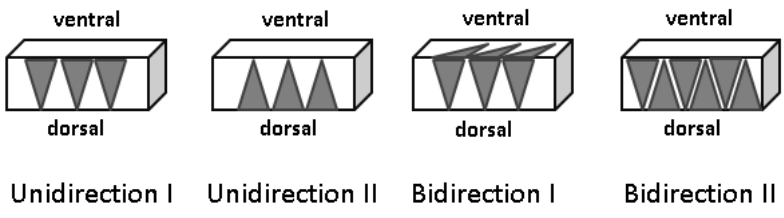

Figure 6-2: Flake core patterns. The grey triangles indicate the direction of flake scars. Unidirection I and II means flake scars only come from one direction. Bidirection I and II means flake scars come from different directions.

There are 12 cores that produce elongated flakes (see example in Figure 6-3.21). Those cores were manufactured on various blanks, such as chunks, nodular and flake. Direct hard hammer percussion is the technique that reduced cores. The median max dimension of the cores is 52.4 mm. Most of cores do not have cortex remained and the median number of scars left is 4. The morphologies of the cores are various, including irregular, column, wedged and cubic. Prepared and plain platforms dominate the core platform types. The cores are only minimally preparation, and the volume is not thoroughly shaped out before starting the production, thus showing significant variation in shape and size. For example, the geometries of these cores vary from circle to cylinder.

6.2.3 Flakes

Among the 1,138 flake pieces studied (see Figure 6-3 for selected specimen), there are 189 complete flakes, 214 retouched flakes, 6 flake breaks and 729 retouched flake breaks. The flaking technique is mainly free hand percussion with hard hammer. Seventeen flakes with lips and diffusive bulbs may indicate the possibility application of soft hammer (see example from Figure 6-3.8).

Table 6-3 summarised the basic flake attributions. The median dimension of complete flakes is 48 x 49 x 16 mm; this is larger than those of scars remained on the cores, suggesting that many of the flakes were obtained outside of the cave. The majority of flake has mass from 10 to 100 g (Figure 6-4A) and maximum dimension from 20 to 80 mm (Figure 6-4B). The median maximum dimension of flakes pieces is ~60 mm. The ratios of length and oriented thickness are shown in Figure 6-4C. The median of the ratios is 3 and more than 86% of the ratios are greater than 2, suggesting that the flakes are relatively thin and indicating a capability of a good knapping control. Figure 6-4D and E show the thickness and width at 25%, 50% and 75% of maximum dimension, respectively. Both the thickness and width at 50 % of maximum dimension are systematically and slightly larger than those at the other parts. This also suggests a good control over the morphology of flakes.

More than 80% of the fakes (including retouched flakes) have no cortex (Figure 6-4F). The cortex proportion of those flakes with cortex is mainly restricted from 5 to 10%. It suggests that most of flakes were obtained on the later stage of reduction. It is likely that hominins took secondary products into the cave before they initially knapped the blank outside.

There are 396 artefacts that have distinguishable platforms, which can be divided into cortex (n=36; 9.1%), plain (n=214; 53.5 %), faceted (n=42; 10.9%), dihederal (n=46; 11.4%) and focus (n=20; 5.1%). Although the plain and cortex platforms make up the largest proportion, flakes with prepared platform frequently appeared, indicating a predetermined strategy during core reduction. Besides, flakes with faceted platform are systematically larger than other platform types (Figure 6-4g), indicating that the hominins deliberate to obtain larger flakes through preparing flake platforms. In other words, the achievement of larger flakes cost more endeavour and require more sophisticated technologies.

Figure 6-3: Photos showing selected cores and flakes. 1-2, 4, single platform cores; 3,4, double platform cores; 6-7, discoid cores; 8, flake probably achieved by soft hammer; 9, truncated facetted; 10-11, Kombewa flakes; 12-18, flakes; 19, pseudo-Levallois point; 20 elongated flake; 21, elongated core.

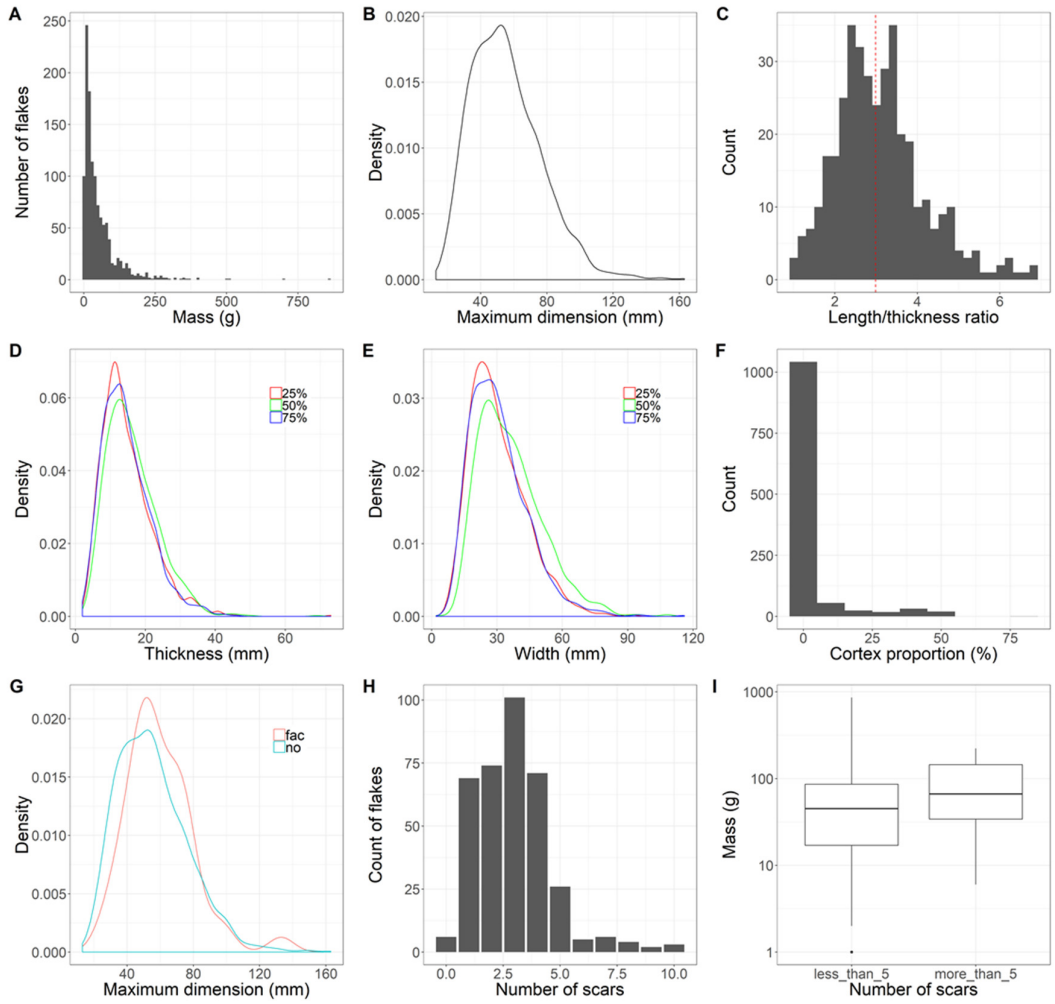

Figure 6-4: Statistical results for flakes. (A, C, F and H) The counts of flakes for different mass, different length/thickness ratios, cortex proportion and number of dorsal scars. The vertical red line in C represents the median value. (B, D, and E) Density distribution of flakes for different maximum dimension, thickness, and width. (G) Comparison of density distributions of flakes with and without faceted platforms. (I) Box plots showing the mass difference between flakes with different scar numbers

Table 6-3. Summary of mean, standard deviation (SD), variable coefficient (CV), quantile values at 25%, 50% and 75% for basic flake attributes.

	length (mm)	maximum dimension (mm)	oriented width (mm)	width at 25% maximum dimension (mm)	width at 50% maximum dimension (mm)	width at 75% maximum dimension (mm)	oriented thickness (mm)	thickness at 25% maximum dimension (mm)	thickness at 50% maximum dimension (mm)	thickness at 75% maximum dimension (mm)	mass (g)	platform width	platform thickness (mm)	scar number	cortex percentage (%)
mean	49.4	62.5	50.3	36.3	41.9	35.2	17.6	16.1	16.6	13.7	68.2	32.8	13.7	2.9	9.4
SD	19.2	22.5	19.2	14.1	15.3	14.8	8.1	7.6	7.8	6.8	81.7	16.8	7.8	1.6	15.1
CV	0.4	0.4	0.4	0.4	0.4	0.4	0.5	0.5	0.5	0.5	1.2	0.5	0.6	0.6	1.6
25%	35.0	48.2	36.0	26.0	30.1	25.0	11.8	10.9	11.0	9.0	18.8	19.9	8.0	2.0	0.0
50%	48.0	60.0	49.0	35.0	41.0	34.0	16.0	15.0	15.0	12.6	45.5	30.9	12.0	3.0	0.0
75%	60.8	76.0	61.7	44.9	51.1	43.0	23.0	20.9	21.0	18.0	90.0	43.0	18.3	4.0	10.0

The median dorsal scar number is 3 (Table 6-3) and flakes with 3 dorsal scars also account to the largest proportion (Figure 6-4H). Flakes with more than 5 scars are rare. In order to test whether the number of scars is related to size of flakes, the mass of flakes with more than 5 scars was compared with those with fewer than (and equal to) 5 scars (Figure 6-4I). It appears that flakes with more than 5 scars are systematically larger than those flakes with fewer scars.

The median dimension of flake platforms is 31x12 mm (Figure 6-5A). The shapes of platform include triangular (n=137; 44%), quadrangle (n=88; 28%), fusiform (n=46; 15%), and gull-wing (n=31; 10%) and with a small number of trapezoid, rectangle and irregular (Figure 6-5B). In order to test the possible relationships between platform shapes and flake dimension, the maximum dimension as well as thickness at 50 % of maximum dimension for different platform shapes is compared (Figure 6-5C and D). It appears that thickness of flakes with gull wing and fusiform platforms are slightly thinner (more concentrated around 10–15 mm), and those with triangular platform are the thickest (around 20 mm). Similar pattern is observed for the maximum dimension, i.e., the triangle platform is more evidenced on larger flakes.

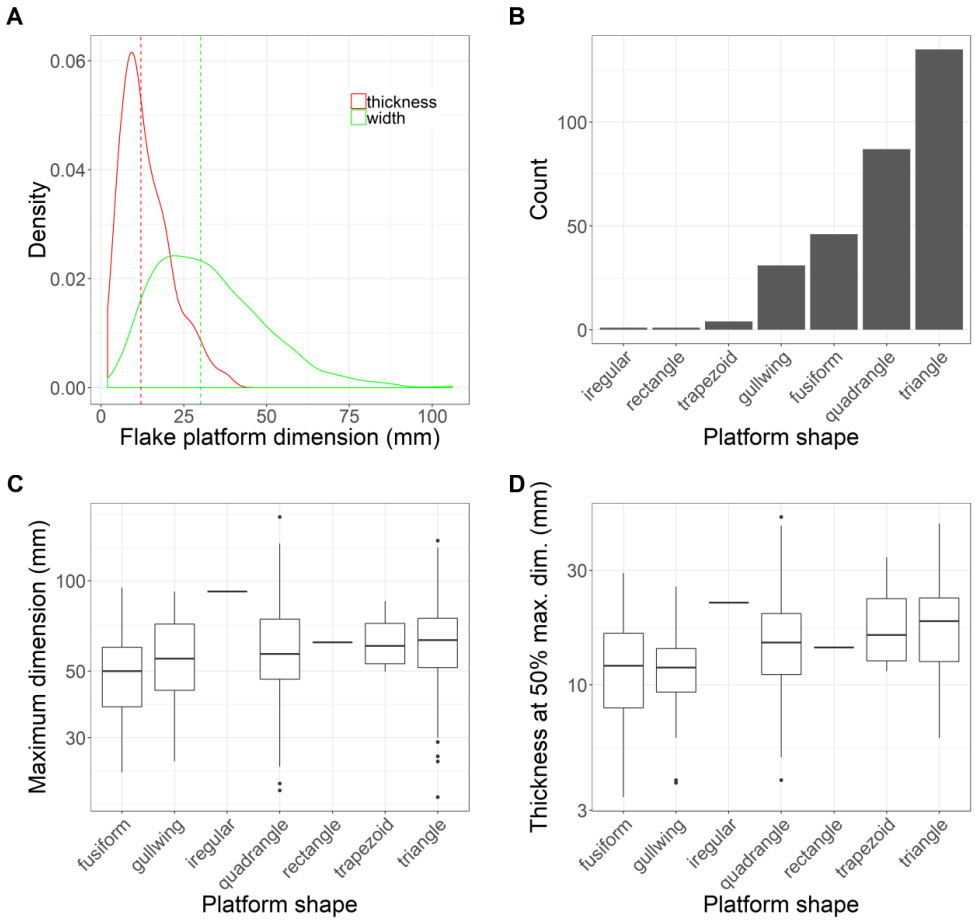

Figure 6-5: (A) Density distribution of flakes' platform thickness and width. The vertical lines represent median values of the corresponding distributions. (B) Number of flakes with different platform shapes. (C) Box plots showing the maximum dimension of flakes with different platform shapes. (D) Box plots showing thickness at 50% maximum dimension of flakes with different platform shapes.

The directions dorsal scars from 356 flakes were recorded. Except 85 scars that have lost the direction landmark, the number of dorsal scars on each direction are shown in Figure 6-6A. Among them, 221 flakes have dorsal scars that have the same directions of the flake. The other major directions are from 2, 3 and 8 (marked in gray semi-circle) suggesting suggests that most of the previous flakes on original cores have similar directions of the scar. In other words, the rotation of the core is limited.

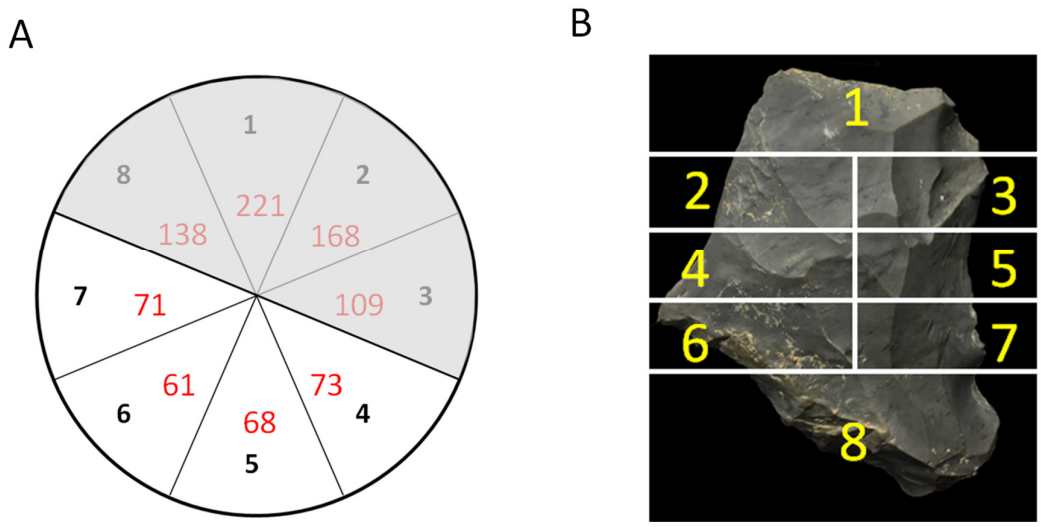

Figure 6-6. (A) Sketch showing the dorsal scar directions of flakes. The numbers in black are directions showing the scar directions (e.g. '1' from platform; '3' from right lateral; '5' from distal; '7' from left lateral). The numbers in red are the counts of dorsal scars that come from this direction. The gray area marks the most frequent dorsal scar directions. (B) Division of 8 sections on a tool.

The likely usage of soft hammer percussion is evidenced on 17 flakes with distinguishable lips and relatively diffusive bulbs of percussion (see example in Figure 6-3.8). A number of retouched flakes show parallel or sub parallel retouched, probably resulted from pressure technique (Dibble, 1994). There were 14 elongated pieces, including 11 elongated flakes, 3 crest flakes (see example in Figure 6-3). The median maximum dimension of them is about 74 mm and their platforms are mainly plain.

6.2.4 Retouch technologies

A total of 1,101 retouched pieces were found in the assemblage, accounting to 49% of lithic assemblage (see examples from Figure 6-7). The median maximum dimension is 54.1 mm. Compared to unretouched flakes, max dimensions and masses of retouched flake are smaller (Figure 6-8A).

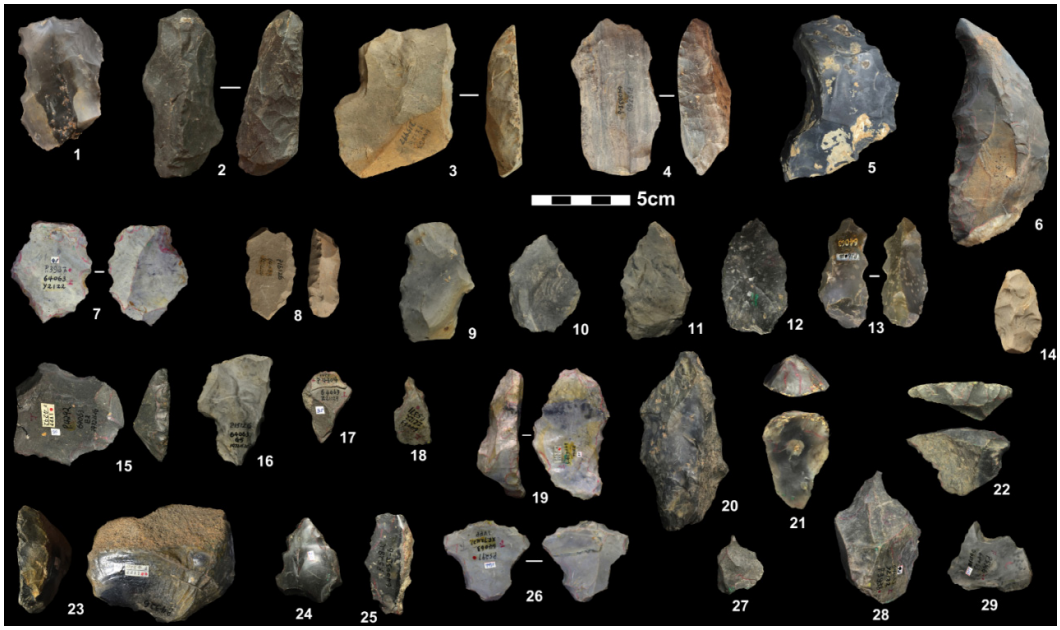

Figure 6-7: Selected retouched pieces. 1, 7, 9, 13 and 26, denticulates; 2-6, 8, 10-12, 14, 15 and 19, scrapers; 16, notch; 17 and 24, point; 18, 27-29, borers; 20, 25, natural backed knives; 21, 23 end scrapers; 22, transverse scrapers;

Given the fact that the tools in Guanyindong are invasively retouched, their smaller size may due to the consumption during recycling and resharpen. Most retouched pieces were made on flakes breaks (~70%) and flake (~20%), a small number of them are made on either chunks or pebbles. Side scrapers and denticulates dominate the sub-division of retouched pieces (65%), followed by borers (6%) and other types (Table 6-1).

The locations and shapes of retouch and the properties of the retouching scars provide us further insight into tool manufactory and management. The types of 1,559 retouched edges from 1,094 retouched pieces were recorded. They include convex, concave, straight, denticulate, end, notch, borer (Figure 6-8B). Among them, straight edge constitutes the largest proportion (n=575) followed by convex (n=395) and concave (n=274). The edge angle of 8 sections from a tool was calculated (each section means different part of the retouched piece, see Figure 6-6B).

Figure 6-8C demonstrates the distribution of edge angle. It shows that degree of section 1 to 8 are similar, mainly constricting from 50° to 80°. The median angle of all edges is 67°. This suggests that the edge angles of the entire blank is not only indiscriminately retouched and used but also relatively steep. More than half of retouched pieces were not only retouched on one edge, instead, they were retouched on 2 or more edges. Those data suggests a high efficient and massive exploitation of blanks that probably due to repeated recycling and resharpen.

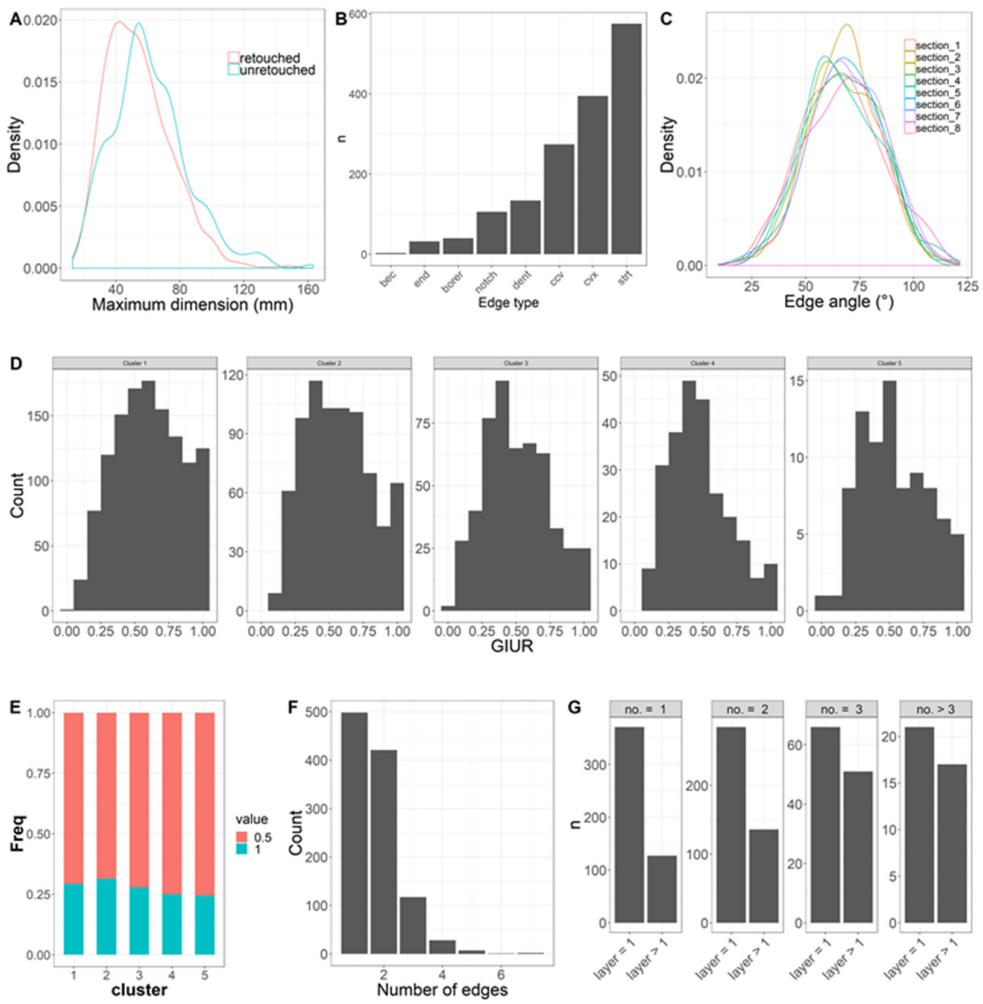

Figure 6-8: (A) Comparison of the density distribution of the maximum dimension between retouched and unretouched flakes. (B) Histogram showing the counts of tools for different edge types. (C) Comparison of edge angles among different sections. (D) Comparison of distribution of GIUR among 5 groups of flakes with different masses. (E) Invasiveness Index if the 5 mass groups of flakes. (F) Histogram showing the counts of tools of different number of edges. (G) The counts of tools that have one and more than one retouching layers for tool with different edge number.

According to index of invasiveness' (Clarkson, 2002) and GIUR (Geometric index of unifacial reduction) analysis (Hiscock and Clarkson, 2005; Hiscock and Tabrett, 2010; Kuhn, 1990), most of the specimens were extensively retouched, i.e., more than 67% of them have GIUR greater than 0.9. In order to investigate whether smaller pieces were more intensively retouched than larger pieces, the flakes was divided into five clusters of sizes based on a dynamic programming algorithm for optimal one-dimensional k-means clustering, which selects optimal number of clusters of flake sizes based on the Gaussian mixture model using BIC. Figure 6-8D and E shows the GIUR and Index of invasiveness distribution according to different size groups. Figure 6-8D shows that the smaller the tools tend to have higher GIUR values. This is constant with the speculation that the size had been considerably influenced by continuous retouch and reuse.

For the index of invasiveness, about 75% of retouching scars did not pass half depth of the section dominate (Figure 6-8E). This does not necessarily mean the inefficiency of retouch. On the contrary, it is due to most of the edge is too steep to allow the retouching scar overpass half depth of the section. Over half of tools have more than 1 edges (Figure 6-8F; count edges by the gap between each single retouch section) and with the edge number increase, the counts of edges that have retouch layers more than 1 increase too (Figure 6-8G). It suggests that the tools are heavily recycled and knappers not only inclined to resharpen the edges with secondary retouch but also attempted to create a new edge when reuse the tool.

For notch (n=79) pieces, the median depth and length is 3.7 and 11.6mm. The majority of notch is Clactonian notches (65%). Ordinary notchs only account for 32%. The rest of notches contain both Clactonian and ordinary notches. The notch edges are steep too. The location of retouching is mainly on one side which defined as longer geometric side of the piece.

6.2.5 Middle Paleolithic complex other than Levallois

6.2.5.1 Discoid Production

Ten discoid cores were identified in the assemblage (see Figure 6-3). Discoid/Mousterian debitage (Boëda, 1993; Bordes, 1961b) has been found in many sites with a significant variability (Jaubert, 1993; Pasty, 2000; Peresani, 1998). The roots of discoid production can trace back to the Oldowan (reviewed by Barsky, 2009; Peresani, 2003). It is considered to be a more simplistic method which was common adopted since the Lower Paleolithic (Picin and Carbonell, 2016; Stout et al., 2010; Vaquero M., 2003). Systematic comparison between Levallois concept and discoid were made by Boeda (Boëda,1995). For a discoid system the core consist of two highly convex surfaces and these surfaces can be used for both flake detachment or as striking platform within a single operational sequence. While for Levallois, the two surfaces are hierarchically related that cannot be reversed and their roles cannot be alternated.

The median maximum dimension of discoid cores in Guanyindong is ~70 mm. The median number of complete flake scars left on discoid core is four. Three of them have cortex covered on the surface. The platforms are mostly plain. Those cores all used recurrent centripetal method to detach removals from platforms extending around the entire periphery of the core.

A variety of end-products of discoid production systems are found from the Guanyindong assemblage including pseudo-Levallois points, short débordant flakes, triangular and quadrangular flakes. Pseudo-Levallois points and débordant flakes appeared in a small quantity. Because both centripetal recurrent Levallois method and discoid production are responsible for these kinds of flakes, so it is hard to separate those by products from either of the productions. Similarly, the debitage of discoid production is also reflected by the large number of triangular flakes. Those flakes always have a triangular scar covering most part of the dorsal surface and creating the ridge that guided the detachment of the flake leading to the parallel or sub-parallel formation of ventral and dorsal surfaces and flat morphology.

Usually, in an industry that contains both Levallois and discoid production aims to produce short, strong, and occasionally pointed implements, as evidenced by pseudo-Levallois points, backed flakes, and

quadrangular or triangular flakes (Delpiano and Peresani, 2017; Peresani, 1998). As stated above, it is hard to exactly distinguish what kind of production system that produces the triangular flakes purely based on individual's morphology and technology. However, with the appearance of pseudo-Levallois points (n=3), backed flakes (n=9), débordant flakes (n=12) and plenty of triangular flakes, it can be concluded that Levallois system and discoid production both coexist at Guanyindong.

6.2.5.2 Quina retouch

Quina production system, typically found in Europe (Delagnes and Meignen, 2006; Lenoir, 1986; Rolland, 1981), is also identified in the Guanyindong assemblage (Figure 6-9). Quina strategy linked to artefacts production, retouch and use (Kuhn, 2013). Quina tools, usually found in cave or shelter sites, commonly refer to tools made on thick or large blanks by using Quina retouch (steep, stepped scalar retouch) (e.g. Turq, 1989). The Quina system in Guanyindong (see example from Figure 6-9) is identifiable from 4 criteria: 1) tools possess distinctive stepped retouch (n=70), 2) steep edges, 3) thick blanks and 4) several retouching phases. The retouching scars on tools produced by the Quina method form a distinctive stepped morphology, especially where those scars overlapped on the retouched edge. The steep cutting edge is related to the rejuvenation of cutting edges after extensive use and blunting, making the edges less efficient, for example when processing hides (Preysler, 2010). Frequent resharpening and recycling to extend the use-life of tools are typical principles of the Quina system (Delagnes and Rendu, 2011).

There is some debate on whether Quina retouch was intentionally produced (e.g. Lenoir, 1986) or whether it is the result of resharpening thick blanks unintentionally (e.g. Dibble, 1987). Nevertheless, the presence of Quina artefacts at Guanyindong indicates intensive retouching activity, which is relevant to understanding mobility patterns of the hominin occupants of the site. Often, Levallois strategies are interpreted as indicators of less mobility than the Quina and discoid-denticulate systems, whose tools were modified by several successive retouching phases, indicating a higher level of mobility (Delagnes and Rendu, 2011). The higher proportion of Qunia relative to Levallois pieces, and traces of invasive tool reduction and constant recycling at Guanyindong may indicate frequent and long distance travel by the hominin occupants of Guanyindong.

Usually, Levallois production indicates a lower transportability of production strategies, while for Quinar and discoid-denticulate system, of which tools always were modified by several successive retouching phases, indicates a higher level of mobility (Delagnes and Rendu, 2011). This is especially true for the case of Guanyindong, since the raw material resource of Guanyindong is relatively close to the site (2–6 km), leading to a stable and easy-to-access supply of raw material. So the extensive retouching would be likely related to reuse and reshape of tools during high mobile activities. This explains why individual tools in Guanyindong having several retouching series appeared with a high occurrence (>50%). Hominins occupy this cave during 170-90 ka (MIS6-5), corresponding to the period of increasing of mobility in Mousterian technological diversity (Delagnes and Rendu, 2011; Geneste, 1985, 1988b, 1990). The invasive tool reduction and constant recycling could have been a response to the growing activities of frequent and long distance travel when their hunting territories expanded in Middle Palaeolithic.

However, there are still debates on whether Quina retouch was intentionally produced (e.g. Lenoir, 1986) or whether it is the result of resharpening thick blanks unintentionally (e.g. Dibble, 1987).

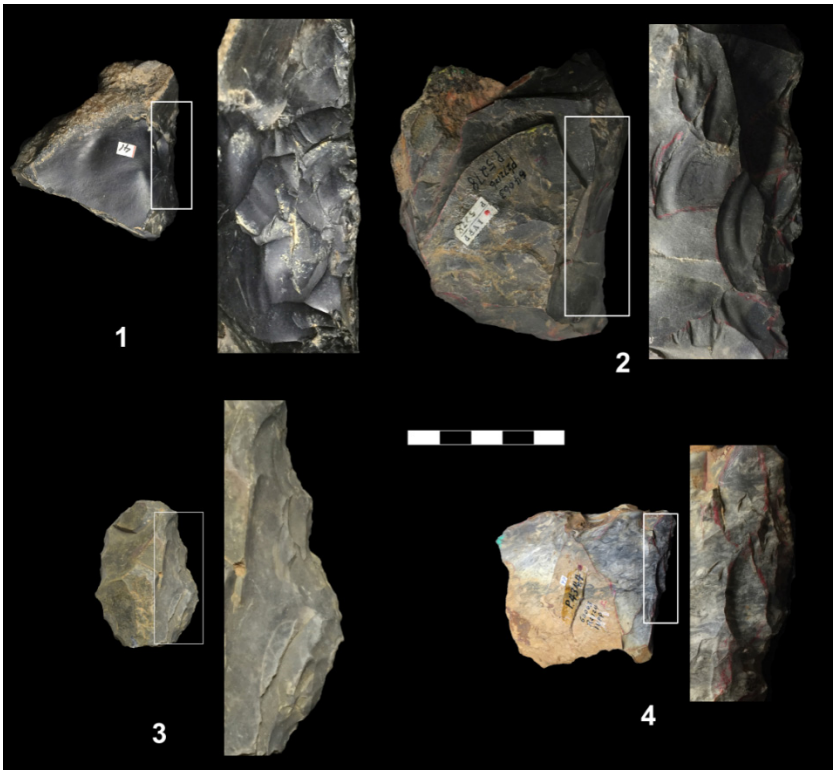

Figure 6-9: Examples of Quina tools. The photos on the right of each panel shows the details in the rectangular of the artefact on the left.

6.2.5.3 Kombewa production

Kombewa production (see examples from Figure 6-3.10-11), firstly found by W.E. Owen (1938, 1939) and further described by Tixier (1980) and Dauvois (1981), has be found in many lithic industries around Africa and Eurasia (see Boëda and Au Présent, 2018; J. Wang, 1994). It is featured by two bulbs left on both upper and lower surface. As one of the predetermined debitage, it needs to firstly achieve a flake with an announced bulb and second to detach the predetermined flake (Kombewa flake; Dauvois, 1981) with desirable shape (usually oval and sharp edge). In Guanyindong assemblage, the kombewa unit consist of 21 flakes (median maximum dimension = 69 mm) with both ventral and dorsal sides that present convex swellings resulted from detachment bulbs and 10 kombewa cores (median maximum dimension = 82.4 mm) most of which are truncated faceting too. Due to morpho-functional quality and to the sharp edges, Kombewa as a knapping technique (Tixier et al., 1980) was mainly used in the Acheuleans assembldge from Africa before the Levallois method (Inizan, 1999) or the mousterians (Casini, 2010). Although this method is perfectly known as production of blanks for core-tools in Africa, it was also applied when producing tiny flakes (Bordes, 1975). Here, kombewa method was utilized to produce relatively small flakes with sharp edges once they are obtained.

6.2.5.4 Truncated faceted

Another preparation form found in Guanyindong assemblage is the presence of 54 truncated faceted pieces that expresses standard metric features and typology. It is identified as the Middle to Upper Paleolithic transition and Early Upper Paleolithic industries of Northern Asia (Shalagina et al., 2015). These pieces usually started from a flake and then knapped along the periphery of the flake and take its ventral side as working surface, ending up as cores with the flake scars on ventral side, indicating the production of invasive flakes from platforms along the dorsal edge. The functions of truncated faceting pieces are controversial (Dibble, 1984; Goren-Inbar, 1988; Nishiaki, 1985; Solecki, 1970). Some believes it is a type of preparated core (Brantingham et al., 2000), while others primarily regard it as tools (Shalagina et al., 2015). In the case of Guanyindong, the relative larger ventral flake scars and improper edges as tools suggest it would be more likely utilized as cores.

The exploitation of flake as blank represent a predetermined concept, owing to the goal products needed to firstly have a plan in mind and prepare the construction of a core. It is regarded as the response to lack of lithic raw materials and to the special strategies of mobility of prehistoric people (Wallace and Shea, 2006). Although about 85% of truncated faceted pieces were made on chert, which is available beyond 2 km from the site, it still might indicate a high mobility of hominins. Because it would be favourable to use comparative larger flake (meidan maximum dimension = 76 mm) as cores to produce the desirable blanks during travelling.

6.3 Patterns in artefact reduction

6.3.1 Patterns in artefact reduction

To understand the technological sequences that produced the artefacts at Guanyindong Cave, flake attributes vary across different sized pieces were investigated. The distribution of flake mass is strongly right-skewed with a long tail, typical of many flaked stone artefact assemblages (Figure 6-10). The unimodal quality of this distribution does not indicate any obvious size classes suitable to use as analytical categories to compare flake attributes in different reduction stages. To divide the flakes in the assemblage into analytical categories, a dynamic programming algorithm for optimal one-dimensional k-means clustering (Wang and Song, 2011) was used. This method selects optimal number of clusters of flake sizes based on the Gaussian mixture model using the BIC. After limiting cluster membership to 30 or more artefacts, five clusters of size classes were found in the Guanyindong Cave flakes that can be used to investigate changes in flaking behaviours relative to size.

Raw materials are uniformly distributed across each size class (Figure 6-11). Cortex location shifts markedly from the left, right and distal areas of the dorsal surface for larger flakes (size class 5), to be found mostly on the platform and right side of the dorsal surface of smaller flakes (size classes 1, 2 and 3). This indicates that most small flakes result from advanced stages of the reduction process. The high proportion of flakes with cortex on the right indicates a repeated sequence of flake removals moving left

to right across the face of a core. Platform shape shows a trend of an increasing proportion of rhombus platforms as flake size decreases. The “gull-wing” (Moore, 2004) platform (also called "platform beveling" (Leader et al., 2017)) is increasingly represented in the smaller size classes. This shape of platform is resulted from detachment of a flake directly behind the location of a previously detached flake, which has been frequently found in Levallois points (Moore, 2003), Nubian Complex (Chiotti et al., 2009) and tula adze blanks (Moore, 2004). This pattern in the Guanyindong assemblage indicates a high degree of precision when producing the smaller flakes.

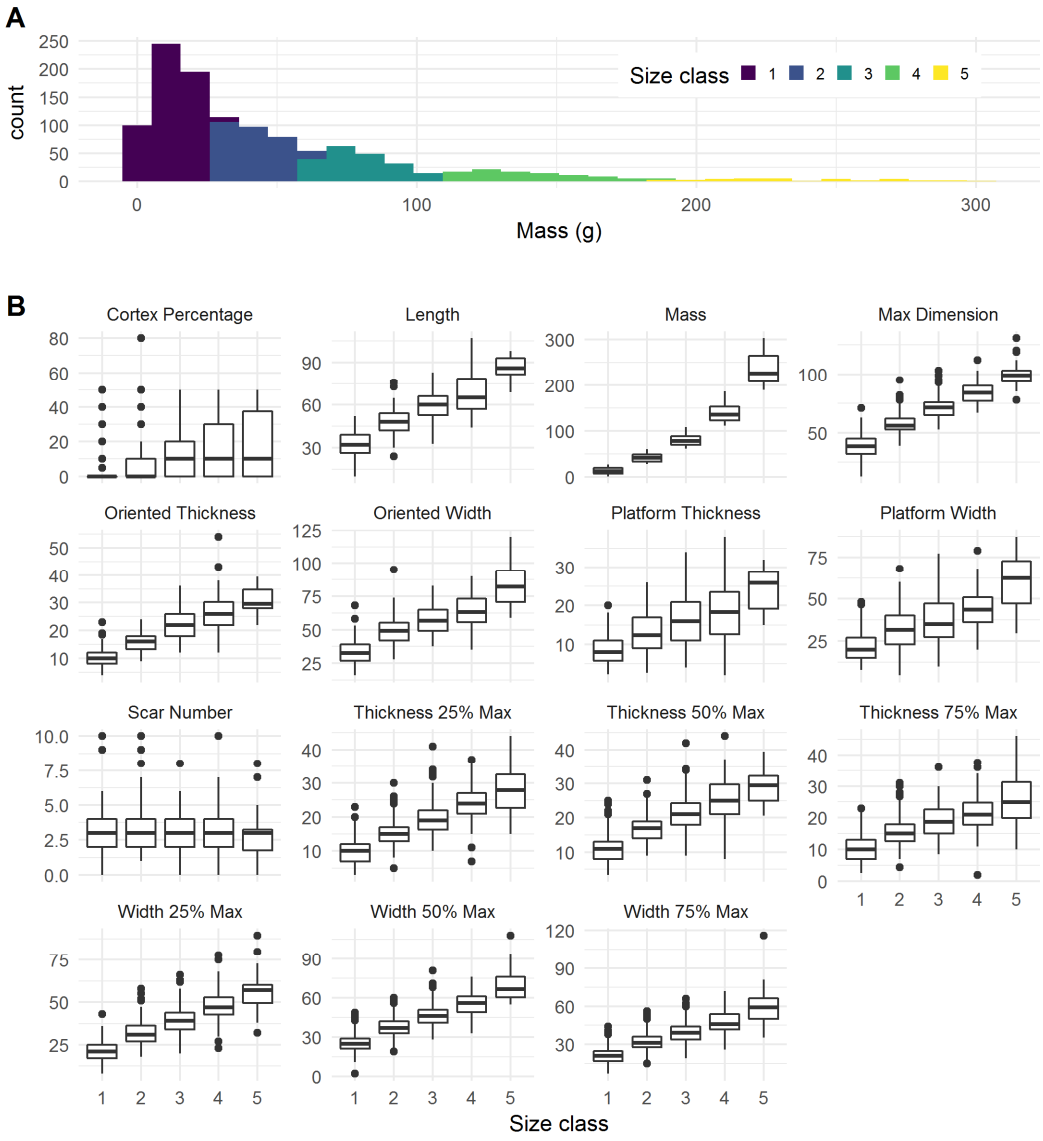

Figure 6-10: Distributions of metric variables on flakes: (A) Histogram of flake lengths, coloured by size class. (B) Box-and-whisker plots of a selection of metric variables to show technological variation across the size classes to reveal the lithic reduction sequence. Linear dimensions measured in mm, mass in g.

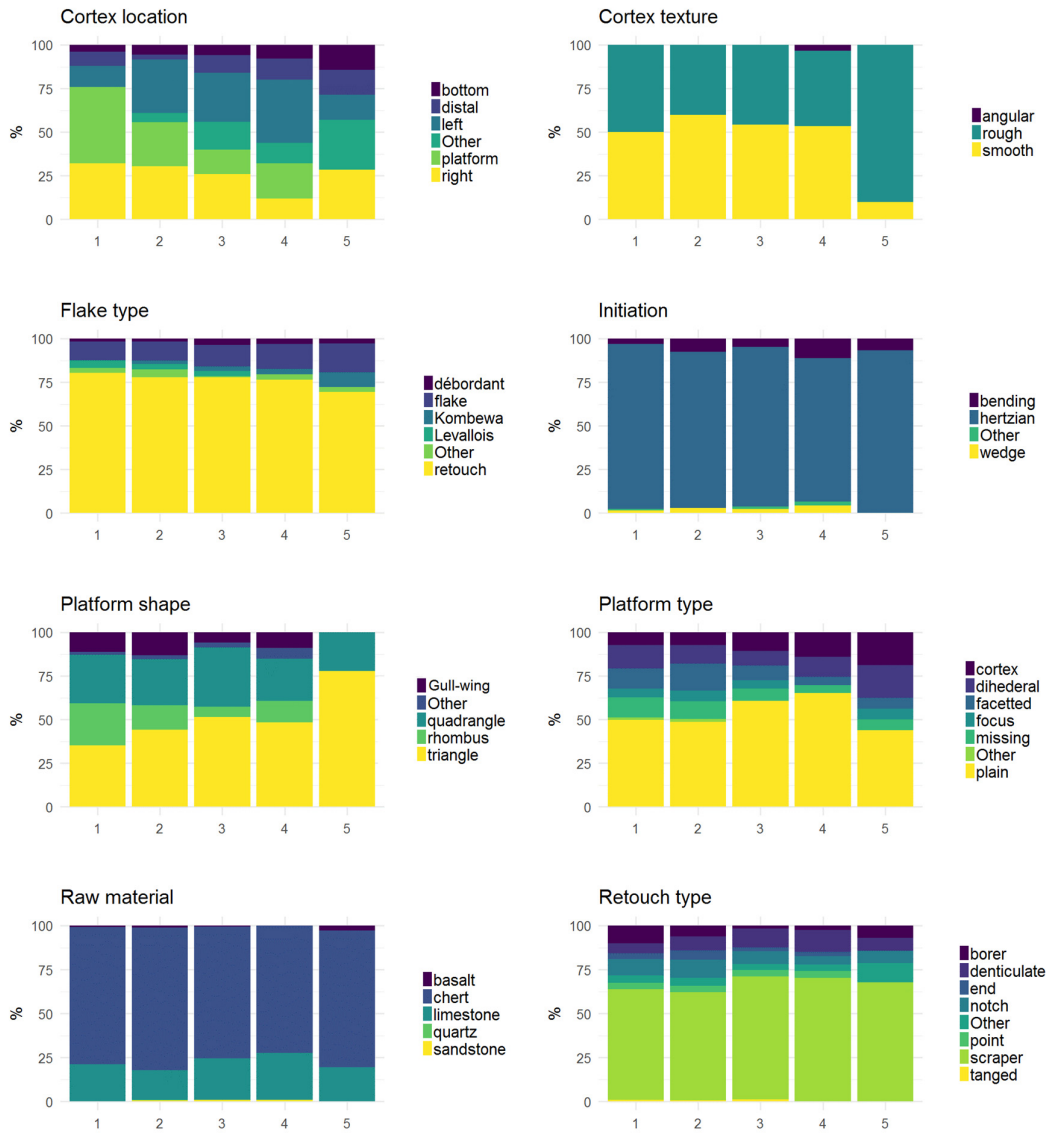

Figure 6-11: Distributions of technological attributes of flakes across the five size classes.

Platform types are highly diverse throughout the reduction sequence. Missing platforms are more common on the smallest flakes. Faceting is only evident on mid- and small-sized flakes (size classes 1, 2, and 3), consistent with a Levallois strategy of preparing cores by flaking across their platforms, resulting in flakes with facetted platforms. The low proportions of faceting on large flakes indicate that this was not a generic technique applied at all reduction stages, but only preferentially applied to certain-sized flakes produced via Levallois processes. We can see further support for this in the distribution of flake types, with Levallois flakes also appearing only in the mid- and small-sized flakes. This indicates a well-controlled reduction strategy where the production of Levallois flakes was constrained to a specific size range. Kombewa flakes are most abundant in the largest size class. This type of flake is distinctive due to having two opposed bulbs of percussion because it is detached at the intersection of the platform and ventral surface of a larger flake. The rarity of Kombewa flake in the smaller sized flakes reflects the high levels of inertia and precision required to detach a flake from a larger flake

The distribution of retouch types shows complex variation across the reduction sequence. Only subtle changes in proportions are evident across the size classes. The three smaller size classes have the greatest diversity and most even distribution of retouch types. This indicates how retouch types present in the larger size class, such as scrapers, notched pieces, borers and denticulate pieces, are transformed into new types, such as tanged pieces, points, and end-scrapers, as reduction of a piece proceeds further and the mass of the pieced is reduced by reduction.

Figure 6-10 shows that as for larger flakes sizes, the oriented thickness and flake thickness (at 25%, 50% and 75% of the length axis) all increase only very slightly, relative to increases in mass, length, oriented width, platform width and platform thickness, which increase substantially. For the most part, flake thickness is thus less than expected for larger flakes. This indicates that the thickness of larger flakes was controlled by the knappers at the start of the reduction sequence, consistent with a deliberate strategy to produce flakes with desirable features in tools, such as capacity for retouch and reduction of torque. The percentage of dorsal cortex varies little, from a median of 10% to 0%, but with a higher range in the larger flakes. This indicates even the largest flakes often do not have much cortex on their dorsal surface, so some pre-processing of the artefacts must have happened before they arrived at Guanyindong Cave. The median and range in the number of flake scars is nearly constant across size classes.

6.3.2 Patterns among layers

Figure 6-12 shows that flakes are slightly larger in the upper layer, and more variable in the thickness dimensions. Limestone is more frequently utilized as a raw material in the upper layer, as well as a small amount of sandstone, which does not appear in the lower level assemblage. This minor increase in raw material breadth in the upper layer may relate to a decrease in the availability of chert on the landscape, perhaps due to increased vegetation cover during MIS 5 that may result in changes in forager mobility strategies. Most of the technological attributes show little difference between the upper and lower layers, indicating that the technological strategies were similar across the two periods. Notable differences include platform shape, where we see higher proportions of rhombus and gull-wing platforms in the lower layer. A much higher proportion of facetted platforms in the lower layer is also seen. The high

frequency of platform faceting in the lower layer is notable because faceting is a key step in the preparation of striking platforms on Levallois cores. While this attribute by itself is not sufficient to identify a piece as Levallois, the high frequency of it in the lower layer is consistent with this period (170–80 ka) as a time when the cave's occupants were producing Levallois technology.

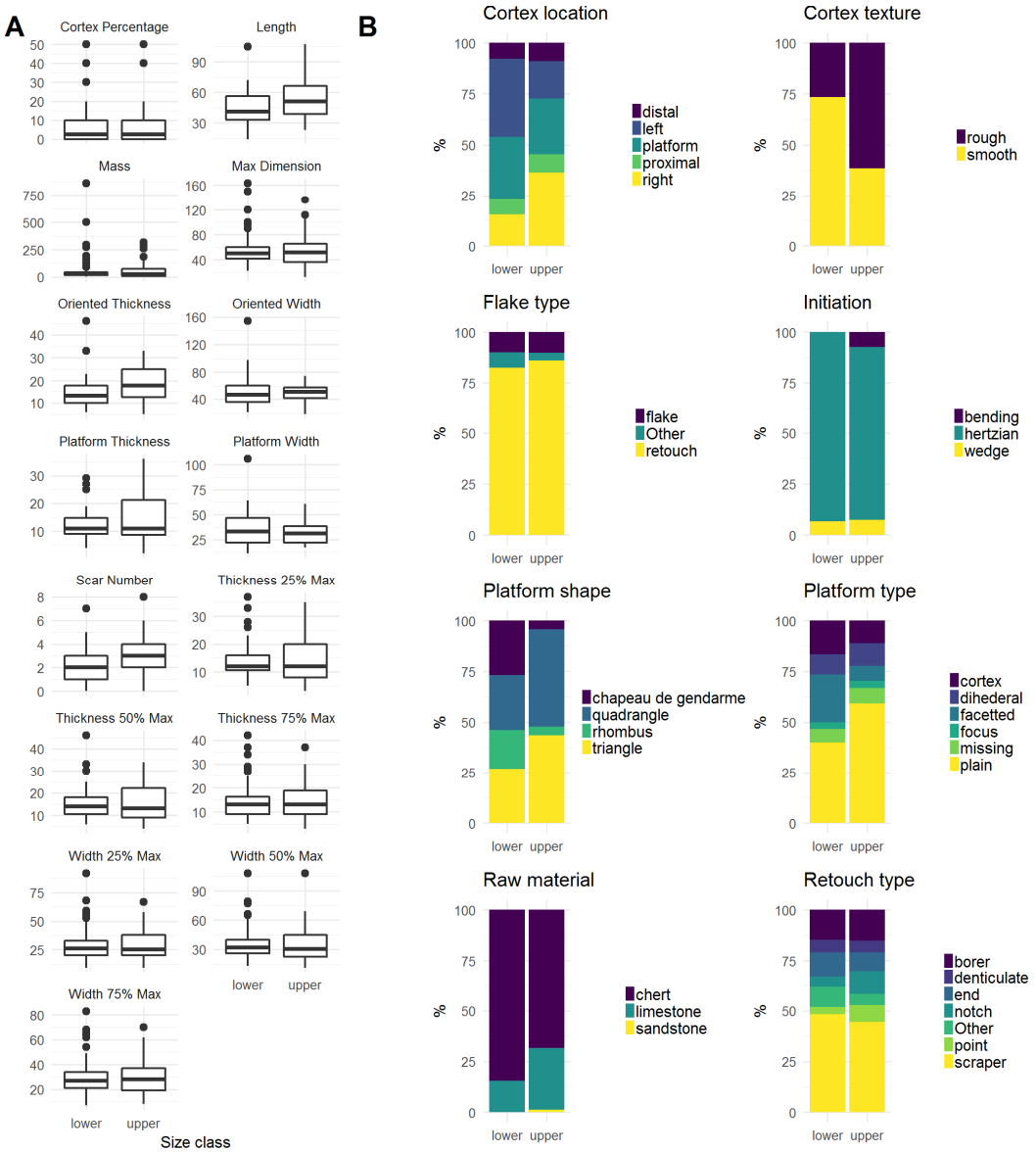

Figure 6-12: Comparison of flakes from the upper (Group A) and lower layers (Group B) of the deposit (n = 204): (A) Metric variables. Linear dimensions measured in mm, mass in g. (B) Technological variables.

6.3.3 Artefact taphonomy

Among the flake pieces in the assemblage, 63% (n = 732) are broken, among which most of them are retouched. Two processes are likely responsible for this high percentage: manufacturing failures during the knapping activity, and energetic taphonomic processes that have damages the artefacts after discard. The generally homogenous nature of the stone indicates that failures during knapping should be expected at a low frequency, assuming a competent knapper. The sedimentary feature of the deposits (characterised by well stratified and sorted silt and sand layers) inside the cave indicates a low-energetic depositional process. Thus, many of the breakages may be attributed to post-depositional processes such as ground surface breakage due to trampling. Many of the artefacts show considerable edge rounding/chipping, indicating some extents of taphonomic influence. For example, trampling and post-depositional processes may have damaged artefact edges in ways that resemble light retouch, which may partly explain the high percentage (46%) of retouched pieces in the whole assemblage. With just two artefacts showing signs of heat treatment, it is, hence, concluded that artefact damage due to excess heating occurred at a negligible rate at Guanyindong Cave. The surface texture of the artefacts is generally fresh, indicating limited weathering from exposure to pedogenic processes. This is probably a result of the cool, dry environment within the rockshelter.

6.4 Summary

To date, many paleolithic sites in southwest China have been found (Cai, 1991; Cao, 1978; Gao, 2012; Qiu, 1985; Wu, 1975; Zhu, 2011), though only a few of them, such as Guanyindong and Panxiandadong (Huang et al., 1997; Miller-Antonio et al., 2004), have been reliably dated to the Late Middle Pleistocene period. Similarly, very few sites from this period contain evidence of technical behaviors found in the Middle Pleistocene in western Eurasia. Evidence of various traits of Middle Palaeolithic technologies in Guanyindong, such as Levallois strategies, multiple blank production techniques including discoid, Kombewa, and various methods on tool manufacture and management such like Quina-like systems, suggests that during MIS 6 – 5 hominins in this area had the comparable abilities as those in Europe and Africa. It remains unclear whether these technical traditions coexisted in or replaced each other over time. Further research at other Late Middle Pleistocene sites in this region may help to establish more detailed pattern and timing of the Middle Palaeolithic production and whether this is a result of technology convergence or cultural transmission needs further evidence and more studies.

Chapter 7: Lithic assemblage and Chronology of Tianhuadong

The content of this chapter is based on an article submitted to the *Quaternary Research*, but with some changes (e.g. excluding the introduction of the site and method description, etc.) made for this thesis.

Yue Hu, Qijun Ruan, Jianhui Liu, Ben Marwick, Bo Li. Luminescence chronology and lithic technology of Tianhuadong Cave, an early Upper Pleistocene Paleolithic site in southwest China. Quaternary Research (accepted).

7.1 Lithic assemblage of the Tianhuadong site

The detailed measurement and analysis of stone artefacts from this site were conducted by Dr. Ruan Qijun from the Yunnan Institute of Cultural Relics and Archeology, and the details have been reported in Ruan et al. (2017). In this thesis, I only briefly summarise the key features of the assemblage to give context to the new OSL ages and discuss the archaeological implication of this site.

Table 7-1 summarises the number of stone artefacts collected from individual cultural layers and surface. Most of the artefacts (n = 114) came from Layer 2, followed by Layer 1 and then Layer 3. The artefacts collected from the surface and individual layers show similar features in the extent of weathering, raw material and typology. There are no clear technological changes through different layers. This, however, does not rule out any systematic difference among different layers, due to the relative small number of artefacts excavated from individual layers. Further excavation may be able to provide more statistically significant information for studying the stratigraphic and chronological evolution in the stone technology. At this stage, hence, it is best to treat the stone artefacts from all layers as a whole assemblage. The entire lithic assemblage consists of cores (n=37), flakes (n=509), tools (n=112), chunks and debris (n=464). Hard hammer percussion is the dominant technique been utilized. The raw materials are dominated by basalt (78%) and there appears to have no major changes in preference in raw material selection over time.

7.1.1 Cores

Selected cores from Tianhuadong site are shown in Figure 7-1. There are two types of core strategies, simple debitage and complex debitage. Cores that demonstrate no signs of preparation or predetermination were classified as the simple debitage (Figure 7-1.1, 4-6). This type of core includes single platform, double platform and multi-platform cores. Other cores show traces of preparation and predetermination or have a relative stable morphology and reduction strategy represent complex debitage (Figure 7-1.2 and 7-1.3). Most cores are knapped simply, yielding a constricted number of flakes with irregular morphologies. There are two cores that resemble the Levallois reduction (Figure 7-1.2 and 7-

1.3) due to the recurrent centripetal scar pattern shown on the upper surface and other criteria such as hierarchical construction. One core displays several parallel scars (Figure 7-1.4).

7.1.2 Flakes

Selected flakes are shown in Figure 7-2. There are 420 complete flakes, which comprise ordinary flakes, elongated flakes, crest flakes, discoidal flakes, Levallois-like flakes and triangle flakes. There are 89 flake breaks including proximal, distal and medial breaks, left and right splits. Elongated flakes are defined as having a length dimension that is two times greater the than width dimension, and with regular ridges on the dorsal side (Figure 7-2.4 to 7-2.8). There are several flakes that have sharp edges and thick centre with centripetal ridges convergent in the middle (Figure 7-2.9 to 7-2.12), which may have been produced from classic discoidal cores. There are a small number of Levallois-like flakes that demonstrate nearly elliptic shapes, centripetal dorsal scars and other features that resemble products obtained from Levallois reduction (Figure 7-2.13 to 7-2.15).

7.1.3 Tools

Tools make up 10% of the entire assemblage. They consist of hammers, sidescrapers, denticulates and notches (see Figure 7-3 for selected tools). The blanks of tools are mainly flakes or broken flakes. Most of them are small and with a low intensively of retouch, leading to irregular morphologies and edge shapes as well as uneven retouching scars. There are only few tools with extensive small retouching. Notably, there are 38 scrapers, which was termed as ‘Quina-like scrapers’ (Ruan et al., 2017) that exhibit similar features with Quina retouch scrapers found in Europe (Figure 7-3). These scrapers are larger than other types of tools and are retouched on thick blanks (most of them are flakes). The retouching scars are stepped and terminate in either step or hinge fractures. Compared with other tools, they have more intensive and invasive retouch and regular morphologies. The retouching scars are evenly distributed, ending up with more normative edge shapes.

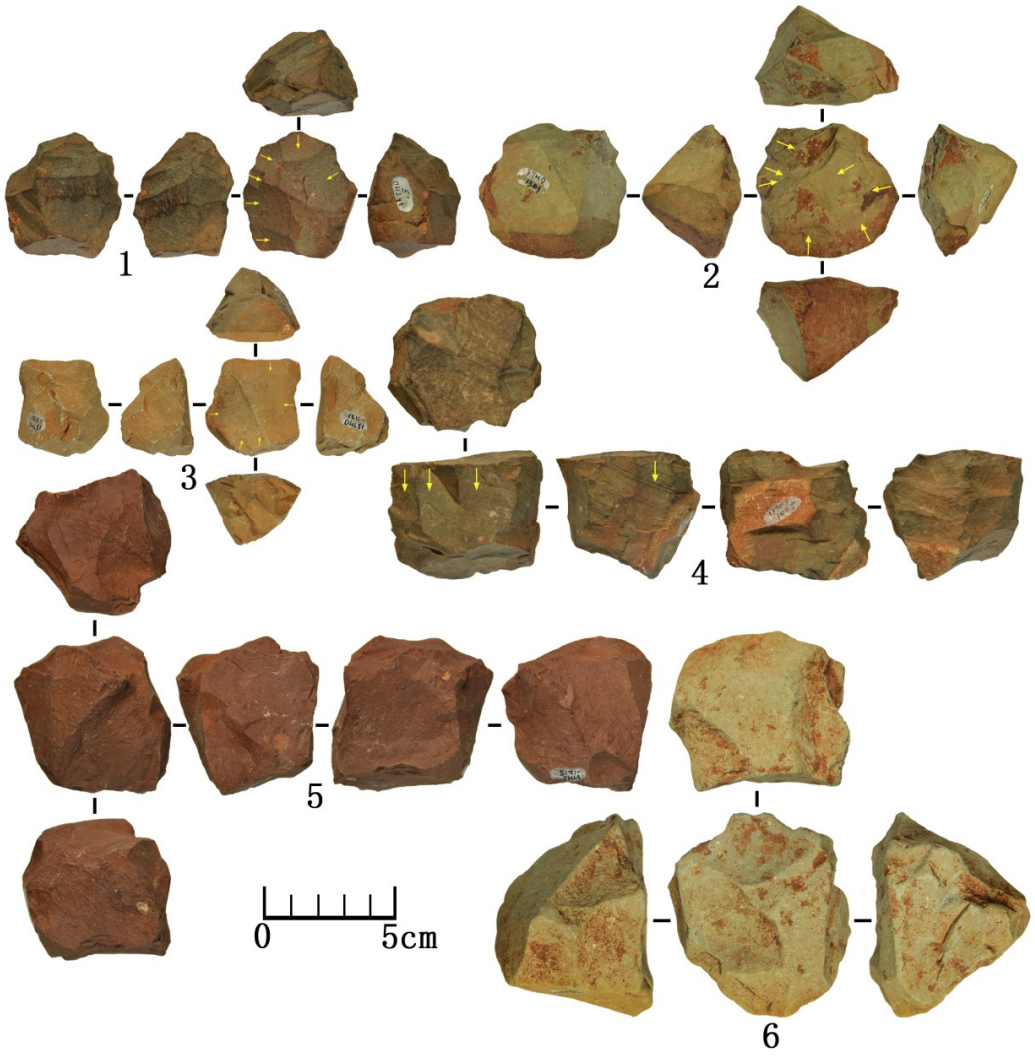

Figure 7-1: Photos showing selected cores from the Tianhuadong site. 1, Discoidal core; 2-3, Prepared cores; 4, Multi-platform core with elongated flaking scars; 5-6, Multi-platform cores. Photo sare from Ruan et al. (2017).

Table 7-1. Statistics on the distribution of stone artefacts collected from cultural layers and surface in the Tianhuadong site.

Layer	Cores	Whole flakes	Flake fragments	Tools					Debris	Total	Proportion (%)
				Broken hammerstones	Scraper	Quina-like scraper	Denticulate	Notch			
Surface	33	317	70	2	33	35	27	4	311	832	74
1	2	43	5	0	0	2	0	1	28	81	7
2a	1	41	9	0	1	1	0	1	46	100	9
2b	0	7	0	0	1	0	1	0	5	14	1
3	1	8	3	0	3	1	0	0	40	56	5
4	0	4	2	0	0	0	0	0	32	38	3

Table 7-2. Dose rate data, equivalent doses (D_e) and OSL ages for sediment samples from the Tianhuadong site.

Sample	Layer	Depth (cm)	Grain size (μm)	Water content (%) [a]	Gamma dose rate (Gy/kyr)	Beta dose rate (Gy/kyr)	Cosmic ray (Gy/kyr) [b]	Total dose rate (Gy/kyr)	D_e (Gy) [c]	Age (kyr) [c,d]
THD-OSL1	1	10	180–212	15 ± 5 (12)	1.84 ± 0.42	1.93 ± 0.11	0.150	3.92 ± 0.43	158 ± 17	40 ± 6
THD-OSL2	2a	30	180–212	15 ± 5 (13)	1.62 ± 0.38	1.80 ± 0.11	0.130	3.56 ± 0.39	186 ± 12	52 ± 7
THD-OSL3	2b	60	180–212	15 ± 5 (12)	1.52 ± 0.32	1.72 ± 0.11	0.115	3.36 ± 0.34	202 ± 9	60 ± 7
THD-OSL4	3	110	180–212	15 ± 5 (10)	1.48 ± 0.31	1.60 ± 0.09	0.110	3.18 ± 0.33	277 ± 17	87 ± 11
THD-OSL5	4	145	180–212	15 ± 5 (15)	1.57 ± 0.28	1.88 ± 0.12	0.105	3.55 ± 0.30	300 ± 22	85 ± 10
THD-OSL6	5	190	180–212	15 ± 5 (16)	1.62 ± 0.32	1.92 ± 0.11	0.100	3.64 ± 0.34	317 ± 15	87 ± 9

[a] Values used for dose rate and age calculations, with measured (field) water contents shown in parentheses.

[b] Values after correction for the zenith angular distribution of cosmic rays.

[c] The D_e and corresponding ages for THD-OSL1 and -OSL2 were based on maximum age model, but they should be considered as minimum ages.

[d] A systematic error of 2% was added (in quadrature) to the propagated random errors in the final ages to allow for any bias associated with calibration of the laboratory beta sources.

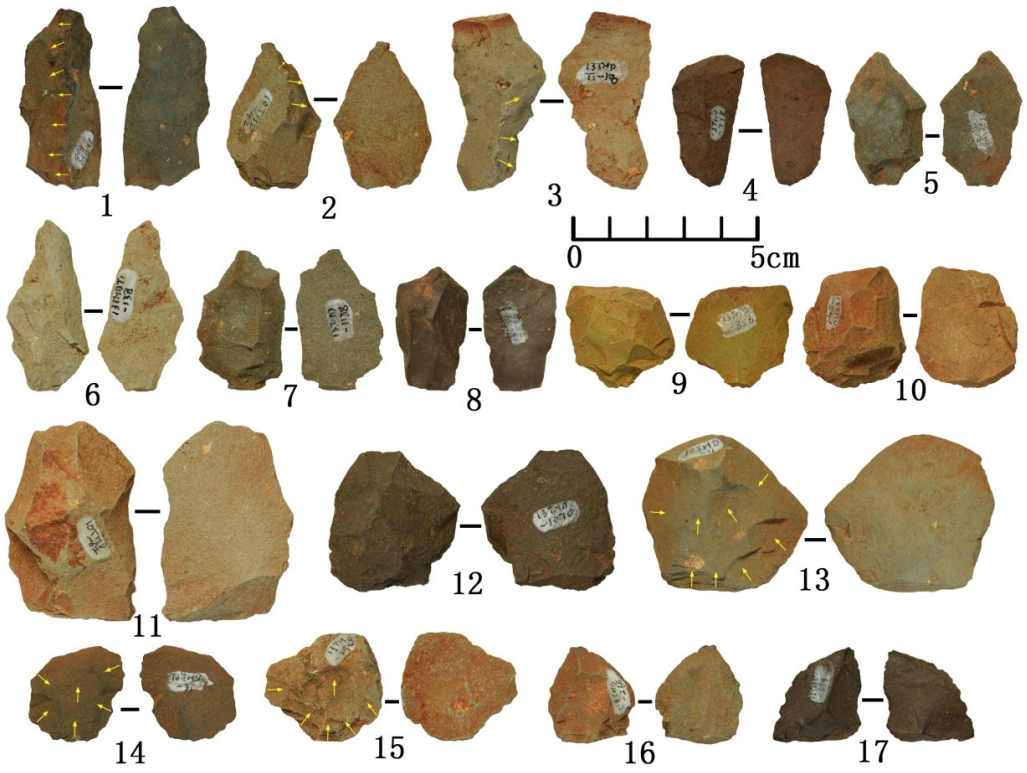

Figure 7-2: Selected flakes from the Tianhuadong site. 1-3, Crested long flakes; 4-8, Elongated flakes; 9-12, Flakes produced from classic discoidal cores; 13-15, flakes with Levallois dorsal scar patterns, 16-17, Triangular flakes. Photos are from Ruan et al. (2017).

Figure 7-3: Selected Quina-like scrapers discovered in the Tianhuadong site. 1-2, Discoidal retouched Quina-like scrapers; 3, Multi-edged Quina-like scraper; 4-7, Semi-discoidal retouched Quina-like scrapers. Photos are from Ruan et al. (2017).

7.2 OSL Dating

Attempts to date the deposits at Tianhuadong using radiocarbon methods have not been successful due to the old age of the dated materials (>50 ka). Previously research tentatively allocated the assemblage to MIS 5-4, because its lithic assemblage exhibits some characteristics that are comparable with Middle Palaeolithic cultures from Europe and Africa (Ruan et al., 2017). In order to provide a firm chronological framework for this site, OSL dating was applied to the artefacts-bearing deposits. Since K-feldspars are rare in the deposits and showed only a dim luminescence signal, this study focused on the quartz minerals to determine the sedimentary ages of the samples.

7.2.1 Sample description and preparation

A total of 6 sediment samples were collected from each of the stratigraphic layer and sub-layers from the north wall of the test trench (Figure 2-6). The samples were collected by hammering opaque steel tubes, each about 5 cm in diameter and ~25 cm long, into the cleaned section face. The samples were prepared using the procedure described in Chapter 3. Quartz grains of 180–212 μm in diameter were purified with HF etching and then used for D_e determination.

7.2.2 Measurement facilities

All OSL measurements were made on an automated Risø TL-DA-20 luminescence reader (see Chapter 3 for details). For OSL measurements, individual quartz grains were mounted onto standard Risø single grain discs, and each grain hole contained 1 grain. The OSL emissions were detected by an Electron Tubes Ltd 9235QA photomultiplier tube fitted with a 7.5-mm Hoya U-340 filter.

The environmental dose rate for etched quartz consists of beta and gamma radiation and cosmic rays. Beta dose rates were measured directly by low-level beta counting of dried, homogenised and powdered sediment samples from the dosimetry bags, using a GM-25-5 multi-counter system (Chapter 2). Gamma dose rates were measured based on the combination of thick source alpha counting (TASC) and beta counting (Chapter 2). The U and Th contents were first obtained based on TASC. The beta dose rate from U and Th were then calculated and subtracted from the beta counting results to estimate the contribution of beta from K; the latter was subsequently used to estimate the K content. The U, Th and K contents were then converted to gamma dose rates based on the conversion factors (Chapter 2). The cosmic-ray dose rates were estimated following Prescott and Hutton (1994), based on the geomagnetic latitude and altitude of the site, as well as the thickness of sediment above each sample. Since these samples were collected immediately in front of a mountain (Figure 2-5B), the overhead mountain shielding was taken into account, i.e., the cosmic-ray dose rates are about 50% of those if there is no mountain shielding. A relative uncertainty of 10% was assigned to account for the systematic uncertainty in the primary cosmic-ray intensity.

The measured water contents of the six samples range from 10 to 16 % (Table 7-2). Since these samples have been stored for a few months since being taken, it is expected that the measured present-day water

contents were slightly underestimated. So, instead of using the in-situ water content, a value of 15 ± 5% was used as an estimate of the long-term water content for all samples. The measured in-situ water contents are within the 1 sigma range of the assumed value. Each of the measured beta and gamma dose rates and the calculated cosmic-ray dose rate were corrected for attenuation by water using the assumed water content.

7.2.3 SAR performance test

The D_e values were determined using a single-aliquot regenerative-dose (SAR) procedure (Galbraith et al., 1999; Murray and Wintle, 2000), which involves measuring the OSL signals from the natural (burial) dose and from a series of regenerative doses, each of which was preheated at a given temperature (e.g., 240 °C) for 10 s prior to optical stimulation by the green laser beam for 1 s at 125°C. A fixed test dose (~10 Gy) was given after each natural and regenerative dose, with the induced test dose OSL signals used to correct for any sensitivity changes during the SAR sequence. A cut-heat to a temperature (e.g., 180°C) lower than the preheat temperature was applied to the test dose. A duplicate regenerative dose was included in the procedure, to check on the validity of sensitivity correction, and a 'zero dose' measurement was made to monitor the extent of any 'recuperation' or 'thermal transfer' induced by the preheat. The OSL infrared depletion-ratio test (Duller, 2003) was applied at the end of the SAR sequence, using an infrared bleach of 100 s at 50°C, to check for feldspar contamination.

In order to find the best suitable experimental conditions, e.g., preheat and cutheat temperatures, dose recovery tests were conducted using a range of preheat and cutheat temperatures (280/180, 260/180, 240/180, 220/180, 200/160 and 180/160 °C). Since the samples are dominant by bright grains (about half of the grains emit detectable OSL signal, Table 7-3), only one single-grain disc (100 grains) was measured for each preheat temperature. In this test, all the grains were bleached for ~30 min using a Dr Hönle solar simulator (model: UVACUBE 400). The bleached grains were then given a dose of ~100 Gy, before being measured using the SAR procedure with different preheat and cut-heat temperatures. To select reliable single-grain D_e results, several rejection criteria the same as those described in Chapter 4 (see section 4.2.3) were applied.

From 26 to 46 grains were accepted for each of the preheat temperatures after applying the above rejection criteria. The measured to given dose ratios (or dose recovery ratios) are summarised as radial plots in Figure 7-4A–F for each of the preheat temperatures, respectively. A central age model (CAM) (Galbraith et al., 1999) was used to calculate the weighted mean recovery ratios for each preheat temperature, and these were shown in each of the radial plots (Galbraith and Roberts, 2012; Galbraith et al., 1999). The distributions of the measured D_e are tightly distributed around a central value, and overdispersion (OD) values are all statistically consistent with zero. The dose recovery results were plotted against the preheat temperature in Figure 7-5A. It is shown that there appears a 'plateau' region between 200 and 260 °C. The recovery ratios are statistically consistent with unity at 1σ for the preheat temperatures at 220 and 240 °C, although the results from 200 and 260 °C are slightly lower than unity. There are significant overestimation and underestimation for the preheat temperature of 180 and 280 °C, respectively.

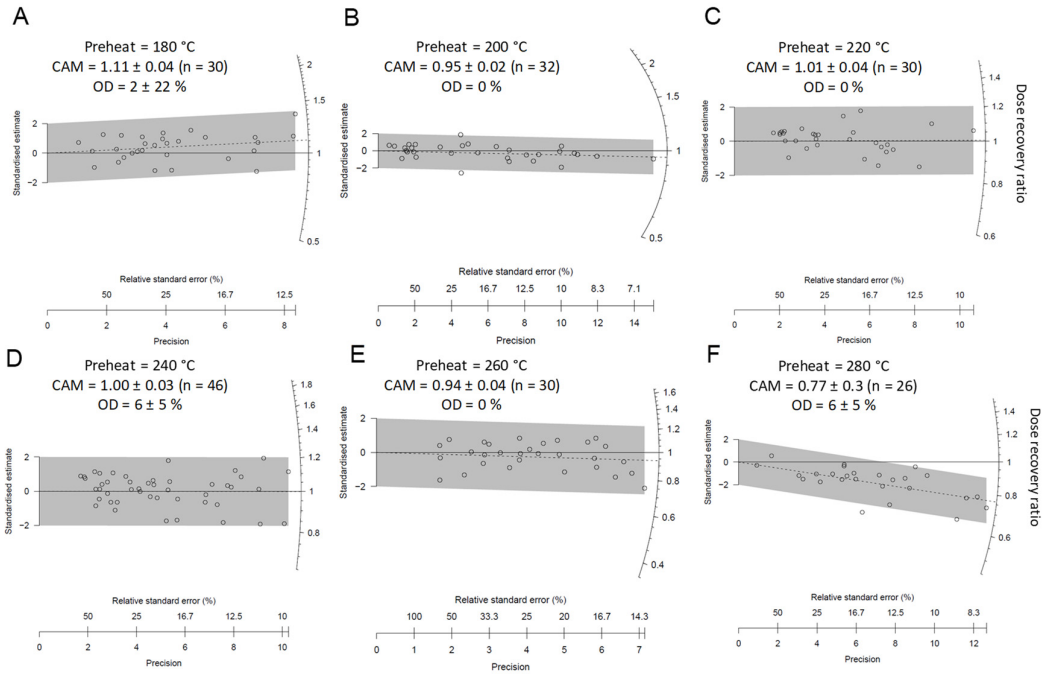

Figure 7-4: Dose recovery results for quartz OSL. (A-F) Radial plots showing the distributions of dose recovery ratios for individual grains for different preheat temperatures (from 280 to 180 °C, respectively) and the CAM and OD values

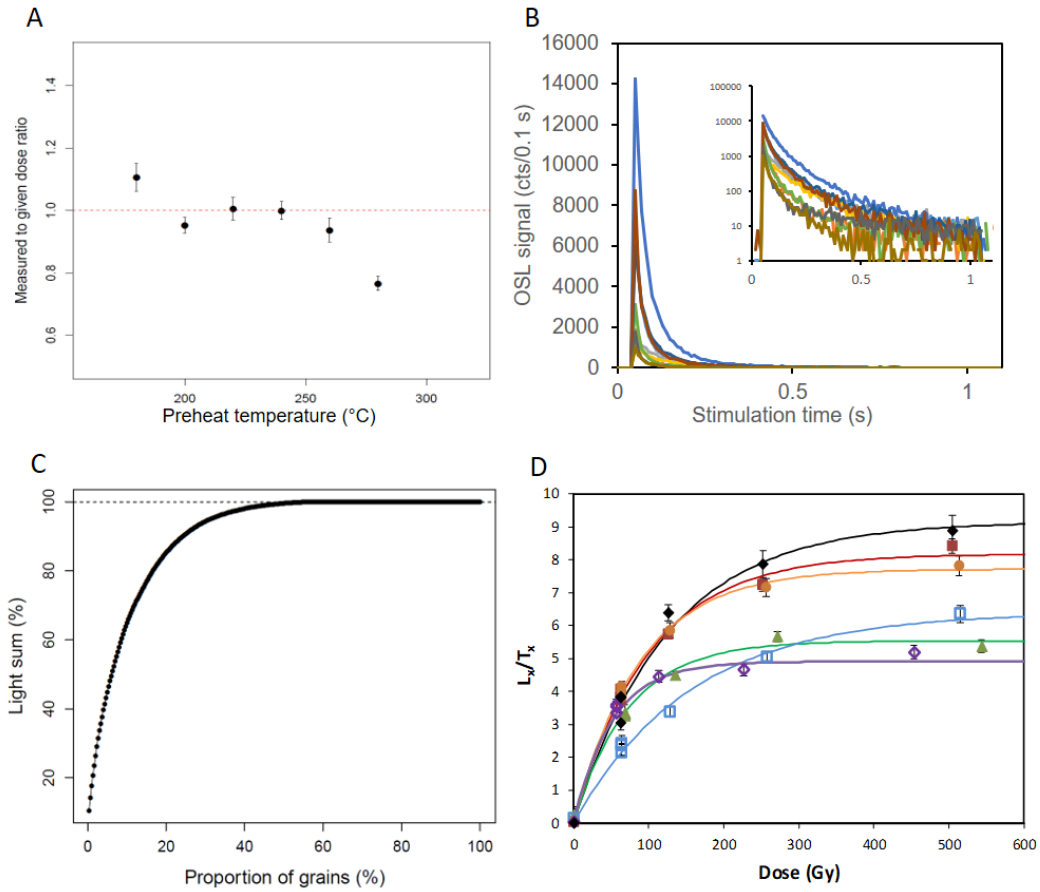

Figure 7-5: (A) The weighted mean dose recovery ratio plotted against preheat temperature. (B) Typical natural OSL decay curves of 10 grains of sample THD-OSL6. The inset shows the same curves in log scale. (C) Distribution of OSL signal intensities from 200 grains of quartz from sample THD-OSL6. Data are plotted as the proportion of the total light sum that originates from the specified percentage of grains. (D) Typical dose response curves from 6 grains of sample THD-6. The sensitivity-corrected (L_x/T_x) dose response curves were well fitted using a single saturating-exponential function of the form $I = I_0(1-\exp^{-D/D_0})$, where I is the L_x/T_x value at regenerative dose D, I_0 is the saturation value of the exponential curve and D_0 is the characteristic saturation dose.

7.2.4 D_e determination

Based on the performance tests shown above, the preheat/cutheat of 240/180°C was applied for measuring D_e values for all the samples. Figure 7-5B shows the natural OSL decay curves of 10 grains from THD-OSL6. The OSL intensity varies significantly from grain to grain, e.g., the net initial OSL intensity varies from a few tens of counts per 0.1 s to more than 10,000 cts per 0.1 s. Despite nearly half of the grains yielded detected OSL signal, about 20% of the grains contribute ~80% of the total OSL signal (Figure 7-5C). Apart from the variation in OSL intensity, the dose response curves from different grains also display a wide range of shapes associated with different saturation doses (Figure 7-5D).

Between 500 and 800 grains were measured to determine D_e for each of the samples, respectively. The same rejection criteria described above are applied to select reliable results. The rejected grains number

of each criterion is summarised in Table 7-3. About 60% of the grains were rejected due to weak signals (i.e., the initial intensity of T_n is below 3σ above the background intensity and/or its relative standard error is more than 20%). Only a few grains of each sample were rejected due to recuperation larger than 5%. Among the grains with detectable OSL signals, from 23% to 49% of them were rejected because their DRC data are too scattered to be fitted reliably. For those grains with satisfactory DRCs, however, there are significant proportions of grains (from 15% up to 57%) that have natural signals saturated. In other words, their L_n/T_n values are consistent or above the saturation levels of the corresponding DRCs, so that they yielded infinite D_e estimates or D_e error. After rejection of these grains, from 10% to 36% of the measured grains yielded reliable and finite D_e estimates.

The distributions of individual D_e values passed through the rejection criteria are shown in radial plots in Figure 7-6 for all the samples. It can be seen that all the samples have a broad range of D_e values, including many values close to zero, indicating that all the samples were affected by post-depositional mixture or intrusion of 'younger' grains. This is especially apparent in the two uppermost samples (THD-OSL1 and -OSL2), which is not surprising because the top layers are disturbed by recent agricultural and engineering activities that might inevitably result in mixture of younger and old grains in the upper layers and intrude some young grains into the deeper layers. Fortunately, the intensity of mixture decreases significantly in lower layers which can be shown from the significant reduction in the number younger grains for the 4 lower samples (THD-OSL3, -OSL4, -OSL5 and -OSL6).

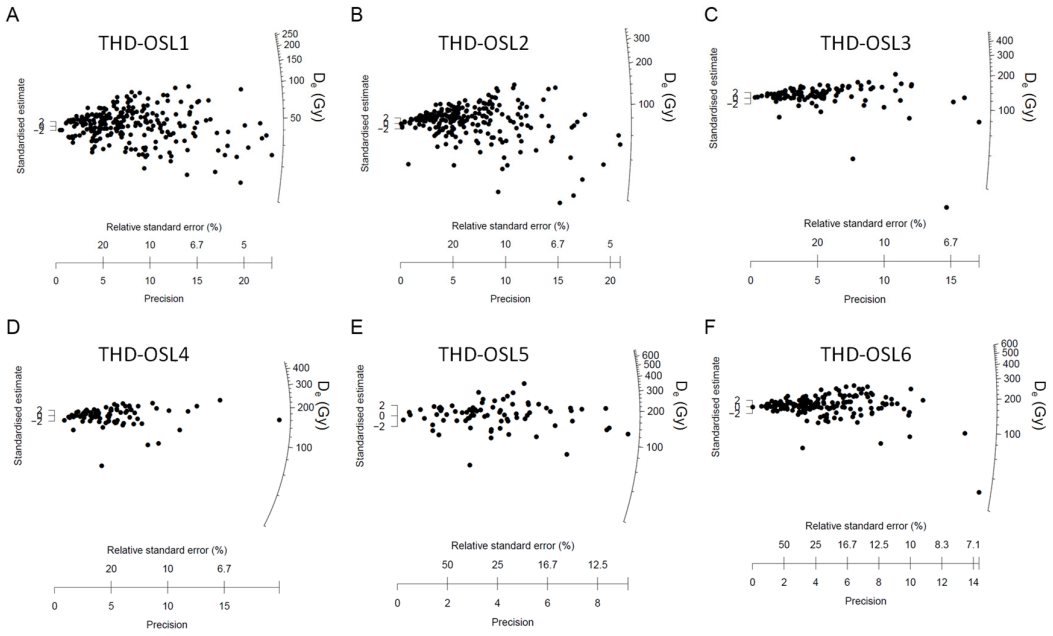

Figure 7-6: SAR De distribution of samples (A-F) D_e distribution for the accept grains of samples THD-OSL1 to -OSL6, respectively.

Table 7-3. Number of single grains or aliquots measured, rejected and accepted for each sample, together with the reasons for their rejection.

Sample	No. of measured	Rejection criteria						Accepted D_e values [b]	Proportion of saturated [c]
		T_n below 3σ above BG [a]	RSE of T_n > 20% [a]	Recuperation > 5%	Poor DRC [a]	D_e by extrapolation	No L_n/T_n intersection		
THD-OSL1	700	139	136	6	119	6	39	255 (36%)	15%
THD-OSL2	700	160	102	3	126	18	52	239 (34%)	23%
THD-OSL3	500	182	87	4	65	6	53	103 (21%)	36%
THD-OSL4	500	167	82	4	84	26	51	86 (17%)	47%
THD-OSL5	800	299	146	0	175	7	95	78 (10%)	57%
THD-OSL6	800	226	124	4	102	13	153	178 (22%)	48%

[a] BG, RSE and DRC represent background, relative standard error and dose response curve, respectively.

[b] The proportion of grains with acceptable D_e values is shown in the parentheses and was calculated as a ratio to the total number of measured grains.

[c] The proportion of saturated grains was calculated as the number of grains with D_e obtained by extrapolation and those without L_n/T_n intersection divided by the total number of grains that passed the first four criteria (columns 3–6).

As shown in Table 7-3, there are considerable proportions of grains (up to ~57%) that have natural signals being saturated, especially for the lower samples. It has been suggested by recent studies that the rejection of a large number of "saturated" grains may cause final D_e considerably underestimated because of the truncation of the full D_e distribution (Duller, 2012b; Guo et al., 2017; Li et al., 2017a; Thomsen et al., 2016). To deal with this problem, similar to the Guanyindong samples (see Chapter 4 for details), the method of analyzing the L_n/T_n distribution and establishing standardised growth curves (SGCs) proposed by Li et al. (2017a) were applied. When using this method, because grains that are saturated are also accepted, it can obtain a full and untruncated distribution of the L_n/T_n ratios with a reliable D_e estimation beyond the conventional limit of ~$2D_0$ using the standard SAR procedure.

First of all, the variability of the DRCs of the samples was investigated. Firstly, poorly-behaved grains were identified and rejected, so that only well-behaved grains with reliable growth curves are analysed. This was achieved based on the same rejection criteria mentioned above, but the DRCs from "saturated" grains are accepted. In Figure 7-7A, all the DRCs (n = 1,464) that pass the rejection criteria were shown for all the samples. From the figure it can be seen that it is impossible to establish a common for all the grains because these DRCs are greatly variable among different grains, indicating that there are multiple groups of grains of different shapes of DRCs. In order to group the DRCs, the ratios between the L_x/T_x values from a large regenerative dose (400 Gy) and a smaller regenerative dose (100 Gy) were calculated. The ratios for individual grains from all the samples are shown in Figure 7-7B. A large range of ratios from ~1 to ~2.5 is observed, indicating that the grains have a wide range of saturation doses. For example, the grains with the L_x/T_x ratios close to 1 correspond to early saturated grains (i.e., there was negligible increase in OSL signal beyond 100 Gy). In contrast, grains with higher L_x/T_x ratios have a larger saturation dose level. A Finite Mixture Model (FMM) (Galbraith and Green, 1990; Galbraith and Roberts, 2012; Roberts et al., 2000) was then applied to statistically identify the number of groups of grains that share similar DRC shapes (or L_x/T_x ratios), as well as estimate the weighted mean ratios for each group. Unlike what was observed for the Guanyindong samples (Chapter 4), at least 7 groups are needed to fully take account the observed spread in the ratios for the samples (Figure 7-7B). In order to establish corresponding SGCs for each of the groups (Figure 7-7C), a least-square normalization (LS-normalization) procedure (Li et al., 2016a) is used to analyze the DRCs from each group. The general order kinetic function (Guralnik et al., 2015) is used to fit the dose-response data from the same groups. The grouping of grains and establishment of SGC for each group were achieved using the combination of two packages *numOSL* (Peng et al., 2013; Peng and Li, 2017) and *Luminescence* (Kreutzer et al., 2012) in R (R Core Team, 2016).

The SGCs for all the groups are shown in Figure 7-7C. It can be seen that different groups have considerably different saturation dose levels, i.e., Group 1 saturated at ~100 Gy but Group 7 shows no sign of saturation up to 600 Gy. To test the validity of grouping and SGC establishment, the ratios between the measured L_x/T_x and the expected values based on the SGC are calculated. The data shows that they are statistically consistent with unity for all the groups; most of these ratios (~90% or more) are consistent with unity at 2σ (Figure 7-7D–J), supporting that the SGCs obtained are reliable. The proportions of grains in each DRC groups are shown in Figure 7-7K for each sample. It is shown that the groups 2, 3, 4 and 5 are dominant in the samples, followed by group 1 and then group 6. Only a small

proportion (less than 3%) of grains falls into group 7 for THD-OSL1, 2, 3 and 4, but they are absent in THD-OSL5 and 6.

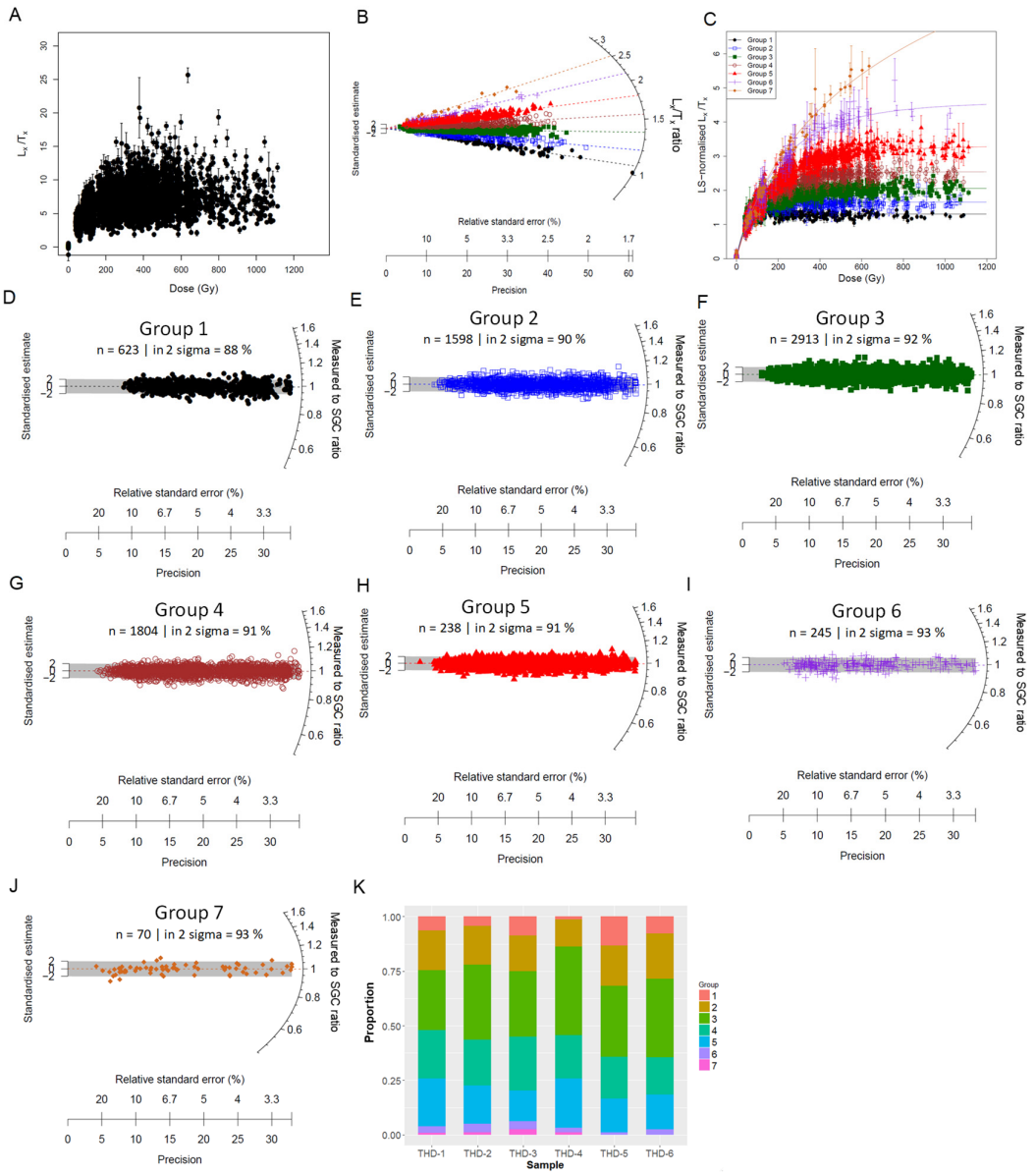

Figure 7-7: (A) Comparisons of all the DRCs that pass the rejection criteria for all the samples. (B) Radial plot showing the distribution of the ratios of L_x/T_x values between two regenerative doses of 400 and 100 Gy for all the accepted grains. The different colour and symbols represent different groups of grains identified using FMM. (C) Comparison of the LS-normalised L_x/T_x values for different groups. The data set for each group were fitted using a GOK function (full lines) and then normalised to unity at 50 Gy. (D–J) Radial plots showing the ratios between the LS-normalised L_x/T_x and the expected values based on the best-fit SGC shown in (C); the shaded band captures 2σ range from unity. The total number of grains (n) and percentage falling inside the 2σ band are shown for each group. (K) Proportion distribution of grains of each DRCs group for each sample.

In order to estimate D_e values for individual groups, the L_n/T_n values for each group were analysed. To allow direct comparison of natural signals among grains from the same group, the L_n/T_n of each group were re-nomalised using the same scaling factors obtained during the LS-normalisation procedure when the SGCs were established for individual groups. Statistical analysis was then conducted to the LS-normalised L_n/T_n values for each group to estimate their 'weighted mean' value. Such value was then projected onto the corresponding SGC to estimate the final D_e for that group. The distribution of LS-normalised L_n/T_n values for individual groups of these samples are shown in the figures from Figure 7-8 to Figure 7-13, respectively.

Similar to the SAR D_e distribution shown in Figure 7-1A and B, the L_n/T_n distributions for the topmost samples THD-OSL1 and 2 show a wide range of values, although a large proportion of the data points are clustered in the upper range, indicating that these samples were affected by intrusion of younger grains. So the maximum age model (MAM) (Olley et al., 2006), adapted from the minimum age model of Gaibraith et al. (1999), was applied to estimate the maximum component in the distribution. In this model, a value of 0.15 was used for σ_b, a parameter representing the expected over-dispersion for a well-bleached and non-distrubed sample. This value is based on the OD values of the L_n/T_n distribution for the lower samples, in which no evidence of post-depositional mixture was observed (e.g., group 5 of THD-OSL5 shown in Figure 7-12E). For the 4 lower samples, all the groups appear to have L_n/T_n values concentrated in a single population, although most of them contain a few grains that have considerably smaller L_n/T_n values. For this reason, the normalised median absolute deviation (nMAD) method was applied to reject outliers. A value of 1.4826 was used as the appropriate correction factor for normal distribution and any log L_n/T_n values with nMADs greater than 1.5 was rejected. This method is effective to reject outliers from the distribution (Figure 7-10 to 7-12). After rejecting the outliers by using the nMAD method, the weighted mean values of the accepted data points were calculated based on the CAM.

The best estimates of L_n/T_n values based on the statistical analysis mentioned above were then projected onto the corresponding SGCs to calculate D_e values for individual groups, which are summarised in Table 7-4. For some groups (e.g., the Groups 6 and 7), insufficient number of grains were accepted so reliable results cannot be obtained. The Group 1 (i.e., the early saturated group) of most samples and the Group 2 and 3 from some samples yielded infinite D_e value because their L_n/T_n statistically lies on the saturation levels of the corresponding SGCs. For the other groups that have higher saturation doses, finite results were obtained and their D_e values are statistically indistinguishable from each other for the same sample. This further confirms that the grouping, SGC establishment and D_e estimates based on L_n/T_n and SGC are reliable. The final D_e values for each sample were, therefore, estiamted based on the weighted mean of the results of the DRC groups that have produced finite D_e values (Table 7-4).

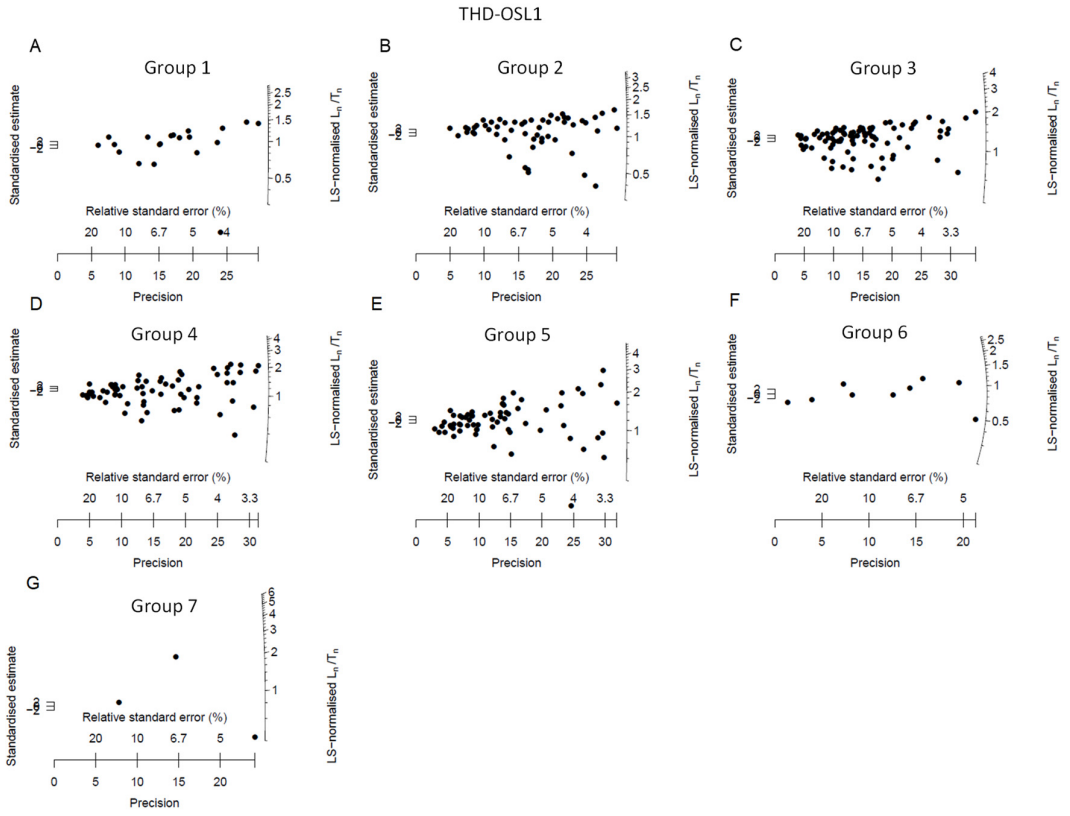

Figure 7-8: Radial plots showing the LS-normalised natural signals (L_n/T_n) of THD-1. (A-D) L_n/T_n calculated by using Maximum Age Model (MAM). The full lines represent the maximum of each groups. (E) L_n/T_n calculated by using CAM.

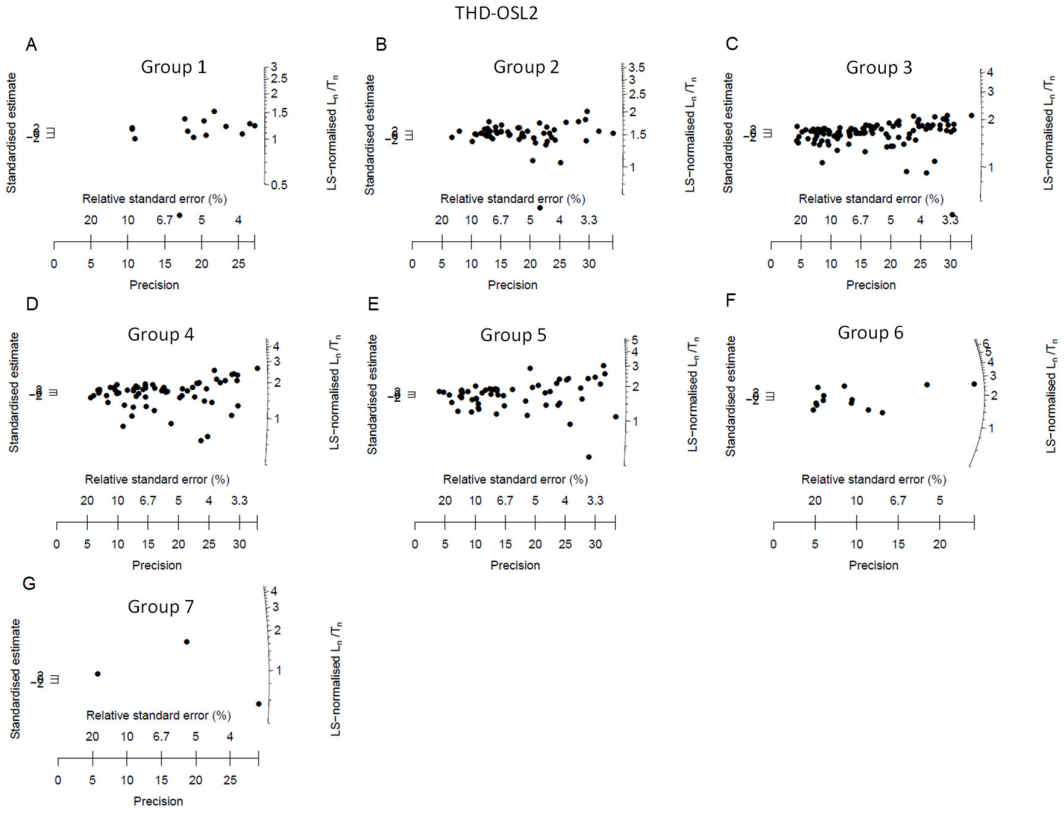

Figure 7-9: Radial plots showing the LS-normalised natural signals (L_n/T_n) of THD-2. (A-E) L_n/T_n calculated by using CAM.

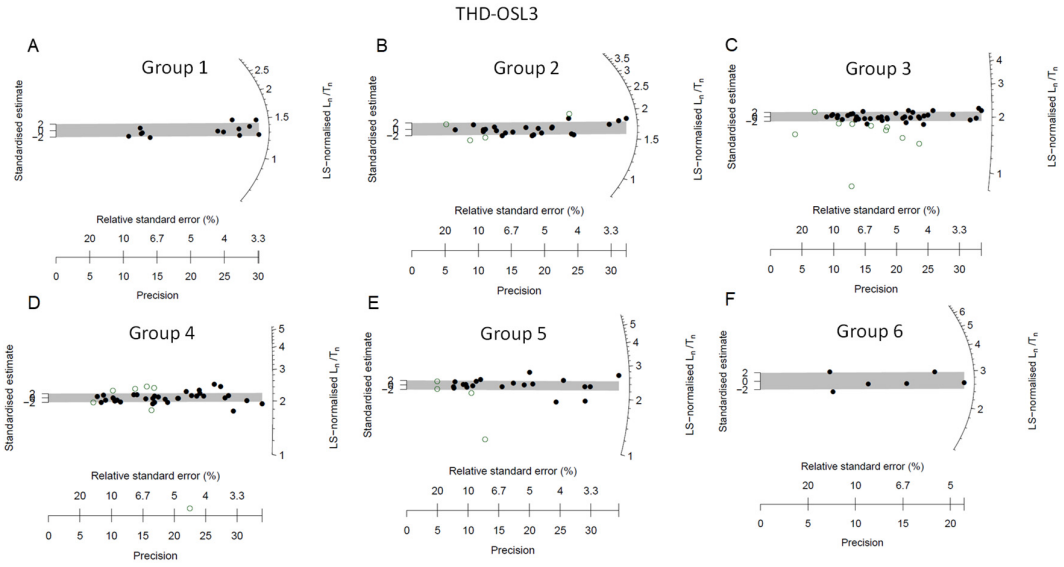

Figure 7-10: Radial plots showing the LS-normalised natural signals (L_n/T_n) of THD-3. (A-D) L_n/T_n calculated by using CAM.

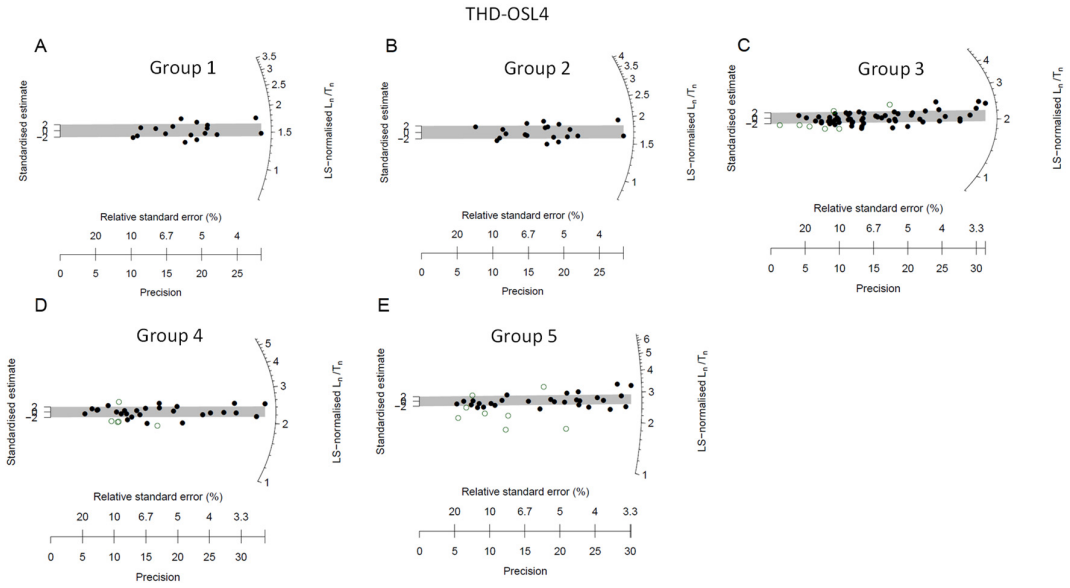

Figure 7-11: Radial plots showing the LS-normalised natural signals (L_n/T_n) of THD-4. (A-D) L_n/T_n calculated by using CAM.

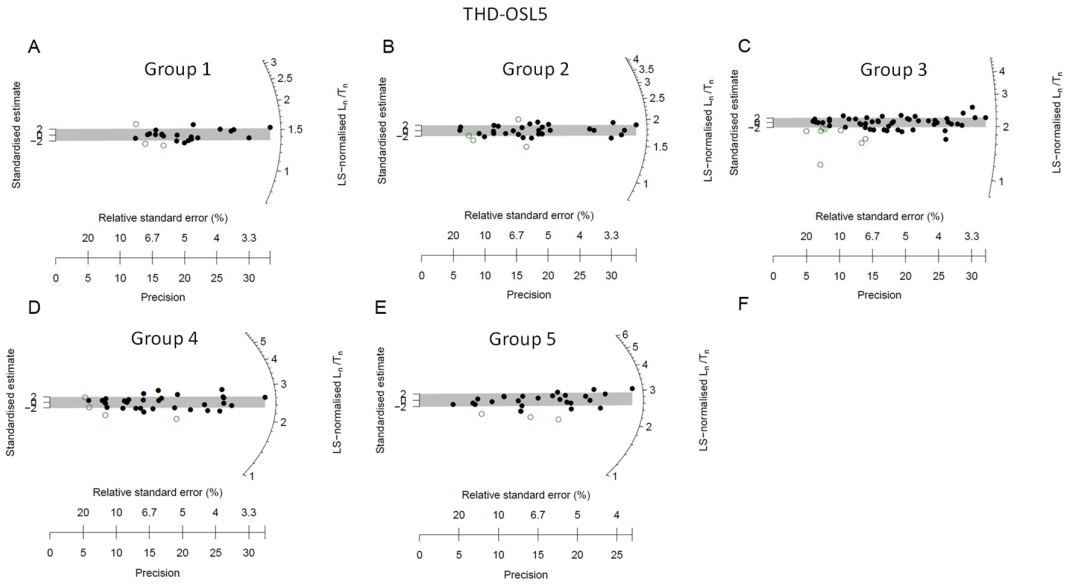

Figure 7-12: Radial plots showing the LS-normalised natural signals (L_n/T_n) of THD-5. (A-E) L_n/T_n calculated by using CAM.

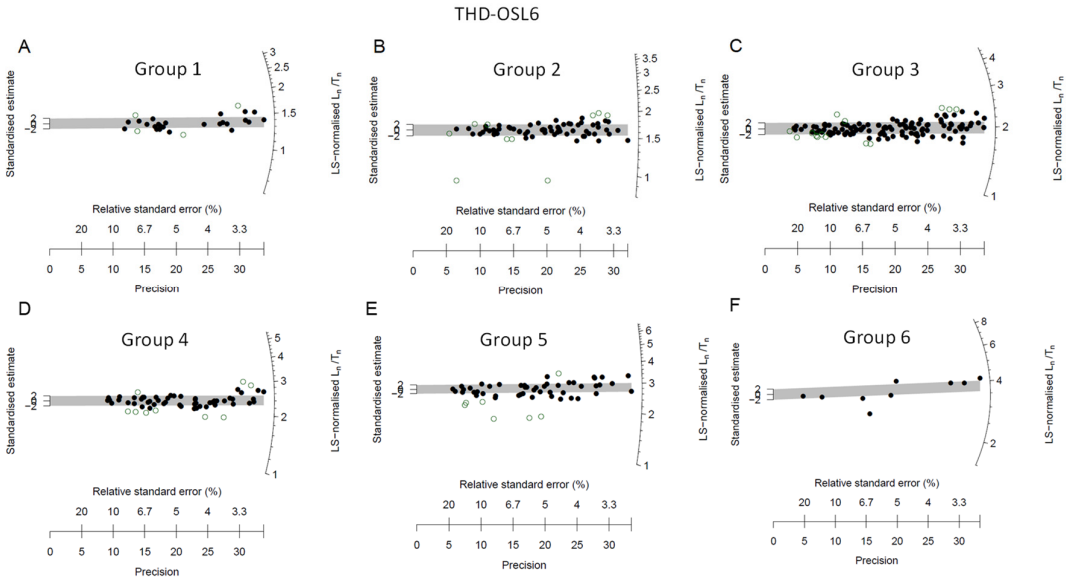

Figure 7-13: Radial plots showing the LS-normalised natural signals (L_n/T_n) of THD-6. (A-D) L_n/T_n calculated by using Maximum Age Model (MAM). The full lines represent the maximum of each group. (E) L_n/T_n calculated by using CAM.

Table 7-4. Summary of number of grains with saturated natural signal and D_e estimation results based on LS-normalised L_n/T_n for individual DRC groups and different grain sizes of each sample.

Sample	DRC Group	No. of accepted grains [a]	No. of saturated grains [b, d]	Over-dispersion (%)	Age model [c]	D_e (Gy) [d]	Final D_e (Gy) [f]
THD-OSL1	1	20 (6.4%)	9 (45%)	63 ± 10	MAM (65%)	saturated	158 ± 17
	2	57 (18.2%)	19 (33%)	51 ± 5	MAM (51%)	144 ± 34	
	3	86 (27.5%)	15 (17%)	60 ± 5	MAM (43%)	156 ± 22	
	4	69 (22%)	6 (9%)	70 ± 6	MAM (16%)	194 ± 68	
	5	69 (22.5%)	5 (7%)	74 ± 6	MAM (16%)	173 ± 64	
	6	9 (3%)	0 (0%)	50 ± 13	- [e]	-	
	7	3 (0.9%)	0 (0%)	89 ± 37	- [e]	-	
THD-OSL2	1	14 (4.4%)	6 (43%)	60 ± 11	MAM (93%)	98 ± 30	186 ± 12
	2	55 (17.4%)	23 (42%)	28 ± 3	MAM (91%)	184 ± 44	
	3	109 (34.4%)	31 (28%)	36 ± 3	MAM (72%)	192 ± 18	
	4	67 (23.2%)	9 (13%)	51 ± 5	MAM (55%)	190 ± 21	
	5	56 (19.4%)	3 (5%)	56 ± 5	MAM (34%)	236 ± 88	
	6	13 (5.7%)	1 (8%)	62 ± 13	- [e]	-	
	7	3 (0.9%)	0 (0%)	63 ± 27	- [e]	-	
THD-OSL3	1	14 (4.4%)	10 (71%)	7 ± 2	nMAD (93%)	saturated	202 ± 9
	2	27 (9.3%)	15 (56%)	9 ± 2	nMAD (85%)	saturated	
	3	50 (21.7%)	26 (52%)	39 ± 4	nMAD (80%)	346 ± 67	
	4	41 (20.1%)	7 (17%)	39 ± 4	nMAD (83%)	189 ± 11	
	5	24 (14%)	3 (13%)	40 ± 6	nMAD (83%)	212 ± 18	
	6	6 (3.6%)	0 (0%)	11 ± 5	nMAD (100%)	192 ± 18	
	7	4 (2.4%)	0 (0%)	43 ± 16	- [e]	-	
THD-OSL4	1	2 (1.3%)	2 (100%)	-	- [e]	-	277 ± 17
	2	20 (13.6%)	16 (80%)	11 ± 2	nMAD (100%)	saturated	
	3	65 (40.1%)	33 (51%)	13 ± 2	nMAD (89%)	356 ± 92	
	4	32 (20.9%)	14 (44%)	16 ± 2	nMAD (84%)	255 ± 28	
	5	37 (22.3%)	7 (19%)	29 ± 4	nMAD (78%)	283 ± 22	
	6	3 (1.8%)	0 (0%)	0	- [e]	-	
	7	2 (1.2%)	0 (0%)	-	- [e]	-	
THD-OSL5	1	24 (13.1%)	20 (83%)	9 ± 2	nMAD (88%)	saturated	300 ± 22
	2	34 (17.3%)	26 (76%)	12 ± 2	nMAD (88%)	saturated	
	3	60 (31.3%)	37 (62%)	33 ± 3	nMAD (87%)	saturated	
	4	35 (17.9%)	17 (49%)	14 ± 2	nMAD (89%)	442 ± 159	
	5	29 (15.5%)	6 (21%)	15 ± 2	nMAD (90%)	295 ± 23	
	6	2 (1.1%)	0 (0%)	-	- [e]	-	
	7	0 (0%)	-	-	- [e]	-	
THD-OSL6	1	28 (14.9%)	21 (75%)	11 ± 2	nMAD (86%)	saturated	317 ± 15
	2	73 (32.2%)	45 (62%)	30 ± 3	nMAD (86%)	saturated	
	3	129 (43.6%)	62 (48%)	11 ± 1	nMAD (89%)	277 ± 24	
	4	60 (18.7%)	26 (43%)	12 ± 1	nMAD (85%)	344 ± 30	
	5	56 (16.1%)	15 (27%)	29 ± 3	nMAD (86%)	332 ± 27	
	6	9 (2.5%)	2 (22%)	21 ± 6	nMAD (100%)	313 ± 56	
	7	0 (0%)	-	-	-	-	

[a] The percentage of grains in each DRC group is shown in parentheses.
[b] The percentage of the 'saturated' grains in each of the DRC group is shown in parentheses.
[c] The percentage of grains picked up by age models for D_e estimation is shown in parentheses.
[d] The D_e shown as 'saturated' means that the weighted mean of LS-normalised L_n/T_n is statistically consistent with the saturation level of the corresponding SGC at 2σ.
[e] The number of grains are insufficient to produce statistically significant results.
[f] The final D_e were obtained based on the weighted mean of the D_e values obtained from each of the groups.

7.2.5 Age estimates

The dose rates, final D_e estimates and ages for all the OSL samples are summarized in Table 7-2. The two samples (THD-OSL1 and 2) taken from the top layers contain a large number of younger grains but the number of younger grains decreased progressively with the depth. This result is consistent with the fact that the top of the trench was used as agricultural land and reworked by engineering activities, resulting in numerous younger grains intruded into the top layers. This suggests that single-grain measurements were able to effectively identify mixture in the deposits for the Tianhuadong site. Furthermore, it is shown that the post-depositional mixture, as a result of agricultural and engineering activities, mostly affected the two uppermost samples and was insignificant for the lower samples (see figures from Figure 7-10 to Figure 7-13).

The ages for the samples from Tianhuadong follow stratigraphic order, indicating good stratigraphic integrity of the deposit, and the reliability of the age measurements. Sample THD-OSL6 from Layer 5, which is archaeologically sterile, was dated to 87 ± 9 ka. Sample THD-OSL5 from Layer 4, associated with both artefacts and fossils, reveals the earliest human occupation at Tianhuadong site at 85 ± 10 ka ago. The ages of the two samples (THD-OSL1 and THD-OSL2) taken from the topmost layers yielded ages of ~40–50 ka.

7.3 Summary

Tianhuadong is another site found in southwest China dated back to early Late Pleistocene. The lithic assemblage consists of artefacts excavated from trend and collected from surface. The lithic industry includes cores, flakes, tools and chunks and debris. Most of cores are simple cores without preparation and achieved by hard hammer percussion. The simplified features are also found in flake and tools. However, the traces of Levallois and Quina retouch can also be detected in the lithic industry, which, certainly, need to be confirmed by further excavation. Another improvement of the study is the application of newly developed method of OSL dating. Because of numerous saturated grains found during the measurement, the age would be underestimated if using traditional SAR method. This study demonstrated that SGC can successfully reduce the influence of saturation problem and yield a more reliable dating result for samples from this site.

Chapter 8: Synthesis and suggestions for future work

In this study, the lithic characteristics and chronology for two Paleolithic sites from Southwest China were studied and have been presented in the preceding chapters. This chapter presents a synthesis of these results, set within a broader regional context of Southwest China. I also finish with some suggestions for future work that will help fill the remaining gaps in our understanding of the cultural development, human evolution and dispersal in this region and more broadly in East Asia.

8.1 The significance of Levallois technique in Southwest China

The earliest age of the Guanyindong lithic assemblage (Chapter 4) post-dates the earliest modern human fossils in Africa at 300–200 ka (Richter et al., 2017), but pre-dates any existing evidence of modern human outside Africa during MIS 5 (~130–80 ka), including the Levant (Shea, 2008) and southern and southwestern China (Liu et al., 2010; Liu et al., 2015). With a secure age of ~170–80 ka, the Levallois artefacts from Guanyindong Cave provide the earliest unequivocal evidence of prepared-core technology in East Asia (Chapter 5), suggesting a geographically more widespread distribution of Levallois prior to the dispersal of *Homo sapiens*. This discovery has two significant implications. First, the Guanyindong assemblage presents a plausible ancestral technology to blade-based technologies during the Late Pleistocene in China, and obviates the need for major population admixture or replacement hypotheses to explain these changes. Instead, demographic events may have occurred earlier in the Middle Pleistocene, leading to the appearance of Levallois concepts in East Asia. This possibility is suggested by the ~100 ka Xuchang crania with its mosaic of Eurasian and Neanderthal features indicating population interactions across Eurasia (Li et al., 2017b). A Middle Pleistocene demographic event is also indicated by aDNA from the Late Pleistocene Tianyuan individual that indicates the divergence of Asians from Europeans had occurred prior to 40 ka (Fu et al., 2013). Second, the emerging evidence of Mode II bifacial tools from archaeological sites in East Asia (Hou et al., 2000; Li et al., 2016b) indicates that the prepared-core technologies from Guanyindong Cave, although rare, may alternatively represent a convergent technological evolution within the Acheulean technology of the same region. This challenges the existing hypotheses for the absence of Middle Pleistocene prepared-core technology in East Asia, including the lack of a strong ancestral Acheulean (Mode II) tradition in this region and local raw stone materials constrained tool-making simple forms. Furthermore, if the use of Levallois concept in Guanyindong was developed *independently*, it could be another evidence supporting the theory of cultural convergence (e.g. Adler et al., 2014; Debono and Goren-Inbar, 2001; Rolland, 1995; Tryon et al., 2005).

Given the absence of human fossils dated to the same period in Southwest China, it is difficult to speculate which species of hominin produced the Guanyindong assemblage. Our findings, however, demonstrate a behavioral capacity compatible with their counterparts from the western hemisphere. The rarity of material traces of these complex behaviors in East Asia, relative to the Old World, therefore, may instead be due to the small, low density populations with weak and/or irregular patterns of social interconnectedness in this region during the Middle Pleistocene. Under these conditions, technological

innovation, transmission and persistence would have been rarer, compared to the high population/high density conditions of Middle Pleistocene sub-Saharan Africa where Levallois is more abundant. Since Guanyindong is one of only a few Palaeolithic sites discovered in South China reliably dated to the Late Middle Pleistocene, the abundance of Mode 3 technology in this region remains an open question.

8.2 The implications of technical diversity of Guanyindong assemblage

Except for the Levallois concept, the MP period in Africa and west Eurasia also demonstrates a remarkable degree of variation in methods for making stone tools (Kuhn, 2013). As an assemblage coexisting with the Middle Palaeolithic of west Eurasia, the Guanyindong industry shows a similar extent of technological behavioural diversity (Chapter 6). In other words, the persistence of various blank production and tool making techniques also indicates a variety of specific processing in the Guanyindong lithic industry. The development of new technologies and diversity in lithic industry could have been responses to several factors, as discussed below.

8.2.1 Response to changing climate and environment

The age of Guanyindong assemblage is associated with the Marine Isotopic Stages 6 and 5, suggesting that the Middle Palaeolithic hominins in Guanyindong cave experienced climate changes from a glacial period (MIS 6) of cooler temperatures to a warmer interglacial condition (MIS 5). To cope with the climate changes, hominins might have to alternate a variety of tool-making strategies to serve various purposes. For example, during harsh climatic conditions, people needed to search ways to maintain the supply by foraging larger territories. According to a model of mobility patterns of Neanderthals (Binford, 1980), portable and multifunctional toolkits which require a low degree of predetermination are likely to be produced for a high residential mobility. This would lead to repeated retouching and re-sharpening. This situation compelled them gradually to make multi-purpose and long-life tools or easily transformed artefacts, such as Quina scrapers since they are reliable, slightly "over-designed" (Bringmans et al., 1998), with a high resharpening or recycling potential (Delagnes and Rendu, 2011). This also stimulates the requirements for the urgency of raw materials with suitable quality, size and availability, which may explain why the majority of artefacts in Guanyindong are made from chert even though raw materials such like limestone, quartz are abundant nearby the cave.

8.2.2 Availability and procurement of raw materials

It is difficult to directly detect the distances that MP hominins forage over territories carrying tools, but we infer this from the distances of how far they procured raw materials. During the MP, the distances of foragers' movements could range from within 5 km up to more than 100 km (Féblot-Augustins, 2009; Gamble, 1999; Geneste, 1985, 1988b, 1990). Hominins of Guanyindong obtained raw materials from a relative close distance, i.e., no further than 20 km and the majority of sources are located within 2–6 km (Leng, 2001; Li et al., 2009b). This suggests that the raw materials with high quality and proper size are

relatively easier to find near the Guanyindong site, which consequently expedite the development of variation in lithic technology, since hominins could spend more effort on tool manufacturing rather than searching for high quality raw materials.

8.2.3 Mobility and hunting-gathering strategies

We could see that there are at least two mobility strategies in Guanyindong, one is indicated by the Levallois system, and the other by Quina and discoid production. In Europe, it was suggested that Levallois tools were adapted to a wide range of activities and enabling a wide range of hunting strategies. Levallois systems represent high extents of predetermination but relatively lower mobility. On the contrary, Quina and discoid systems are suitable for a high seasonal mobility (Delagnes and Rendu, 2011). In Guanyindong, Levallois was favourable because they can be used directly for cutting or scraping tasks. However, their volume and sharp edges limited their potence to resharpen or recycle. In addition, the energy and time spending on searching for suitable raw materials and volumetric preparation for the single purpose (Levallois blanks or blades) can be used as diagnostic evidence for a low transportability in Guanyindong. In contrast, the Quina tools or discoid systems, which do not heavily rely on high quality raw materials and high extent of predetermination, their long use-life and less elaborate reduction sequence enable hominins to carry them across a larger landscape for general use, since they are more portable, multifunctional toolkit and more likely subject to retouch and re-sharpening (Binford, 1980; Hovers, 1997). Hence, we can infer that the diversity among Guanyindong lithics facilitated strategic flexibility in land usage, and extended radiations around living sites. With the convenience of diverse flake productions and tool manufactures and managements, the foragers' strategies and daily activities of Guanyindong hominins could efficiently deal with complicated topography such as mountainous and lake landscapes among different seasons and climate fluctuations during the glacial and inter-glacial periods (MIS 6 and 5).

8.2.4 Demography

Demographic changes have been emerged as a key explaination to prehistoric cultural varibles (Henrich, 2004; Powell et al., 2009; Shennan, 2001). When the populations are relatively small, the cultural transmit depends largely on the opportunity (Neiman, 1995), resulting in loss of cultural elements or decreasing the diversity in lithic assemblage.

In Africa, where there has been most genetical diverse, sustained growth in population, and efficient social transmission networks (Henrich, 2004; Lycett and Norton, 2010; Tishkoff and Kidd, 2004), major technological innovations from Mode 1 to Mode 3 appeared and spread during the Early to Middle Pleistocene (Asfaw et al., 1992; Roche et al., 1999; Semaw S, 2003; Tryon and McBrearty, 2002; Tryon et al., 2005). In contrast, the East Asia lies in a remote region far from the migration origin points in Africa and Western Europe during the Early and Middle Pleistocene and the geological barriers created by the Himalaya–Karakorum mountain range, the Tibetan Plateau, the deserts of central Asia prevent the human migration into these regions (Dennell, 2004; Schick and Toth, 1993). The long distance of travel from the original population source may lead to the reduction in their effective population size and

weakness or irregular pattern of social interconnectedness. Actually, defining population size using either 'cultural parents' (Shennan, 2001) or 'the number of interacting social learners' (Henrich, 2004) is hardly practical (Collard et al., 2016). Nevertheless, many proxies from genetics suggest population of modern human decrese as the travel distance increase (Prugnolle et al., 2005; Ramachandran et al., 2005). Although using which to predict the population size is debated for years (French, 2015, 2016; Kuhn, 2012; Mellars and French, 2013), another least feasible proxy is the archaeological records (quantities of sheltered sites and retouched stone artifacts). The archaeological records disparity between East Asia and other parts of the Old World before Upper Pleistocene indicates East Asia is a low degree of colonisation (Dennell, 2003).

Therefore, it was suggested that the less frequent occurrence of Acheulean and Levallois sites is pertinent to this factor (Lycett and Norton, 2010). However, the technological behaviours reflected by blank production, tool manufacture and management from the Guanyindong assemblage suggest the lithic technological complexity was influenced by the demographic growth during MP in the other parts of the Old World (Stiner et al., 1999). The large variation of technological patterns in Guanyindong, therefore, may be a reflection of complicated demographic conditions.

8.2.5 Diversity in hominin species

Compared to Europe and Africa, Asia (especially East Asia) had more complicated patterns of directional paleobiological changes, regional continuity and interregional population dynamics during the late Middle and early Late Pleistocene, based on evidence from several human fossil sites, Xuchang, Xujiayao, Dali, Maba and Daoxian (Athreya and Wu, 2017; Li et al., 2017c; Liu et al., 2015; Wu and Bruner, 2016; Wu et al., 2014). Unlike the MP of Europe and MSA of Africa, which were dominantly occupied by Neanderthals and *Homo sapiens*, respectively, the MP of East and Southeast Asia have been occupied by at least four species: Denisova (Chen et al., 2019; Reich et al., 2010), *Homo sapiens (Liu et al., 2015)*, *Homo erectus* (Indriati et al., 2011; Swisher et al., 1996), *Homo floresiensis* (Brown et al., 2004; Morwood et al., 2004; Sutikna et al., 2016), and *Homo luzonensis* (Détroit et al., 2019). Because of the long range of ages of the Guanyindong assemblage (~170 to ~80 ka), it is possible that the diversities and advancement in lithic technological patterns were results of alternating occupations of different technical-tradition holding groups. Obviously, the possible candidates of the tool makers in Guanyindong could be attributed to Denisovans, *Homo sapiens, Archaic Homo sapiens* or even some other unknown hominin groups. Given the lack of fossil and ancient DNA results in this region, the existing evidence is still insufficient to ascribe the complex technological behaviors to any of the hominin groups.

8.3 The dating results and cultural importance of Tianhuadong cave

Based on the single grain analysis of samples from Tianhuadong, human occupation of the site spans about 40–90 ka, corresponding to MIS 3–5c. During this period, global climate records indicate several glacial and interglacial cycles leading to temperature and environment fluctuations (Lisiecki and Raymo, 2005). Nonetheless, according to the analysis of stone artefacts from Tianhuadong (Ruan, 2017), there were no major changes in the lithic technology and raw materials during this time span, indicating that the relationship between environmental changes and stone artefact technologies are weak during this time. This suggests that the technological strategies used at Tianhuadong were sufficient to be equally effective under a wide range of environmental conditions.

Besides, the technologies of the Tianhuadong assemblage indicate a mix of simple and complex reduction. Retouch techniques at Tianhuadong are mainly simple knapping along the edge of flakes, consistent with other sites from the same region, such like Xiangbidong (~50 ka, Dali Bai autonomous prefecture cultural relics management institute et al., 2015), Yushuiping (40–20 ka; Gao, 2012), Laohudong (30–18 ka; Zhu, 2011) and Longtanshang locality 2 (~30 ka; Qiu, 1985). Apart from that, the Tianhuadong assemblage also exhibits characters that are similar to the MP cultures from Africa and west Eurasia. The appearance of Levallois-like products at Tianhuadong is consistent with other nearby sites (e.g., Guanyindong and Panxiandadong). Additionally, the Quina-like scrapers are also similar to those from the MP sites from Europe and Africa. Compared to the sites Panxiandadong and Guanyindong, Tianhuadong shares many similarities in tool making, such as core-flake tools and hard hammer percussion. However, neither raw material procurement nor exploitation, core preparation, invasion and regularity of retouch at Tianhuadong is as complex and systematically present throughout the assemblage as found at Panxiandadong and Guanyindong.

In addition to the Levallois-like core and Qunia-like retouched tools, the majority of the stone artefacts from Tianhuadong also exhibit various types of scrapers, denticulates and notches resulting from invasive retouch on some of the tools. However, the small number of stone artefacts recovered from Tianhuadong prevents a comprehensive comparison with other assemblages. Levallois elements have also reported from a younger site Dahe (44–35 ka) (Ji, 2008) in the same region, indicating there might be a long-term technological transmission or population interaction in southwest Asia during the late Middle Pleistocene. Based on the available information, we could draw a preliminary sketch for the late Pleistocene of semi-isolated human groups learning some technologies from their forebears or neighbors, with small numbers of these Levallois elements persisting through time. One reason why these technologies did not become more dominant in archaeological assemblages may be due to the low availability of raw materials with predictable flaking qualities, e.g., chert is rarely available in this region. Another contributing factor may be the constraints of relatively smaller effective population sizes that limit the propagation and long-term persistence of new technologies (Lycett and Norton, 2010).

Although the record remains sparse, the results from Tianhuadong highlight the importance of the MIS 5 out of Africa dispersal. One possible implication of the finds at Tianhuadong is that the MIS 5 dispersal potentially resulted in the appearance of Levallois in East Asia. A second implication is that a southern,

or lower-latitudes, MIS 5 dispersal route may now be more plausible. However, we currently lack the evidence to robustly link the appearance of Levallois in southwestern China to a dispersal event. Hopefully, future work will lead to skeletal or ancient DNA evidence that can indicate how isolated or connected the human populations in southwest China.

8.4 Comaprison between Guanyindong and Tianhuadong

The locations, chronology and technological complex of Tianhuadong and Guanyindong make them two of the few sites that suitable to study the technology development in south China during Late Middle Pleistocene. Both of them are located in southwest China (Tianhuadong is ~600 km to the southwest of Guanyindong), and the occupation periods for the two sites are overlapping during MIS 5, suggesting the hominin groups lived in both sites probably had been coping with similar environmental and climatic fluctuations. The lithic assemblages of both sites consist of cores, flakes, tools and debris. Side-scrapers and denticulates dominate the tool types for both sites. What is interesting is that both of these sites have the element of Levallois concept and 'Quina' retouch. In Guanyindong, the Levallois cores and flakes are more typical abundant, however, these products in Tianhuadong are fewer and less typical. Similarly, the 'Quina' tools of Tianhuadong are fewer and less typical than those from Guanyindong.

The similarity and difference between the technology and assemblages from two sites could be explained by demographic events that happened during that period. The low effective population density and weak social connection might have led to the disappearance of certain technologies. Another possible underlying mechanism is the availability of raw materials and function of site exploitation. The majority stone artefacts in Guanyindong are chert, while basalt was dominantly used in Tianhuadong. The widely use of chert would provide better knapping physical properties to facilitate the complexity of the cultural remains in Guanyindong.

8.5 The validity of MP in China

Since 1970s (Boriskovsky, 1978), the validity of 'Middle Palaeolithic' in China has been questioned and been heavily debated. Some have suggested the term 'Middle Palaeolithic' should be abandoned and the stage of Palaeolithic in China should be replaced by two stages, i.e., Lower and Upper Palaeolithic (Gao, 1999; Gao and Norton, 2002). Despite that, some 'slow' changes during the Late Middle Pleistocene were noticed, although Gao and colleagues argued that this gradual progress is insufficient to support the division of two separate cultural periods. These changes include 1) the block-on-block method declined and disappeared; 2) the use of hard hammer percussion to produce more regular flakes; 3) tools types increased and retouch was more controlled. Some scholars have also noticed the similar trend during MP (Du, 2003; Kei, 2012; Li et al., 2019; Wang, 2005; Yang et al., 2016). Hence, the key issue underlying

this debate is whether those changes during Late Middle and early Late Pleistocene are quantitative or qualitative.

According to this study and several previous studies (Huang et al., 1997; Li et al., 2019; Otte et al., 2017), the initial appearance of Levallois concept appeared in several sites in China prior to the Upper Palaeolithic. Although hard-hammer percussion is the only technique used during the reduction, without a doubt, it qualitatively varies from simple and opportunistic core reduction. In addition, rather than utilizing the local and poor workable raw material, knappers from Guanyindong exploited chert as the main raw material from more remote sources. The deliberate choose of fine materials no matter the distance is also beneficial to the manufacture of the tools. We could also see that when finer raw materials are available and the effects of poor-quality in raw material on typological variability, technological attributes decrease. Local hominins might be able to develop more skilled technologies on good raw materials, which then might enable them to apply these skills on even less predictable materials such like limestone (Otte et al., 2017). Furthermore, the diversity in technological patterns as shown in Guanyindong and Tianhuadong, such like discoid, quinar, truncated faceting, is comparable with its counterparts in west, suggesting similar changes in this area during Late Middle Pleistocene. These progresses could not happen if the technological behaviors have not qualitatively changed.

Furthermore, although complexity shown in only a few sites is inadequate to fully sustain the MP in China, we should be aware that this weakness could be owing to the rarity of archaeological sites that have been dated back to Late Middle Pleistocene and early Late Pleistocene in China. The main MP-claimed sites with reliable dates and more than 100 artefacts in China are extremely limited, for examples, Jinniushan (170–300 ka) (Gao and Norton, 2002; Lu, 1989; Tiemei et al., 1994), Zhoukoudian locality 15 (155–284 ka) (Shen et al., 2004), Xujiayao (260–370 ka) (Ao et al., 2017), Dingcun (128–336 ka) (Yang et al., 2014), Dali (247–300 ka) (Li and Lotter, 2019), Lingjing (90–125 ka) (Li et al., 2019), Wulanmulun (50–65 ka) (Rui et al., 2015), and most of which were found in North China. The sites with complex technologies, such like Guanyindong, Tianhuadong and Panxiandadong, were all found in southwest China.

In sum, although prepared core reductions and a diverse range of tools are best demonstrated as a whole in the study sites, especially in Guanyindong, the technological innovations found in them are not special cases in Southwest China. Element of technological changes can be traced in several sites in north China with a geological age slightly after them. They include the Tongtiandong cave (Yu et al., 2018; Li and Lotter, 2019), Sanlongdong Cave (Li and Lotter, 2019) and Jinsitai (Li et al., 2018) found in Mongolia and Xinjiang in northern China, respectively. The technological pattern of MP or even Mousterian culture are even more obvious, letting alone the Shuidonggou (c. 30,000–11,000 BP) (Boëda et al., 2013; Li et al., 2013a; Li et al., 2013b; Madsen et al., 2001; Niu et al., 2016; Pei et al., 2012), where a full complex of Levallois and blade Mousterian lithic assemblages were found. Owing to the fragmental evidence of prepared core technology, we are still a long way from a strong conclusion about the evolutionary trajectory of this behavior, as well as the human groups that lived there. However, according to the current knowledge, no matter the appearance of changes is caused by technological

convergence or diffusion, the demographic dynamics in this region around 300–100 ka is far more complicated than we previously thought.

8.6 Suggestions for future work

Although this thesis has made much progress in establishing firm chronology and identifying MP lithic features (such as Levallois) for two late Middle Pleistocene sites in Southwest China, further studies are needed to resolve the remaining gaps in understandings the human dispersal and evolution in this area during Late Middle Pleistocene.

First, we cannot come to a conclusion on who inhabited this region and made the MP assemblages based on stone aritfacts themselves. Therefore, further excavations are required to search for human fossils or sediment DNA to identify the species of hominins inhabited this region.

Second, because most artefacts from Guanyindong have lost their original excavation provenance information, we could not tell whether the MP traits were actually concentrated in a specific time period or accounted for the entire occupation. Thus, further excavations of the site in a more controlled way are required. Detailed geoarchaeological and palaeoenvironment studies are also needed to study the site formation process and relationship between technology and environment.

Third, reliable chronologies for Middle Palaeolithic sites should be established, not only in southwest China but in other regions of East Asia. This is fundamental to resolve debates about the presence or absence of the 'Middle Palaeolithic' stage in China. Furthermore, systematic lithic technological analysis and comparisons of assemblages from a range of sites, are necessary to test variability of the Chinese Palaeolithic and the validity of three-stage or two-stage models in the division of Chinese Palaeolithic. Only when reliable chronological, geological and archaeological studies are combined will the spatial and temporal development of Palaeolithic technologies be finally understood.

Bibliography or List of References

Abdulla, M., Ahmed, I., Assawamakin, A., Bhak, J., K Brahmachari, S., Calacal, G., Chaurasia, A., Chen, C.-H., Chen, J., Chen, Y., Chu, J., de la Paz, E.M., De Ungria, M.C., Delfin, F., Edo, J., Fuchareon, S., Ghang, H., Gojobori, T., Han, J., Zilfalil, B., 2009. Mapping Human Genetic Diversity in Asia. Science 326, 1541-1545.

Adam, A., 2002. Les pointes pseudo-Levallois du gisement moustérien Le Rissori, à Masnuy-Saint-Jean (Hainaut, Belgique). L'Anthropologie 106, 695-730.

Adler, D.S., Wilkinson, K.N., Blockley, S., Mark, D.F., Pinhasi, R., Schmidt-Magee, B.A., Nahapetyan, S., Mallol, C., Berna, F., Glauberman, P.J., Raczynski-Henk, Y., Wales, N., Frahm, E., Jöris, O., MacLeod, A., Smith, V.C., Cullen, V.L., Gasparian, B., 2014. Early Levallois technology and the Lower to Middle Paleolithic transition in the Southern Caucasus. Science 345, 1609-1613.

Aitken, M.J., 1985. Thermoluminescence dating. Academic press, London.

Aitken, M.J., 1998. An Introduction to Optical Dating. Oxford University Press, Oxford.

Aitken, M.J., Smith, B.W., 1988. Optical dating - recuperation after bleaching. Quaternary Science Reviews 7, 387-393.

Akhilesh, K., Pappu, S., Rajapara, H.M., Gunnell, Y., Shukla, A.D., Singhvi, A.K., 2018. Early Middle Palaeolithic culture in India around 385–172 ka reframes Out of Africa models. Nature 554, 97.

Ambrose, S.H., 1998. Chronology of the Later Stone Age and food production in East Africa. Journal of Archaeological Science 25, 377-392.

Ameloot-van der Heijden, N., Dupuis, C., Limondin, N., Munaut, A.V., Puissegur, J.J., 1996. The Middle Palaeolithic open air site of Salouel. L'Anthropologie 100, 555-573.

An, Z., 1965. Trial excavation of the Paleolithic cave of Hsiaonan-hai in Anyang, Honan. Acta Archaeologica Sinica 1, 1-26.

Andrews, J.E., Singhvi, A.K., Kailath, A.J., Kuhn, R., Dennis, P.F., Tandon, S.K., Dhir, R.P., 1998. Do stable isotope data from Calcrete record Late Pleistocene monsoonal climate variation in the Thar Desert of India? Quat. Res. 50, 240-251.

Ao, H., Liu, C.-R., Roberts, A.P., Zhang, P., Xu, X., 2017. An updated age for the Xujiayao hominin from the Nihewan Basin, North China: Implications for Middle Pleistocene human evolution in East Asia. Journal of Human Evolution 106, 54-65.

Arnold, L.J., Roberts, R.G., 2009. Stochastic modelling of multi-grain equivalent dose (De) distributions: Implications for OSL dating of sediment mixtures. Quaternary Geochronology 4, 204-230.

Arnold, L.J., Demuro, M., Pares, J.M., Arsuaga, J.L., Aranburu, A., de Castro, J.M.B., Carbonell, E., 2014. Luminescence dating and palaeomagnetic age constraint on hominins from Sima de los Huesos, Atapuerca, Spain. Journal of Human Evolution 67, 85-107.

Arsuaga, J.L., Martínez, I., Arnold, L.J., Aranburu, A., Gracia-Téllez, A., Sharp, W.D., Quam, R.M., Falguères, C., Pantoja-Pérez, A., Bischoff, J., Poza-Rey, E., Parés, J.M., Carretero, J.M., Demuro, M., Lorenzo, C., Sala, N., Martinón-Torres, M., García, N., Alcázar de Velasco, A., Cuenca-Bescós, G., Gómez-Olivencia, A., Moreno, D., Pablos, A., Shen, C.C., Rodríguez, L., Ortega, A.I., García, R., Bonmatí, A., Bermúdez de Castro, J.M., Carbonell, E., 2014. Neandertal roots: Cranial and chronological evidence from Sima de los Huesos. Science 344, 1358.

Asfaw, B., Beyene, Y., Suwa, G., Walter, R.C., White, T.D., WoldeGabriel, G., Yemane, T., 1992. The earliest Acheulean from Konso-Gardula. Nature 360, 732-735.

Athreya, S., Wu, X., 2017. A multivariate assessment of the Dali hominin cranium from China: Morphological affinities and implications for Pleistocene evolution in East Asia.

Bae, C.J., Douka, K., Petraglia, M.D., 2017. On the origin of modern humans: Asian perspectives. Science 358, eaai9067.

Bahain, J.-J., 2007. La méthode de datation par résonance de spin électronique (ESR) au Muséum national d'histoire naturelle. Vingt ans de recherches méthodologiques et d'applications géochronologiques. Université Michel de Montaigne - Bordeaux III.

Balescu, S., Tuffreau, A., 2004. La phase ancienne du Paléolithique moyen dans la France septentrionale (stades isotopiques 8 à 6) : apports de la datation par luminescence des séquences lœssiques. Archaeological Almanac 16, 5-22.

Bamforth, D.B., 1991. Technological organization and hunter-gatherer land use: a California example. American Antiquity 56, 216-234.

Bar-Yosef, O., Belfer-Cohen, A., 2013. Following Pleistocene road signs of human dispersals across Eurasia. Quatern Int 285, 30-43.

Bar-Yosef, O., Kuhn, S.L., 1999. The big deal about blades: Laminar technologies and human evolution. American Anthropologist 101, 322-338.

Bar-Yosef, O., Van Peer, P., 2009. The chaîne opératoire approach in Middle Paleolithic archaeology. Current Anthropology 50, 103-131.

Bar-Yosef, O., Vandermeersch, B., Arensburg, B., Belfer-Cohen, A., Goldberg, P., Laville, H., Meignen, L., Rak, Y., Speth, J.D., Tchernov, E., Tillier, A.-m., Weiner, S., 1992. The Excavations in Kebara Cave, Mt. Carmel. Current Anthropology 33, 497-550.

Bar-Yosef, O., Wang, Y., 2012. Paleolithic archaeology in China. Annual Review of Anthropology 41, 319-335.

Barkai, R., Gopher, A., Lauritzen, S.E., Frumkin, A., 2003. Uranium series dates from Qesem Cave, Israel, and the end of the Lower Palaeolithic. Nature 423, 977-979.

Barsky, D., 2009. An Overview of Some African and Eurasian Oldowan Sites: Evaluation of Hominin Cognition Levels, Technological Advancement and Adaptive Skills, in: Hovers E., B.D.R. (Ed.), Interdisciplinary Approaches to the Oldowan. Springer, New York.

Barzilai, O., Malinsky-Buller, A., Ackermann, O., 2006. Kefar Menachem West: a Lower Paleolithic site in the southern Shephela, Israel. J. Israel Prehist. Soc 36, 7-38.

Berna, F., Goldberg, P., 2007. Assessing Paleolithic pyrotechnology and associated hominin behavior in Israel.

Beyries, S., 1993. Analyse fonctionnelle de l'industrie lithique du niveau CA: rapport pr´eliminaire et directions de recherche, in: Tuffreau, A. (Ed.). Maison des Sciences de l'Homme, Paris, pp. 53-61.

Biagi, P., 2006. The Levalloisian assemblages of Sindh (Pakistan) and their importance in the Middle Palaeolithic of the Indian subcontinent.

Binford, L.R., 1980. Willow smoke and dogs' tails: hunter-gatherer settlement systems and archaeological site formation. American Antiquity 45, 4-20.

Blackwell, B., Schwarcz, H.P., 1988. Datation des spéléothèmes de la grotte Vaufrey par la famille de l'Uranium, in: Rigaud, J.-P. (Ed.), La Grotte Vaufrey: Paléoenvironnement, chronologie, activités humaines. Mémoires de la Société Préhistorique Française, Paris, pp. 365–380.

Blinkhorn, J., 2014. Late Middle Palaeolithic surface sites occurring on dated sediment formations in the Thar Desert. Quatern Int 350, 94-104.

Blinkhorn, J., Achyuthan, H., Petraglia, M., Ditchfield, P., 2013. Middle Palaeolithic occupation in the Thar Desert during the Upper Pleistocene: the signature of a modern human exit out of Africa? Quaternary Science Reviews 77, 233-238.

Boëda, E., 1986. Approche technologique du concept Levallois et évaluation de son champ d'application: étude de trois gisement saaliens et weichseliens de la France septentrionale. Paris 10.

Boëda, E., 1991. Approche de la variabilité des systèmes de production lithique des industries du paléolithique inférieure et moyen: chronique d'une variabilité attendue. Techniques Culture 17–18, 31–79.

Boëda, E., 1993. Le débitage discoïde et le débitage Levallois récurrent centripède. Bulletin de la Société préhistorique française 90, 392-404.

Boëda, E., 1994. Le Concept Levallois: Variabilité des Méthodes. CNRS.

Boëda, E., 1995. Levallois: A volumetric construction, methods, a technique., in: Dibble, H., Bar-Yosef, O. (Eds.), The Definition and Interpretation of Levallois Technology. Prehistory Press, Madison, pp. 41–68.

Boëda, E., Au Présent, P., 2018. Techno-logique & Technologie Une Paléo-histoire des objets lithiques tranchants. @rchéo-éditions.

Boëda, E., Connan, J., Dessort, D., Muhesen, S., Mercier, N., Valladas, H., Tisnérat, N., 1996. Bitumen as a hafting material on Middle Palaeolithic artefacts. Nature 380, 336-338.

Boëda, E., Geneste, J.-M., Meignen, L., 1990. Identification de chaînes opératoires lithiques du Paléolithique ancien et moyen. Paléo 2, 43-80.

Boëda, E., Hou, Y.M., Forestier, H., Sarel, J., Wang, H.M., 2013. Levallois and non-Levallois blade production at Shuidonggou in Ningxia, North China. Quatern Int. 295, 191-203.

Boismier, W.A., Schreve, D.C., White, M.J., Robertson, D.A., Stuart, A.J., Etienne, S., Andrews, J., Coope, G.R., Field, M.H., Green, F.M.L., Keen, D.H., Lewis, S.G., French, C., Rhodes, E.D., Schwenninger, J.L., Tovey, K., Donahue, R.E., Richards, M.P., O'Connor, S., 2003. A Middle Palaeolithic Site at Lynford Quarry, Mundford, Norfolk: Interim Statement. Proceedings of the Prehistoric Society 69, 315-324.

Bolton, L., 2015. Assessing the origins of Levallois through Lower Palaeolithic core variation: A comparative study of Simple Prepared Cores in northwest Europe. University of Southampton.

Bordes, F., 1961a. Mousterian Cultures in France. Science 134, 803-810.

Bordes, F., 1961b. Typologie du Paléolithique Ancien et Moyen. Centre National de la Recherche Scientifique, Paris.

Bordes, F., 1969. Reflections on typology and techniques in the Paleolithic. Arctic Anthropology 6, 1-29.

Boriskovsky, P.I., 1978. Some problems of the Palaeolithic of South and Southeast Asia, in: Ikawa-Smith, F. (Ed.), Early Palaeolithic in South and East Asia. Mouton, The Hague, pp. 87-97.

Bøtter-Jensen, L., Andersen, C.E., Duller, G.A.T., Murray, A.S., 2003. Developments in radiation, stimulation and observation facilities in luminescence measurements. Radiation Measurements 37, 535-541.

Botter-Jensen, L., Bulur, E., Duller, G.A.T., Murray, A.S., 2000. Advances in luminescence instrument systems. Radiation Measurements 32, 523-528.

Bøtter-Jensen, L., Ditlefsen, C., Mejdahl, V., 1991. Combined OSL (infrared) and TL studies of feldspars. Nuclear Tracks and Radiation Measurements 18, 257-263.

Bøtter-Jensen, L., Duller, G.A.T., Poolton, N.R.J., 1994. Excitation and emission-spectrometry of stimulated luminescence from quartz and feldspars. Radiation Measurements 23, 613-616.

Bøtterjensen, L., Mejdahl, V., 1988. Assessment of beta dose rate using a GM multicounter system. Nuclear Tracks and Radiation Measurements 14, 187-191.

Bourguignon, L., 1996. La conception de debitage quina. Quaternaria Nova VI, 149-166.

Brantingham, P.J., Kuhn, S.L., 2001. Constraints on Levallois core technology: A Mathematical Model. Journal of Archaeological Science 28, 747-761.

Brantingham, P.J., Kuhn, S.L., Kerry, K.W., 2004. The Early Upper Paleolithic beyond Western Europe. Univ of California Press.

Brantingham, P.J., Olsen, J.W., Rech, J.A., Krivoshapkin, A.I., 2000. Raw material quality and prepared core technologies in northeast Asia. Journal of Archaeological Science 27, 255-271.

Brenet, M., Folgado, M., Lenoble, A., Bertran, P., Viellevigne, E., Guibert, E., 2008. Interprétation de la variabilité technologique de deux industries du Paléolithique moyen ancien du Bergeracois: Cantalouette 1 et Combe Brune 3 (Creysse, Dordogne). Bulletin de la Société Préhistorique Française, 57-81.

Brennan, B.J., 2003. Beta doses to spherical grains. Radiation Measurements 37, 299-303.

Bringmans, P.M.M.A., Meijs, E., Gullentops, F., Cordy, J., Vermeersch, P., Warrimont, J.P.d., Groenendijk, A., 1998. Human Presence and Lithic Variability at the Middle Palaeolithic Valley Settlements at Veldwezelt-Hezerwater (Limburg, Belgium), in: Demarsin, B. (Ed.), Neanderthals In Europe, pp. 89-100.

Brown, F.H., Fuller, C.R., 2008. Stratigraphy and tephra of the Kibish Formation, southwestern Ethiopia. Journal of Human Evolution 55, 366-403.

Brown, P., Sutikna, T., Morwood, M.J., Soejono, R.P., Jatmiko, Saptomo, E.W., Due, R.A., 2004. A new small-bodied hominin from the Late Pleistocene of Flores, Indonesia. Nature 431, 1055-1061.

Brumm, A., Moore, M.W., 2012. Biface distributions and the Movius line: a southeast Asian perspective. Australian Archaeology 74, 34-46.

Buraczynski, J., Butrym, J., 1987. Thermoluminescence stratigraphy of the loess in the southern Rhinegraben. In: Pesci, M. (Ed.), Loess and Environment, in: Pesci, M. (Ed.), Loess and Environment, Catena Supplement, pp. 81-94.

Cahen, D., 1981. Les industries préhistoriques des nappes alluviales de Petit-Spiennes et de Mesvin. Notae Praehistoricae Tervuren 1, 70-74.

Cahen, D., Haesaerts, P., Watteyne, D., 1985. La nappe alluviale de Petit-Spiennes et le début du débitage levallois dans la vallée de la Haine. Archaeologia Belgica Bruxelles 1, 7-16.

Cai, H., Wang, X., Xu, C, 1991. Paleolith of Bianbian cave at Bijie county, Guizhou province. Acta Anthropologica Sinica 10, 50-57.

Callow, P., Cornford, J.M., 1986. La Cotte de St. Brelade, 1961-1978: excavations by C.B.M. McBurney. Kluwer Academic, Norwich, UK.

Cao, Z., 1978. Palaeolithic site found in Xiaohuidong cave at Shuicheng, Guizhou Province. Vertebrata Palasiatica 16, 67-72.

Carbonell, E., Rodríguez, X.P., 2008. El Paleolítico Inferior En Cataluña. VELEIA 24-25, 331-343.

Cârciumaru, M., Ion, R.-M., Niţu, E.-C., Ştefănescu, R., 2012. New evidence of adhesive as hafting material on Middle and Upper Palaeolithic artefacts from Gura Cheii-Râşnov Cave (Romania). Journal of Archaeological Science 39, 1942-1950.

Casini, A., 2010. The meaning of "Kombewa" method in Middle Palaeolithic: techno-economic analysis of lithic assemblages from Riparo Tagliente (VR), Carapia (RA), Podere Camponi (BO) and Fossato Conca d'Oro (MT). Annali dell'Università di Ferrara, Sezione di Museologia Scientifica e Naturalistica, 6-123.

Castañeda, I.S., Mulitza, S., Schefuß, E., Lopes dos Santos, R.A., Sinninghe Damsté, J.S., Schouten, S., 2009. Wet phases in the Sahara/Sahel region and human migration patterns in North Africa. Proceedings of the National Academy of Sciences 106, 20159.

Chazan, M., 1997. Redefining levallois. Journal of Human Evolution 33, 719-735.

Chen, F., Welker, F., Shen, C.-C., Bailey, S.E., Bergmann, I., Davis, S., Xia, H., Wang, H., Fischer, R., Freidline, S.E., Yu, T.-L., Skinner, M.M., Stelzer, S., Dong, G., Fu, Q., Dong, G., Wang, J., Zhang, D., Hublin, J.-J., 2019. A late Middle Pleistocene Denisovan mandible from the Tibetan Plateau. Nature 569, 409-412.

Chiotti, L., Dibble, H.L., Olszewski, D.I., McPherron, S.P., Schurmans, U.A., 2009. Middle Palaeolithic lithic technology from the western high desert of Egypt. Journal of Field Archaeology 34, 307-318.

Chlachula, J., Drozdov, N.I., Ovodov, N.D., 2003. Last Interglacial peopling of Siberia: the Middle Palaeolithic site Ust'-Izhul', the upper Yenisei area. Boreas 32, 506-520.

Clark, G., 1969. World Prehistory: A New Outline, Cambridge University Press.

Clark, J.D., Beyene, Y., WoldeGabriel, G., Hart, W.K., Renne, P.R., Gilbert, H., Defleur, A., Suwa, G., Katoh, S., Ludwig, K.R., Boisserie, J.-R., Asfaw, B., White, T.D., 2003. Stratigraphic, chronological and behavioural contexts of Pleistocene Homo sapiens from Middle Awash, Ethiopia. Nature 423, 747-752.

Clarkson, C., 2002. An Index of Invasiveness for the measurement of unifacial and bifacial retouch: a theoretical, experimental and archaeological verification. Journal of Archaeological Science 29, 65-75.

Clarkson, C., Jacobs, Z., Marwick, B., Fullagar, R., Wallis, L., Smith, M., Roberts, R.G., Hayes, E., Lowe, K., Carah, X., Florin, S.A., McNeil, J., Cox, D., Arnold, L.J., Hua, Q., Huntley, J., Brand, H.E.A., Manne, T., Fairbairn, A., Shulmeister, J., Lyle, L., Salinas, M., Page, M., Connell, K., Park, G., Norman, K., Murphy, T., Pardoe, C., 2017. Human occupation of northern Australia by 65,000 years ago. Nature 547, 306-310.

Collard, M., Vaesen, K., Cosgrove, R., Roebroeks, W., 2016. The empirical case against the 'demographic turn' in Palaeolithic archaeology. Philosophical Transactions of the Royal Society B: Biological Sciences 371, 20150242.

Colonge, D., Jarry, M., Delfour, G., Fondeville, C., Arnoux, T., Berthet, A.-L., 2010. De la transition paléolithique inférieur-moyen dans la vallée de la Garonne: l'Acheuléen supérieur de Raspide 2 (Blagnac, Haute-Garonne). Bulletin de la Société préhistorique française 107, 205-225.

Conard, N., 1990. Laminar Lithic Assemblages from the Last Interglacial Complex in Northwestern Europe. Journal of Anthropological Research 46, 243-262.

Cyrek, K., Sudoł, M., Czyżewski, Ł., Osipowicz, G., Grelowska, M., 2014. Middle Palaeolithic cultural levels from Middle and Late Pleistocene sediments of Biśnik Cave, Poland. Quatern Int 326, 20-63.

D'Errico, F., 2008. Le rouge et le noir: implications of early pigment use in Africa, the near East and Europe for the origin of cultural modernity. Goodwin Series 10, 168-174.

Dali Bai autonomous prefecture cultural relics management institute, Yunnan Institute of Cultural Relics and Archeology, Jianchuan Institute of Cultrual Relics, 2015. Study of the Jianchuan Xiangbidong Paleolithic site. Cultural Relics Publishing House, Beijing.

Dauvois, M., 1981. De la simultanéité des concepts Kombewa et Levallois dans l'Acheuléen du Maghreb et du Sahara nord-occidental, in: Roubet C., H.H.J., Souville G. (Ed.), Préhistoire Africaine, Paris, pp. 313-321.

Debono, H., Goren-Inbar, N., 2001. Note on a link between Acheulian handaxes and the Levallois method.

Delagnes, A., 1995. Variability within Uniformity: three Levels of Variability within Levallois System, in: Bar-Yosef, O., Dibble, H. (Eds.), The definition and interpretation of Levallois technology. Prehistory Press, Madison, Wisconsin, pp. 201-212.

Delagnes, A., Jaubert, J., Meignen, L., 2007. Les technocomplexes du Paléolithique moyen en Europe occidentale dans leur cadre diachronique et géographique, pp. 213-229.

Delagnes, A., Meignen, L., 2006. Diversity of lithic production systems during the Middle Paleolithic in France: are there any chronological trends? Springer US, Boston, MA, pp. 85-107.

Delagnes, A., Rendu, W., 2011. Shifts in Neandertal mobility, technology and subsistence strategies in western France. Journal of Archaeological Science 38, 1771-1783.

Delagnes, A., Roche, H., 2005. Late Pliocene hominid knapping skills: The case of Lokalalei 2C, West Turkana, Kenya. Journal of Human Evolution 48, 435-472.

Delagnes, A., Ropars, A., 1996. Paléolithique moyen en pays de Caux (Haute-Normandie). Le Pucheuil, Ettoutteville: Deux gisements de plein air en milieu loessique. Éditions de la Maison des Sciences de l'Homme, Paris.

Delpiano, D., Peresani, M., 2017. Exploring Neanderthal skills and lithic economy. The implication of a refitted Discoid reduction sequence reconstructed using 3D virtual analysis. Comptes Rendus Palevol 16, 865-877.

deMenocal, P.B., 2004. African climate change and faunal evolution during the Pliocene–Pleistocene. Earth and Planetary Science Letters 220, 3-24.

Dennell, R., 2003. Dispersal and colonisation, long and short chronologies: how continuous is the Early Pleistocene record for hominids outside East Africa? J. Hum. Evol. 45, 421-440.

Dennell, R.W., 2004. Hominid Dispersals and Asian Biogeography during the Lower and Early Middle Pleistocene, c. 2.0-0.5 Mya. Asian Perspectives 43, 205.

Dennell, R., 2009. The Palaeolithic settlement of Asia. Cambridge University Press, Cambridge.

Dennell, R., 2016. Life without the Movius Line: The structure of the East and Southeast Asian Early Palaeolithic. Quatern Int 400, 14-22.

Derevianko, A., Olsen, J.W., Tseveendorj, D., Krivoshapkin, A., Petrin, V.T., Brantingham, P.J., 2000. The stratified cave site of Tsagaan Agui in the Gobi altai (Mongolia). Archeology, Ethnology, and Anthropology of Eurasia 1, 23-36.

Derevianko, A.P., M.V. Shunkov & S.V. Markin, 2014. The dynamics of the Paleolithic industries in Africa and Eurasia in the Late Pleistocene and the issue of the Homo sapiens Origin Institute of Archaeology and Ethnography SB RAS, Novosibirsk.

Derevianko, A.P., Postnov, P., Rybin, E.P., Kuzmin, Y., Keates, S.G., 2005. The Pleistocene peopling of Siberia: A review of environmental and behavioral aspects. Indo-Pacific Prehistory Association Bulletin 25, 57-68.

Derevianko, A.P., Shunkov, M.V., Agadjanian, A.K., Baryshnikov, G.F., Malaeva, E.M., Ulianov, V.A., Kulik, N.A., Postnov, A.V., Anoikin, A.A., 2003. Paleoenvironment and Paleolithic human occupation of Gorny Altai: subsistence and adaptation in the vicinity of Denisova Cave, Institute of Archaeology and Ethnography, Siberian Branch of the Russian Academy of Sciences, Novosibirsk.

Détroit, F., Mijares, A.S., Corny, J., Daver, G., Zanolli, C., Dizon, E., Robles, E., Grün, R., Piper, P.J., 2019. A new species of Homo from the Late Pleistocene of the Philippines. Nature 568, 181-186.

Devièse, T., Karavanić, I., Comeskey, D., Kubiak, C., Korlević, P., Hajdinjak, M., Radović, S., Procopio, N., Buckley, M., Pääbo, S., Higham, T., 2017. Direct dating of Neanderthal remains from the site of Vindija Cave and implications for the Middle to Upper Paleolithic transition. Proceedings of the National Academy of Sciences 114, 10606.

Dibble, A.D.a.H.L., 1994. Handbook of Paleolithic Typology: Lower and Middle Paleolithic of Europe. University of Pennsylvania, Philadelphia.

Dibble, H., 1984. The Mousterian Industry from Bisitun Cave (Iran). Paleorient 10.

Dibble, H., McPherron, S., Goldberg, P., Sandgathe, D., 2018. The Middle Paleolithic Site of Pech de l'Azé IV.

Dibble, H.L., 1987. The Interpretation of Middle Paleolithic Scraper Morphology. American Antiquity 52, 109-117.

Dibble, H.L., 1995. Biache Saint-Vaast, Level IIA: A comparison of analytical approaches. The definition and interpretation of Levallois technology, 93-116.

Dibble, Harold L., McPherron, Shannon P., 2006. The Missing Mousterian. Current Anthropology 47, 777-803.

Diez-Martín, F., Sánchez Yustos, P., Uribelarrea, D., Baquedano, E., Mark, D.F., Mabulla, A., Fraile, C., Duque, J., Díaz, I., Pérez-González, A., Yravedra, J., Egeland, C.P., Organista, E., Domínguez-Rodrigo, M., 2015. The Origin of the Acheulean: the 1.7 million-year-old site of FLK west, Olduvai Gorge (Tanzania). Scientific Reports 5, 17839.

Douka, K., Jacobs, Z., Lane, C., Grun, R., Farr, L., Hunt, C., Inglis, R.H., Reynolds, T., Albert, P., Aubert, M., Cullen, V., Hill, E., Kinsley, L., Roberts, R.G., Tomlinson, E.L., Wulf, S., Barker, G., 2014. The chronostratigraphy of the Haua Fteah cave (Cyrenaica, northeast Libya). Journal of Human Evolution 66, 39-63.

Douze, K., Delagnes, A., 2016. The pattern of emergence of a Middle Stone Age tradition at Gademotta and Kulkuletti (Ethiopia) through convergent tool and point technologies. Journal of Human Evolution 91, 93-121.

Du, S., 2003. Changes in the relationship between human behaviour and the environment in the Nihewan basin following the Middle to Late Palaeolithic period. Archaeology and Relics 2, 22-26.

Du, S., 2006. Cultural features of the Middle Palaeolithic of northern China and related questions, in: K. Zhong, X.G., Ningxia Institute of Cultural Relics and Archaeology (Ed.), Papers on the Palaeolithic period—commemorating the 80th anniversary of the discovery of the Shuidonggou site. Wenwu press, Beijing, pp. 17-23.

Duller, G.A.T., 2003. Distinguishing quartz and feldspar in single grain luminescence measurements. Radiation Measurements 37, 161-165.

Duller, G.A.T., 2006. Single grain optical dating of glacigenic deposits. Quaternary Geochronology 1, 296-304.

Duller, G.A.T., 2012a. Cross-talk during single grain optically stimulated luminescence measurements of quartz and feldspar. Radiation Measurements 47, 219-224.

Duller, G.A.T., 2012b. Improving the accuracy and precision of equivalent doses determined using the optically stimulated luminescence signal from single grains of quartz. Radiation Measurements 47, 770-777.

Duller, G.A.T., Botter-Jensen, L., Kohsiek, P., Murray, A.S., 1999a. A high sensitivity optically stimulated luminescence scanning system for measurement of single sand-sized grains. Radiation Protection Dosimetry 84, 325-330.

Duller, G.A.T., Botter-Jensen, L., Murray, A.S., Truscott, A.J., 1999b. Single grain laser luminescence (SGLL) measurements using a novel automated reader. Nuclear Instruments & Methods in Physics Research Section B-Beam Interactions with Materials and Atoms 155, 506-514.

Enzel, Y., Bar-Yosef, O., 2017. Quaternary of the Levant: Environments, Climate Change, and Humans. Cambridge University Press, Cambridge.

Eren, M.I., Lycett, S.J., 2012. Why Levallois? A morphometric comparison of experimental 'preferential' Levallois flakes versus debitage flakes. PLoS ONE 7, e29273.

Eren, M.I., Lycett, S.J., 2016. A Statistical Examination of Flake Edge Angles Produced During Experimental Lineal Levallois Reductions and Consideration of Their Functional Implications. Journal of Archaeological Method and Theory 23, 379-398.

Fain, J., Soumana, S., Montret, M., Miallier, D., Pilleyre, T., Sanzelle, S., 1999. Luminescence and ESR dating - Beta-dose attenuation for various grain shapes calculated by a Monte-Carlo method. Quaternary Science Reviews 18, 231-234.

Faivre, J.-P., 2012. A material anecdote but technical reality. Lithic Technology 37, 5-24.

Falguères, C., Bahain, J.-J., Pérez-González, A., Mercier, N., Santonja, M., Dolo, J.-M., 2006. The Lower Acheulian site of Ambrona, Soria (Spain): ages derived from a combined ESR/U-series model. Journal of Archaeological Science 33, 149-157.

Falguères, C., Bahain, J.-J., Saleki, H., 1997. U-Series and ESR Dating of Teeth from Acheulian and Mousterian Levels at La Micoque (Dordogne, France). Journal of Archaeological Science 24, 537-545.

Falguères, C., Bahain, J.-J., Yokoyama, Y., Arsuaga, J.L., Bermudez de Castro, J.M., Carbonell, E., Bischoff, J.L., Dolo, J.-M., 1999. Earliest humans in Europe: the age of TD6 Gran Dolina, Atapuerca, Spain. Journal of Human Evolution 37, 343-352.

Farrand, W.R., 1979. Chronology and palaeoenvironment of levantine prehistoric sites as seen from sediment studies. Journal of Archaeological Science 6, 369-392.

Féblot-Augustins, J., 2009. Revisiting European Upper Paleolithic raw material transfers: the demise of the cultural ecological paradigm? Lithic Materials and Paleolithic Societies, pp. 25-46.

Feathers, J.K., 2003. Single-grain OSL dating of sediments from the Southern High Plains, USA. Quaternary Science Reviews 22, 1035-1042.

Fernandes, P., Raynal, J.-P., Moncel, M.-H., 2008. Middle Palaeolithic raw material gathering territories and human mobility in the southern Massif Central, France: first results from a petro-archaeological study on flint. Journal of Archaeological Science 35, 2357-2370.

Foley, R., Lahr, M.M., 1997. Mode 3 Technologies and the Evolution of Modern Humans. Cambridge Archaeological Journal 7, 3-36.

Fontana, F., Moncel, M.H., Nenzioni, G., Onorevoli, G., Peretto, C., Combier, J., 2013. Widespread diffusion of technical innovations around 300,000 years ago in Europe as a reflection of anthropological and social transformations? New comparative data from the western Mediterranean sites of Orgnac (France) and Cave dall'Olio (Italy). Journal of Anthropological Archaeology 32, 478-498.

Freeman, L.G., 1977. Palaeolithic Archaeology and Palaeoanthropology in China, in: Howells, W.W., Tsuchitani, P.J. (Eds.), Paleoanthropology in the People's Republic of China: A Trip Report of the American Paleoanthropology Delegation: Submitted to the Committee on Scholarly Communication with the People's Republic of China. National Academies, pp. 79-114.

French, J.C., 2015. The demography of the Upper Palaeolithic hunter–gatherers of Southwestern France: A multi-proxy approach using archaeological data. Journal of Anthropological Archaeology 39, 193-209.

French, J.C., 2016. Demography and the Palaeolithic Archaeological Record. Journal of Archaeological Method and Theory 23, 150-199.

Fu, Q., Hajdinjak, M., Moldovan, O.T., Constantin, S., Mallick, S., Skoglund, P., Patterson, N., Rohland, N., Lazaridis, I., Nickel, B., Viola, B., Prüfer, K., Meyer, M., Kelso, J., Reich, D., Pääbo, S., 2015. An early modern human from Romania with a recent Neanderthal ancestor. Nature 524, 216.

Fu, Q., Meyer, M., Gao, X., Stenzel, U., Burbano, H.A., Kelso, J., Pääbo, S., 2013. DNA analysis of an early modern human from Tianyuan Cave, China. Proceedings of the National Academy of Sciences 110, 2223-2227.

Gagnepain, J., Gaillard, C., 2003. La grotte de la Baume Bonne (Quinson, Alpes de Haute-Provence): synthèse chronostratigraphique et séquence culturelle d'après les fouilles récentes (1988-1997), La grotte de la Baume Bonne (Quinson, Alpes de Haute-Provence) : synthèse chronostratigraphique et séquence culturelle d'après les fouilles récentes (1988-1997). John and Erica Hedges Ltd, Rennes, France, pp. 73-86.

Galbraith, R.F., Green, P.F., 1990. Estimating the component ages in a finite mixture. Nuclear Tracks and Radiation Measurements 17, 197-206.

Galbraith, R.F., Roberts, R.G., 2012. Statistical aspects of equivalent dose and error calculation and display in OSL dating: An overview and some recommendations. Quaternary Geochronology 11, 1-27.

Galbraith, R.F., Roberts, R.G., Laslett, G.M., Yoshida, H., Olley, J.M., 1999. Optical dating of single and multiple grains of quartz from jinmium rock shelter, northern Australia, part 1, Experimental design and statistical models. Archaeometry 41, 339-364.

Gamble, C., 1999. Palaeolithic societies of Europe. Cambridge University Press, Cambridge.

Gamble, C., Marshall, G., 2001. The shape of handaxes, the structure of the Acheulian world. Oxbow Books, Oxford.

Gao, F., Min, R., Li, B., Duan, C., 2012. The significance of the first archaeological excavation of Yushuiping sites in Nujiang in: Zhang, Y., Li, S. (Ed.), The Nu Nationality in the Canyon. Yunnan univeristy press, Yunnan Province, China.

Gao, X., 1999. A discussion of the 'Chinese Middle Paleolithic'. Acta Anthropologica Sinica 18, 1-16.

Gao, X., 2013. Paleolithic Cultures in China: Uniqueness and Divergence. Current Anthropology 54, S358-S370.

Gao, X., Norton, C.J., 2002. A critique of the Chinese 'Middle Palaeolithic'. Antiquity 76, 397-412.

Gemble, C., 1986. The Paleolithic Settlement of Europe. Cambridge University Press, Cambridge.

Geneste, J.-M., 1985. Analyse lithique d’industries moustériennes du Perigord: uneapproche technologique du comportement des groupes humains au Paléolithique Moyen. Université de Bordeaux.

Geneste, J.-M., 1988a. Les industries de la grotte Vaufrey: technologie du débitage, économie et circulation de la matière première, in: Rigaud, J.-P. (Ed.), Paléoenvironnements, Chronologie et Activités Humaines, pp. 441-517.

Geneste, J.-M., 1988b. Syste`mes d'approvisionnement en matie`res premie`res au pale´olithique moyen et au pale´olithique supe´rieur en Aquitaine, in: Kozlowski, M.O.a.J.K. (Ed.), La mutation. Universite´ de Lie`ge, Lie`ge, pp. 61-70.

Geneste, J.-M., 1990. De´velopment des syste`mes de production lithique au cours du pale´olithique moyen en Aquitaine septentrionale, in: Farizy, C. (Ed.), Pale´olithique moyen recent et pale´olithique supe´rieur ancien en Europe: ruptures et transitions, pp. 203-123.

Geneste Jean-Michel, H.P., 1996. Production et utilisation de l'outillage lithique dans le Mouste´rien du sud-ouest de la France: les Tares a` Sourzac, Valle´e de l'Isle, Dordogne. Quaternaria Nova 6, 343-368.

Gilead, I., 1991. The Upper Paleolithic period in the Levant. J. World Prehist. 5, 105-154.

Gliganic, L.A., Jacobs, Z., Roberts, R.G., Dominguez-Rodrigo, M., Mabulla, A.Z.P., 2012. New ages for Middle and Later Stone Age deposits at Mumba rockshelter, Tanzania: Optically stimulated luminescence dating of quartz and feldspar grains. Journal of Human Evolution 62, 533-547.

Goldberg, P., Dibble, H., Berna, F., Sandgathe, D., McPherron, S., Turq, A., 2012. New evidence on Neandertal use of fire: Examples from Roc de Marsal and Pech de l'Azé IV.

Goren-Inbar, N., 1988. Too Small to Be True? Reevaluation of Cores on Flakes in Levantine Mousterian Assemblages. Lithic Technology 17, 37-44.

Grimaldi, S., 1998. Analyse technologique, chaîne opératoire et objectifs techniques. Torre in Pietra (Rome, Italie). Torre in Pietra (Rome, Italy). Technological analysis, chaîne opératoire and technical objectives. Paléo, 109-122.

Grün, R., Brink, J.S., Spooner, N.A., Taylor, L., Stringer, C.B., Franciscus, R.G., Murray, A.S., 1996. Direct dating of Florisbad hominid. Nature 382, 500-501.

Grün, R., Eggins, S., Kinsley, L., Moseley, H., Sambridge, M., 2014. Laser ablation U-series analysis of fossil bones and teeth. Palaeogeography, Palaeoclimatology, Palaeoecology 416, 150-167.

Grun, R., Stringer, C., 2000. Tabun revisited: revised ESR chronology and new ESR and U-series analyses of dental material from Tabun C1. Journal of Human Evolution 39, 601-612.

Grun, R., Stringer, C., McDermott, F., Nathan, R., Porat, N., Robertson, S., Taylor, L., Mortimer, G., Eggins, S., McCulloch, M., 2005. U-series and ESR analyses of bones and teeth relating to the human burials from Skhul. Journal of Human Evolution 49, 316-334.

Guérin, G., Mercier, N., Adamiec, G., 2011. Dose-rate conversion factors: update. Ancient TL 29, 5-8.

Guibert, P., Bechtel, F., Bourguignon, L., Brenet, M., Couchoud, I., Delagnes, A., Delpech, F., Detrain, L., Duttine, M., Folgado, M., Jaubert, J., Lahaye, C., Lenoir, M., Maureille, B., Texier, J.-P., Turq, A., Vieillevigne, E., Villeneuve, G., 2008. Une base de données pour la chronologie du Paléolithique moyen dans le Sud-Ouest de la France, in: Jaubert, J., Bordes, J.-G., Ortega, I. (Eds.), Les sociétés du Paléolithique dans us Grand Sud-Ouest : nouveaux gisements, nouveaux résultats, nouvelles méthodes. Bulletin de la Société Préhistorique Française 47, pp. 19-40.

Guo, Y.-J., Li, B., Zhang, J.-F., Yuan, B.-Y., Xie, F., Roberts, R.G., 2016. Luminescence ages for three 'Middle Palaeolithic' sites in the Nihewan Basin, northern China, and their archaeological and palaeoenvironmental implications. Quat. Res. (USA) 85, 456-470.

Guo, Y.J., Li, B., Zhang, J.F., Yuan, B.Y., Xie, F., Roberts, R.G., 2017. New ages for the Upper Palaeolithic site of Xibaimaying in the Nihewan Basin, northern China: implications for small‐tool and microblade industries in north‐east Asia during Marine Isotope Stages 2 and 3. J. Quat. Sci. 32, 540-552.

Guralnik, B., Li, B., Jain, M., Chen, R., Paris, R.B., Murray, A.S., Li, S.H., Pagonis, V., Valla, P.G., Herman, F., 2015. Radiation-induced growth and isothermal decay of infrared-stimulated luminescence from feldspar. Radiation Measurements 81, 224-231.

Haesaerts, P., Koulakovskaya, L.V., 2006. La séquence paléosedimentaire de Korolevo (Ukraine transcarpathique): contexte chronostratigraphique et chronologique, in: Koulakovskaya, L.V. (Ed.), The European Middle Paleolithic Shlyakh, Kiev, Ukraine, pp. 21-38.

Harmand, S., Lewis, J.E., Feibel, C.S., Lepre, C.J., Prat, S., Lenoble, A., Boës, X., Quinn, R.L., Brenet, M., Arroyo, A., Taylor, N., Clément, S., Daver, G., Brugal, J.-P., Leakey, L., Mortlock, R.A., Wright, J.D., Lokorodi, S., Kirwa, C., Kent, D.V., Roche, H., 2015. 3.3-million-year-old stone tools from Lomekwi 3, West Turkana, Kenya. Nature 521, 310.

Hawkins, A.L., Smith, J.R., Giegengack, R., McDonald, M.M.A., Kleindienst, M.R., Schwarcz, H.P., Churcher, C.S., F., W.M., Nicoll, K., 2001. New research on the prehistory of the escarpment in Kharga Oasis, Egypt. NYAME AKUMA 55, 8-14.

Hayden, B., 1993. The cultural capacities of Neandertals: a review and re-evaluation. Journal of Human Evolution 24, 113-146.

Henrich, J., 2004. Demography and cultural evolution: How adaptive cultural processes can produce maladaptive losses-The Tasmanian case. American Antiquity 69, 197-214.

Henshilwood, C.S., D'Errico, F., Yates, R., Jacobs, Z., Tribolo, C., Duller, G.A., Mercier, N., Sealy, J.C., Valladas, H., Watts, I., 2002a. Emergence of modern human behavior: Middle Stone Age engravings from South Africa. Science 295, 1278-1280.

Herries, A.I.R., 2011. A Chronological Perspective on the Acheulian and Its Transition to the Middle Stone Age in Southern Africa: The Question of the Fauresmith. International Journal of Evolutionary Biology 2011, 25.

Hidjrati, N., Kimball, L.R., Koetje, T.A., 2003. Middle and Late Pleistocene investigations of Myshtulgaty Lagat (Weasel Cave) North Ossetia, Russia. Antiquity 77, 298.

Higham, T., Compton, T., Stringer, C., Jacobi, R., Shapiro, B., Trinkaus, E., Chandler, B., Gröning, F., Collins, C., Hillson, S., O'Higgins, P., FitzGerald, C., Fagan, M., 2011. The earliest evidence for anatomically modern humans in northwestern Europe. Nature 479, 521.

Hiscock, P., Clarkson, C., 2005. Experimental evaluation of Kuhn's geometric index of reduction and the flat-flake problem. Journal of Archaeological Science 32, 1015-1022.

Hiscock, P., Clarkson, C., 2009. The reality of reduction experiments and the GIUR: reply to Eren and Sampson. Journal of Archaeological Science 36, 1576-1581.

Hiscock, P., Tabrett, A., 2010. Generalization, inference and the quantification of lithic reduction. World Archaeology 42, 545-561.

Hiscock, P., Turq, A., Faivre, J.-P., Bourguignon, L., 2009. Quina Procurement and Tool Production, pp. 232-246.

Hoffecker, J., 2003. Desolate landscapes: Ice-Age settlement in Eastern Europe, Rutgers University Press, New Bruns-wick, NJ.

Holloway, R.L., 1992. Culture: A Human Domain. Current Anthropology 33, 47-64.

Hou, Y.M., 2003. Naming and preliminary study on the category of the ''Donggutuo core''. Acta Anthropologica Sinica 22, 79– 292.

Hou, Y.M., 2004. Two cases of early man in China: A small tool industry from Donggutuo (northern Nihewan Basin) and a large tool industry from Longgupo (southern Yangtze River), 18th International Senckenberg Conference 2004 in Weimar.

Hou, Y.M., Potts, R., Yuan, B.Y., Guo, Z.T., Deino, A., Wang, W., Clark, J., Xie, G., Huang, W., 2000. Mid-Pleistocene Acheulean-like Stone Technology of the Bose Basin, South China. Science 287, 1622.

Hovers, E., 1997. Variability of Levantine Mousterian Assemblages and Settlement Patterns: Implications for Understanding the Development of Human Behavior. The Hebrew University of Jerusalem.

Hovers, E., 2009. The lithic assemblages of Qafzeh Cave. Oxford University Press.

Huang, W., 2000. Stratigraphical basic of the Paleolithic sequence of China. Acta Anthropologica Sinica 19.

Huang, W., Hou, Y., Gao, L., 2009. 'Western Elements' in the Chinese Palaeolithic as viewed in a framework of early human cultural evolution. Acta Anthropologica Sinica 28, 16-24.

Huang, W., Hou, Y., Si, X., 1997. Stone industry from Panxian Dadong, a cave-site of southeastern China. Acta Anthropologica Sinica 16, 171-192.

Huang, W.W., 1989. Bifaces in China. Human Evolution 4, 87–92.

Hublin, J.-J., Ben-Ncer, A., Bailey, S.E., Freidline, S.E., Neubauer, S., Skinner, M.M., Bergmann, I., Le Cabec, A., Benazzi, S., Harvati, K., Gunz, P., 2017. New fossils from Jebel Irhoud, Morocco and the pan-African origin of Homo sapiens. Nature 546, 289.

Hublin, J.J., 2009. The origin of Neandertals. Proceedings of the National Academy of Sciences of the United States of America 106, 16022-16027.

Hublin, J.J., Barroso, C., Medina Lara, P., Fontugne, M., Reyss, J.L., 1995. The Mousterian site of Zafarraya (Andalucia, Spain): dating and implications on the Palaeolithic peopling processes of Western Europe. Comptes Rendus de l'Academie des Sciences Serie 2, Sciences de la Terre et des Planetes 321, 931-937.

Huntley, D.J., Godfreysmith, D.I., Haskell, E.H., 1991. Light-induced emission-spectra from some quartz and feldspars. Nuclear Tracks and Radiation Measurements 18, 127-131.

Huntley, D.J., Godfreysmith, D.I., Thewalt, M.L.W., 1985. Optical dating of sediments. Nature 313, 105-107.

Hütt, G., Jaek, I., Tchonka, J., 1988. Optical dating: K-feldspars optical response stimulation spectra. Quaternary Science Reviews 7, 381-385.

Ichikawa, Y., 1965. Dating of ancient ceramics by thermoluminescence. Bulletin of the Institute of Chemical Research, Kyoto University 43, 1-6.

Indriati, E., Swisher, C.C., Lepre, C., Quinn, R.L., Suriyanto, R.A., Hascaryo, A.T., Grun, R., Feibel, C.S., Pobiner, B.L., Aubert, M., Lees, W., Anton, S.C., 2011. The age of the 20 meter Solo River Terrace, Java, Indonesia and the survival of Homo erectus in Asia. Plos One 6.

Inizan, M.-L., Reduron-Ballinger, M., Roche, H., Tixier, J., 1999. Technology and Terminology of Knapped Stone. CREP, Nanterre, Paris.

J. Norton, C., Gao, X., Feng, X., 2009. The East Asian Middle Paleolithic Reexamined, pp. 245-254.

J. Wang, F.H.T., Y.R. Wang, 1994. The report of excavation and survey at the Dingcun Site. Journal of Chinese Antiquity, 1-75.

Jacobs, Z., Duller, G.A.T., Wintle, A.G., 2003. Optical dating of dune sand from Blombos Cave, South Africa: II - single grain data. Journal of Human Evolution 44, 613-625.

Jacobs, Z., Duller, G.A.T., Wintle, A.G., 2006a. Interpretation of single grain De distributions and calculation of De. Radiation Measurements 41, 264-277.

Jacobs, Z., Duller, G.A.T., Wintle, A.G., Henshilwood, C.S., 2006b. Extending the chronology of deposits at Blombos Cave, South Africa, back to 140ka using optical dating of single and multiple grains of quartz. Journal of Human Evolution 51, 255-273.

Jacobs, Z., Li, B., Shunkov, M.V., Kozlikin, M.B., Bolikhovskaya, N.S., Agadjanian, A.K., Uliyanov, V.A., Vasiliev, S.K., O'Gorman, K., Derevianko, A.P., Roberts, R.G., 2019. Timing of archaic hominin occupation of Denisova Cave in southern Siberia. Nature 565, 594-599.

Jacobs, Z., Roberts, R.G., 2007. Advances in optically stimulated luminescence dating of individual grains of quartz from archeological deposits. Evol Anthropol 16, 210-223.

Jacobs, Z., Roberts, R.G., Galbraith, R.F., Deacon, H.J., Grun, R., Mackay, A., Mitchell, P., Vogelsang, R., Wadley, L., 2008a. Ages for the Middle Stone Age of Southern Africa: Implications for Human Behavior and Dispersal. Science 322, 733-735.

Jarry, M., D., C., L.A., L., V., M., 2007. Les Bosses (La Magdelaine, Lot, France): Un gisement paléolithique moyen antérieur à l'avant-dernier Interglaciaire sur la moyenne terrasse du Lot. Société Préhistorique Française, Paris.

Jaubert, J., 1993. Le gisement paléolithique moyen de Mauran (Haute-Garonne): Techno-économie des industries lithiques. Bulletin de la Société préhistorique française 90, 328-335.

Jaubert, J., Bordes, J.G., 2008. Les sociétés du Paléolithique dans un Grand Sud-Ouest de la France: nouveaux gisements, nouveaux résultats, nouvelles méthodes. Société préhistorique française, p. 370.

Jaubert, J., Farizy, C., 1995. Levallois debitage: exclusivity, absence, or coexistence with other operative schemes (Garonne Basin, SW France). In: Dibble H. L. & Bar-Yosef O. (Eds), The Definition and Interpretation of Levallois Technology. Monographs in World Archaeology No. 23.

Jaubert, J., Lorblanchet, M., Laville, H., Slott-Moller, R., Turq, A., Brugal, J.-P., 1990. Les chasseurs d'aurochs de La Borde: Un site du Paleolithique moyen (Livernon, Lot). Paris: Editions de la Maison des sciences de l'homme.

Jaubert, J., Servelle, C., 1996. L'Acheuléen dans le bassin de la Garonne (région Midi Pyrénées): état de la question et implications, in: Tuffreau, A. (Ed.), L'Acheuléen dans l'Ouest de l'Europe. University of Sciences & Technology, Centre d'Etudes et Recherches Préhistoriques, Lille, France, pp. 77-108.

Jelinek, A.J., 1982. The Tabun cave and Paleolithic man in the Levant. Science 216, 1369-1375.

Ji, X.L., Chengwu; Tan, Huizhong; Zhang, Xiaoling; Ao, Xiujuan; You, Pingping, 2008. The discovery of palaeolithic site-Dahe, at Fuyuan. Chinese cultural heritage 28, 78-83.

Jia, L., Wei, Q., Li, C., 1979. Report on the excavation of Hsuchiayao man site in 1976. Verterbrata Palasiatica 17, 277-293.

Johnson, C.R., McBrearty, S., 2010. 500,000 year old blades from the Kapthurin Formation, Kenya. Journal of Human Evolution 58, 193-200.

Jungner, H., Huntley, D.J., 1991. Emission-spectra of some potassium feldspars under 633-Nm stimulation. Nuclear Tracks and Radiation Measurements 18, 125-126.

Kadowaki, S., Omori, T., Nishiaki, Y., 2015. Variability in Early Ahmarian lithic technology and its implications for the model of a Levantine origin of the Protoaurignacian. Journal of Human Evolution 82, 67-87.

Karkanas, P., Schepartz, L.A., Miller-Antonio, S., Wang, W., Huang, W., 2008. Late Middle Pleistocene climate in southwestern China: inferences from the stratigraphic record of Panxian Dadong Cave, Guizhou. Quaternary Science Reviews 27, 1555-1570.

Keates, S.G., 2010. Evidence for the earliest Pleistocene hominid activity in the Nihewan Basin of northern China. Quatern Int 223-224, 408-417.

Kei, Y.M., 2012. The Middle Palaeolithic in China a review of current interpretations. Antiquity 86, 619-626.

Kimbel, W.H., Walter, R.C., Johanson, D.C., Reed, K.E., Aronson, J.L., Assefa, Z., Marean, C.W., Eck, G.G., Bobe, R., Hovers, E., Rak, Y., Vondra, C., Yemane, T., York, D., Chen, Y., Evensen, N.M., Smith, P.E., 1996. Late PlioceneHomoand Oldowan Tools from the Hadar Formation (Kada Hadar Member), Ethiopia. Journal of Human Evolution 31, 549-561.

Klein, R.G., 1999. The Human Career. University of Chicago Press, Chicago.

Krause, J., Fu, Q., Good, J.M., Viola, B., Shunkov, M.V., Derevianko, A.P., Pääbo, S., 2010. The complete mitochondrial DNA genome of an unknown hominin from southern Siberia. Nature 464, 894-897.

Krause, J., Orlando, L., Serre, D., Viola, B., Prufer, K., Richards, M.P., Hublin, J.-J., Hanni, C., Derevianko, A.P., Paabo, S., 2007. Neanderthals in central Asia and Siberia. Nature 449, 902-904.

Kreutzer, S., Schmidt, C., Fuchs, M.C., Dietze, M., Fischer, M., Fuchs, M., 2012. Introducing an R package for luminescence dating analysis. Ancient TL 30, 1-8.

Krivoshapkin, A., Shalagina, A., Baumann, M., Shnaider, S., Kolobova, K., 2018. Between Denisovans and Neanderthals: Strashnaya Cave in the Altai Mountains. Antiquity 92, e1.

Krivoshapkin, A.I., Kuzmin, Y., Jull, A.J.T., 2010. Chronology of the Obi-Rakhmat Grotto (Uzbekistan): First Results on the Dating and Problems of the Paleolithic Key Site in Central Asia. Radiocarbon 52, 549-554.

Kuhn, S.L., 1990. A geometric index of reduction for unifacial stone tools. Journal of Archaeological Science 17, 581-593.

Kuhn, S.L., 1995. Mousterian Lithic Technology. Princeton University Press, Princeton.

Kuhn, S.L., 2012. Chapter 6 - Emergent Patterns of Creativity and Innovation in Early Technologies, in: Elias, S. (Ed.), Developments in Quaternary Sciences. Elsevier, pp. 69-87.

Kuhn, S.L., 2013. Roots of the Middle Paleolithic in Eurasia. Current Anthropology 54, S255-S268.

Kuhn, S.L., Hovers, E., 2013. Alternative Pathways to Complexity: Evolutionary Trajectories in the Middle Paleolithic and Middle Stone Age: An Introduction to Supplement 8. Current Anthropology 54, S176-S182.

Kuman, K., Clarke, R.J., 2000. Stratigraphy, artefact industries and hominid associations for Sterkfontein, Member 5. Journal of Human Evolution 38, 827-847.

Langley, M., Clarkson, C., Ulm, S., 2008. Behavioural complexity in Eurasian Neanderthal populations: a chronological examination of the archaeological evidence. Cambridge Archaeological Journal 18, 289-307.

Leader, G., Abdolahzadeh, A., Lin, S.C., Dibble, H.L., 2017. The effects of platform beveling on flake variation. Journal of Archaeological Science: Reports 16, 213-223.

Leakey, M.D., 1971. Olduvai Gorge, 3. Excavations in Beds I and II, 1960-1963. Cambridge University Press, Cambridge.

Leng, J., 2001. Early Paleolithic technology in Eastern and Southern Asia / Jian Leng. J. and E. Hedges: Archaeopress, Oxford.

Lenoir, M., 1986. Un mode d'obtention de la retouche Quina dans le Mousterien de Combe Grenal (Domme, Dordogne). Bulletin de la Soci´et´e d'Anthropologie du Sud-Ouest XXI, 153-160.

Li, B., Jacobs, Z., Roberts, R.G., 2016a. Investigation of the applicability of standardised growth curves for OSL dating of quartz from Haua Fteah cave, Libya. Quaternary Geochronology 35, 1-15.

Li, B., Jacobs, Z., Roberts, R.G., Galbraith, R., Peng, J., 2017a. Variability in quartz OSL signals caused by measurement uncertainties: Problems and solutions. Quaternary Geochronology 41, 11-25.

Li, B., Roberts, R.G., Jacobs, Z., Li, S.H., 2015. Potential of establishing a 'global standardised growth curve' (gSGC) for optical dating of quartz from sediments. Quaternary Geochronology 27, 94-104.

Li, F., 2014. Fact or fiction: The Middle Palaeolithic in China. Antiquity 88, 1303-1309.

Li, F., Gao, X., Chen, F., Pei, S., Zhang, Y., Zhang, X., Liu, D., Zhang, S., Guan, Y., Wang, H., 2013a. The development of Upper Palaeolithic China: new results from the Shuidonggou site. Antiquity 87, 368-383.

Li, F., Kuhn, S.L., Chen, F., Wang, Y., Southon, J., Peng, F., Shan, M., Wang, C., Ge, J., Wang, X., Yun, T., Gao, X., 2018. The easternmost Middle Paleolithic (Mousterian) from Jinsitai Cave, North China. Journal of Human Evolution 114, 76-84.

Li, F., Kuhn, S.L., Gao, X., Chen, F.-y., 2013b. Re-examination of the dates of large blade technology in China: A comparison of Shuidonggou Locality 1 and Locality 2. Journal of Human Evolution 64, 161-168.

Li, H., Kuman, K., Li, C., 2016b. What is currently (un)known about the Chinese Acheulean, with implications for hypotheses on the earlier dispersal of hominids. Comptes Rendus Palevol 17, 120-130.

Li, H., Li, Z.-y., Gao, X., Kuman, K., Sumner, A., 2019. Technological behavior of the early Late Pleistocene archaic humans at Lingjing (Xuchang, China). Archaeological and Anthropological Sciences 11, 3477-3490.

Li, H., Lotter, M.G., 2019. Lithic production strategies during the late Middle Pleistocene at Dali, Shaanxi Province, China: implications for understanding late archaic humans. Archaeological and Anthropological Sciences 11, 1701-1712.

Li, S.H., 1991. Removal of the thermally unstable signal in optical dating of K-feldspar. Ancient TL 9, 26-29.

Li, Y., 1993. On the division of the Upper Paleolithic industries of China. Acta Anthropologica Sinica 12, 214-223.

Li, Y., Hou, Y., Boëda, E., 2009a. Mode of débitage and technical cognition of hominids at the Guanyindong site. Chinese Science Bulletin 54, 3864-3871.

Li, Y., Wen, B., 1986. Guanyindong: A Lower Paleolithic Site at Qianxi County, Guizhou Province. Cultural Relics Press Beijing.

Li, Y.H., 2009. Tehnological study of lithic industry of the Guanyindong site, Guizhou province, south-west of China. The Institute of Vertebrate Paleontology and Paleoanthropology, Chinese Academy of Sciences, Beijing, China.

Li, Y.H., Hou, Y.M., Boëda, E., 2009b. Mode of débitage and technical cognition of hominids at the Guanyindong site. Chinese Science Bulletin 54, 3864-3871.

Li, Z.-Y., Wu, X.-J., Zhou, L.-P., Liu, W., Gao, X., Nian, X.-M., Trinkaus, E., 2017b. Late Pleistocene archaic human crania from Xuchang, China. Science 355, 969-972.

Lian, O.B., Roberts, R.G., 2006. Dating the Quaternary: progress in luminescence dating of sediments. Quaternary Science Reviews 25, 2449-2468.

Lieberman, P., 1975. On the origins of language: an introduction to the evolution of human speech. Macmillan, New York.

Lin, S., 1996. Comparison of technological mode of Paleolithic culture between China and the West Acta Anthropologica Sinica 15, 1-20.

Lipo, C.P., Madsen, M.E., 2001. Neutrality, "style", and drift: building models for studying cultural transmission in the archaeological record, in: Hurt, G.M., Rakita, G.F.M. (Eds.), Style and Function: Conceptual Issues in Evolutionary Archaeology. Bergin and Garvey, Westport, Connecticut, pp. 91-118.

Lisiecki, L.E., Raymo, M.E., 2005. A Pliocene-Pleistocene stack of 57 globally distributed benthic δ18O records. Paleoceanography 20, PA1003.

Liu, D., Wang, X., Gao, X., Xia, Z., Pei, S., Chen, F., Wang, H., 2009. Progress in the stratigraphy and geochronology of the Shuidonggou site, Ningxia, North China. Chinese Science Bulletin 54, 3880.

Liu, W., Jin, C.-Z., Zhang, Y.-Q., Cai, Y.-J., Xing, S., Wu, X.-J., Cheng, H., Edwards, R.L., Pan, W.-S., Qin, D.-G., An, Z.-S., Trinkaus, E., Wu, X.-Z., 2010. Human remains from Zhirendong, South China, and modern human emergence in East Asia. Proceedings of the National Academy of Sciences 107, 19201-19206.

Liu, W., Martinon-Torres, M., Cai, Y.-j., Xing, S., Tong, H.-w., Pei, S.-w., Sier, M.J., Wu, X.-h., Edwards, R.L., Cheng, H., Li, Y.-y., Yang, X.-x., de Castro, J.M.B., Wu, X.-j., 2015. The earliest unequivocally modern humans in southern China. Nature 526, 696-699.

Locht, J.-L., Antoine, P., Hérisson, D., Gadebois, G., Debenham, N., 2010. Une occupation de la phase ancienne du Paléolithique moyen à Therdonne (Oise). Chronostratigraphie, production de pointes Levallois et réduction des nucléus. Gallia préhistoire, 1-32.

Lu, Z., 1989. Date of the Jinniushan man and his position in human evolution. Jiaohai Wenwu Xuekan 1, 44-45.

Lycett, S.J., 2007a. Is the Soanian techno-complex a Mode 1 or Mode 3 phenomenon? A morphometric assessment. Journal of Archaeological Science 34, 1434-1440.

Lycett, S.J., 2007b. Why is there a lack of Mode 3 Levallois technologies in East Asia? A phylogenetic test of the Movius-Schick hypothesis. Journal of Anthropological Archaeology 26, 541-575.

Lycett, S.J., Eren, M.I., 2013. Levallois economics: an examination of 'waste' production in experimentally produced Levallois reduction sequences. Journal of Archaeological Science 40, 2384-2392.

Lycett, S.J., Norton, C.J., 2010. A demographic model for Palaeolithic technological evolution: The case of East Asia and the Movius Line. Quatern Int 211, 55-65.

Madsen, D.B., Li, J., Brantingham, P.J., Gao, X., Elston, R.G., Bettinger, R.L., 2001. Dating Shuidonggou and the Upper Paleolithic blade industry in North China. Antiquity 75, 706-716.

Malinsky-Buller, A., 2016. The Muddle in the Middle Pleistocene: The Lower–Middle Paleolithic Transition from the Levantine Perspective. J. World Prehist. 29, 1-78.

Mallick, R., Frank, N., 2002. A new technique for precise uranium-series dating of travertine micro-samples. Geochimica et Cosmochimica Acta 66, 4261-4272.

Marks, A.E., Brugal, J.-P., Chabai, V.P., Monigal, K., Goldberg, P., Hockett, B., Peman, E., Elorza, M., Mallol, C., 2002. Le gisement pléistocène moyen de Galeria Pesada (Estrémadure, Portugal): premiers résultats. PALEO 14, 77-100.

Martinón-Torres, M., Wu, x.j., Bermúdez de Castro, J.-M., Xing, S., Liu, W., 2017. Homo sapiens in the Eastern Asian Late Pleistocene. Current Anthropology 58, S434-S448.

Marwick, B., Clarkson, C., O'Connor, S., Collins, S., 2016. Early modern human lithic technology from Jerimalai, East Timor. Journal of Human Evolution 101, 45-64.

Mathias, C., 2016. After the Lower Palaeolithic: Lithic ramification in the early Middle Palaeolithic of Orgnac 3, layer 2 (Ardèche, France). Quatern Int 411, 193-201.

McBrearty, S., Brooks, A.S., 2000. The revolution that wasn't: a new interpretation of the origin of modern human behavior. Journal of Human Evolution 39, 453-563.

McDougall, I., Brown, F.H., Fleagle, J.G., 2005. Stratigraphic placement and age of modern humans from Kibish, Ethiopia. Nature 433, 733-736.

Meignen, L., 2002. Hayonim Cave Lithic Assemblages in the Context of the Near Eastern Middle Paleolithic, pp. 165-180.

Mejdahl, V., 1979. Thermoluminescence Dating - Beta-Dose Attenuation in Quartz Grains. Archaeometry 21, 61-72.

Mejdahl, V., 1985. Thermo-Luminescence Dating Based on Feldspars. Nuclear Tracks and Radiation Measurements 10, 133-136.

Mellars, P., French, J.C., 2013. Population changes across the Neanderthal-to-modern-human transition in western France: A reply to Dogandžić and McPherron (2013). J. Hum. Evol. 65, 330-333.

Mellars, P., 2006a. Going east: New genetic and archaeological perspectives on the modern human colonization of Eurasia. Science 313, 796-800.

Mellars, P., 2006. Why did modern human populations disperse from Africa ca. 60,000 years ago? A new model. Proceedings of the National Academy of Sciences 103, 9381.

Mellars, P.A., 1995. The Neanderthal legacy: an archaeological perspective from Western Europe. Princeton University Press.

Mercier, N., Falguères, C., 2007. Field gamma dose-rate measurement with a NaI(Tl) detector: re-evaluation of the "threshold" technique. Ancient TL 1.

Mercier, N., Valladas, H., 2003. Reassessment of TL age estimates of burnt flints from the Paleolithic site of Tabun Cave, Israel. Journal of Human Evolution 45, 401-409.

Mercier, N., Valladas, H., Bar-Yosef, O., Vandermeersch, B., Stringer, C., Joron, J.L., 1993. Thermoluminescence Date for the Mousterian Burial Site of Es-Skhul, Mt. Carmel. Journal of Archaeological Science 20, 169-174.

Mercier, N., Valladas, H., Froget, L., Joron, J.L., Reyss, J.L., Weiner, S., Goldberg, P., Meignen, L., Bar-Yosef, O., Belfer-Cohen, A., Chech, M., Kuhn, S.L., Stiner, M.C., Tillier, A.M., Arensburg, B., Vandermeersch, B., 2007. Hayonim Cave: a TL-based chronology for this Levantine Mousterian sequence. Journal of Archaeological Science 34, 1064-1077.

Michel, V., Shen, G., Shen, C.C., Wu, C.C., Vérati, C., Gallet, S., Moncel, M.H., Combier, J., Khatib, S., Manetti, M., 2013. Application of U/Th and $^{40}Ar/^{39}Ar$ dating to orgnac 3, a Late Acheulean and Early Middle Palaeolithic site in Ardèche, France. PLOS ONE 8.

Miller-Antonio, S., Schepartz, L.A., Karkanas, P., Yamei, H., et al., 2004. Lithic Raw Material Use at the Late Middle Pleistocene Site of Panxian Dadong. Asian Perspectives 43, 314.

Mishra, S., Venkatesan, T.R., Rajaguru, S.N., Somayajulu, B.L.K., 1995. Earliest Acheulian Industry from Peninsular India. Current Anthropology 36, 847-851.

Misra, V.N., 2001. Prehistoric human colonization of India. J. Biosci. 26, 491-531.

Moncel, M.-H., xe, xe, ne, Moigne, A.-M., Sam, Y., Combier, J., 2011. The Emergence of Neanderthal Technical Behavior: New Evidence from Orgnac 3 (Level 1, MIS 8), Southeastern France. Current Anthropology 52, 37-75.

Monnier, G., Bisson, M., Klein, R., McNabb, J., Fluck, H., Moncel, M., Straus, L., Tuffreau, A., Monnier, G., 2006. The Lower/Middle Paleolithic periodization in western Europe: an evaluation. Current Anthropology 47, 709-744.

Monnier, G.F., Missal, K., 2014. Another Mousterian Debate? Bordian facies, *chaîne op eratoire* technocomplexes, and patterns of lithic variability in the western European Middle and Upper Pleistocene. Quatern Int 350, 59-83.

Moore, M.W., 2003. Flexibility of Stone Tool Manufacturing Methods on the Georgina River, Camooweal, Queensland. Archaeology in Oceania 38, 23-36.

Moore, M.W., 2004. The tula adze: Manufacture and purpose. Antiquity 78, 61-73.

Morgan, L., Renne, P., 2008. Diachronous dawn of Africa's Middle Stone Age: New $^{40}Ar/^{39}Ar$ ages from the Ethiopian Rift.

Morin, E., Delagnes, A., Armand, D., Castel, J.-C., Hodgkins, J., 2014. Millennial-scale change in archaeofaunas and their implications for Mousterian lithic variability in southwest France. Journal of Anthropological Archaeology 36, 158-180.

Morwood, M.J., Soejono, R.P., Roberts, R.G., Sutikna, T., Turney, C.S.M., Westaway, K.E., Rink, W.J., Zhao, J.X., Van Den Bergh, G.D., Due, R.A., Hobbs, D.R., Moore, M.W., Bird, M.I., Fifield, L.K., 2004. Archaeology and age of a new hominin from Flores in eastern Indonesia. Nature 431, 1087-1091.

Movius, H., 1969. Lower Paleolithic archaeology in southern Asia and the Far East. Humanities Press, New York.

Movius, H.L., 1948. The Lower Palaeolithic cultures of southern and eastern Asia. Transactions of the American Philosophical Society 38, 329-420.

Murray, A.S., Olley, J.M., 2002. Precision and accuracy in the optically stimulated luminescence dating of sedimentary quartz: a status review. Geochronometria 21, 1-16.

Murray, A.S., Roberts, R.G., 1998. Measurement of the equivalent dose in quartz using a regenerative-dose single-aliquot protocol. Radiation Measurements 29, 503-515.

Murray, A.S., Wintle, A.G., 2000. Luminescence dating of quartz using an improved single-aliquot regenerative-dose protocol. Radiation Measurements 32, 57-73.

Neiman, F.D., 1995. Stylistic variation in evolutionary perspective: implications for decorative diversity and inter-assemblage distance in Illinois Woodland ceramic assemblages. American Antiquity 60, 7-36.

Nelson, M.C., 1991. The study of technological organization. Archaeological Method and Theory 3, 57-100.

Nishiaki, Y., 1985. Truncated-facetted flakes from Levantine Mousterian assemblage, Bulletin of the Department of Archaeology (The University of Tokyo). The Univ. of Tokyo, Tokyo, pp. 215-226.

Niu, D., Pei, S., Zhang, S., Zhou, Z., Wang, H., Gao, X., 2016. The Initial Upper Palaeolithic in Northwest China: New evidence of cultural variability and change from Shuidonggou locality 7. Quatern Int 400, 111-119.

Noble, W.D., I., 1996. Human Evolution, Language and Mind: A Psychological and Archaeological Inquiry Cambridge University Press, Cambridge.

Norton C.J., Jin J., J.H., 2009. The evolution of modern human behavior in East Asia: Current perspectives. Evol. Anthropol. 18, 247-260.

Norton, C.J., Bae, K., 2008. The Movius Line sensu lato (Norton et al., 2006) further assessed and defined. Journal of Human Evolution 55, 1148-1150.

Norton, C.J., Bae, K., Harris, J.W.K., Lee, H., 2006. Middle Pleistocene handaxes from the Korean Peninsula. Journal of Human Evolution 51, 527-536.

Olley, J.M., Murray, A., Roberts, R.G., 1996. The effects of disequilibria in the uranium and thorium decay chains on burial dose rates in fluvial sediments. Quaternary Science Reviews 15, 751-760.

Otte, M., 1995. The nature of Levallois. The definition and interpretation of Levallois technology, 117-124.

Otte, M., Weiwen, H., Hu, Y., Hou, Y., 2017. Panxian Dadong et le Levallois chinois. L'Anthropologie 121, 255-269.

Otte, M., Yalçinkaya, I., Kozlowski, J., Bar-Yosef, O., López Bayón, I., Taskiran, H., 1998. Long-term technical evolution and human remains in the Anatolian Palaeolithic. Journal of Human Evolution 34, 413-431.

Otte, M.H., WW; Hu, Y; Hou, YM, 2017. Panxian Dadong et le Levallois chinois. L'anthropologie in press.

Owen, W.E., 1938. The Kombewa Culture, Kenya Colony, Man. Royal Anthropological Institute of Great Britain and Ireland, pp. 203-205.

Owen, W.E., 1939. An Amateur field collector in Kavirondo. African Affairs XXXVIII, 124-132.

Pappu, S., Gunnell, Y., Akhilesh, K., Braucher, R., Taieb, M., Demory, F., Thouveny, N., 2011. Early Pleistocene Presence of Acheulian Hominins in South India. Science 331, 1596.

Pasty, J.-F., 1997. Étude technologique du site atérien d'El-Azrag (Mauritanie). Paléo 9, 173-190.

Pasty, J.-F., 2000. Le gisement Paléolithique moyen de Meillers (Allier): un exemple de la variabilité du débitage Discoïde. Bulletin de la Société préhistorique française 97, 165-190.

Patrick, M.M.A., Bringmans, E.M., Frans Gullentops, Jeanmarie Cordy, Pierre Vermeersch, Jean Pierre de Warrimont, Albert Groenendijk, 1998. Human Presence and Lithic Variability at the Middle Palaeolithic Valley Settlements at Veldwezelt-Hezerwater (Limburg, Belgium), in: Demarsin, B. (Ed.), NEANDERTHALS IN EUROPE, pp. 89-100.

Pavlov, P., Roebroeks, W., Svendsen, J.I., 2004. The Pleistocene colonization of northeastern Europe: a report on recent research. Journal of Human Evolution 47, 3-17.

Pei, S., Gao, X., Wang, H., Kuman, K., Bae, C.J., Chen, F., Guan, Y., Zhang, Y., Zhang, X., Peng, F., Li, X., 2012. The Shuidonggou site complex: new excavations and implications for the earliest Late Paleolithic in North China. Journal of Archaeological Science 39, 3610-3626.

Pei, W.C., 1939. A preliminary study on a new Palaeolithic station known as locality 15 within the Choukoudien region. Bull. Geol. Soc.China 19, 147-187.

Pei, W.C., Woo, J.K., Chia, L.P., Chow, M.C., Liu, H.T., Wang, C.Y, 1958. Report on the Excavation of Palaeolithic Sites at Tingtsun, Hsiangfenhsien, Shansi Province, China. Science Press, Beijing.

Pei, W.C., Yuan, C.S., Lin, Y.P., Chang, Y.Y., Tsao, C.T., 1965. Discovery of Paleolithic chert artefacts in Kuan-Yin-Tung Cave in Chien-Hsi-Hsien of Kweichow Province. Vertebrata Palasiatica 9, 270-279.

Pei, W.C., Yuan, C.S., Lin, Y.P., Chang, Y.Y., 1965. Discovery of palaeolithic chert artefacts in Kuan-Yin-Tung cave in Chien-Hsi-Hsien of Kweichow Province. Vertebreta Palasiatica 9, 270-279.

Peng, J., Dong, Z., Han, F., Long, H., Liu, X., 2013. R package numOSL: numeric routines for optically stimulated luminescence dating. Ancient TL 31: 41-48.

Peng, J., Li, B., 2017. Single-aliquot Regenerative-Dose (SAR) and Standardised Growth Curve (SGC) Equivalent Dose Determination in a Batch Model Using the R Package 'numOSL'. Ancient TL 35, 32-53.

Peng, J., Pagonis, V., Li, B., 2016. On the intrinsic accuracy and precision of the standardised growth curve (SGC) and global-SGC (gSGC) methods for equivalent dose determination: A simulation study. Radiation Measurements 94, 53-64.

Peresani, M., 1998. La variabilité du débitage discoïde dans la grotte de Fumane (Italie du Nord)/The variability of discoid production at the grotte de Fumane Paléo 10, 123-146.

Peresani, M., 2003. Discoid lithic technology: advances and implications. Archaeopress, Oxford.

Perpère, M., 1986. Apport de la typométrie à la définition des éclats Levallois: l'exemple d'Ault. Bulletin de la Société préhistorique française, 115-118.

Petraglia, M., Korisettar, R., Boivin, N., Clarkson, C., Ditchfield, P., Jones, S., Koshy, J., Lahr, M.M., Oppenheimer, C., Pyle, D., Roberts, R., Schwenninger, J.L., Arnold, L., White, K., 2007. Middle paleolithic assemblages from the Indian subcontinent before and after the Toba super-eruption. Science 317, 114-116.

Petraglia, M.D., Alsharekh, A., Breeze, P., Clarkson, C., Crassard, R., Drake, N.A., Groucutt, H.S., Jennings, R., Parker, A.G., Parton, A., Roberts, R.G., Shipton, C., Matheson, C., al-Omari, A., Veall, M.-A., 2012. Hominin Dispersal into the Nefud Desert and Middle Palaeolithic Settlement along the Jubbah Palaeolake, Northern Arabia. PLOS ONE 7, e49840.

Petraglia, M.D., Shipton, C., 2008. Large cutting tool variation west and east of the Movius Line. Journal of Human Evolution 55, 962-966.

Picin, A., 2017. Technological adaptation and the emergence of Levallois in Central Europe: new insight from the Markkleeberg and Zwochau open-air sites in Germany. J. Quat. Sci., 1-13.

Picin, A., Carbonell, E., 2016. Neanderthal mobility and technological change in the northeastern of the Iberian Peninsula: The patterns of chert exploitation at the Abric Romaní rock-shelter.

Picin, A., Peresani, M., Falguères, C., Gruppioni, G., Bahain, J.-J., 2013. San Bernardino Cave (Italy) and the Appearance of Levallois Technology in Europe: Results of a Radiometric and Technological Reassessment. PLOS ONE 8, e76182.

Pigeot, N., 1991. Réflexions sur l'histoire technique de l'Homme: de l'évolution cognitive à l'évolution culturelle. Pale´o 3, 167-200.

Porat, N., Chazan, M., Grün, R., Aubert, M., Eisenmann, V., Horwitz, L.K., 2010. New radiometric ages for the Fauresmith industry from Kathu Pan, southern Africa: Implications for the Earlier to Middle Stone Age transition. Journal of Archaeological Science 37, 269-283.

Powell, A., Shennan, S., Thomas, M.G., 2009. Late Pleistocene Demography and the Appearance of Modern Human Behavior. Science 324, 1298-1301.

Prescott, J.R., Hutton, J.T., 1988. Cosmic-ray and gamma-ray dosimetry for TL and electron-spin-resonance. Nuclear Tracks and Radiation Measurements 14, 223-227.

Prescott, J.R., Hutton, J.T., 1994. Cosmic-ray contributions to dose rates for luminescence and ESR dating - large depths and long-term time variations. Radiation Measurements 23, 497-500.

Preusser, F., Chithambo, M.L., Götte, T., Martini, M., Ramseyer, K., Sendezera, E.J., Susino, G.J., Wintle, A.G., 2009. Quartz as a natural luminescence dosimeter. Earth-Science Reviews 97, 184-214.

Preysler, J., 2010. Experimental Approach to the Function and Technology of Quina Side-Scrapers, In Hugo Nami (Ed) Essays in Honor of Errett Callahan, Edition: Ediciones de Arqueología Contemporánea, Chapter: 7, Ediciones de Arqueología Contemporánea, pp.172-202.

Prugnolle, F., Manica, A., Balloux, F., 2005. Geography predicts neutral genetic diversity of human populations. Curr Biol 15, R159-R160.

Qiu, Z., Zhang, Y., 1985. Human tooth and Paleoliths found at locality 2 of Longtanshan, Chenggong, Kunming. Acta Anthropologica Sinica 4, 233-241.

R Core Team, 2016. R: A language and environment for statistical computing. Vienna, Austria.

Ramachandran, S., Deshpande, O., Roseman, C.C., Rosenberg, N.A., Feldman, M.W., Cavalli-Sforza, L.L., 2005. Support from the relationship of genetic and geographic distance in human populations for a serial founder effect originating in Africa. Proceedings of the National Academy of Sciences of the United States of America 102, 15942.

Reich, D., Green, R.E., Kircher, M., Krause, J., Patterson, N., Durand, E.Y., Viola, B., Briggs, A.W., Stenzel, U., Johnson, P.L.F., Maricic, T., Good, J.M., Marques-Bonet, T., Alkan, C., Fu, Q.,

Mallick, S., Li, H., Meyer, M., Eichler, E.E., Stoneking, M., Richards, M., Talamo, S., Shunkov, M.V., Derevianko, A.P., Hublin, J.J., Kelso, J., Slatkin, M., Pääbo, S., 2010. Genetic history of an archaic hominin group from Denisova cave in Siberia. Nature 468, 1053-1060.

Révillion, S. and Tuffreau, A., 1994. Les industries laminaires au Pal´eolithique moyen, Paris. CNRS.

Révillion, S., 1995. Technologie du débitage laminaire au Paléolithique moyen en Europe septentrionale: état de la question. Bulletin de la Société préhistorique française 92, 425-442.

Richter, D., Grün, R., Joannes-Boyau, R., Steele, T.E., Amani, F., Rué, M., Fernandes, P., Raynal, J.-P., Geraads, D., Ben-Ncer, A., Hublin, J.-J., McPherron, S.P., 2017. The age of the hominin fossils from Jebel Irhoud, Morocco, and the origins of the Middle Stone Age. Nature 546, 293-296.

Richter, J., 2011. When Did the Middle Paleolithic Begin?, in: Conard, N.J., Richter, J. (Eds.), Neanderthal Lifeways, Subsistence and Technology: One Hundred Fifty Years of Neanderthal Study. Springer Netherlands, Dordrecht, pp. 7-14.

Roberts, H.M., Duller, G.A.T., 2004. Standardised growth curves for optical dating of sediment using multiple-grain aliquots. Radiation Measurements 38, 241-252.

Roberts, M.B., Stringer, C.B., Parfitt, S.A., 1994. A hominid tibia from Middle Pleistocene sediments at Boxgrove, UK. Nature 369, 311-313.

Roberts, R., Bird, M., Olley, J., Galbraith, R., Lawson, E., Laslett, G., Yoshida, H., Jones, R., Fullagar, R., Jacobsen, G., Hua, Q., 1998. Optical and radiocarbon dating at Jinmium rock shelter in northern Australia. Nature 393, 358-362.

Roberts, R.G., Galbraith, R.F., Olley, J.M., Yoshida, H., Laslett, G.M., 1999. Optical dating of single and multiple grains of quartz from jinmium rock shelter, northern Australia, part 2, Results and implications. Archaeometry 41, 365-395.

Roberts, R.G., Galbraith, R.F., Yoshida, H., Laslett, G.M., Olley, J.M., 2000. Distinguishing dose populations in sediment mixtures: a test of single-grain optical dating procedures using mixtures of laboratory-dosed quartz. Radiation Measurements 32, 459-465.

Roberts, R.G., Jacobs, Z., Li, B., Jankowski, N.R., Cunningham, A.C., Rosenfeld, A.B., 2015. Optical dating in archaeology: thirty years in retrospect and grand challenges for the future. Journal of Archaeological Science 56, 41-60.

Roche, H., Delagnes, A., Brugal, J.P., Feibel, C., Kibunjia, M., Mourre, V., Texier, P.J., 1999. Early hominid stone tool production and technical skill 2.34 Myr ago in West Turkana, Kenya. Nature 399, 57.

Roe, D.A., 2014. The lower and middle Palaeolithic periods in Britain. Routledge.

Roebroeks, J.W.M.T., A., 1999. Palaeoenvironment and settlement patterns of the Northwest Europe¬an Middle Palaeolithic, in: Gamble, W.R.a.C. (Ed.), The Middle Palaeolithic Occupation of Europe. University of Leiden, Leiden, pp. 121-138.

Rolland, N., 1981. The Interpretation of Middle Palaeolithic Variability. Man 16, 15-42.

Rolland, N., 1995. Levallois technique emergence: single or multiple? A review of the Euro-African record. Prehistory Press, Madison, Wisconsin.

Rolland, N., 2010. The early human occupation of high latitudes, Boreal, continental and periglacial habitats: Middle Palaeolithic milestones in northern Eurasia. Acta Universitatis Wratislaviensis 3027, 15-46.

Rose, J.I., Usik, V.I., Marks, A.E., Hilbert, Y.H., Galletti, C.S., Parton, A., Geiling, J.M., Černý, V., Morley, M.W., Roberts, R.G., 2011. The Nubian Complex of Dhofar, Oman: An African Middle Stone Age Industry in Southern Arabia. PLOS ONE 6, e28239.

Rots, V., 2009. The functional analysis of the Mousterian and Micoquian assemblages of Sesselfelsgrotte, Germany. Tool use and Hafting in the European Late Middle Paleolithic. Quartär: Jahrbuch für Erforschung des Eiszeitalters und Seiner Kulturen.

Rousseeuw, P.J., Croux, C., 1993. Alternatives to the Median Absolute Deviation. Journal of the American Statistical Association 88, 1273-1283.

Rousseeuw, P.J., Debruyne, M., Engelen, S., Hubert, M., 2006. Robustness and Outlier Detection in Chemometrics. Critical Reviews in Analytical Chemistry 36, 221-242.

Ruan, Q.J., Liu, J.H., Hu, Y., Li, B., Yang, C.C., Luo, X.R., 2017. A study of stone artefacts found in the Tianhuadong Paleolithic site, Heqing, Yunnan. Acta Anthropologica Sinica 36, 1-16.

Rui, X., Zhang, J.-F., Hou, Y.-M., Yang, Z.-M., Liu, Y., Zhen, Z.-M., Zhou, L.-P., 2015. Feldspar multi-elevated-temperature post-IR IRSL dating of the Wulanmulun Paleolithic site and its implication. Quaternary Geochronology 30, 438-444.

Ryssaert, C., 2006a. Lithische technologie te Mesvin IV: selectiecriteria voor geretoucheerde werktuigen en hun relatie met Levalloiseindproducten. Anthropologica Et Praehistorica 117, 13-33.

Ryssaert, C., 2006b. Some new insights in an old collection: lithic technology at Mesvin IV. Notae Praehistoricae 26, 91-99.

Sandgathe, D., 2004. Alternative Interpretation of the Levallois Reduction Technique. Lithic Technology 29, 147-159.

Santonja, M., Villa, P., 1990. The Lower Paleolithic of Spain and Portugal. J. World Prehist. 4, 45-94.

Santonja, M., Villa, P., 2006. The Acheulian of Western Europe, in: Goren-Inbar, N., Sharon, G. (Eds.), Axe age: Acheulian tool-making from quarry to discard. Equinox, London; Oakville, CT.

Schick, K., Toth, N., 1993. Making Silent Stones Speak: Human Evolution and the Dawn of Technology. Simon and Schuster, New York.

Schick, K.D., 1994. The Movius Line reconsidered: Perspectives on the earlier Palaeolithic of Eastern Asia, in: Corruccini, R.S., Ciochon, R. (Eds.), Integrative Paths to the Past: Palaeoanthropological Advances in Honour of F. Clark Howell. Prentice Hall, New Jersey, pp. 569-596.

Schick, K.D., 1998. A comparative perspective on Paleolithic cultural patterns. Plenum Press, New York.

Schick, K.D., Zhuan, D., 1993. Early paleolithic of China and eastern Asia. Evol. Anthropol. 2, 22-35.

Schlanger, N., 1996. Understanding Levallois: lithic technology and cognitive archaeology. Cambridge Archaeological Journal 6, 231-254.

Schlanger, N., 2008. Understanding Levallois: Lithic Technology and Cognitive Archaeology. Cambridge Archaeological Journal 6, 231-254.

Schlebusch, C., Malmström, H., Günther, T., Sjödin, P., Coutinho, A., Edlund, H., R. Munters, A., Vicente, M., Steyn, M., Soodyall, H., Lombard, M., Jakobsson, M., 2017. Southern African ancient genomes estimate modern human divergence to 350,000-260,000 years ago.

Schwarcz, H.P., Grün, R., Vandermeersch, B., Bar-Yosef, O., Valladas, H., Tchernov, E., 1988. ESR dates for the hominid burial site of Qafzeh in Israel. Journal of Human Evolution 17, 733-737.

Scott, B., Ashton, N., Lewis, S., Parfitt, S., White, M., 2011. Technology and landuse in the early Middle Palaeolithic of the Thames valley, in: Ashton, N., Lewis, S., Stringer, C. (Eds.), The Ancient Human Occupation of Britain. Elsevier, Amsterdam, pp. 67-89.

Scott, R., 2006. The early middle Palaeolithic of Britain; origins, technology and landscape. Durham University.

Semaw, S., Renne, P., Harris, J.W.K., Feibel, C.S., Bernor, R.L., Fesseha, N., Mowbray, K., 1997. 2.5-million-year-old stone tools from Gona, Ethiopia. Nature 385, 333-336.

Semaw S, R.M., Quade J, Renne PR, Butler RF, Dominguez-Rodrigo M, Stout D, Hart WS, Pickering T, Simpson SW., 2003. 2.6-Million-Year-Old Stone Tools and Associated Bones from OGS-6 and OGS-7, Gona, Afar, Ethiopia. Journal of Human Evolution 45, 169-177.

Shalagina, A.V., Krivoshapkin, A.I., Kolobova, K.A., 2015. Truncated-faceted pieces in the Paleolithic of northern Asia. Archaeology, Ethnology and Anthropology of Eurasia 43, 33-45.

Shea, J.J., 2013. Measuring Lithic Artefacts, Stone Tools in the Paleolithic and Neolithic Near East: A Guide. Cambridge University Press, Cambridge, pp. 334-346.

Shea, J.J., 2003. The Middle Paleolithic of the East Mediterranean Levant. J. World Prehist. 17, 313-394.

Shea, J.J., 2008. Transitions or turnovers? Climatically-forced extinctions of Homo sapiens and Neanderthals in the east Mediterranean Levant. Quaternary Science Reviews 27, 2253-2270.

Shea, J.J., 2011. Homo sapiens is as homo sapiens was: Behavioral variability versus "behavioral modernity" in paleolithic archaeology. Current Anthropology 52, 1-35.

Shea, J.J., 2014. Sink the Mousterian? Named stone tool industries (NASTIES) as obstacles to investigating hominin evolutionary relationships in the Later Middle Paleolithic Levant. Quatern Int 350, 169-179.

Shen, G.J., Gao, X., Zhao, J.-x., Collerson, K.D., 2004. U-series dating of Locality 15 at Zhoukoudian, China, and implications for hominid evolution. Quat. Res. 62, 208-213.

Shen, G.J., Jin, L.H., 1992. U-series dating of speleothem samples from Guanyindong Cave at Qianxi County, Guizhou Province. Acta Anthropologica Sinica 11, 93-100.

Shennan, S., 2001. Demography and Cultural Innovation: a Model and its Implications for the Emergence of Modern Human Culture. Cambridge Archaeological Journal 11, 5-16.

Shimelmitz, R., Barkai, R., Gopher, A., 2011. Systematic blade production at late Lower Paleolithic (400-200 kyr) Qesem Cave, Israel. Journal of Human Evolution 61, 458-479.

Shimelmitz, R., Kuhn, S.L., 2017. The toolkit in the core: There is more to Levallois production than predetermination. Quatern Int 464, 81-91.

Shimelmitz, R., Weinstein-Evron, M., Ronen, A., Kuhn, S.L., 2016b. The Lower to Middle Paleolithic transition and the diversification of Levallois technology in the Southern Levant: Evidence from Tabun Cave, Israel. Quatern Int 409, 23-40.

Shirokov, V.N., Volkov R. B., Kosintsev, P.A., Lapteva, E.G., 2011. Paleoliticheskaya stoyanka Bogdanovka (Yuzhnyy Ural). Rossiyskaya arkheologiya 1, 111-125.

Slavinskiy, V.S., Rybin, E.P., 2015. Levallois Convergent Unidirectional Typical Technology in Southern Siberia and the Northern Part of Central Asia: Variability, Distribution, Chronology. Stratum Plus 2015, 285-307.

Slimak, L., 1999. Mise en évidence d'une composante laminaire et lamellaire dans un complexe moustérien du Sud de la France/Evidence of blade and bladelet debitage in a Mousterian complex from Southern France. Pale´o 11, 89-110.

Slon, V., Hopfe, C., Weiß, C.L., Mafessoni, F., de la Rasilla, M., Lalueza-Fox, C., Rosas, A., Soressi, M., Knul, M.V., Miller, R., Stewart, J.R., Derevianko, A.P., Jacobs, Z., Li, B., Roberts, R.G., Shunkov, M.V., de Lumley, H., Perrenoud, C., Gušić, I., Kućan, Ž., Rudan, P., Aximu-Petri, A., Essel, E., Nagel, S., Nickel, B., Schmidt, A., Prüfer, K., Kelso, J., Burbano, H.A., Pääbo, S., Meyer, M., 2017. Neandertal and Denisovan DNA from Pleistocene sediments. Science 356, 605.

Slon, V., Mafessoni, F., Vernot, B., de Filippo, C., Grote, S., Viola, B., Hajdinjak, M., Peyrégne, S., Nagel, S., Brown, S., Douka, K., Higham, T., B. Kozlikin, M., V. Shunkov, M., P. Derevianko, A., Kelso, J., Meyer, M., Prüfer, K., Pääbo, S., 2018. The genome of the offspring of a Neandertal mother and a Denisovan father. Nature 561, 113–116.

Smith, B.W., Rhodes, E.J., Stokes, S., Spooner, N.A., 1990. The Optical Dating of Sediments Using Quartz. Radiation Protection Dosimetry 34, 75-78.

Smith, M.A., Prescott, J.R., Head, M.J., 1997. Comparison of ^{14}C and luminescence chronologies at Puritjarra rock shelter, central Australia. Quaternary Science Reviews 16, 299-320.

Solecki, R.L.S., R. S., 1970. A new secondary flaking technique at the Nahr Ibrahim cave site, Lebanon. Bulletin Du Musee De Beyrouth 23, 137-142.

Soressi, M., D'Errico, F., 2007. Pigments, gravures, parures: les comportements symboliques controversés de Néandertaliens. In Bernard Vandermeersch & Bruno Maureille (Ed.), Les Néandertaliens: Biologie et cultures (pp. 297-309). Paris: Édition CTHS.

Spooner, N.A., Aitken, M.J., Smith, B.W., Franks, M., Mcelroy, C., 1990. Archaeological Dating by Infrared-Stimulated Luminescence Using a Diode-Array. Radiation Protection Dosimetry 34, 83-86.

Stiner, M.C., Munro, N.D., Surovell, T.A., Tchernov, E., Bar-Yosef, O., 1999. Paleolithic Population Growth Pulses Evidenced by Small Animal Exploitation. Science 283, 190.

Stokes, S., Ingram, S., Aitken, M.J., Sirocko, F., Anderson, R., Leuschner, D., 2003. Alternative chronologies for Late Quaternary (Last Interglacial-Holocene) deep sea sediments via optical dating of silt-sized quartz. Quaternary Science Reviews 22, 925-941.

Stout, D., Semaw, S., Rogers, M.J., Cauche, D., 2010. Technological variation in the earliest Oldowan from Gona, Afar, Ethiopia. Journal of Human Evolution 58, 474-491.

Stringer, C., 2002. Modern human origins: progress and prospects. Philosophical Transactions of the Royal Society of London. Series B: Biological Sciences 357, 563-579.

Stringer, C.B., Grun, R., Schwarcz, H.P., Goldberg, P., 1989. ESR dates for the Hominid burial site of ES Skhul in Israel. Nature 338, 756-758.

Sun, X., Mercier, N., Falgueres, C., Bahain, J.-J., Despriee, J., Bayle, G., Lu, H., 2010. Recuperated optically stimulated luminescence dating of middle-size quartz grains from the Palaeolithic site of Bonneval (Eure-et-Loir, France). Quaternary Geochronology 5, 342-347.

Sutikna, T., Tocheri, M.W., Morwood, M.J., Saptomo, E.W., Jatmiko, Awe, R.D., Wasisto, S., Westaway, K.E., Aubert, M., Li, B., Zhao, J.X., Storey, M., Alloway, B.V., Morley, M.W., Meijer, H.J.M., Van Den Bergh, G.D., Grün, R., Dosseto, A., Brumm, A., Jungers, W.L., Roberts, R.G., 2016. Revised stratigraphy and chronology for Homo floresiensis at Liang Bua in Indonesia. Nature 532, 366-369.

Svendsen, J.I., Heggen, H.P., Hufthammer, A.K., Mangerud, J., Pavlov, P., Roebroeks, W., 2010. Geo-archaeological investigations of Palaeolithic sites along the Ural Mountains – On the northern presence of humans during the last Ice Age. Quaternary Science Reviews 29, 3138-3156.

Swisher, C.C., Rink, W.J., Antón, S.C., Schwarcz, H.P., Curtis, G.H., Widiasmoro, A.S., 1996. Latest *Homo erectus* of Java: Potential Contemporaneity with *Homo sapiens* in Southeast Asia. Science 274, 1870-1874.

Teihard de Chardin TD, L.F., 1924. On the discovery of a Palaeolithic industry in northern China. Bulletin of the Geological Society of China 3, 45-50.

Tensorer, J.-M.L., Jagher, R., Rentzel, P., Hauck, T., Ismail-Meyer, K., Pümpin, C., Wojtczak, D., 2007. Long-term site formation processes at the natural springs Nadaouiyeh and Hummal in the El Kowm Oasis, Central Syria. Geoarchaeology 22, 621-640.

Thiébaut, C., Claud, E., Deschamps, M., Discamps, E., Soulier, M.-C., Mussini, C., Sandrine, C., Rendu, W., Brenet, M., David, C., Coudenneau, A., Gerbe, M., Guibert, P., Jaubert, J., Laroulandie, V., Maureille, B., Mourre, V., Santos, F., 2014. Diversité des productions lithiques du Paléolithique moyen récent (OIS4-OIS3): enquête sur le rôle des facteurs environnementaux, fonctionnels et culturels.

Thissen, J., 2006. Die Paläolithischen Freilandstationen von Rheindahlen im Löss Zwischen Maas und Niederrhein. Rheinische Ausgrabungen 59, Verlag Philipp von Zabern, Mainz, Germany.

Thomsen, K.J., Murray, A.S., Buylaert, J.P., Jain, M., Hansen, J.H., Aubry, T., 2016. Testing single-grain quartz OSL methods using sediment samples with independent age control from the Bordes-Fitte rockshelter (Roches d'Abilly site, Central France). Quaternary Geochronology 31, 77-96.

Tiemei, C., Quan, Y., En, W., 1994. Antiquity of Homo sapiens in China. Nature 368, 55-56.

Tishkoff, S.A., Kidd, K.K., 2004. Implications of biogeography of human populations for 'race' and medicine. Nature Genetics 36, S21.

Tite, M.S., 1966. Thermoluminecent dating of ancient ceramics: a reassessment. Archaeometry 9, 155-169.

Tixier, J., Inizan, M.L., Roche, H., 1980. Préhistoire de la pierre taillé 1: terminologie e technologie. Centre de Recherches et d'études Pré-historiques, Valbone.

Tryon, C.A., 2006. Middle Stone Age Lithic Technology of the Kapthurin Formation (Kenya). Current Anthropology 47, 367-375.

Tryon, C.A., Faith, J.T., 2013. Variability in the Middle Stone Age of Eastern Africa. Current Anthropology 54, S234-S254.

Tryon, C.A., McBrearty, S., 2002. Tephrostratigraphy and the Acheulian to Middle Stone Age transition in the Kapthurin Formation, Kenya. Journal of Human Evolution 42, 211-235.

Tryon, C.A., McBrearty, S., 2006. Tephrostratigraphy of the Bedded Tuff Member (Kapthurin Formation, Kenya) and the nature of archaeological change in the later middle Pleistocene. Quat. Res. (USA) 65, 492-507.

Tryon, C.A., McBrearty, S., Texier, P.-J., 2005. Levallois Lithic Technology from the Kapthurin Formation, Kenya: Acheulian Origin and Middle Stone Age Diversity. African Archaeological Review 22, 199-229.

Tryon, C.A., Tyler, F., J., 2013. Variability in the Middle Stone Age of Eastern Africa. Current Anthropology 54, S234-S254.

Tuffreau, A., 1982. The transition Lower/Middle Palaeolithic in Northern France, in: Ronen, A. (Ed.), The Transition from the Lower to Middle Palaeolithic and the Origin of Modern Man. British Archaeological Reports, International Series, Oxford, pp. 137-149.

Tuffreau, A., 2001. L'Acheuléen dans la vallée de la Somme et Paléolithique moyen dans le Nord de la France: données récentes. Centre d'études et de recherches préhistoriques, Université des sciences et technologies de Lille.

Turner, R.C., Radley, J.M., Mayneord, W.V., 1958. The alpha-ray activity of human tissues. British Journal of Radiology 31, 397-402.

Turq, A., 1989. Approche technologique et économique du faciès Moustérien de type Quina: étude préliminaire. Bulletin de la Société préhistorique française 86, 244-256.

Turq, A., 2000. Paléolithique inférieur et moyen entre Dordogne et Lot. Bulletin de la Société préhistorique française 98, 338-339.

Valladas, H., Mercier, N., Hershkovitz, I., Zaidner, Y., Tsatskin, A., Yeshurun, R., Vialettes, L., Joron, J.-L., Reyss, J.-L., Weinstein-Evron, M., 2013. Dating the Lower to Middle Paleolithic transition in the Levant: A view from Misliya Cave, Mount Carmel, Israel. Journal of Human Evolution 65, 585-593.

Valladas, H., Reyss, J.L., Joron, J.L., Valladas, G., Bar-Yosef, O., Vandermeersch, B., 1988. Thermoluminescence dating of Mousterian Troto-Cro-Magnon' remains from Israel and the origin of modern man. Nature 331, 614-616.

Van Baelen, A., Meijs, E., Van Peer, P., de Warrimont, J.-P., De Bie, M., 2007. An early Middle Palaeolithic site at Kesselt-Op de Schans (Belgian Limburg). Preliminary result. Notae Praehistoricae 27, 19-26.

Van Peer, P., 1992. The Levallois reduction strategy. Prehistory Press.

Van Peer, P., Fullagar, R., Stokes, S., Bailey, R.M., Moeyersons, J., Steenhoudt, F., Geerts, A., Vanderbeken, T., De Dapper, M., Geus, F., 2003. The Early to Middle Stone Age Transition and the Emergence of Modern Human Behaviour at site 8-B-11, Sai Island, Sudan. Journal of Human Evolution 45, 187-193.

Vandenberghe, J., Roebroeks, W., van Kolfschoten, T., 1993. Maastricht-Belvédère: Stratigraphy. Palaeoenvironment and Archaeology of the Middle and Late Pleistocene Deposits. Part II. Mededelingen Rijks Geologische Dienst, Leiden, Netherlands.

Vandermeersch, B., 1982. The first Homo sapiens sapiens in the Near East. British Archaeological Research, Oxford.

Vaquero M., C.E., 2003. A temporal perspective on the variabilityof the discoid method in the Iberian Peninsula., in: Peresani, M. (Ed.), Discoid Lithic Technology. Advances and Implication, Oxford, pp. 67-82.

Vasil'ev, S.A., Kuzmin, Y.V., Orlova, L.A., Dementiev, V.N., 2002. Radiocarbon-based chronology of the Paleolithic in Siberia and its relevance to the peopling of the New World. Radiocarbon 44, 503-530.

Wadley, L., Jacobs, Z., 2004. Sibudu Cave, KwaZulu-Natal: Background to the excavations of Middle Stone Age and Iron Age occupations. South African Journal of Science 100, 145-151.

Wallace, I.J., Shea, J.J., 2006. Mobility patterns and core technologies in the Middle Paleolithic of the Levant. Journal of Archaeological Science 33, 1293-1309.

Wang, H., Deng, C., Zhu, R., Wei, Q., Hou, Y., Boëda, E., 2005. Magnetostratigraphic dating of the Donggutuo and Maliang Paleolithic sites in the Nihewan Basin, North China. Quat. Res. 64, 1-11.

Wang, H., Song, M., 2011. Ckmeans. 1d. dp: optimal k-means clustering in one dimension by dynamic programming. The R journal 3, 29.

Wang, S.J., 2007. The Paleolithic Open-air Sites in the Luonan Basin, China. Science Press, Beijing.

Wang, W., Liu, J., Hou, Y., Si, X., Huang, W., Schepartz, L.A., Miller-Antonio, S., 2004. Panxian Dadong, South China: establishing a record of Middle Pleistocene climatic changes. Asian Perspectives 43, 302-313.

Wang, X.K., Wei, J., Chen, Q.J., Tang, Z.W., Wang, C.X., 2010. A Preliminary study on the excavation of the Jinsitai Cave site. Acta Anthropologica Sinica 29, 15-32.

Wang, Y., 2000. Palaeolithic Archaeology Cultural Relics Publishing House, Beijing.

Wang, Y., 2005. Roots of Pleistocene Hominids and Cultures in China. Science Press, Beijing.

Wang, Y., 2017. Late Pleistocene Human Migrations in China. Current Anthropology 58, S504-S513.

Watteyne, D., 1985. Petit-Spiennes: industrie (s) a débitage Levallois et para-Levallois. Notae Praehistoricae 5.

Westaway, K.E., Louys, J., Awe, R.D., Morwood, M.J., Price, G.J., Zhao, J.x., Aubert, M., Joannes-Boyau, R., Smith, T.M., Skinner, M.M., Compton, T., Bailey, R.M., van den Bergh, G.D., de Vos, J., Pike, A.W.G., Stringer, C., Saptomo, E.W., Rizal, Y., Zaim, J., Santoso, W.D., Trihascaryo, A., Kinsley, L., Sulistyanto, B., 2017. An early modern human presence in Sumatra 73,000–63,000 years ago. Nature 548, 322.

Westaway, R., Bridgland, D., White, M., 2006. The Quaternary uplift history of central southern England: evidence from the terraces of the Solent River system and nearby raised beaches. Quaternary Science Reviews 25, 2212-2250.

White, M., Ashton, N., 2003. Lower Palaeolithic core technology and the origins of the Levallois method in North-Western Europe. Current Anthropology 44, 598-608.

White, M., Ashton, N., Scott, B., 2011. The emergence, diversity and significance of the Mode 3 (prepared core) technologies. The ancient human occupation of Britain, 53-66.

White, M.J., Scott, B., Ashton, N., 2006. The Early Middle Palaeolithic in Britain: Archaeology, settlement history and human behaviour. J. Quat. Sci. 21, 525-541.

White, T.D., Asfaw, B., DeGusta, D., Gilbert, H., Richards, G.D., Suwa, G., Clark Howell, F., 2003. Pleistocene Homo sapiens from Middle Awash, Ethiopia. Nature 423, 742-747.

Wil Roebroeks, C.G., 1999. The Middle Palaeolithic Occupation of Europe. University of Leiden.

Wintle, A.G., 2008. Luminescence dating: where it has been and where it is going. Boreas 37, 471-482.

Wintle, A.G., Huntley, D.J., 1980. Thermoluminescence dating of ocean sediments. Canadian Journal of Earth Sciences 17, 348-360.

Wintle, A.G., Murray, A.S., 1999. Luminescence sensitivity changes in quartz. Radiation Measurements 30, 107-118.

Wintle, A.G., Murray, A.S., 2006. A review of quartz optically stimulated luminescence characteristics and their relevance in single-aliquot regeneration dating protocols. Radiation Measurements 41, 369-391.

Wiśniewski, A., 2014. The beginnings and diversity of Levallois methods in the early Middle Palaeolithic of Central Europe. Quatern Int 326, 364-380.

Wisniewski, A., Fridrich, J., 2010. Early Middle Palaeolithic activity exemplified by the industry from Becov I, A-III-6 and other sites of Central Europe. Middle Palaeolithic Human Activity and Palaeocology: New discoveries and Ideas, in: Burdukiewicz, J.M., Wisniewski, A. (Eds.), Middle Palaeolithic Activity and Palaeoecology. Studia Archeologiczne 41, Biblioteka Cyfrowa, Wydawnictwa Uniwersytetu Wroclawskiego, Wroclaw, Poland, pp. 217–243.

Wood, B., Richmond, B.G., 2000. Human evolution: taxonomy and paleobiology. Journal of Anatomy 197, 19-60.

Wu, M.W.L.Z., Yinyun; Zhang, Senshui, 1975. Ancient Human fossils and cultural remains in Tongzi, Guizhou Province. Vertebrata Palasiatica 13, 14-23.

Wu, X.-j., Bruner, E., 2016. The endocranial anatomy of maba 1. American Journal of Physical Anthropology 160, 633-643.

Wu, X.-J., Crevecoeur, I., Liu, W., Xing, S., Trinkaus, E., 2014. Temporal labyrinths of eastern Eurasian Pleistocene humans. Proceedings of the National Academy of Sciences 111, 10509.

Wurz, S., 2013. Technological trends in the Middle Stone Age of South Africa between MIS 7 and MIS 3. Current Anthropology 54, S305-S319.

Wynn, T., Coolidge, F.L., 2004. The expert Neandertal mind. Journal of Human Evolution 46, 467-487.

Xie, G., Bodin, E., 2007. Paleolithic industries of the Bose Basin (South China). L'Anthopologie 111, 182–206.

Yang, S.-X., Hou, Y.-M., Pelegrin, J., 2016. A Late Acheulean Culture on the Chinese Loess Plateau: The techno-economic behavior of the Dingcun lithic industry. Quatern Int 400, 73-85.

Yang, S.-X., Petraglia, M.D., Hou, Y.-M., Yue, J.-P., Deng, C.-L., Zhu, R.-X., 2017. The lithic assemblages of Donggutuo, Nihewan basin: Knapping skills of Early Pleistocene hominins in North China. PLOS ONE 12, e0185101.

Yang, S.X., Huang, W.W., Hou, Y.M., Yuan, B.Y., 2014. Is the Dingcun lithic assembly a "chopper-chopping tool industry", or "Late Acheulian"? Quatern Int 321, 3-11.

Yi, S., Clark, G.A., 1983. Observations on the Lower Palaeolithic of Northeast Asia. Current Anthropology 24, 181-202.

Yu, J.J., Wang, Y.P., He, J.N., Feng, Y., Li, Y.L., Li, W.C., 2018. The Tongtian Dong Site in Jeminay County, Xinjiang. Archaeology 7, 4-14.

Yuan, S.X., Chen, T.M., Gao, S.J., 1986. Uranium series chronological sequence of some Paleolithic sites in South China. Acta Anthropologica Sinica 5, 179-190.

Zhang, J.F., Huang, W.W., Hu, Y., Yang, S.X., Zhou, L.P., 2015. Optical dating of flowstone and silty carbonate-rich sediments from Panxian Dadong Cave, Guizhou, southwestern China. Quaternary Geochronology 30, 479-486.

Zhang, M.L., Yuan, D.X., Lin, Y.S., Cheng, H., Qin, J.M., Zhang, H.L., 2004. The record of paleoclimatic change from stalagmites and the determination of termination II in the south of Guizhou Province, China. Science in China Series D: Earth Sciences 47, 1-12.

Zhang, P., Huang, W., Wang, W., 2010. Acheulean handaxes from Fengshudao, Bose sites of South China. Quatern Int 223-224, 440-443.

Zhang, S., 1985. Preliminary investigation of the Middle Paleolithic in north China. Prehistory research 1, 8-16.

Zhang, S., 1990. Regional industrial gradual advance and cultural exchange of Paleolithic in North China. Acta Anthropologica Sinica 9, 322-333.

Zhu, Z., Dennell, R., Huang, W., Wu, Y., Qiu, S., Yang, S., Rao, Z., Hou, Y., Xie, J., Han, J., Ouyang, T., 2018. Hominin occupation of the Chinese Loess Plateau since about 2.1 million years ago. Nature 559, 608-612.

Zhu, Z., Ji, X., 2011. Study on the stone artefacts from the Laohu Cave Paleolithic site, Baoshan County, Yunnan Research of China's frontier archaeology 4.

Ziegler, M., Simon, M.H., Hall, I.R., Barker, S., Stringer, C., Zahn, R., 2013. Development of Middle Stone Age innovation linked to rapid climate change. Nature Communications 4, 1905.

Zilhão, J., 2007. The Emergence of Ornaments and Art: An Archaeological Perspective on the Origins of "Behavioral Modernity". Journal of Archaeological Research 15, 1-54.

Zimmerman, D.W., 1971. Thermoluminescent dating using fine grains from pottery. Archaeometry 13, 29-52.

Appendices

Appendix A: detailed description of 9 examples of Levallois pieces from Guanyindong.

Recurrent Levallois core

Core P15948 (Figures 5-1.1 and 5-2.1) was made on black fine grained chert. It presents all stages of reduction and manufacture of Levallois core. The upper surface is covered with several scars come from different directions forming a centripetal scar pattern. Before flaking on the debitage surface, the core was knapped along the edge to prepare the striking platform. The fractures of the predetermined flakes are parallel to the plane of the flake release surface and striking platform surface. The dimension of the core is 56 x 62 x 21 mm.

Core P15266 (Figures 5-1.6 and 5-2.6) was made on chert with rough cortext partially remained on the lower surface. On the upper surface, several previous scars were removed to form convexities to influence the pattern of detachment of the final blank. On the striking platform surface several removals distributed along the circumference of the core with small removals along the edge to create a proper flaking angle. The upper surface (working surface) and lower surface formed a plane that cannot exchange and the axe of percussion is perpendicular to the hinge. The dimension of the core is 30 x 42 x 40 mm.

Core P16502-1 (Figures 5-1.4 and 5-2.4) was made on limestone. The scar pattern of the upper surface was radially produced by removing several flakes. The lower surface was partially prepared along the edge to create a proper striking platform. The intersection of these two surfaces is parallel to the fracture plane of predetermined blank. The size of the core is 101 x 72 x 34 mm.

Preferential Levallois core

Core P4265 (Figures 5-1.2 and 5-2.2) was made on chert with few cortex remains. Most parts of the previous convexity preparatory flake scars were taken away by the final detachment of the predetermined blanks. The fracture of the removal is paralleled with the intersection of the upper and lower surface. The lower surface is covered by plenty of platform preparation scars. The dimension of the core is 72 x 75 x 23mm.

Core P5262 (Figures 5-1.3 and 5-2.3) was made on chert. The upper and lower surface intersected a plane which is parallel to the fracture plane of the final flake. The platform where the final flake knapped off was carefully prepared and other preparations present along the core circumference. The final determined flake was knapped from the prepared platform and took away most parts of the previous convexity preparatory flake scars.

Core P16383 (Figure 5-1.5 and 5-2.5) was made on limestone. It is a Nubian-like core with a large flake scar on the upper surface. The Nubian system is a subset of the preferential Levallois core reduction method, aiming to obtain flakes and points with predetermined size and form (Van Peer, 1992). This

system was found mainly in Africa and Arabia during MIS 5. This core resembles the Nubian Type 1/2 (Will, 2015). In order to produce a distal ridge that can control the final flake, a combination of distal and lateral removals was formed. The dimension is 61 x 51 x 18 mm.

Levallois flakes and tools

Flake P15002 (Figure 5-1.7 and 5-3A.1) was made on fine grained chert. The platform is faceted. One big scar covers the major part of dorsal side with several previous scars coming from different directions left on the margin. It was probably obtained by using recurrent method. The size of the flake is 63 x 62 x 13 mm.

Flake P15951(Figure 5-1.8 and 5-3A.2) was made on chert with the dimension of 65 x 52 x 17 mm, which has a centripetal dorsal scar pattern, indicating that the convexity of original preferential core is maintained by detachment along the circumference of the core.

Tool P5348 (Figure 5-1.17 and 5-3B.1) is a scraper made on a Levallois blank. The original flake has a radial pattern on the dorsal side and then it was alternating retouched along the edge on both sides.

Appendix B: The published manuscript from this thesis.

Hu, Y., Marwick, B., Zhang, J.-F., Rui, X., Hou, Y.-M., Yue, J.-P., Chen, W.-R., Huang, W.-W., Li, B., 2019. Late Middle Pleistocene Levallois stone-tool technology in southwest China. Nature 565, 82–85.

Hu, Y., Marwick, B., Zhang, JF. *et al.* Late Middle Pleistocene Levallois stone-tool technology in southwest China. *Nature* **565,** 82–85 (2019). https://doi.org/10.1038/s41586-018-0710-1